INFORMATION TO USERS

This manuscript has been reproduced from the microfilm master. UMI films the text directly from the original or copy submitted. Thus, some thesis and dissertation copies are in typewriter face, while others may be from any type of computer printer.

The quality of this reproduction is dependent upon the quality of the copy submitted. Broken or indistinct print, colored or poor quality illustrations and photographs, print bleedthrough, substandard margins, and improper alignment can adversely affect reproduction.

In the unlikely event that the author did not send UMI a complete manuscript and there are missing pages, these will be noted. Also, if unauthorized copyright material had to be removed, a note will indicate the deletion.

Oversize materials (e.g., maps, drawings, charts) are reproduced by sectioning the original, beginning at the upper left-hand corner and continuing from left to right in equal sections with small overlaps.

Photographs included in the original manuscript have been reproduced xerographically in this copy. Higher quality 6" x 9" black and white photographic prints are available for any photographs or illustrations appearing in this copy for an additional charge. Contact UMI directly to order.

ProQuest Information and Learning
300 North Zeeb Road, Ann Arbor, MI 48106-1346 USA
800-521-0600

Development of Zeolite based Acid Catalysts for the Synthesis of Methyl tertiary butyl Ether

Si Tuan LE

A Thesis

in

The Department

of

Chemistry & Biochemistry

Presented in Partial Fulfilment of the Requirements
for the Degree of Doctor of Philosophy at
Concordia University
Montreal, Quebec, Canada

October 2000

ABSTRACT

Development of zeolite based catalysts for the gas phase synthesis of Methyl tertiary butyl Ether

Si Tuan LE, Ph.D.
Concordia University, 2000

Methyl tertiary butyl ether (MTBE) an antiknock additive presently used in gasoline blends as a safer alternative to lead compounds, is currently synthesized industrially from methanol and isobutene over an acidic ion-exchange resin Amberlyst-15. This commercial catalyst, although very active, still suffers from several drawbacks such as thermal instability, acid leaching, and need of a high methanol over isobutene ratio. Zeolites for their higher thermal stability and shape selectivity, were thus proposed to remedy to such disadvantages. However, they did not show a surface acidity which is as high as that of the organic resin.

In gas phase synthesis of MTBE, the incorporation of an organic superacid trifluoromethanesulfonic acid onto the the zeolite surface have shown an important enhancement in catalytic activity and product selectivity for the large pore sized Y-type zeolite. However this method did not increase significantly the catalytic activity of the medium pore sized ZSM-5 zeolite, because of limited diffusion phenomena.

ZSM-5 zeolite, when doped with fluorine species in relatively low concentration using ammonium fluoride as precursor, and subsequently activated stepwise at high temperatures, showed two maxima for the MTBE yield. The first maximum occurring at the final activation temperature 325°C, corresponded to the positive effect of chemisorbed HF acidic species onto the zeolite surface. The second maximum occurring at 450°C, provided the highest MTBE yield and is attributed to the increased Brønsted acid sites density and strength resulting from the reaction of zeolite surface with the proton from the «proton-fluoride» ions pair. Data obtained from different characterization techniques such as FTIR, ^{27}Al MAS-NMR, XRD, NH_3-TPD, BET, MeOH adsorption tests, Fluoride-SIE and Pyridine adsorption tests supported the proposed mechanism for the modification of the fluorine treated ZSM-5 surface as a function of final activation temperatures.

Controlled desilication of ZSM-5 zeolite by treatment with an aqueous solution of sodium carbonate under mild conditions has provided materials having much lower Si/Al ratio with an unchanged zeolite structure. The desilicated ZSM5 zeolite exhibited a higher Brønsted acid sites density compared to the parent zeolite and showed a significant increase of MTBE conversion.

The combination of these two modification techniques, i.e. desilication followed by incorporation of fluorine / thermal treatment produced a highly efficient catalyst: the yield of MTBE obtained was higher than that of the commercial catalyst and no isobutene dimer by-products were formed owing to

the shape selectivity of ZSM-5 structure. With respect to the parent zeolite, the total acid density increased by almost 80 % and the formation of some stronger acid sites were observed. This new inorganic catalyst can be advantageously applied to a wide range of acido-catalysed reactions up to 450°C which require a high surface acidity, a pronounced shape-selectivity and a strong chemical resistance.

ACKNOWLEDGEMENTS

I wish to express my sincere gratitude to my thesis supervisor Dr. Raymond Le Van Mao for his precious guidance and direction throughout the course of this research and in the preparation of this thesis, and to my co-supervisor, Dr. Georges Denes for his precious support and helpful discussions in the writing of my thesis.

I would also like to thank the members of my research committee, Dr. P.H. Bird, Dr. D. Jack and Dr. O.S. Tee for their time and helpful suggestions during my research.

I am greatly indebted to my mother Nguyen Ngoc Bich, my aunt Le Thi Ty Peroz, to Dr. Vi Kien Luong, Mrs Marilyn Mai Lien LE, my brothers Le Si Phat, Le Si Dat, my sisters Le Ngoc Loan, Le Ngoc Tram, Le Ngoc Tuyet and Miss Lam Nguyet Minh for their precious supports and continous encouragements.

I also thank to all members and my friends of the Catalysis Laboratory, Dr. R. Carli, Dr. J.H. Yao, Dr. S.Y. Xiao, Dr. L. Heeribout, Dr. V. Semmer, Dr. A. Muntasar, Dr. M.A. Saberi, Dr. D. Ohayon, Miss N. Borsuk, Mr. M. Fairbain, Mr. S. Melancon and especially Dr. R. Patterson Mr. F. Nudo and J. Kolokotronis for their helpful technical assistance. Finally, I also wish to express my sincere thanks to Mrs Carole Coutts for always giving me good advice, and to Dr. A. Lesir for his patience in reading this manuscript.

In precious memory of my father,

the late, Mr. LE Si Giai

TABLE OF CONTENTS

LIST OF FIGURES

Chapter 1

Chapter 2

Chapter 3

LIST OF TABLES

Chapter 1

Chapter 3

LIST OF ABBREVIATIONS

A-15	Amberlyst-15
BET	Brunauer Emmett and Teller
BTX	Benzene, Toluene and Xylene
DEE	Diethyl Ether
DME	Dimethyl Ether
DTA	Differential Thermal Analysis
ETBE	Ethyl Tertiary Butyl Ether
FCC	Fluid Catalytic Cracking
FID	Flame Ionization Detector
FTIR	Fourier Transform Infrared Spectroscopy
GC	Gas Chromatography
GC-MSD	Gas Chromatography - Mass Spectrometry Detector
HC	Hydrocarbon
HF	Hydrogen Fluoride
HY	Faujasite type zeolite in the acid form
IR	Infrared Spectroscopy
LPG	Liquefied Petroleum Gases
MAS-NMR	Magic Angle Spinning Nuclear Magnetic Resonance
MON	Motor Octane Number
MTBE	Methyl Tertiary Butyl Ether
MTG	Methanol To Gasoline
RON	Research Octane Number
SBU	Secondary Building Unit
SEM	Scanning Electron Microscopy
T_c	Contact Time
TCD	Thermal Conductivity Detector

TFA	Tri Fluoromethanesulfonic Acid
TGA	Thermal Gravimetric Analysis
TPD	Temperature Programmed Detector
WHSV	Weight Hourly Space Velocity
XPS	X-ray Photoelectron Spectroscopy
$\mathbf{Y_i}$	Yield of product i
ZSM	Zeolite Socony Mobil

CHAPTER I

INTRODUCTION

1.1 MTBE an antiknock additive to transportation fuels.

Knock phenomenon , heard outside the engine as a pinging sound, is caused by the premature auto-ignition of the end gas in the combustion chamber just before the piston reaches the summit of its cycle. This results in a significant loss of engine power, damage to the engine and harmful emissions of unburnt hydrocarbons in exhaust gases. The basic principle involved in the elimination of knock is delaying the fuel ignition long enough, until the piston reaches the summit of its cycle. Several organic compounds known for their ability to delay the auto-ignition process, have been introduced into gasoline blends to suppress the knock. They are characterized by the octane number which reflects their specific resistance to knock.

A scale of octane number was introduced in the early 1900 in order to evaluate the antiknock characteristics of hydrocarbons mixture. Iso-octane (2,2,4-trimethylpentane) exhibiting the best antiknock characteristic was assigned a value of 100, whereas n-heptane for its poor antiknock resistance was assigned a value of zero. This designation was applied to gasoline blends in comparison with a reference mixture of known percentage of iso-octane and n-heptane which gives the same anti-knock performance under standard conditions in a test engine. The higher the octane number the better their antiknock characteristics.

Since 1922, lead compounds such as tetraethyl lead (TEL) and tetramethyl lead (TML) were widely used as gasoline additives for their remarkable

effectiveness in suppressing knock. However due to their detrimental effects on the environment including effects on human health such as lower IQ, hyperactivity, reducing learning ability as well as their deactivating action on catalytic mufflers (covering of the catalyst surface), their use in gasoline blends have been recently banned in most industrialized countries.

As substitutes to lead compounds, oxygenates such as alcohols (ethanol, methanol) and ethers (methyl tert-butyl ether, ethyl tert-butyl ether, tert-amyl methyl ether) have been proposed by refiners as alternate sources of octane additives (1). Owing to a fairly high octane blending value (Table 1.0), a relatively low volatility and positive effects on the reduction of carbon monoxide, unburnt hydrocarbons and NO_x in automobile exhaust gases (2,3), methyl tert-butyl ether (MTBE) is the oxygenate of choice approved by the US Environmental Protection Agency as of 1990, to be blended into gasoline at 11 vol % (4a). Compared to alcohols which may cause phase separation in gasoline in the presence of water, MTBE does not present this demixing problem nor evolves any toxic products of incomplete combustion in engines as do aromatic hydrocarbons (4b). In addition, with its specifications close to those of gasolines, MTBE does not require any dramatic modifications of engine technology (5). Ethyl tert-butyl ether (ETBE), a related compound to MTBE having a comparable reaction enthalpy (6a), although having similar antiknock characteristics, is not widely used because of its higher toxic emissions of CO_2, CO, and benzene in exhaust gases, and of a doubled cost

	Boiling Point (°F)	Blending vapor Pressure (psi)	Average octane (R+M)/2	Oxygen content wt %	Blending limits vol %	wt %
Alcohols						
Methanol	148	60	120	50	–	–
Ethanol	173	18	115	35	10	3.7
MeOH Blend	145/180	31	108	35	9.5	3.7
GTBA	181	12	100	21	16	3.7
Ethers						
MTBE	131	8	110	18	15	2.7
ETBE	161	4	111	16	13	2.0
TAME	187	1	106	16	13	2.0

R : Research octane number

M : Motor octane number

GTBA : Gasoline grade tertiary butyl alcohol

MTBE : Methyl tertiary butyl ether

ETBE : Ethyl tertiary butyl ether

TAME : Tertiary amyl methyl ether

Table 1.0 : Physical properties of fuel oxygenates (ref. 23)

of ethanol used as starting material at the present time (6b). TAME, another cousin to MTBE, is also not widely produced by refiners because of its less favorable thermodynamic equilibrium considerations with respect to MTBE (8).

For some industrial processes requiring high purity isobutene (> 99.9 %) as feedstock (e.g. the production of synthetic polyisobutylene rubbers), MTBE also represents a valuable starting material for the production of pure isobutene by thermal decomposition over acidic catalyst and thus is used in many areas as an alternative form of transportation for isobutene (7a). Another application of industrial interest making use of the highly reactive character of the tertiary butyl carbenium from isobutene is the use of MTBE reaction as a means for the quantitative separation of isobutene from 1-butene in C4 petroleum cuts (7b,7c).

The volume of the global gasoline pool is so large that the incorporation of 10-15% of an ether has a huge impact in terms of oxygenate demand. In consequence, MTBE is the fastest growing chemical of the 1990s with a worldwide annual capacity amounting to 24 million tons (Mt) in 1997 (Figure 1.0.a) and a projected increase to nearly 36 Mt by the year 2000 (8a).

Recently, the presence of MTBE was discovered in water supplies at very low concentrations (even below the taste and odor threshold) in areas that use reformulated gasoline, such as California, Maine, New Jersey and others. Since it is an ether, MTBE behaves more like non-reactive alkanes (8b), is very soluble in water and is much less biodegradable than esters. Investigations of higher MTBE

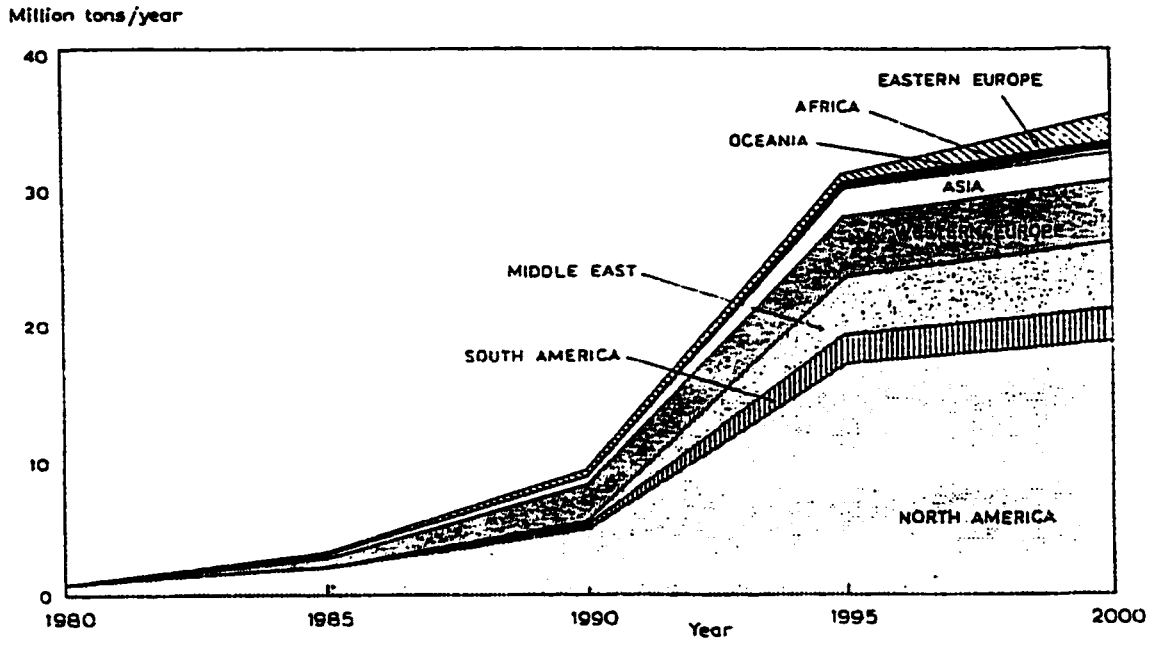

Figure 1.0.a : Projected growth of the MTBE capacity by region (source : SRI International, ref. 24)

concentrations detected in several municipal water wells, revealed the existence of leaking underground storage tanks which are the sources from which MTBE was able to migrate through water tables and enter water sources (8c).

In the affected areas, simultaneous health complaints such as headaches, nausea, dizziness, irritated eyes, nose, and throat, arose and were associated with the use of the oxygenated additive MTBE in reformulated gasoline (8d). Although toxicologic and medical studies have been extensively carried out to investigate the exact cause of the above health problems and their possible link to the presence of MTBE in waters, there is still no clear evidence of ailments linkage with the use of MTBE as an oxygenated additive (8e). Under public pressure in the affected areas and from public agencies such as the Environmental Protection Agency, the American Lung Association and the Natural Resources Defense Council, the state of California has decided on October 22nd, 1999 to ban the use of MTBE as a clean-fuel additive in reformulated gasoline by the year 2003, so as to reduce its negative impacts on the quality of drinking water and its potential harmful effects on human health (8f). Nevertheless, all the remaining states of the USA and the rest of the world still allow the use of MTBE and consider it to be the oxygenated additive of choice to be blended in reformulated gasoline, owing to its outstanding antiknock characteristics and environmentally clean-fuel properties (8c).

1.1.1 Chemical aspects of the MTBE synthesis.

In industry, MTBE is currently produced from the exothermic ($\Delta H_{298\ K}$ = – 37.7 kJ/mol) liquid phase reaction of methanol and isobutene (IB) contained in C4 stream hydrocarbons (9). Only MeOH reacts with IB, all other hydrocarbons remain unreacted. The reaction is catalyzed by a strong acidic macroreticular ion-exchange resin, Amberlyst 15 (A-15), under a pressure ranging from 12 to 20 atms and is maintained at temperatures ranging from 60 °C to 70 °C, according to the following equilibrium reaction (10) :

$$CH_3OH + (CH_3)_2CCH_2 \rightleftharpoons (CH_3)_3COCH_3$$

Methanol Isobutene MTBE

The reaction is equilibrium limited (Figure 1.0.b) : higher conversion to ether is favored at low temperatures due to thermodynamic equilibrium where reaction rates are lower. Conversely conversion to ether is lower at high temperatures where the reverse decomposition of MTBE becomes significant despite a higher reaction rate (11).

From several kinetic studies (12,13a), the mechanistic description which has widely gained acceptance postulates a change of the mechanism depending upon the presence or absence of an excess of MeOH over IB. In the former case in which a polar medium exists around the acid sites, the sulfonic acid groups are dissociated and the protons are solvated owing to an excess of alcohol. The rate determining step of the etherification reaction is the protonation of IB by the

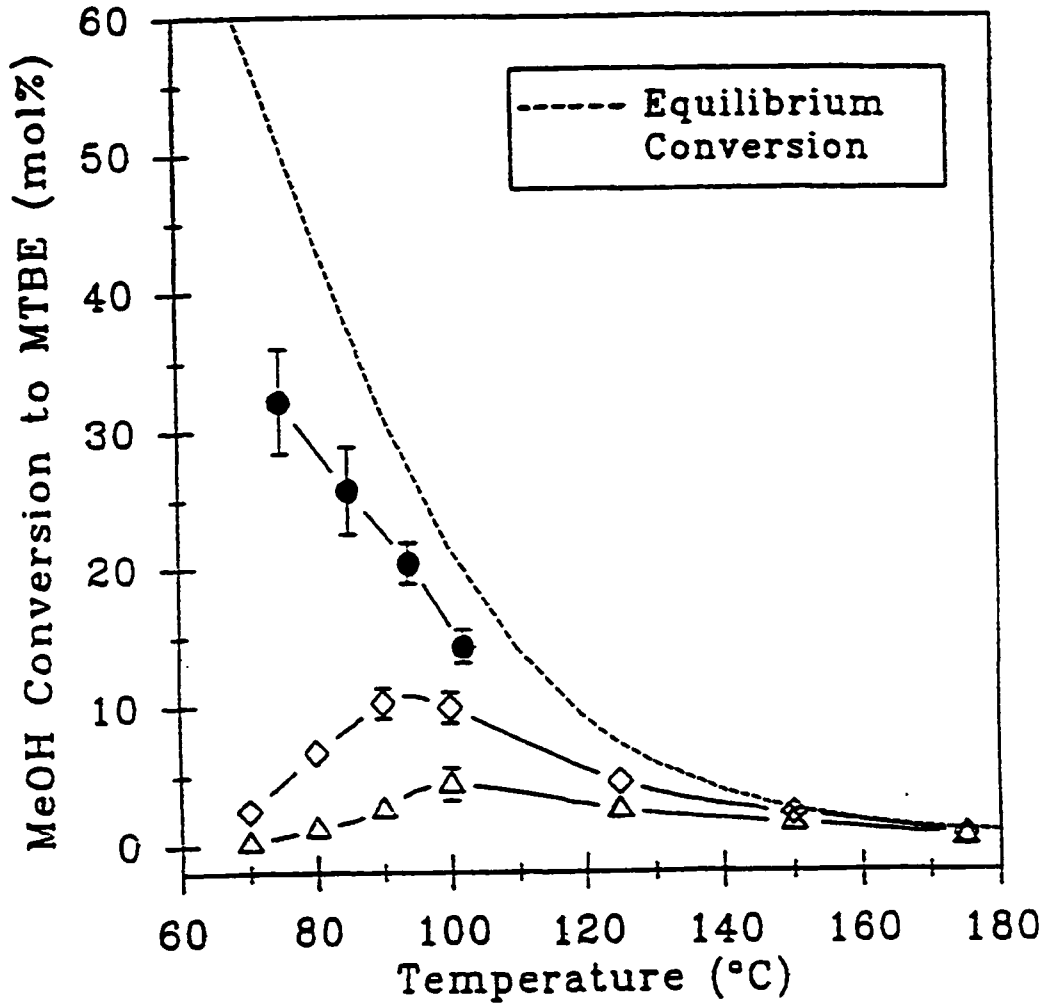

Figure 1.0.b : Effect of temperature on the conversion of methanol to MTBE
MeOH / IB = 0.5, WHSV = 20 hr^{-1}, p(IB) = 27.6 kPa,
(●) Amberlyst – 15, (◇) H-ZSM-5, (Δ) LZ210-12 (Ref. 99.a)

solvated protons, forming a stable tertiary carbenium ion (Figure 1.1). In the next step the carbenium ion reacts with the nucleophilic methanol to form a protonated ether. After deprotonation, the ether molecule so formed diffuses out of the catalyst bed. This mechanism is referred to as specific acid catalysis. In the mechanism proposed for the nonpolar medium where MeOH is not in excess, the active sites of the catalyst is claimed to play a dual role of proton donor (acid) and nucleophilic toward the substrate (22). No proton transfer step like that in the previous case is involved, however instead, the catalyst interacts with the reactants and products exclusively by hydrogen bonding and the reaction is concerted. As described in Figure 1.2, the proposed transition state for this mechanism comprises five participants (three SO_3H groups, MeOH, and IB) in a cyclic arrangement which subsequently dissociates into the reaction products. This mechanism is referred to as general acid catalysis. In industrial process of MTBE production, since a high MeOH to IB moloar ratio (1.24:1) is used, the first mechanism involving a tertiary carbenium prevails.

1.1.2 Technological aspects of MTBE synthesis and literature review

In liquid phase synthesis, the high yield of MTBE production (17) in terms of isobutene conversion (92-93%) is ascribed to the large pore structure in the mesopore range (25-35 nm) of A-15 resin which facilitates the diffusion of reactants and products molecules. However, despite a high activity due to the open

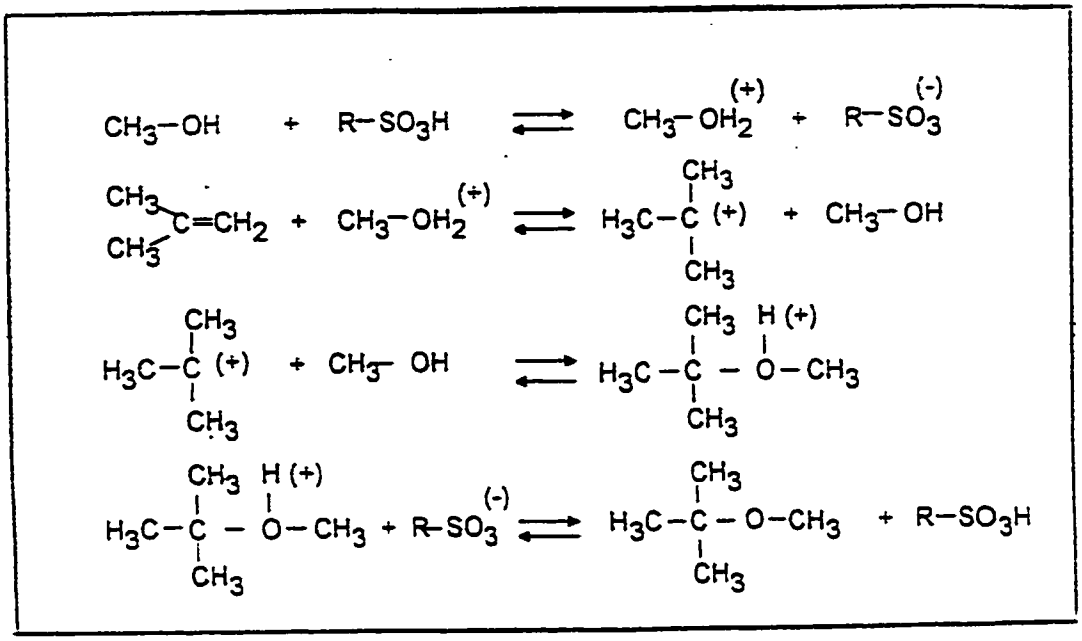

Figure 1.1: Reaction steps in MTBE synthesis (ref. 11)
Specific acid catalysis

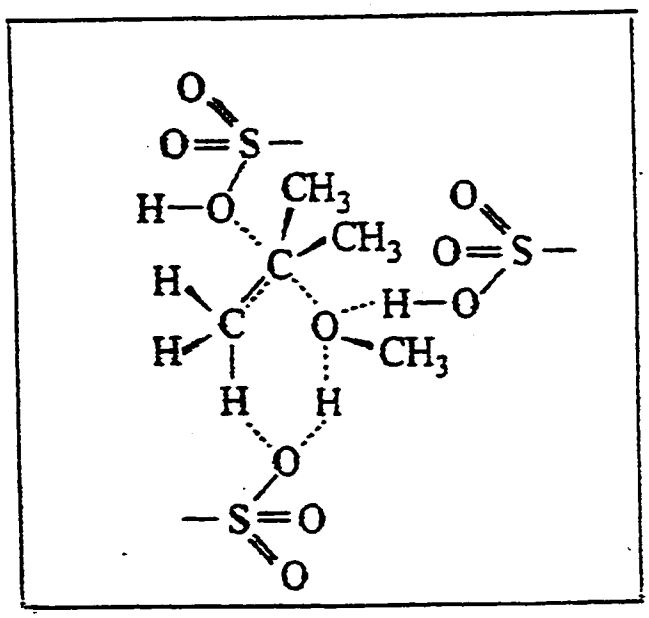

Figure 1.2: Proposed transition state for MTBE formation (ref. 25)
General acid catalysis

structure of A-15, the industrial production of MTBE suffers from several disadvantages, namely the production of undesired by-products, the recycling of unreacted methanol, thermal instability of A-15 resin, acid corrosion and the quite costly medium pressure applied to maintain the reaction medium in liquid phase.

The main side reactions are the dimerization and oligomerization of isobutene (18). The significant amount of diisobutene (8-10 %), by-products of dimerization of isobutene, i.e. the isomers 2,4,4-trimethyl-1-pentene and 2,4,4-trimethyl-2-pentene (19) represents a serious loss of isobutene feed. This reflects a lack of selectivity to MTBE due to the large pore size of A-15 resin (20) which favors the formation of large diisobutene molecules. Oligomer molecules, consisting mainly of tri- and tetramers of IB (21), have an adverse effect of fouling the resin pore structure, thereby decreasing the useful life of A-15 catalyst (17). To minimize unwanted dimerization and oligomerization of IB, refiners have to use an excess of methanol in the feed with a methanol to IB molar ratio up to 2:1. This leads to an additional step of recycling unreacted methanol causing extra costs to MTBE production (14). Other side reactions of less importance are the formation of tert-butanol by reaction of IB with water as feed impurity and the formation of dimethyl ether and water by the condensation of two molecules of methanol. The water produced from methanol condensation constitutes an additional source of impurity which can react with IB to form tert-butanol by-product (21).

The main drawback of the A-15 resin catalyst is its thermal instability even at low temperatures (18). At normal operating temperatures from 60 °C to 70 °C, the leaching of sulfonic acid groups from the resin surface to the reaction medium has been recorded with serious corrosion problems of various portions of the apparatus. In the long term, it is the main cause of deterioration of the resin catalyst (19). In further distillation separation steps consecutive to MTBE synthesis where heating is involved, the amount of effused acid substances released in the reaction medium represents a serious risk of decomposition of MTBE back to methanol and IB since MTBE contains a tertiary carbon atom (20).

In recent years, several studies have been devoted, mainly in our catalysis laboratory, to the gas phase synthesis of MTBE and ETBE over acidic zeolites for its numerous advantages over the liquid phase synthesis (17, 5). Compared to the A-15 resin, zeolite materials present the advantages of higher chemical and thermal stabilities up to 700 °C and a better diffusion of gaseous reactants and products. Acid leaching from the catalyst surface, usually encountered with the A-15 resin, is not observed with zeolite catalysts. The narrower pore structure of zeolite within the micropore range (5.4 - 7.4 Å) contributes to a better shape selectivity to MTBE and ETBE products and thereby prevents the loss of IB feed by dimerization and oligomerization. The latter feature represents a real economic advantage over the liquid phase synthesis with A-15 resin where up to 10 % IB

feed are lost through the conversion to diisobutene and IB oligomer by-products. A lower MeOH to IB molar ratio, equal to unity, is needed which requires much less effort to recycling MeOH if gas phase synthesis of MTBE and ETBE is applied on an industrial scale processes. In the gas phase, the synthesis of MTBE is carried out at much lower pressure (1 atm or slightly higher), below the liquefaction pressure of IB as required in liquid phase synthesis but at a slightly higher temperature (80 °C).

1.2 Zeolites

Zeolites are a class of porous crystalline aluminosilicates based on a rigid three-dimensional framework with well defined cavities and channels of molecular dimensions ranging from 3 to 10 Å in diameter. The general formula for the composition of a zeolite in the hydrated form is :

$$M_{x/n}^{n+} [(AlO_2)_x (SiO_2)_y]^{x-} z H_2O$$

where exchangeable cations M of valence n are used to neutralize the negative charge associated with the framework aluminum ions. Typical cations include alkali metals, e.g. Na^+, K^+, alkaline earth metals, e.g. Ca^{2+}, Ba^{2+}, NH_4^+, and H^+.

The primary building unit of zeolites structures is a tetrahedron composed of a central Si or Al atom (commonly called T-atoms) surrounded by four oxygen atoms, namely $[SiO_4]^{4-}$ or $[AlO_4]^{5-}$. Figure 1.3.a depicts primary units represented by the vertices of the network and connected to each other by straight lines which

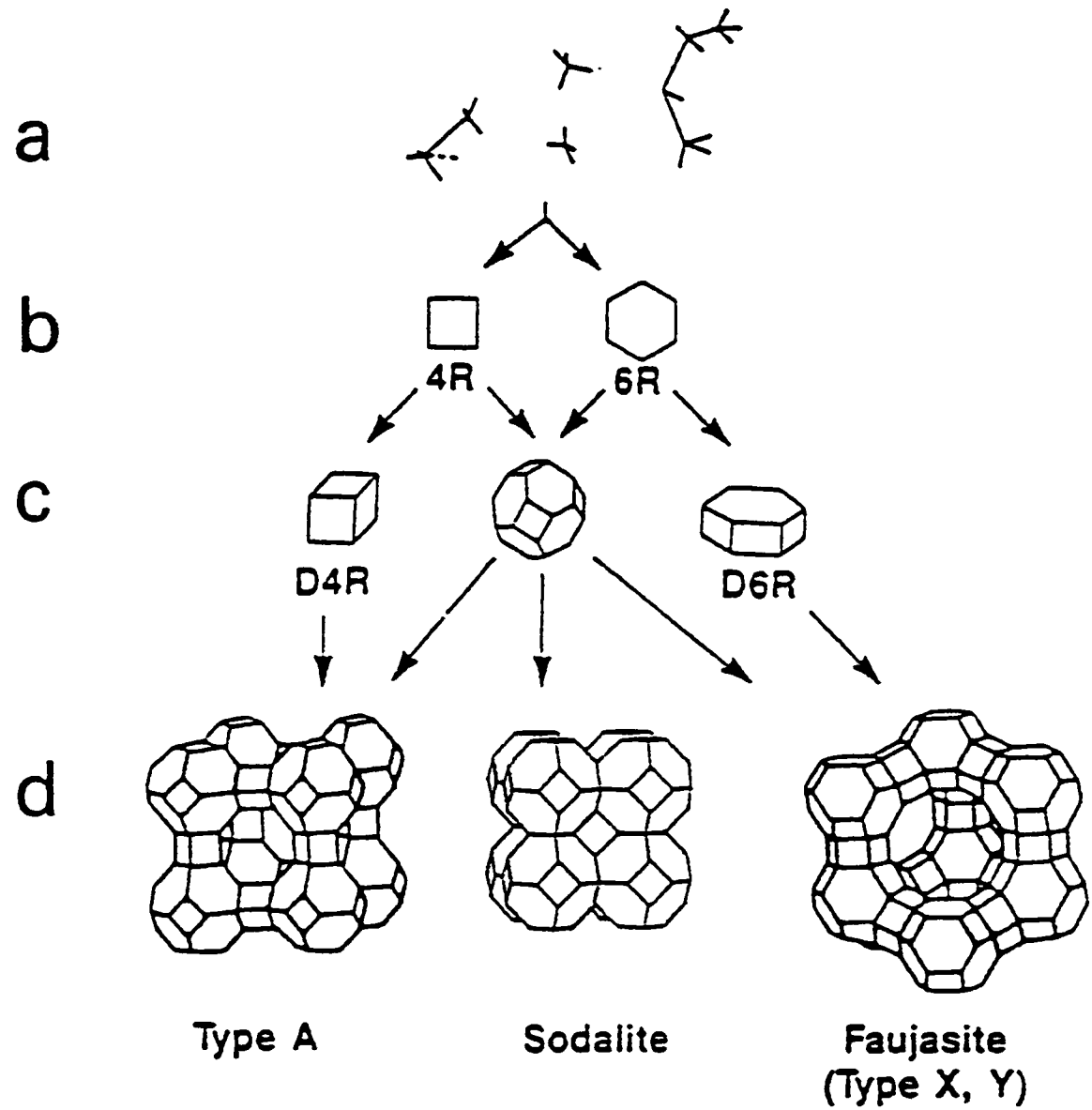

Figure 1.3 : Structural composition of zeolite framework (ref. 32)
a) Primary units b) Secondary units
c) Tertiary units or building polyhedra d) Zeolite structures
(D : double, R : ring)

schematically represent the T-O-T bridges (37). These tetrahedra are joined so that each of the four oxygen anions is shared in turn with another silica or alumina tetrahedron to form a wide range of small secondary building units (SBU), as shown in Figure 1.3.b . These SBU are interconnected to produce a wide range of tertiary building units or building polyhedra (Figure 1.3.c) which in turn are arranged in a three dimensional fashion to form extended characteristic frameworks of the various zeolite crystal structures (Figure 1.3.d). In these structural diagrams the corners of the polyhedra represent Si or Al atoms and the connecting lines the shared oxygen atoms. The combination of tetrahedra containing Si and Al atoms to form the aluminosilicate framework create a negative charge on the Al atoms which is balanced by a non-framework cations M^{n+} to give electrical neutrality.

To date, about 38 naturally occurring zeolites have been identified and synthesized, but in the quest for new catalysts more than 130 synthetic zeolites have been developed with a large variety of framework structures (26, 27). These structures have high thermal and chemical stabilities making them useful materials in a wide range of important industrial processes such as catalysis, separations, purifications and ion exchange.

In general zeolites do not have Si/Al ratios below unity. This implies that each Al atom cannot have another Al atom in its second coordination sphere. This observation was rationalized by Loewenstein (28) in terms of the Al-O-Al

avoidance rule on the distribution of Al atoms within the zeolite structure: such an arrangement of Al atoms involving two adjacent negative charges would create an electrical instability in the zeolite framework and is therefore ruled out. The Si/Al ratio also represents a convenient way for classification of zeolites according to their silica and alumina framework contents. Generally, the higher the silica to alumina ratio, the more thermally stable is the zeolite.

Owing to the existence of a three-dimensional channel network interconnected to cavities or voids, zeolites possess very large internal surface areas as determined from BET nitrogen adsorption technique (29). The external surface area only represents a few percent of the total surface area (30) which ranges from 400 up to 1000 m^2/g as observed for some of the most commonly used zeolites in heterogeneous catalysis:

(a) zeolite A : $\approx$ 600 m^2/g (c) zeolite Y : $\approx$ 750 m^2/g

(b) zeolite X : $\approx$ 650 m^2/g (d) zeolite ZSM-5 : $\approx$ 400 m^2/g

The important structural feature that make zeolites unique is the uniform size of pore apertures which have dimensions approximately equal to those of many molecules converted in catalytic processes as demontrasted in Figure 1.4. Thus, zeolites were named "molecular sieves" by Mc Bain in 1932, since they can discriminate between molecules on the basis of molecular size and shape. Molecules smaller than the aperture size are admitted to penetrate through the pore system while those larger are not.

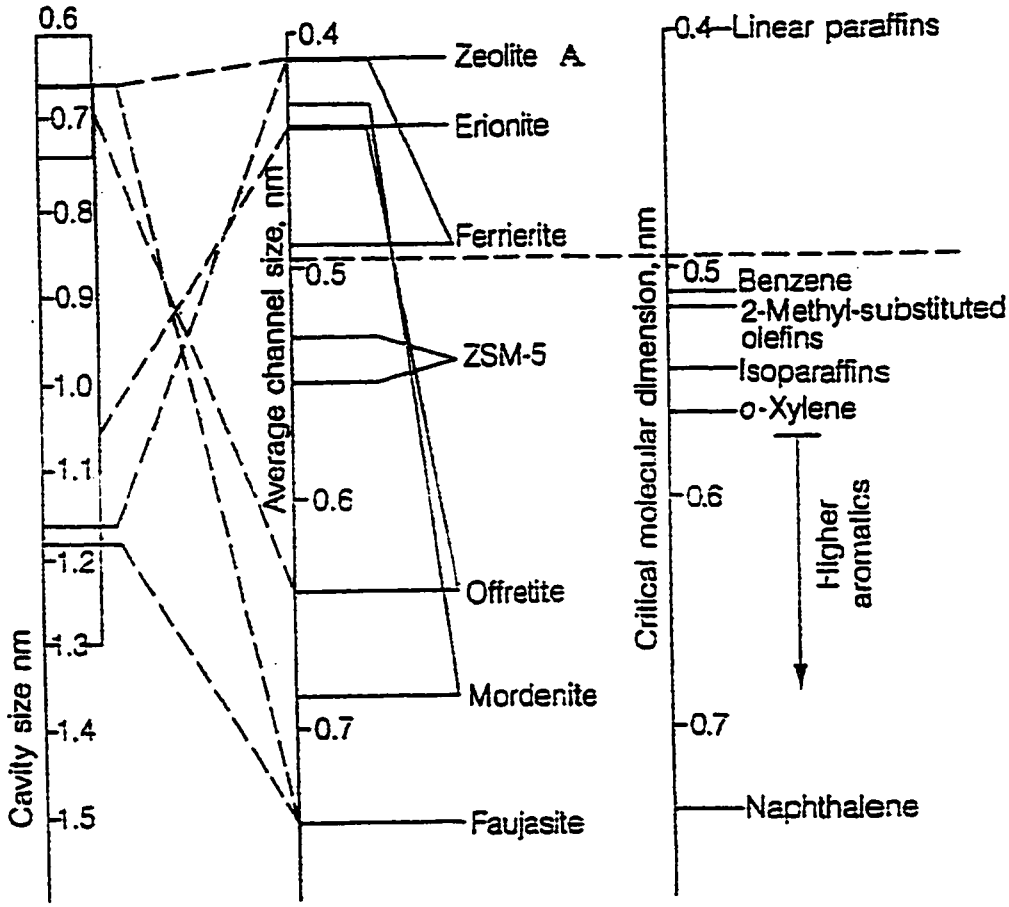

Figure 1.4 : Pore dimensions of zeolites and critical dimensions of some hydrocarbons (ref. 31)

Zeolites are classified according to the size of these apertures. Table 1.1 includes the number of oxygen atoms (8, 10 or 12) in the aperture of each zeolite and the aperture dimension : the smallest being 4.0 Å and the largest being 7.4 Å. The size of the aperture is also dependant on the size of the exchangeable cations. With zeolite A, the effective pore diameter is 3 Å when the cation is K^+, 3.8 Å when it is Na^+ and 4.3 Å when it is Ca^{2+}.

1.2.1 ZSM-5 and Y zeolites.

The novelty of the use of organic cations such as tetrapropyl ammonium as template during zeolite synthesis, lead Mobil Oil scientists to the discovery of the industrially interesting ZSM-5 zeolite. The acronym ZSM-5 stands for Zeolite Socony Mobil – number five in the series of materials produced. This synthetic zeolite belongs to the family of the silica rich pentasil zeolites with Si / Al ratios ranging from 20 up to infinity (33). The corresponding Aluminum free structure is referred to as silicalite.

The ZSM-5 structure is based on the double five ring unit (D5R) as the secondary building block and a characteristic stacking of sequences of layers of 10-membered oxygen rings which forms a network of 3D intersecting channels within the crystal. ZSM-5 exhibits two pore types in the medium diameter range, one sinusoidal channel with pore opening 5.1 Å × 5.5 Å and the other straight channel with pore opening 5.4 Å × 5.6 Å as shown in Figure 1.5. ZSM-5

Zeolite	Number of Oxygens in the Ring	10 × Aperture Dimensions, nm
Chabazite	8	3.6 × 3.7
Erionite	8	3.6 × 5.2
Zeolite A	8	4.1
ZSM-5 (or silicalite)	10	5.1 × 5.5 ; 5.4 × 5.6
ZSM-11	10	5.1 × 5.5
Heulandite	10	4.4 × 7.2
Ferrierite	10	4.3 × 5.5
Faujasite	12	7.4
Zeolite L	12	7.1
	12	7.0
Mordenite	12	6.7 × 7.0
Offretite	12	6.4

Table 1.1 : Zeolites and their pore aperture dimensions (ref. 31)

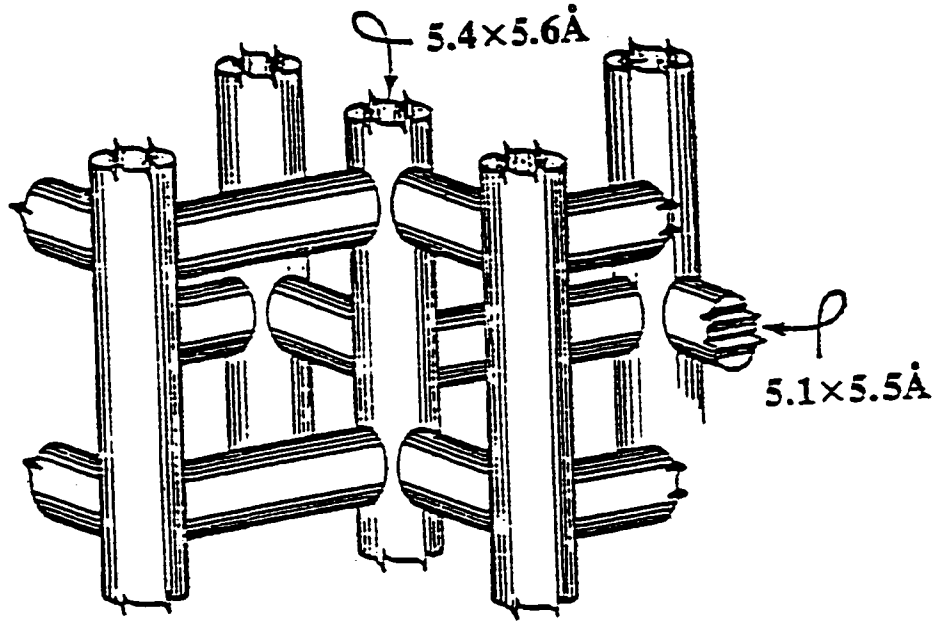

Figure 1.5 Structure of ZSM-5 zeolite. (ref. 60)

crystallizes in the orthorhombic system with space group Pnma and lattice constants a = 20.1 Å, b = 19.9 Å and c = 13 Å. The unit cell contents of the Na form are :

$$Na_n\ Al_n\ Si_{96-n}\ O_{192}\ \sim 16\ H_2O$$

where n < 27 and is typically about 3 .

This new class of synthetic zeolite possesses unusual catalytic properties mainly due to:

(i) a unique dual channel structure in the intermediate diameter range which confers to ZSM-5 a pronounced affinity for linear paraffins and para-substituted aromatics hydrocarbons

(ii) a high thermal stability and hydrophobic character owing to a high silicon content in the framework, and

(iii) a high acid strength (high Si/Al molar ratio) which makes ZSM-5 behave as a superacid capable of cracking paraffins at high temperatures (34).

The synthetic X and Y zeolites and the naturally occurring faujasite zeolite all have the same framework structure which is sketched in Figure 1.6. The unit cell of the faujasite type zeolites containing 192 silica and alumina tetrahedra is cubic with a unit cell dimension of 25 Å. The structural composition of Y zeolite is characterized by a Si/Al molar ratio of about 2.5 whereas for the X zeolite this ratio is about 1.3 . Each sodalite subunit in the structure is connected to four other sodalites by six bridged oxygen atoms connecting the hexagonal faces of two

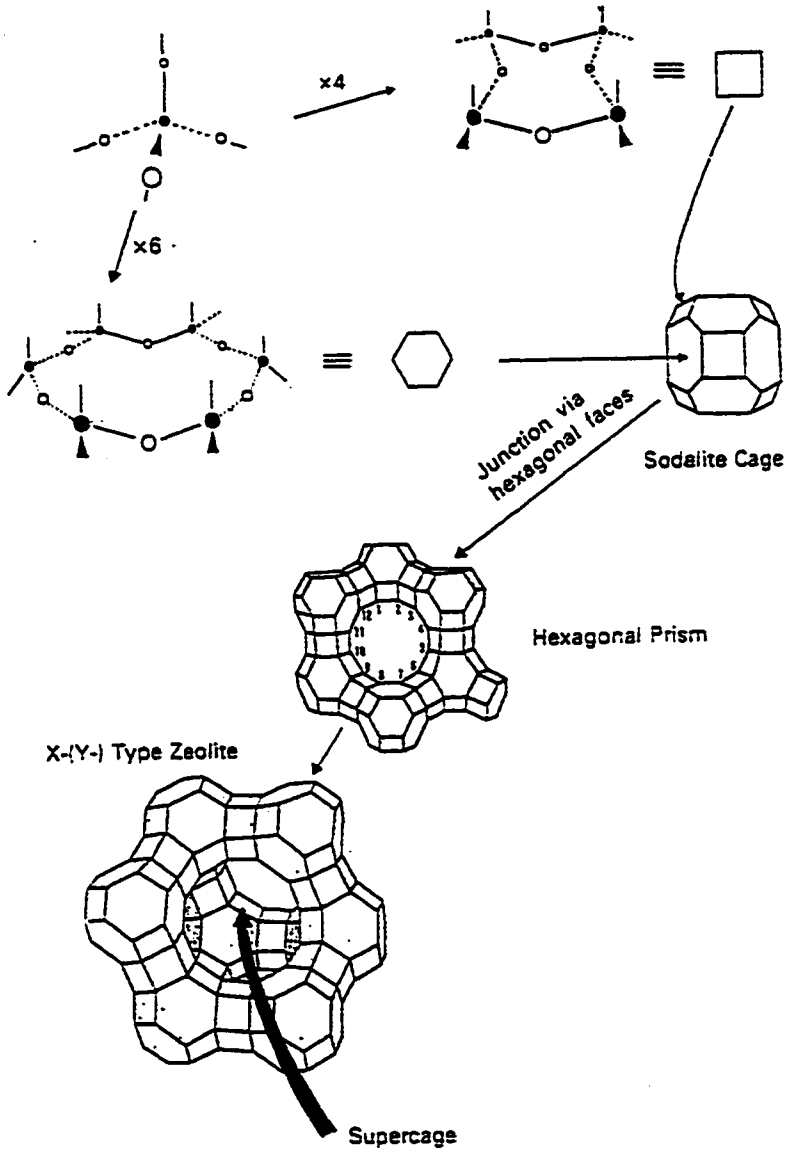

Figure 1.6 Structural composition of Y zeolite (ref. 35)

adjacent sodalites as shown in Figure 1.6 . This structure results in a supercage (or α-cage) surrounded by ten sodalite units which is sufficient large to lodge a sphere with a diameter of 12 Å. The opening to this large cavity is a twelve membered oxygen ring with a diameter of 7.4 Å (35). Each cavity is connected to four other cavities, which in turn are connected to adjacent three-dimensional cavities to form a highly porous framework structure.

Due to their large pore system of 7.4 Å in diameter which can accommodate larger hydrocarbon molecules, faujasite type zeolites have been extensively used in petroleum industry for the catalytic cracking of the gas oil fraction into smaller gasoline-range molecules.

1.2.2 Acidity of zeolites

The reactivity and selectivity of molecular sieve zeolites as catalysts are determined by the surface acidity of active sites. The framework aluminum atoms negatively charged and balanced by extra-framework cations, represent potential active acid sites (46). The acidic properties of zeolites are mainly dependent on the Si / Al molar ratio as well as the temperature of activation.

In zeolites, acid sites are classified according to the classical Brønsted and Lewis acid models. Brønsted acidity corresponds to proton donor acidity, while Lewis acidity corresponds to electron pair acceptor acidity. Brønsted acidity occurs when the cations used to balance the negatively charged framework are

protons (H^+). A trigonally coordinated aluminum atom possessing a vacant orbital that can accept an electron pair, behaves like a Lewis acid site.

In the majority of the as-synthesized commercial zeolites, the cation is sodium Na^+ and the corresponding zeolite is referred to as the sodium form (Figure 1.7.a). To obtain the acid form of zeolites, sodium ions are replaced by protons by ion-exchange with an ammonium salt (Figure 1.7.b), followed by calcination at high temperatures to decompose NH_4^+ ions into H^+ and NH_3 (Figure 1.7.c). After the liberation of ammonia, protons are bonded with surface oxygens to give the bridging form -SiO(H)Al- of Brønsted acid sites. An equilibrium exists between this bridging form and the form in which silanol (–SiOH) group is adjacent to a tricoordinate aluminum that constitutes the Lewis acid site (Figure 1.7.d). A further increase in calcination temperature (> 500°C) of the zeolite results in the dehydroxylation process (33) where Brønsted acid sites are converted to Lewis acid sites (Figure 1.8).

The catalytic activity of zeolites is also determined by : (i) the strength of the acid sites, (ii) their density within the zeolite matrix as well as (iii) their accessibility. The strength of zeolite acidity is characterized by the varying ability at which protons are transferred from different surface acid sites to the adsorbed chemical species. It arises from the non-homogeneous distribution of aluminum atoms within the zeolite structure as indicated by Electron Microprobe Analysis (EPA) and X Ray Photoelectron Spectroscopy (XPS), showing a higher aluminum

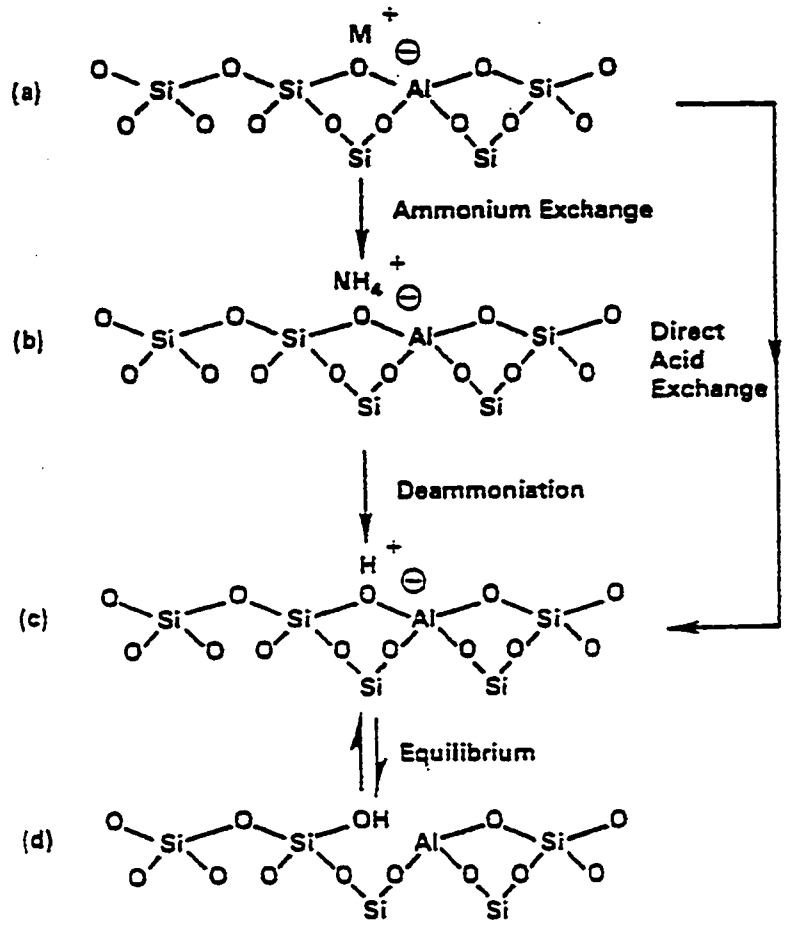

Figure 1.7 : Diagram of a zeolite framework surface (ref. 37)
(a) the as-synthesized form, M^+ is a metal cation (b) the ammonium form (c) the acid form produced by thermal treatment (d) an equilibrium form with the acid form showing a silanol group adjacent to a tricoordinate Aluminum.

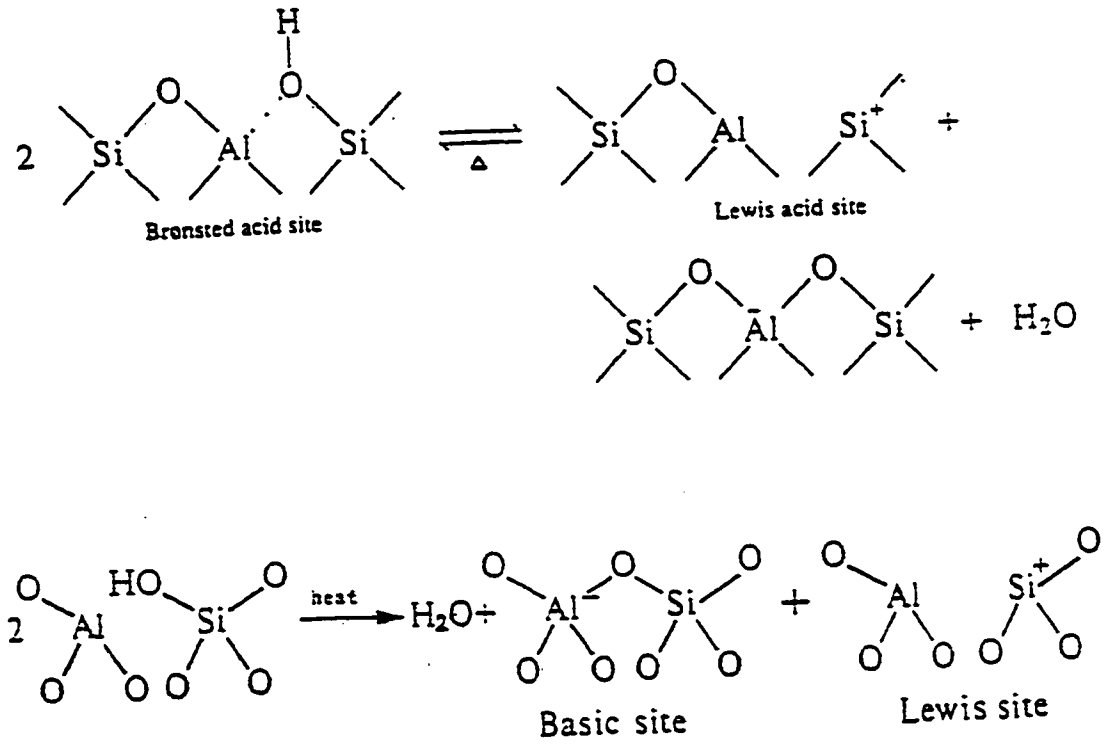

Figure 1.8 : Formation of Lewis acid site from Bronsted acid site (ref. 38)

concentration on the surface compared to the bulk of zeolite crystal mainly for those larger than 5 microns (39,40). The result is a wide range of acidity strengths in zeolite, commonly classified as strong, medium and weak by the characterization technique of ammonia temperature desorption (NH_3-TPD).

As for the density of acid sites, it is directly related to the Si/Al molar ratio, since each aluminum site corresponds to a Brønsted acid sites. In general, the lower the aluminum content of a zeolite or the higher the Si/Al ratio, the stronger the associated Brønsted acidity. The greatest proton donor strength is characteristic of aluminum sites having the smallest number of aluminum neighbors (40).

The non-uniformities of zeolite structure ranging from cracks and defaults which are visible by electron microscopy within the zeolite crystals to located variations in the surroundings of individual silicon and aluminum atoms as detected by ^{29}Si and ^{27}Al MAS-NMR techniques (38), greatly affect the accessibility of adsorbed molecules to the acid sites.

Several characterization techniques have been developed to qualitatively and quantitatively estimate the acid sites and the relation between catalytic behavior of zeolite and their acidity. The most widely used techniques are : ammonia temperature programmed desorption (NH_3-TPD) (42), FTIR spectroscopy (43) and a catalytic test reaction of n-hexane cracking (45).

The temperature programmed desorption of adsorbed NH_3 molecules is used to characterize the amount and strength of Brønsted acid sites. Ammonia is the preferred adsorbing / desorbing gas because of its small size (kinetic diameter: 2.62 Å) and its strong basicity ($pK_b = 4.75$). It can reach practically all the acid sites at a given temperature. Upon desorption at a programmed temperature rise, NH_3 molecules will gradually desorb from the acid sites at various temperatures depending on the strength of the acid sites. The latter aspect is exhibited by the profile of the NH_3 desorption curve. In some cases (46,47), depending on the heating rate one observes three distinct NH_3 desorption peaks, usually identified as weak, medium and strong, for the corresponding acid sites. The higher the desorption temperature, the more strongly adsorbed the NH_3, therefore the stronger the acid strength. The total volume of desorbed NH_3 is related to the total amount of Brønsted acid sites present in the zeolite.

Infrared spectroscopy (IR) has proved to be a valuable tool in characterizing hydroxyl species on the surface of molecular sieves and in measuring Brønsted and Lewis acidity (48). The major objective of the infrared spectroscopic studies in the literature has been an attempt to correlate infrared-induced acid properties with the results of activity measurements from acid catalyzed reactions. IR studies of ZSM-5 zeolite have revealed two hydroxyl stretching bands, one at approximately 3605 cm^{-1} and another at approximately 3720 cm^{-1}. The band at 3605 cm^{-1} has been identified as the hydroxyl stretch

associated with the bridging Al-O(H)-Si (49). The band at 3720 cm^{-1} has been attributed to the terminal silanol SiOH groups on the external crystal surface. Strong bases such as pyridine and ammonia have been widely used as probe molecules in adsorption / desorption studies for the determination of Brønsted and Lewis acidity by IR spectroscopy (42,50). A stretching vibration at ca. 1540 cm^{-1} is attributed to the pyridinium ion, i.e. the Brønsted-bound pyridine, whereas the stretching vibration at ca. 1450 cm^{-1} is attributed to the coordinated pyridine or Lewis bound pyridine. A combination band or overlapping band at ca. 1485 cm^{-1} is due to both Lewis and Brønsted-bound pyridine stretching vibrations (42). As for adsorbed ammonia, Brønsted-bound and Lewis-bound species are characterized respectively by the 1475 cm^{-1} and the 1630 cm^{-1} stretching bands (51).

Mortier (52) proposed an enhanced electron donor–acceptor interaction as shown in Figure 1.9 which emphasizes the reactive aspect of acidity in zeolites. The resonance structure I is a fully bridged oxygen with a weakly bonded proton while the structure II is a silanol with a weak Lewis acid interaction of the hydroxyl oxygen with the Al. The actual situation is a resonance hybrid. The interaction of the unshared electron pair from the silanol oxygen with the vacant orbital of tricoordinated Al weakens the O-H bond and thereby increases its acidity. According to Mortier, there would be a significant stabilization of the bond structure within the whole zeolite matrix resulting from the electronic

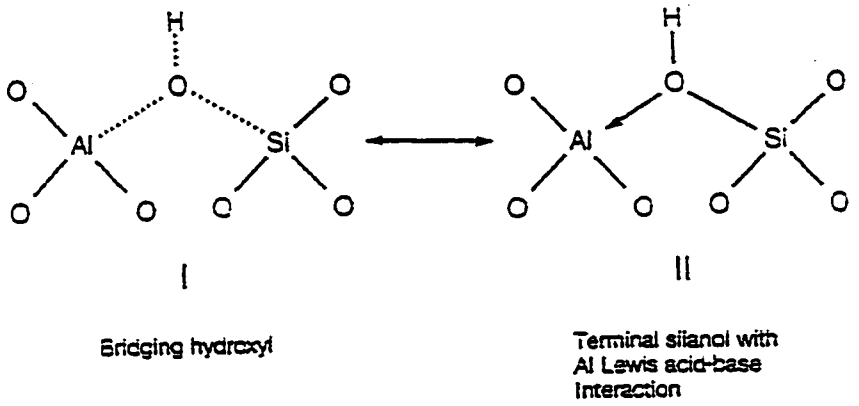

Figure 1.9 : Resonance model of Al-(OH)-Si bond structure (ref. 53)

structure of the Al-O and Si-O bonds becoming more equivalent, which implies a dominance of structure I in the resonance.

1.2.3 Shape selectivity

The highly crystalline structure, a regular channel system and a uniform pore size distribution in the range 4 – 13 Å are among the principal features that zeolites offer over other catalyst materials. The concept of shape selectivity arises from the fact that zeolites are able to recognize, discriminate and selectively adsorb molecules with precisions that can be less than 1 Å (54). The size or diameter of the zeolite pore openings is determined by the number of tetrahedral units or alternatively, oxygen atoms, required to form the pore and the nature of the cations that are present inside or at the mouth of the pore. To date zeolites are commonly classified according to three categories of small, medium and large pore corresponding respectively to 8, 10 and 12 ring openings as shown in Table 1.1. The way in which the channel systems are interconnected in 2D or 3D as well as the existence of connecting supercages within the structure also affect the shape selectivity of zeolites. Tables 1.2 (56) and 1.3 (57) show respectively the types of pore, and aperture of the zeolites and the kinetic diameter of some typical reactants frequently encountered in catalysis.

For instance, in zeolite materials where the pore system is just large enough to admit small monosubstituted paraffins, the rate of diffusion for the isoparaffins

Zeolite	Pore type	Cage size (nm)	Aperture (nm)
H-ZSM-5	Channel		0.54 x 0.56
	Intersection	0.9	0.52 x 0.58
Erionite	Cage	1.3 x 0.63	0.36 x 0.52
Mordenite	Channel		0.67 x 0.70
Faujasite	Intersecting Cavities	1.0 to 1.3	0.74
H-NaX	Supercage	1.0 to 1.3	0.74

Table 1.2 : Dimensions of zeolite channels and apertures (ref. 56)

	Kinetic diameter (Å)
He	2.6
H_2	2.89
O_2	3.46
N_2	3.64
NO	3.17
CO	3.76
CO_2	3.3
H_2O	2.65
NH_3	2.6
CH_4	3.8
C_2H_2	3.3
C_2H_4	3.9
C_3H_8	4.3
n-C_4H_{10}	4.3
Cyclopropane	4.23
i-C_4H_{10}	5.0
SF_6	5.5
Neopentane	6.2
$(C_4F_9)_3N$	10.2
Benzene	5.85
Cyclohexane	6.0

Table 1.3 : Kinetic diameters of various molecules, based on the Lennard - Jones relationship (ref. 57)

is substantially less than the rate of diffusion of n-paraffins (63). Between the small pore ZSM-5 zeolite (5.5 Å) and the larger pore Y zeolite (7.4 Å) the difference of diffusion rate for n-paraffin can amount to several order of magnitude. This significant difference can reverse the order of the reaction selectivity, giving rise to higher reaction rates for the reactant molecules of smaller critical dimension (63).

One can distinguish various types of shape selectivities (59) depending on whether pore size limits the ingress or egress of reactant or product molecules or the formation of certain transition states (see Figure 1.10).

Reactant shape selectivity occurs when only part of the reactant molecules are small enough to pass through the catalyst pores, the remaining reactants being too large to diffuse through (Figure 1.10.a). Since the large majority of the active sites are located inside the pore and channel system, only suitable-sized reactant molecules can diffuse in to react. This situation can be illustrated by the selective hydrogenation reaction over Pt containing Ca-A zeolite where only linear molecules such as propylene and 1-butene can enter the pores to react whereas bulky isobutylene molecules remains nearly nonreactive (55).

Product shape selectivity is observed when some slowly diffusing product molecules cannot rapidly escape from the pore system and have to undergo secondary reactions or when some products molecules are too bulky to diffuse out of the crystal. The latter are either converted to less bulky molecules (e.g., by

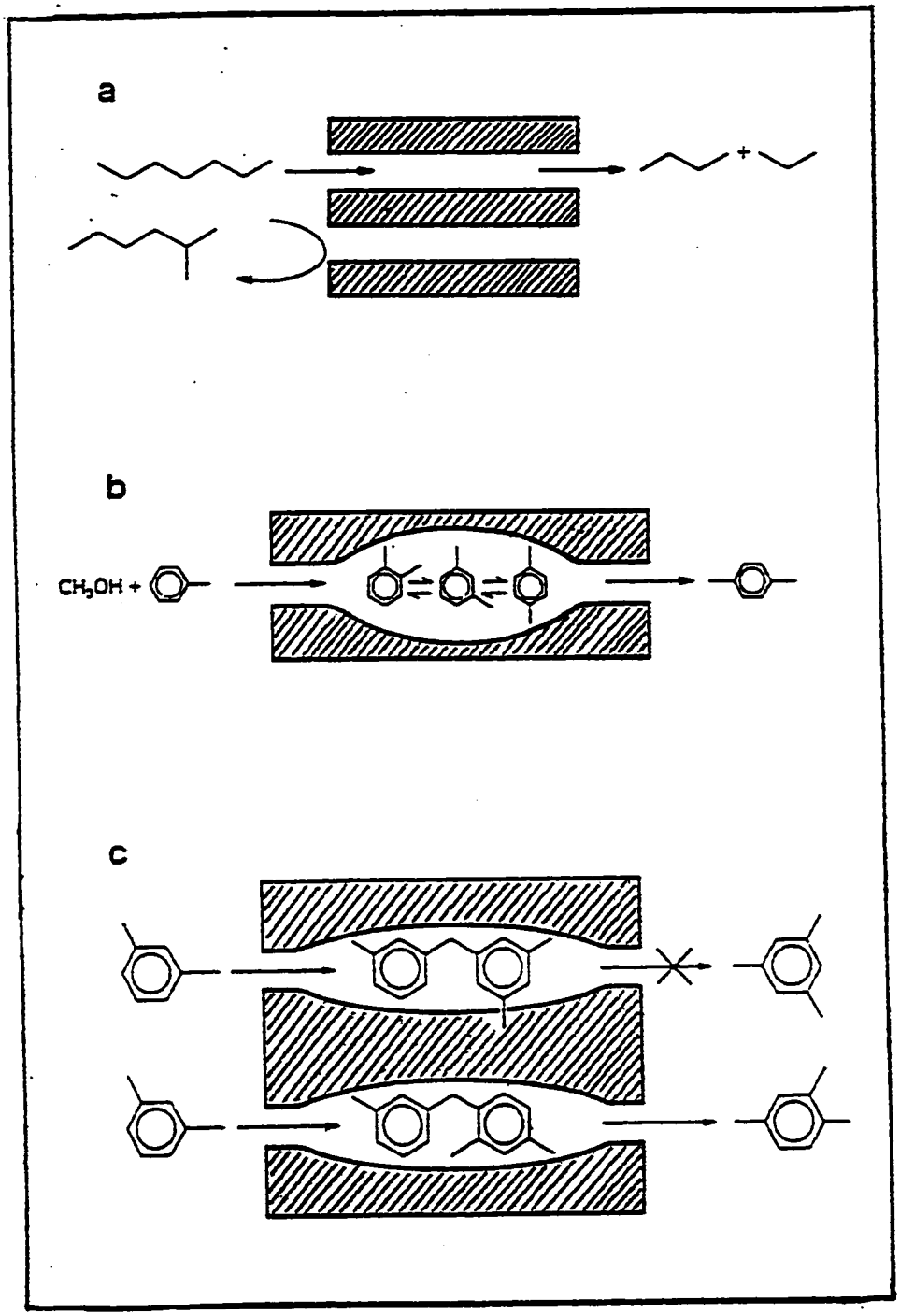

Figure 1.10 Shape selectivity in zeolites (ref. 59)
(a) reactant shape selectivity
(b) product shape selectivity
(c) transition state selectivity

equilibration) or eventually deactivate the catalyst by blocking the pores and channels. For instance in the alkylation of toluene over ZSM-5 zeolite the largely predominant product is p-xylene because of its highest diffusivity and minimal steric hindrance compared to the ortho and para isomers (58) as illustrated in Figure 1.10.b. The diffusion coefficient for p-xylene in ZSM-5 is approximately 103 times faster than that of either ortho or meta xylene (65).

In the third type of shape selectivity, restricted transition-state selectivity occurs when certain reactions are prevented because the corresponding transition state would require more space than available within the channel and cavities. In this case, neither the reactants nor the potential products are prevented from diffusing through the pores, only the formation of the bulky transiton state is hindered. The reactions requiring smaller transition states will proceed unhindered. An example of this case is the acid-catalyzed transalkylation of a dialkylbenzene over mordenite zeolite as shown in Figure 1.10.c (59).

The fourth type of shape selectivity originating from the molecular traffic control may occur in zeolites with more than one type of pore system like ZSM-5 zeolite. The reactant molecules may preferentially enter the crystal structure through one of the pore systems while the products diffuse out by the other as illustrated in Figure 1.11, resulting in the decrease of the counter-diffusion phenomenon.

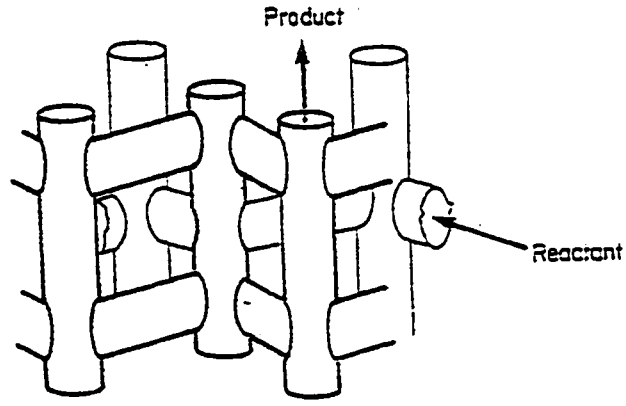

Figure 1.11 : Molecular traffic control in the straight elliptical and zigzag circular channels of ZSM-5 zeolite (ref. 59)

1.2.4 Diffusion in zeolites

The void spaces in the crystalline structure of zeolites provide a high capacity for adsorbates, referred to as guest molecules. Adsorption and diffusion in the pores cannot take place unless the guest molecules are small enough to fit through the apertures. The size of the pore openings that determines the molecular sieving ability of a zeolite depends essentially, for each type of zeolite, on the number of tetrahedral units required to form the pore and also on the nature of the cations that are present in or at the mouth of the pore (62). The diffusion of molecules within the narrow zeolite pores is often slow, since the molecules may barely fit through the apertures and may be roughly described as the hopping of molecules from site to site over significant energy barriers (38).

A qualitative representation of the diffusion process in the pores of solids is shown in Figure 1.12. The effective diffusion coefficient D is shown as a function of the pore size. For large pores, the interactions between the diffusing molecules predominate over those with the walls of the solid, and the transport of molecules through the pores is described by the molecular diffusion of Fick's law. When the pores are smaller, the interactions with the pore walls predominate and the molecules are moved forward by successive collisions with the pore walls instead of being propelled by the succeeding molecules. This type of molecular transport is referred to as Knudsen diffusion. In case of zeolites having very small pore size in the range of molecular dimensions, the diffusion of molecules through the pores

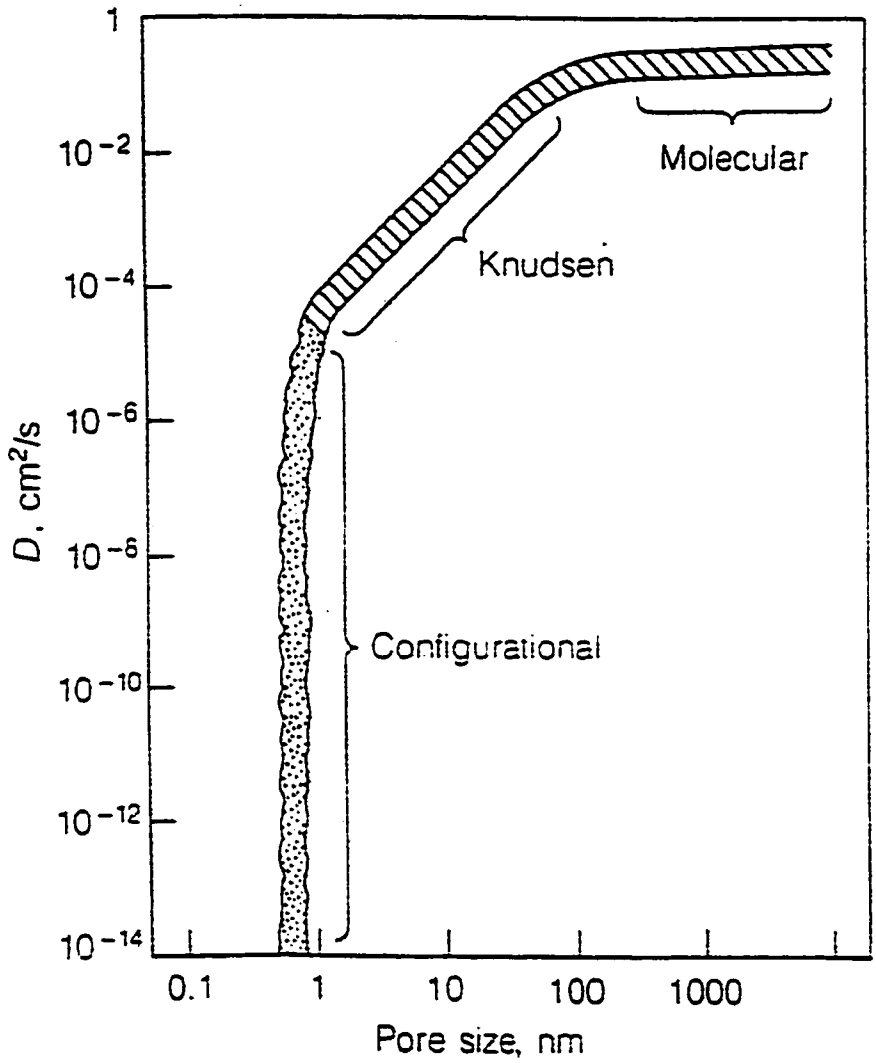

Figure 1.12 Variation of diffusivity of molecules as a function of pore size of various porous solids (ref. 61)

and channels depends strongly on the aperture size since the molecules can barely pass through the pores. This mode of transport is termed configurational diffusion (61).

Almost all of the catalytic active sites are located inside the pores and channels of the zeolite crystals. In a typical catalytic process, the diffusion of reactant molecules to these active sites occurs according to the following steps :

(i) diffusion of reactant molecules from the bulk phase to the crystal interface

(ii) diffusion of reactants through the pore system

(iii) adsorption at the active site

(iv) reaction of the catalyst-reactant complex

(v) desorption of product molecules from the active site

(vi) counter diffusion of products from the pore system to the crystal interface

(vii) transfer of products from the crystal interface to the bulk phase.

Steps 3 to 5 are strictly chemical and consecutive to each other while the transfer steps 1 and 7 are strictly physical and occur separately from the chemical reaction (61). However the transport steps 2 and 6 occurring inside the pore system cannot be separated from the chemical steps 3 to 5 and take place simultaneously with the chemical reaction. Figure 1.13 illustrates the possible different physical and chemical steps starting from a reactant A and ending in a reaction product B via a heterogeneously catalyzed reaction path (64).

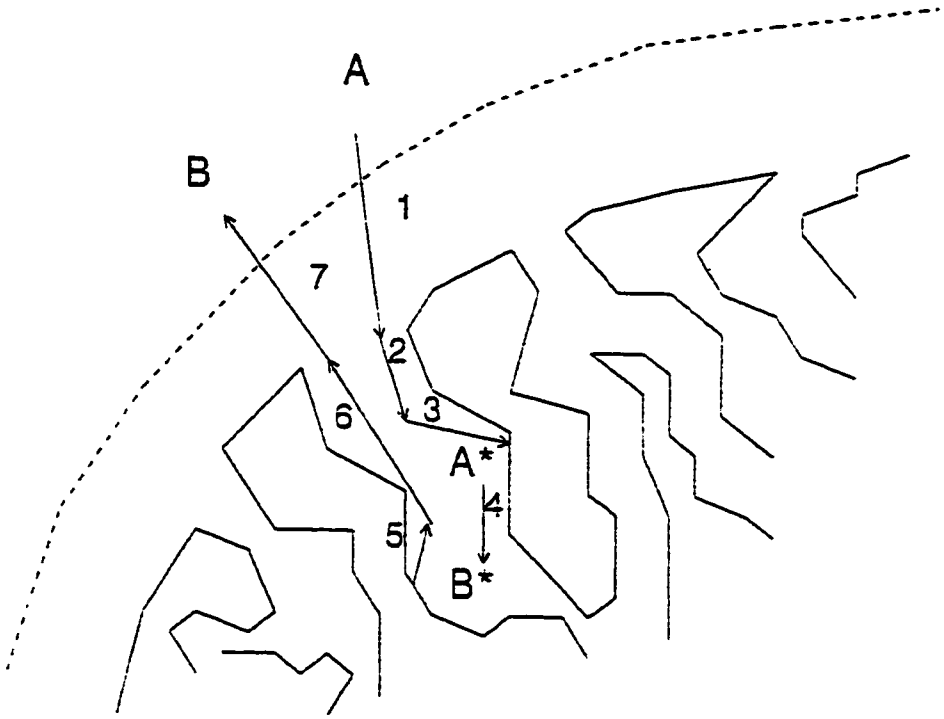

Figure 1.13 Chemical and physical steps involved in the heterogeneously catalysed reaction A → B (* : active site) (ref. 64)

1.2.5 Major industrial applications of zeolites as catalysts

Owing to their unique structural and chemical properties, zeolite materials are finding widespread applications in a diversity of areas, i.e. separations, purifications, adsorption, ion exchange and mainly in catalysis. Although discovered in 1756, the large scale applications of zeolites as catalysts only began in 1959 with Union Carbide using Y zeolite as an isomerization catalyst, and then in 1962 using X zeolite as a cracking catalyst. Early work done by Plank and Rosinski found that the incorporation of a small amount of zeolite in the then-standard silica/alumina catalyst improved significantly the cracking performance of crude oils in the production of petrol (58). Since then for decades, zeolites have found application as catalysts in the oil refining and petrochemical industry, because of their superior activity, stability and selectivity in major conversion and upgrading process as compared to their amorphous equivalents. In oil refining and petrochemical industries, the main catalyzed processes are hydrocarbon cracking, isomerization, hydrocracking, alkylation of aromatics,... These zeolite-catalyzed processes exploit the high acid site density and strength associated with the large internal surface area as well as the uniform pore size system. The major employment of zeolites is as acid cracking catalysts, and zeolites account for over 99% of the world's petrol production from crude oils. An estimate of the world consumption of zeolite materials for this purpose amounts to some 400,000 tons annually, of which 350,000 tons are used for cracking (58). In terms of financial

market size, catalysts represent the largest annual market volume of some 750 billions US$ on a total zeolite market of 1,250 billions US$ (66a). In recent years, research efforts have been put on the increase of the pore size of molecular sieves, aiming at structures with pores greater than 10 Å in diameter in order to meet the present need of selective conversion of the heavier oil molecules or bulky chemical compounds which cannot enter the pores of the currently used zeolites.

1.3 Objectives and thesis presentation

In this chapter, the general background of previous work on the synthesis of MTBE and the main features of zeolite materials related to this work have been reviewed.

Chapter two will deal with the preparation of three different types of acidic catalysts, i.e. the TFA acid loaded Y and ZSM-5 zeolite, the fluorinated ZSM-5 and the fluorinated desilicated ZSM-5, and their characterization with different techniques: AAS, XRD, BET surface measurement, ammonia-TPD, FTIR, methanol adsorption tests, fluorine-SIE, and solid state NMR. Also included in this chapter are the operating conditions, experimental set-up, and the catalytic testing of these catalysts.

In chapter three, a comparison between the activity of TFA-Y and TFA-ZSM-5 will be studied, as well as the interpretation of the two MTBE yield maxima observed for the fluorinated ZSM-5. The two step enhancement of acidity

from the combination of desilication and fluorine treatment will be discussed. A mechanism of the zeolite surface modification as a function of final activation temperatures will be proposed based on the results of catalytic testings and different characterization techniques.

The conclusion will be given in chapter four.

CHAPTER II

EXPERIMENTAL

In this chapter, the experimental methods used in this research work are described. They include the preparation and characterization of the catalysts, and testing the catalytic activity.

2.1 Preparation of catalysts

2.1.1 Source of chemicals

All the chemicals and zeolite materials used in the preparation and characterization of catalysts were purchased from several suppliers listed as follows :

Chemicals	*Purity*	*Suppliers*
Ammonium chloride	(99.5 %)	Fisher Scientific Co.
Ammonium fluoride	(98.5 %)	Aldrich Chemical Co.
Bentonite USP grade	(99.5 %)	Anachemia
Isobutene CP grade	(99.9 %)	Linde
Methanol	(99.8 %)	Fisher Scientific Co.
NH_4-Y zeolite	–	Linde
Nitrogen HP grade	(99.9 %)	Air Product
Na-ZSM-5 zeolite (Zeocat PZ 2/30)	–	Chemie Uetikon
Potassium bromide	(99+ %)	Aldrich Chemical Co.
Pyridine	(99+ %)	Aldrich Chemical Co.

Sodium carbonate	(99.5 %)	Fisher Scientific Co.
Trifluoromethanesulfonic acid	(99 %)	Fluka Chemie A

2.1.2 HY and HZSM-5 zeolites

The acid form of the Y zeolite was obtained by activating the LZY-82 sample (the ammonium form of Y-type zeolite in powder supplied by Linde) in air at 550 °C for overnight.

The acid form of ZSM-5 zeolite referred to as HZSM-5, were prepared by repeated ion exchange of the commercially available sodium form ZSM-5 (Na-ZSM-5) according to the following procedure. The Na-ZSM-5 was brought into contact with an aqueous solution of 10 wt. % ammonium chloride, using 1 gram of zeolite per 10 ml of solution. The ion exchange operation was performed at 80 °C for 1 hour, after which the used solution was decanted and a new fresh NH_4Cl solution was added. This treatment was repeated 5 times, after which the solid was washed on the filter several times with distilled water and dried at 120 °C. The acid form of ZSM-5 was finally generated by activation at 450 °C in air overnight.

The final zeolite catalysts were prepared according to the following procedure: the powdered acid form of the parent zeolite was intimately mixed with 10 wt. % bentonite used as binder and the mixture was then made into a malleable paste with distilled water (about 1 ml of water was added for each gram of zeolite). It is worth mentioning that the bentonite clay used here (supplied from

Anachemia, USP Lab-grade) was the purest material found in the market, having the following chemical composition in wt. % of dried form : silica = 64-71, aluminum oxide = 20-23, magnesium oxide = ca. 4, Fe oxide = 4-5, sodium and potassium oxide = 3-4, calcium and titanium oxide all less than 1 %. The final extrudates in the cylindrical form of 0.3 cm in length and 1 mm in diameter were dried at 120 °C for 12 hours and activated in air at 450 °C overnight. The acid form of HY and HZSM-5 extrudates are hereafter called "parent zeolites".

2.1.3 Trifluoromethane sulfonic acid modified Y and ZSM-5 zeolites

The trifluoromethane sulfonic (or triflic acid, TFA) acid loading (3 wt. %) was done according to the following procedure. About 0.3 g of TFA (CF_3SO_3H, 99 % from Fluka Chemie AG) were dissolved in 15 ml of pure acetone. This solution was then added slowly to 10 g of Y or ZSM-5 zeolite powder in the acid form contained in a beaker. The resulting suspension was stirred gently then was allowed to settle in the beaker, covered with a watch glass and allowed to dry in air at room temperature. The solid obtained was washed quickly with 5 ml of acetone and then heated at 120 °C in air for 12 hours. The final extrudate catalysts were prepared by admixing with 10 wt. % bentonite binder according to the procedure previously described in section 2.1.2 and are referred to as "TFA/Y" and "TFA/ZSM-5" catalysts.

2.1.4 Fluorine loaded ZSM-5 zeolites

The fluorine loading into the HSM-5 zeolite was carried out according to the incipient wetness technique (102, 125). According to this technique, only a minimum volume of the adsorbate solution, i.e. the ammonium fluoride solution, is added to the porous zeolite material in order to fill in exclusively its pore and channel system (66.b). Upon subsequent drying, the adsorbate materials (NH_4F ions) incorporated precipitate inside the pore and channel network rather than on the outer surface of the zeolite crystals. In the particular case, this method was applied as follows : 10 g of HZSM-5 zeolite extrudates were impregnated with a minimum volume (17 ml) of an aqueous solution of ammonium fluoride by means of a medicine dropper. The ammonium fluoride solution was carefully added dropwise directly onto the zeolite extrudates so as to prevent the solution from spilling on the walls or bottom of the glass container. The concentration of fluoride ions of such solutions varied from 0.05×10^{-3} to 3.10×10^{-3} mol g^{-1}, i.e. from 0.095 to 5.89 wt. % of fluoride. The wet extrudates were allowed to dry at room temperature overnight, then dried at 120 °C in air overnight. The F^- loaded catalyst extrudates were activated stepwise in air at 250 °C for 5 hours then at a temperature T_f for other 4 hours, T_f being the temperature of final activation ranging from 300 °C to 500 °C.

2.1.5 Fluorinated - desilicated ZSM-5 zeolites

(i) The desilicated Na-DZSM5 was obtained by treating the Na-ZSM5 (Zeocat PZ 2/30, sodium form, powder, Chemie Uetikon, Switzerland) with an aqueous solution of 0.8 M sodium carbonate containing 0.01 M sodium hydroxide, 1 g of zeolite being treated by 20 ml of solution. The mixture was heated at 80 °C under mild stirring for 4 hours. The mixture was allowed to settle, then the liquid supernatant was rapidly removed. A fresh solution of Na_2CO_3 / NaOH (0.8 M / 0.01 M) was added, and the suspension was again very gently stirred at 80 °C for a further 4 hours. This procedure was repeated a third time so that the entire operation lasted 12 hours. The suspension was filtered and the solid washed on the filter with distilled water several times. The product was dried in an oven at 120 °C overnight. A weight loss of 6.2 % was generally observed after the desilication step with the following chemical composition characteristics : Si/Al = 18.0 and Na/Al = 3.9. It was shown that the addition of sodium hydroxide to the sodium carbonate solution is designed to adjust the initial pH of the suspension for a more efficient desilication process (67).

The desilicated solid product obtained was then thoroughly washed according to the following procedure : the suspension resulting from the addition of 30 ml of water to 1 g of the solid product was heated under very mild stirring at 80 °C for 4 hours, then was allowed to settle. The liquid supernatant was removed rapidly after. A fresh volume of water was added, and the suspension was mildly

stirred at 80 °C again for a further period of 4 hours. This procedure was repeated twice. The desilicated Na-DZSM5 zeolite was then washed on the filter and dried in an oven at 120 °C overnight. For this step, the weight loss was about 23.7 % with the the chemical composition of Si/Al = 14.1 and Na/Al = 1.0 (68).

In previous work, it was shown that such a drastic washing procedure was necessary to remove most of the soluble Si-containing species formed during desilication, which were still trapped in the "corroded" pore network of the zeolite (69).

(ii) The preparation of the acid form of the parent ZSM-5 zeolite and the desilicated Na-DZSM5 zeolite by repeated ion exchange with NH_4Cl, as well as the preparation of the corresponding final extrudate catalysts by admixing with 10 wt. % bentonite binder were done according to the procedures previously described in section 2.1.2.

(iii) The fluorine loading into the H-ZSM5 and H-DZSM5 extrudates was carried out according to the incipient wetness technique described in section 2.1.4 for a F^- loading content of 1.87×10^{-3} mol g^{-1} (i.e. 3.55 wt. %) and the final extrudate catalysts were activated stepwise in air at 250 °C for 5 hours and then at 450 °C for 4 hours. The final catalysts are hereafter referred to as H-ZSM5/F3 and H-DZSM5/F3 respectively.

(iv) The Amberlyst 15, purchased from Aldrich, was used as reference catalyst in this work without any further treatment.

2.2 Characterization of catalysts

The physical and chemical properties of the final extrudate catalysts are characterized by the following techniques :

- Atomic absorption spectrometry (AA)
- X-ray powder diffraction (XRD)
- Determination of the BET surface area and pore size distribution
- Ammonia temperature programmed desorption (NH_3-TPD)
- Fourier transform Infrared spectroscopy (FTIR)
- Methanol adsorption tests
- Selective ions electrodes techniques
- Solid state NMR

2.2.1 Atomic absorption spectrometry

Atomic absorption spectrometry was used to determine the concentration of the heavier elements of zeolite materials, i.e. : Si, Al, and Na. A zeolite sample of approximately 1.2 g was weighed, calcined at 800 °C for one hour in a platinum cruicible, then it was reweighed to obtain the dry weight of the sample. 0.9 g of a fusion mixture (consisting of potassium carbonate and lithium tetraborate in a 2:1 ratio) was added to the calcined zeolite sample, thoroughly mixed and heated for another one hour. The resulting solid was dissolved in a strong mineral acid solution of 4 ml of concentrated HCl and 10 ml of 10 vol.% H_2SO_4 . The resulting

slurry was transferred to a beaker covered with a watch glass then gently heated until a clear solution was obtained. A volume of 5 ml hydrogen peroxide (30 %) was then added, and the solution was heated until effervescence has stopped. The solution was then diluted to 100 ml in a volumetric flask and subsequent dilute solutions were prepared for atomic absorption analysis with a Perkin Elmer Model 503 instrument. The content in metal oxides were computed by referring to external standards of the corresponding metals. From the atomic absorption spectrometric results, the silicon to aluminum ratio of different zeolite materials were obtained.

2.2.2 X-ray powder diffraction

Zeolites materials, being crystalline solids, have a characteristic diffraction pattern that can be used to identify their particular structure and to determine their degree of crystallinity. The diffraction of X-rays from zeolite crystallites produces a scattering pattern which is specific of the periodic arrangement of regular arrays of atoms (or ions) located within the zeolite structure. The peak position is governed by the Bragg equation :

$$n\lambda = 2d\sin\theta$$

where n is the order of diffraction (integer number), λ the wavelength of the incident X-ray beam, d the distance between two adjacent planes in the family of

plane in diffracting position, and θ the scattering angle being equal to the incident angle.

A sample of zeolite powder (0.6 g) was finely ground and pressed in a plexiglas sample holder. The X-ray powder diffraction pattern was recorded on the Phillips PW 1050/25 diffractometer operating at 40 kV and 20 mA, which was automated with the SIE Ray 112 system from Sietronics. The data were collected at an angular velocity of 1° (2θ) / min with a step size of 0.05° (2θ), using the Kα radiation of copper (λ = 1.54178 Å). The observed diffraction pattern was then compared with the reference pattern of the parent ZSM-5 zeolite, to verify that the structure of the zeolite sample has not changed upon treatment. The determination of the "relative crystallinity" (RC %) or "degree of crystallinity" was based on the intensity of the characteristic peaks in the 2θ range from 22.5 ° to 25 ° (2θ) in accordance with the method of Kulkarni et al. (70). The relative crystallinity, calculated after background correction, was taken as the sum of the peak area of the zeolite sample divided by the sum of the peak area of the parent zeolite material that is taken as reference for 100 % crystallinity. The degree of crystallinity was calculated using the following formula (86) :

$$RC\ \% = \frac{\text{Peak area of zeolite sample between } 2\theta = 22.5\,^\circ - 25\,^\circ}{\text{Peak area of reference sample between } 2\theta = 22.5\,^\circ - 25^\circ}$$

2.2.3 Measurement of the BET surface area

The most important method of determining the total surface area of a solid material is the BET method developed by Brunauer, Emmett and Teller in 1938 (71). In this method, the monolayer and multilayer adsorption model allow to determine the total surface area of porous materials and their pore structure characteristics such as the pore size distribution, the average pore size and the total pore volume. These parameters are very important in studying the relationship between the morphology and pore structure of zeolites with their catalytic activity.

The principle involved in the determination of the total surface area is based on the monolayer adsorption of gaseous adsorbate molecules (usually nitrogen) onto the zeolite surface, occurring at very low pressures. From the volume of adsorbate corresponding to a monolayer coverage and the area occupied by each molecule on the surface, the total surface area of porous materials can be calculated.

The basic assumptions of the BET model are as follows (72) :

1. A fixed number of adsorption sites.
2. The second and subsequent layers are adsorbed directly on the first layer.
3. There are no lateral interactions between neighboring molecules adsorbed within a layer.
4. There is a constant heat of adsorption within each layer
5. The heat of adsorption in the first layer is E_A ; for all other layers, the heat

of adsorption is equal to the heat of liquefaction E_L .

6. There is an infinite adsorption at the saturation conditions of the adsorbate.

7. There is an equilibrium between the adsorbed species and the gas phase.

The BET physisorption model is described in Figure 2.0. The physical and mathematical treatment of these hypotheses lead to the formulation of the well known BET equation:

$$\frac{P}{V(P_o - P)} = \frac{1}{V_m C} \times \frac{(C-1)}{V_m C}\frac{P}{P_o} \qquad (2.0)$$

where V = volume of N_2 gas physisorbed at pressure P

V_m = volume of N_2 gas physisorbed in a monolayer cover

P = pressure of N_2 gas in equilibrium with the surface

P_o = saturation pressure of N_2 gas at liquid N_2 temperature (77 K)

C = a constant characteristic of the adsorbent – adsorbate interaction. The constant C is related exponentially to the heats of adsorption E_A and liquefaction E_L of the adsorbate gas : $C = \exp (E_A - E_L) / RT$ (2.1)

where : R = ideal gas constant and T = absolute temperature (K)

At very low partial pressures approximately between 0.05 and 0.35, the graph of $P / V(P_o - P)$ versus P / P_o shows a straight line from which the value of V_m can be evaluated :

$V_m = 1 / (\text{slope} + \text{intercept})$

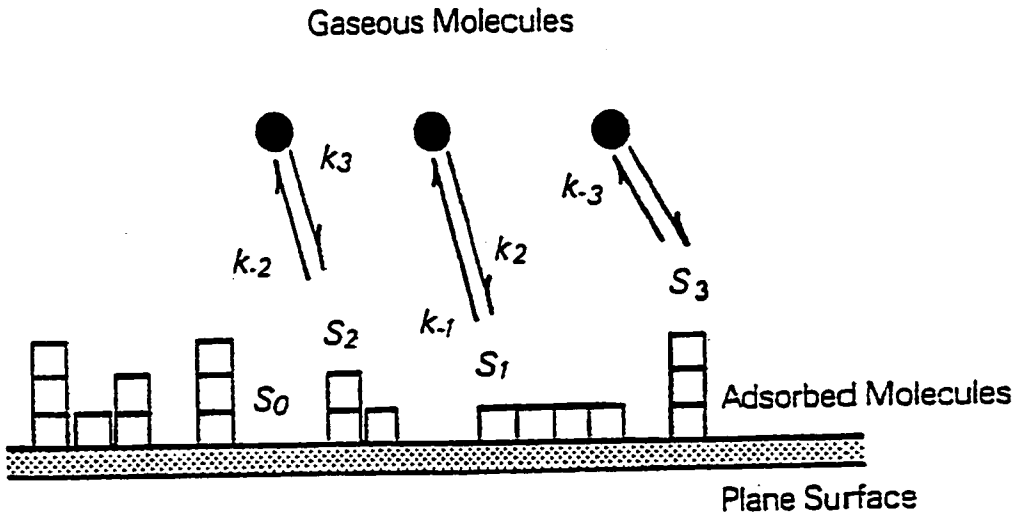

S_0 Fraction of Surface Not Covered
S_1 Fraction of Surface Covered With One Molecule
S_2 Fraction of Surface Covered With Two Molecules
S_3 Fraction of Surface Covered With Three Molecules

Figure 2.0 : BET physisorption model (ref. 72)

The total surface area of the porous catalyst can be calculated from V_m according to the following equation (73) :

$$S_{BET}\ (m^2/g) = a_m \ . N_A V_m / \gamma_m$$

where : N_A = Avogadro's number

a_m = area occupied by a N_2 adsorbate molecule ($16.2 \times 10^{-20}\ m^2$)

V_m = volume of N_2 gas physisorbed in a monolayer coverage (m^3/g of zeolite material)

and γ_m = molar volume of the N_2 adsorbate ($22.4 \times 10^{-3}\ m^3\ mole^{-1}$).

The zeolite sample was first outgassed at 220°C overnight under high vacuum condition (10^{-3} mmHg) before the nitrogen adsorption-desorption isotherm was recorded at the temperature of liquid nitrogen, 77 K, by the Micromeritics ASAP 2000 instrument. The BET surface area, the BJH pore size distribution (75) and the average pore diameter were obtained from these isotherms.

2.2.4 Ammonia adsorption and temperature programmed desorption

The ammonia adsorption and temperature programmed desorption (NH_3-TPD) method was used to study the total surface acidity and the acid strength distribution of the acidic zeolite catalysts (76,77). The following assumptions are made regarding the adsorption and desorption of ammonia molecules (78) : (i) the intracrystalline zeolite surface is homogeneous and the amount of ammonia

adsorbed in the experiment is less than that required for a monolayer coverage, (ii) no readsorption of ammonia takes place during the desorption stage, and (iii) there is no lateral interactions between the neighboring adsorbed ammonia molecules.

2.2.4.1 TPD profile : the distribution of strength of acid sites

The NH_3-TPD experiments were performed according to the technique described by R. Le Van Mao et al. (79) using the set-up of Figure 2.1. The temperature of the furnace was monitored by a multi-program controller. In a typical run, the final zeolite extrudates (1.0 gram) were dried at 120 °C overnight then activated at 300 °C for 3 hours under pre-dry helium flow of 20 ml/min and cooled down to 100 °C. In order to prevent the physisorption phenomenon, the adsorption of ammonia took place at 100 °C with pre-dried ammonia (over 4A zeolite beads) flowing at 20 ml/min during 45 minutes. The catalyst being saturated with ammonia was then flushed with helium flow of 20 ml/min at 100 °C for 3 hours in order to remove any physisorbed ammonia molecules on the zeolite surface or within the reactor system. The desorption of ammonia was carried out gradually by heating the catalyst from 100 °C to 630 °C in a flow of helium at 20 ml/min and according to a linear heating program at a rate of 13 °C /min. The desorbed ammonia was measured by a thermal conductivity detector set at 150 °C and recorded by an HP 3392A integrator which was interfaced to a gas chromatograph HP 5890. The NH_3-TPD profile obtained qualitatively showed the

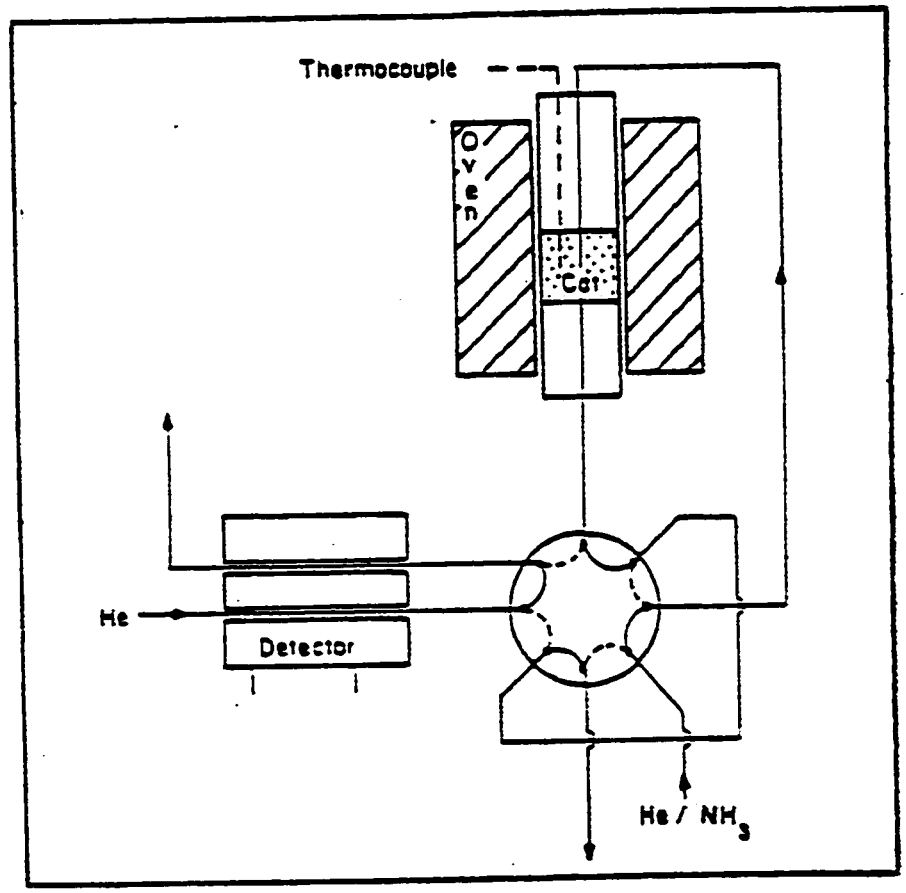

Figure 2.1 : Ammonia temperature programmed desorption experimental set-up

amount of ammonia desorbed at increasing temperature intervals which corresponds to the distribution of acid strengths of the total surface acidity. As a general rule, the higher the desorption temperature of ammonia which resulted from a strong binding energy, the stronger the corresponding acid sites.

Since the ammonia desorption phase was achieved according to a linear temperature program, it is difficult to evaluate the acid strength distribution because of the overlap of different desorbed ammonia peaks. Therefore, in order to estimate semi-quantitaively the acid strength distribution from the ammonia TPD profile, the raw desorption curve was deconvoluted into distinct peaks represented by the dashed lines. According to previous works on the characterization of zeolite acidity (94.b), the acid strength of ZSM-5 can be classified in four levels : weak, medium, strong and very strong. The corresponding temperature ranges for the desorption peaks are 250 – 400°C, 400 – 500°C, 500 – 600°C and 600 – 650°C. Based on this classification, the deconvolution technique was done manually on the raw ammonia TPD profile such that at each desorption temperature, the sum of heights of each deconvoluted peak is equal to the height of the total desorption curve. The sum of the area of all deconvoluted peaks are then assumed to be equal to 100 %.

2.2.4.2 Determination of the acid site density

The measurement of the acid density was carried out with the same ammonia TPD set-up. Great care was taken in order to minimize the physisorbed

NH_3 by a vigorous flushing of the catalyst with nitrogen (20 ml/min) at 100 °C for 3 hours prior to the desorption phase. During the NH_3 desorption operation, the nitrogen stream that carried the desorbed ammonia was bubbled into an excess of a dilute solution of 0.02 N HCl. After the desorption step, the excess HCl was back-titrated with a 0.05 N NaOH solution in accordance with literature (80). From the original HCl concentration, the total amount of adsorbed ammonia corresponding to the number of zeolite acid sites was calculated.

2.2.5 Fourier transform Infrared spectroscopy

Fourier transform infrared spectra were recorded on the Nicolet Magna IR spectrometer model 500, in the 400 – 4000 cm^{-1} range with a resolution of 1 cm^{-1}, using the transmission mode. The samples were prepared as pellets of zeolite /KBr (1:50) mixture of ca. 20 mg. The nature of the surface acid sites was investigated by chemical adsorption of pyridine on the clean zeolite surface according to the following procedure. The zeolite wafers held by an O-ring, were first outgassed under vacuum (10^{-2} mmHg) at 180 °C for 4 hours for the removal of any traces of moisture. They were then exposed to pyridine vapor at 150 °C for 3 hours to allow the chemisorption of pyridine molecules onto zeolite acid sites and then to a desorption step under vacuum (10^{-2} mmHg) for 1 hour at 80 °C for the removal of any physically adsorbed pyridine. The pyridine chemisorbed zeolite wafers were

thus kept in a glass vacuum chamber until FT-IR analysis was performed at room temperature.

The characteristic absorption bands at 1547, 1446 and 1491 cm^{-1} were assigned to the pyridine adsorbed on the Brønsted acid sites (B), the Lewis acid sites (L) and on both acid sites (B,L) respectively (81). However, no data on the OH groups in the conventional range (3400 – 3800 cm^{-1}) will be reported because the drastic treatments (high vacuum and high temperature in a special "catalytic chamber" for FTIR instrument) required for obtaining absolutely cleaned zeolite surfaces (from water molecules), would significantly disturb the F species which were simply chemisorbed in some treated zeolite samples.

2.2.6 Methanol adsorption tests

Methanol adsorption tests were used to determine the adsorption properties of the modified ZSM-5 zeolite surface with regard to methanol being the main reactant of the MTBE synthesis reaction. The experimental set-up used in the present work is similar to that of (82), and is described in Figure 2.2. It consists mainly of two parts: a chamber for evacuation at high temperatures and a vapor adsorption system. The empty sampling tube was accurately weighed, then filled with zeolite powder (ca. 1.0 g) and evacuated at 230 °C for 4 hours to remove adsorbed moisture. The cooled tube was weighed again and transferred to the adsorption system heated at 80 °C and maintained under a vacuum of 10^{-2} Torr.

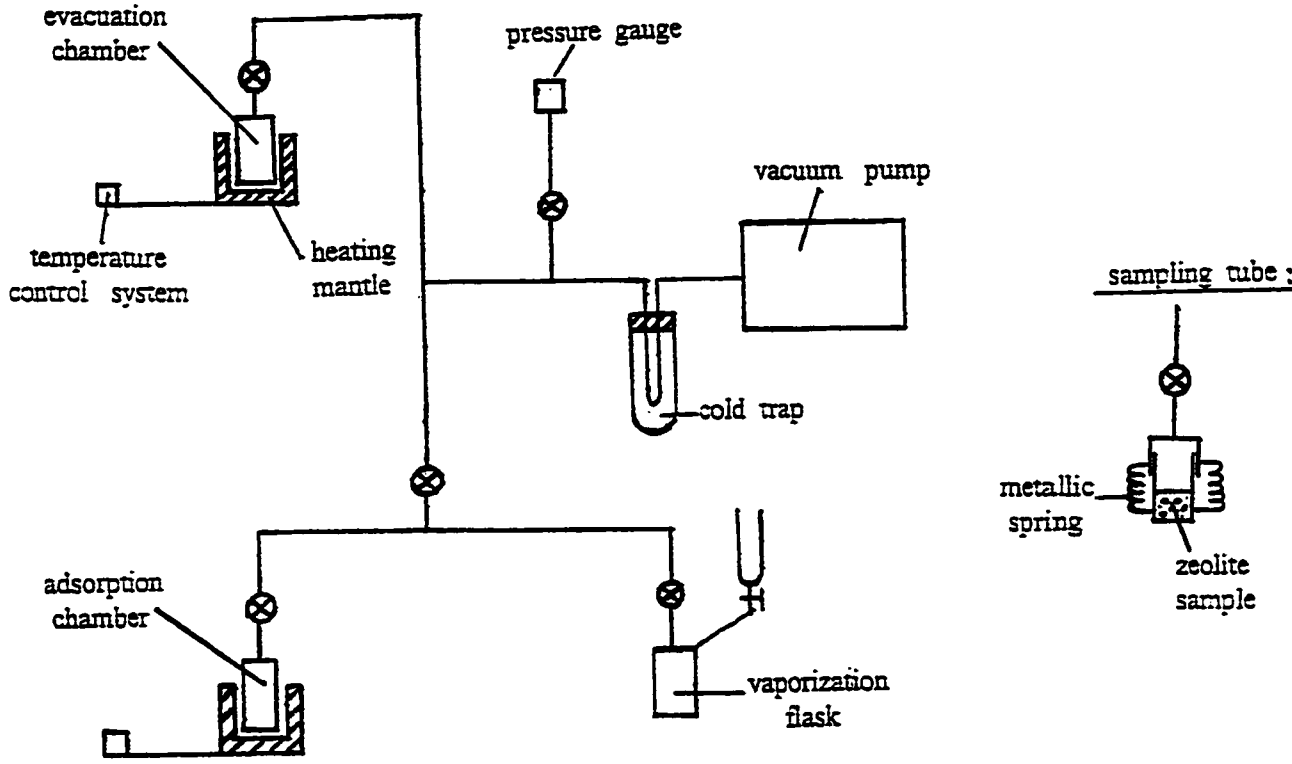

Figure 2.2 : Experimental set-up for methanol adsorption tests

The same evacuation procedure was repeated for the vaporization flask maintained at room temperature and isolated from the adsorption chamber. To ensure that methanol uptake is mainly adsorbed within the intracrystalline channel system of zeolite sample (83), a low methanol vapor pressure was created within the adsorption chamber. This was done by pouring 4 ml of methanol into the vaporization flask previously evacuated at about 10^{-2} Torr. At room temperature, a well defined methanol vapor pressure of about 122 Torr was developed. Then the adsorption chamber and the vaporization flask were put in contact for the methanol vapor to expand to the zeolite sample zone which was heated at 80 °C. It is worth mentioning that the activation temperature of 80°C used here was intended to simulate the reaction conditions. The zeolite sample was left in contact with methanol vapor at 80 °C for five to seven days for the adsorption to complete. During this chemisorption period, the increasing weight of the zeolite sample (contained in the adsorption flask) was carefully recorded every 24 hours until no further weight gain could be measured. The sampling tube was weighed and the equilibrium adsorption capacity was calculated by the following formula :

$$MeOH_{Chemi} = \frac{\text{weight of adsorbed methanol vapor}}{\text{weight of activated zeolite sample} \times 32.04}$$

From this equation, the derived molar ratio $R_{Me/Al}$ was defined as the ratio of the number of methanol molecules chemisorbed per framework Al site.

2.2.7 Selective Fluoride ions electrode analysis

The effective fluoride ions content of the fluorine treated H-ZSM5 and desilicated H-DZSM5 was determined by the fluoride ion selective electrode (model Orion 94-09) analysis. An approximate mass of 1.0 g of zeolite sample was calcined at 800 °C for one hour, then fused in a mixture of potassium carbonate and lithium tetraborate (in a 2:1 ratio) at 800 °C for another hour. The resulting solid was dissolved in a strong mineral acid then the volume was adjusted to 50 ml with a total ionic strength adjustor TISAB II from Orion. A series of standard fluoride ion solutions were prepared in the same conditions. The fluoride content of the unknown samples were determined from the standard calibration curve.

2.2.8 Solid state NMR

The nuclear magnetic resonance (NMR) spectra of zeolite materials were obtained at room temperature on a Varian VXR 300 FT-NMR spectrometer operating at 78.159 MHz for ^{27}Al and using superconducting solenoid magnets and amplifiers for final radio frequency pulse generation. A VXR 4000 model computer system was used for data acquisition and processing. ^{27}Al magic angle spinning MAS-NMR were obtained using probes with a spinning rate of 6 kHz. The ^{27}Al line positions (chemical shifts) were referred to $[Al(H_2O)_6]^{3+}$ as zero

chemical shift. These MAS-NMR spectra were recorded at the University of Ottawa.

2.2.9 Thermal analysis (DTA-TGA)

Thermal analyses of zeolite catalyst samples were performed on the PL Thermal Sciences STA 1500 instrument interfaced to an IBM PS/2 computer.The flow rate of dry air carrier gas was 30 ml/min and 12 to 18 mg of catalyst sample were used in each run. The linear heating rate of the system was programmed to 10°C/min. The platinum crucibles were used for both the sample pan and the reference pan. In the reference pan, 15 mg of calcined alumina was loaded as reference.

In general, the change in weight of a catalyst sample, as recorded in the thermogravimetric analysis curve (TGA), with the increasing temperature was used for the determination of the amount of species incorporated as well as the limit of thermal stability of the zeolite sample. The differential thermal analysis curve (DTA) recorded simultaneously gave information on eventual phase changes of the zeolite sample upon thermal treatment and the thermodynamic nature of the phase change.

2.3 Catalytic activity testing

2.3.1 Experimental set-up

The experimental set-up of the reactor system used for the catalytic testing of the fluorinated HZSM-5, the desilicated HZSM-5 and the fluorinated desilicated HZSM-5, shown in Figure 2.3 was identical to that used for the dehydration of ethanol (84a). The final extrudate catalyst was loaded into a fixed bed tubular reactor of 2 cm internal diameter and 38 cm in length which was heated by a digitally controlled furnace. The methanol reactant was fed into a vaporization flask by an injection syringe the rate of which was monitored by an infusion pump. The isobutene feed and the nitrogen carrier gas connected in-line with a flowmeter were flowed into a vaporization flask heated at 80 °C where they were mixed together with methanol before passing through the catalyst bed for the reaction to take place. A chromel-alumel thermocouple positioned in a thermocouple well located at the center of the catalyst bed, was connected to a digital meter unit to monitor the temperature of the catalyst bed. The hot outstream gas product mixture was condensed into a liquid collector flask immersed in an ice bath maintained at ca. −10 °C while the remaining gaseous products separated from the liquid phase passed through a glass bulb from which gas sampling was performed.

As for the HY zeolite and the triflic acid treated HY zeolite, the experimental set-up for catalytic testing (3) is shown in Figure 2.4. A stainless-

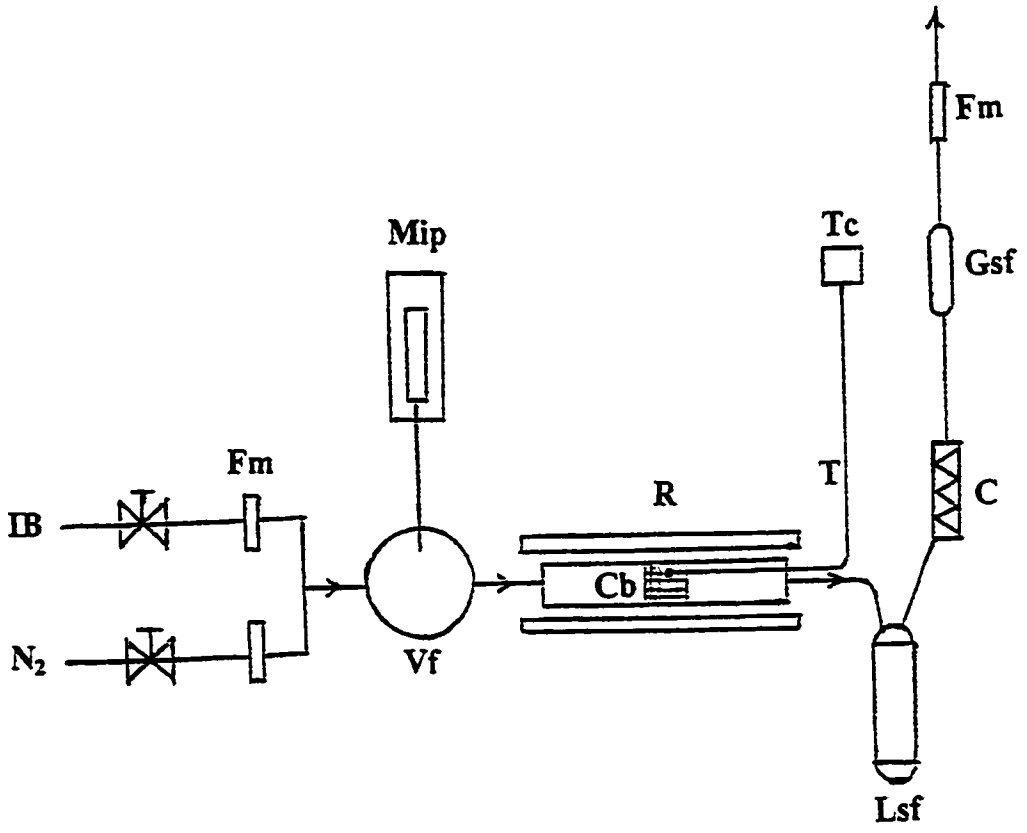

Figure 2.3 : Experimental set-up for catalytic testing of the fluorine treated and desilicated ZSM-5 zeolites

IB: Isobutene; N_2: Nitrogen carrier gas; **Fm**: flowmeter; **Vf**: vaporization flask; **Mip**: Methanol infusion pump; **R**: reactor system; **Cb**: catalyst bed; **Lsf**: liquid sampling flask; **C**: condenser; **Gsf**: gas sampling flask; **T**: thermocouple (chromel-alumel), **Tc** : digital temperature controller.

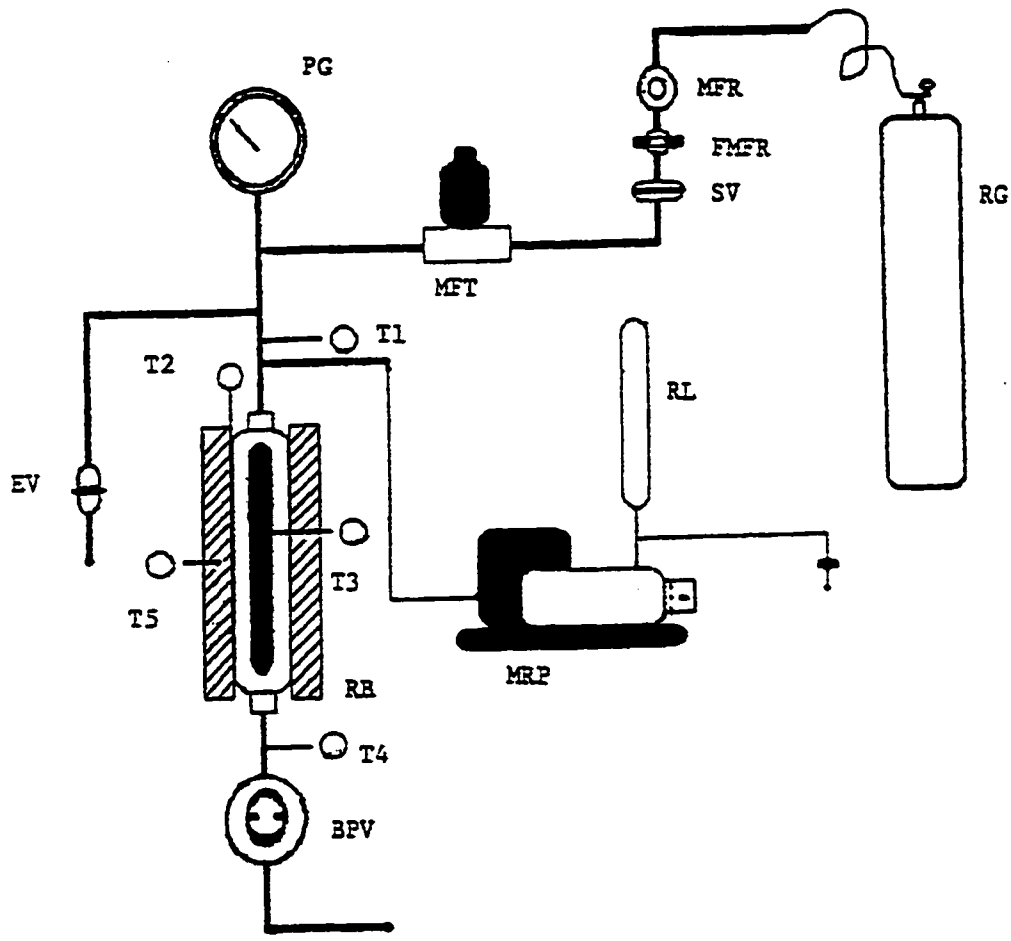

Figure 2.4 : Experimental set-up for catalytic testing of the TFA treated zeolites

RG: Gas reservoir; RL: Liquid reservoir; T*i*: Thermocouples; RB: Reactor body; PG: Pressure gauge; MFT: Mass flow transducer; MRP: Milton Roy pump; MFR: Mass flow regulator; FMFR: (Fine) mass flow regulator; SV: shut off valve; BPV: Back pressure regulator; EV: Emergency valve.

steel fixed - bed reactor 2.5 cm in diameter and 30 cm in length vertically mounted was used. The reactor had a preheating zone and a reaction zone that were monitored by two chromel-alumel thermocouples introduced into two thermocouple wells positioned at the center of the reactor. The temperature control was achieved by adjusting the power input to each zone. Nitrogen was used as carrier gas and the flow rate was monitored by using a gas transducer connected to a digital mass flowmeter and a gas volume totalizer.

2.3.2 Operating conditions

Since the gas phase synthesis of MTBE (or ETBE) within the zeolite structure was strongly related to steric considerations, the acid catalyzed MTBE (or ETBE) reaction was considered as model reaction for the evaluation of the catalytic activity of modified zeolite catalysts. The normal operating conditions used in the testing of HZSM-5 type zeolites were as follows:

– reaction pressure : 1 Atm

– reaction temperature : 80 ± 0.5 °C (70 °C to 90 °C in the case of the study of the effect of temperature on the catalytic activity)

– weight of dehydrated catalyst : 3.0 g

– weight hourly space velocity (weight of total feed per hour / weight of catalyst): 0.5 hr^{-1}

– molar ratio (methanol / isobutene) : 1.0

– reaction duration : 5 hours

– nitrogen carrier gas : 10 ml / min

– flow rate of isobutene feed : 0.017 mole / hour

– methanol feed rate : 0.017 mole / hour

The operating conditions used for the testing of HY type zeolites were similar to those indicated above except for the following conditions :

– reaction temperature : 55 – 100 °C (± 0.5 °C)

– weight of catalyst : 10 – 12 g

– flow rate of isobutene feed : 0.07 mole / hour

– methanol feed rate : 0.07 mole / hour

– molar ratio (methanol / isobutene) : 1.0

– reaction duration : 4 hours

After being loaded into the reactor, the zeolite catalyst was reactivated in-situ under a pre-dried nitrogen flow of 10 ml / min at 150 °C for 2 hours in order to remove any adsorbed moisture and then cooled down under N_2 flow until the desired reaction temperature was stabilized. Prior to reaction, methanol was first injected into the reactor at the above mentioned rate for about 15 minutes in order to saturate the active acid sites and to prevent the eventual oligomerization of isobutene that might block the pore system to the diffusion of reactants. Isobutene was the last reactant to be fed into the reactor just before the start of the reaction.

Previous experiments performed with simultaneous admission of both reactants have resulted in a dramatically low yield of MTBE and a gradual change in the appearance of the catalyst from the normal white to the yellow brown color. After the reaction was finished, isobutene was the first reactant to be removed (for the same reasons as mentioned earlier) then the catalyst was flushed with nitrogen during 15 minutes for the complete removal of all reactants and products remaining inside the zeolite catalyst.

The gas phase and liquid phase products were analyzed using a Hewlett-Packard gas chromatograph Model 5890 equipped with a FID detector, a 50 m length PONA (84b) type capillary column (fused silica coated with a crosslinked dimethyl polysiloxane polymer as a stationary phase) and a reporting integrator Model HP-3392. As internal standard for both gaseous and liquid phase products, 2,2-dimethylbutane was used. About 7.0 g of 1-Octanol was used as solvent in the liquid sampling flask to collect the organic liquid products prior to chromatographic analysis. The 1-Octanol peak was considered as solvent in the chromatogram and was excluded from the final product distribution.

As in the case of other acido-catalyzed reactions such as dehydration of alcohols (79), aromatization of light alkanes (84c), etc., the contribution of the bentonite component to the overall catalytic activity of the catalyst was ruled out by doing some tests with extrudates made of 100 % bentonite (surface area = 28.6 m^2/g and average pore size = 8 nm) and by using the same reaction conditions. In

fact, there were no production of MTBE and no conversion of isobutene and methanol into diisobutene and dimethyl ether, respectively.

2.3.3 Product calculations

The product calculations were made on the carbon atom basis. Product yields were expressed in C atom percent rather than in the usual moles percent because it allows us to visualize the number of carbon atoms of isobutene (or the alcohol) converted into carbon containing products, independently from the molecular length or the chemical composition of such products (85). Chromatographic peak areas were converted to carbon atoms using 2,2-dimethylbutane as internal standard and the corresponding correction factors for the FID detector. The combination of the gaseous phase product and liquid phase product gave the final product result.

The yield of the MTBE (or ETBE) product was calculated as follows:

$$Y_{i-MTBE}\,(\text{C-atom \%}) = 4/5 \times (NC_i / NC_f) \times 100$$

where NC_i and NC_f represent the number of carbon atoms of the MTBE (or ETBE) product and isobutene feed respectively.

The yield of diisobutene (C-8) by-products namely the 2,4,4-trimethyl-1-pentene and its isomer 2,4,4-trimethyl-2-pentene was calculated as follows :

$$Y_{i-C\text{-}8}\,(\text{C-atom \%}) = (NC_i / NC_f) \times 100$$

where NC_i and NC_f represent the number of carbon atoms of the isobutene dimer and isobutene feed respectively.

The selectivity toward reaction product (i) was calculated as follows :

S_i (C-atom %) = NC_i / (NC_{MTBE} + NC_{C8}) × 100

where NC_i is the number of carbon atoms of product (i) in the outstream gases.

In particular in the synthesis of ETBE, the yields of diethyl ether and hydrocarbons other than oligomers of isobutene were expressed as :

Y_{DEE} (C-atom %) = (NC_{DEE} / NC_{ETOH}) × 100

where NC_{DEE} and NC_{ETOH} are the number of carbon atoms of diethyl ether product and ethanol feed respectively.

Y_{HCC} (C-atom %) = (NC_{HCC} / NC_{ETOH}) × 100

where NC_{HCC} is the number of carbon atoms of hydrocarbons other than oligomers of isobutene.

The reagent contact time t_C and the weight hourly space velocity (WHSV) were defined as follows :

t_C (expressed in hours) = W_{CAT} / F_{REAG}

WHSV (expressed in hr^{-1}) = F_{REAG} / W_{CAT}

where W_{CAT} and F_{REAG} are the weight of the catalyst (in gram) and the total flow rate of the reagents (in g/hr), respectively. Satisfactory reproducibilities with

respect to different reaction runs performed over the same catalyst at the same operating conditions were within 4 %.

2.3.4 Kinetic studies

In this research work, kinetic studies were conducted for the TFA doped HY zeolite used in the synthesis of MTBE and ETBE. The experimental set-up for kinetic testing and product analysis was similar to that for the catalytic testing.

The apparent activation energy E_a was determined by using the Arrhenius equation:

$$k = A \exp(-E_a / RT)$$

where k is the rate constant proportional to the initial reaction rate r_o , E_a the apparent activation energy, A, the pre-exponential factor and R, the universal gas constant. E_a was calculated from the initial rates r_o of MTBE or ETBE conversion corresponding to contact times lower than 3.0 hours and at different reaction temperatures ranging from 345 K (72 °C) to 371 K (98 °C). Higher reaction temperatures are not recommended because of the decomposition of MTBE or ETBE (88). The experimental data of the MTBE or ETBE conversion were fit to a function f(t) of the contact time (t) using non-linear regression curve fitting. The initial reaction rate was determined by taking the derivative of the function f(t) at zero contact time, as follows:

$$r_o = \lim_{t \to 0} \frac{d[C_t]}{dt} = \lim_{t \to 0} \frac{d[f(t)]}{dt}$$

where C_t is the conversion expressed in % C-atoms.

and t is the contact time (hour)

For each catalyst, the initial rate r_o was determined for three different reaction temperatures and the apparent activation energy E_a was evaluated from the plot of ln r_o versus $10^3 / T$ the slope of which was ($- E_a / 10^3 R$).

CHAPTER III

RESULTS AND DISCUSSION

3.1 Zeolites as catalysts.

The commercial catalyst Amberlyst-15 resin (Table 3.0) presently used in the synthesis of MTBE, although giving a high performance (13b) in the liquid phase synthesis (92 - 93 % yield), still suffers at the present time from several drawbacks, mainly the high pressure requirement (16-18 atm), the acid leaching from the resin surface, and the production of isobutene oligomers as by-products. The latter aspect constitutes a major economic disadvantage (15) in terms of loss of isobutene reactants, which could not be recycled as is methanol in the industrial processes. Because of these restrictive factors, considerable effort have been focused on the search for alternative catalysts which do not present these drawbacks. In this perspective, inorganic materials such as zeolites represented promising candidates and were thus proposed to carry out the etherification reaction in gas phase in order to remedy these drawbacks. With very high chemical and thermal stability up to 700 °C, zeolite catalysts do not present the problem of acid leaching at the surface as presently encountered with the commercial A-15 resin.

Two zeolite catalysts were proposed for these preliminary studies of catalytic activity : the ZSM-5 and the Y zeolites, having a Si/Al molar ratio of 20.5 and 2.5 respectively. The reaction was carried out according to the following conditions : reaction temperatures ranging from 60 °C to 95 °C at 1 atm, weight of catalyst : 11 g, Isobutene / MeOH molar ratio : 1.0 - 1.1, and a reaction duration of

Table 3.0 : Physico-chemical properties of the commercial Amberlyst-15 resin (Ref. 99)

Skeleton	styrene-divinylbenzene
Structure	macroporous
Active group	sulfonic
Degree of cross-linking	20 %
Maximum temperature operation	120 °C
Surface area	43 m^2/g
Porosity	33 %
Acid density	4.81 meq / L
Mean pore diameter	240 Å
Density	1.012 g/ml
Sulfur content	13.8 wt. %

4 hours. The catalytic results are reported in Tables 3.1 and 3.2 and on Figure 3.1, in % C-atom of MTBE yield as a function of reaction temperature. For comparison purpose, the MTBE synthesis was carried out on the commercial A-15 resin in the gas phase with the same conditions and the results are reported in Table 3.3.

The data clearly showed a maximum of MTBE yield for each catalyst versus reaction temperature. The commercial A-15 presented a maximum MTBE yield of 48.5 % at 71 °C with a steadily increasing yield of C-8 by-products up to 13.84 % at 80 °C. The sharp decrease of MTBE yield above 74 °C was due to larger amounts of by-products formed. For the HZSM-5 and HY zeolites, the maxima MTBE yields of 39.1 % and 26.7 % were observed at 84 °C and 85 °C respectively, with no formation of C-8 by-products for the HZSM-5 zeolite but with a significant yield of by-products formation for the HY zeolite. The lower yield of MTBE obtained at higher reaction temperatures is due to the limiting effect of the thermodynamic equilibrium which favors the decomposition of MTBE at elevated temperatures (11). At this stage, the difference in catalytic activity of these three catalysts in terms of maximum MTBE yield obtained, corresponded to the following sequence :

A-15 > H-ZSM-5 > H-Y

This sequence reflects the situation in terms of acid density and strength of these catalysts. In particular, the Y-type zeolite although having a much higher acid density (4.76 meq H^+ / g) than that of the ZSM-5 type zeolite (0.78 meq H^+ /

Table 3.1 : Yield of MTBE in % C-atom as a function of reaction temperature obtained with the parent HZSM-5 zeolite.

Reaction temperature (°C)	MTBE Yield (% C-atom)	C-8 Yield (% C-atom)	Selectivity to MTBE (%)
68	15.7	0.0	100
70	19.8	0.0	100
80	33.9	0.0	100
82	35.8	0.0	100
83	38.7	0.0	100
84	39.1	0.0	100
85	37.2	0.0	100
90	32.8	0.0	100
91	31.3	0.0	100
92	32.1	0.0	100

Table 3.2 : Yield of MTBE in % C-atom as a function of reaction temperature obtained with the parent HY zeolite.

Reaction temperature (°C)	MTBE Yield (% C-atom)	C-8 Yield (% C-atom)	Selectivity to MTBE (%)
70	8.2	0.53	93.9
75	10.9	0.92	92.2
80	18.5	1.42	92.9
85	26.7	1.98	93.1
87	23.9	2.37	91.0
92	10.4	4.60	69.3

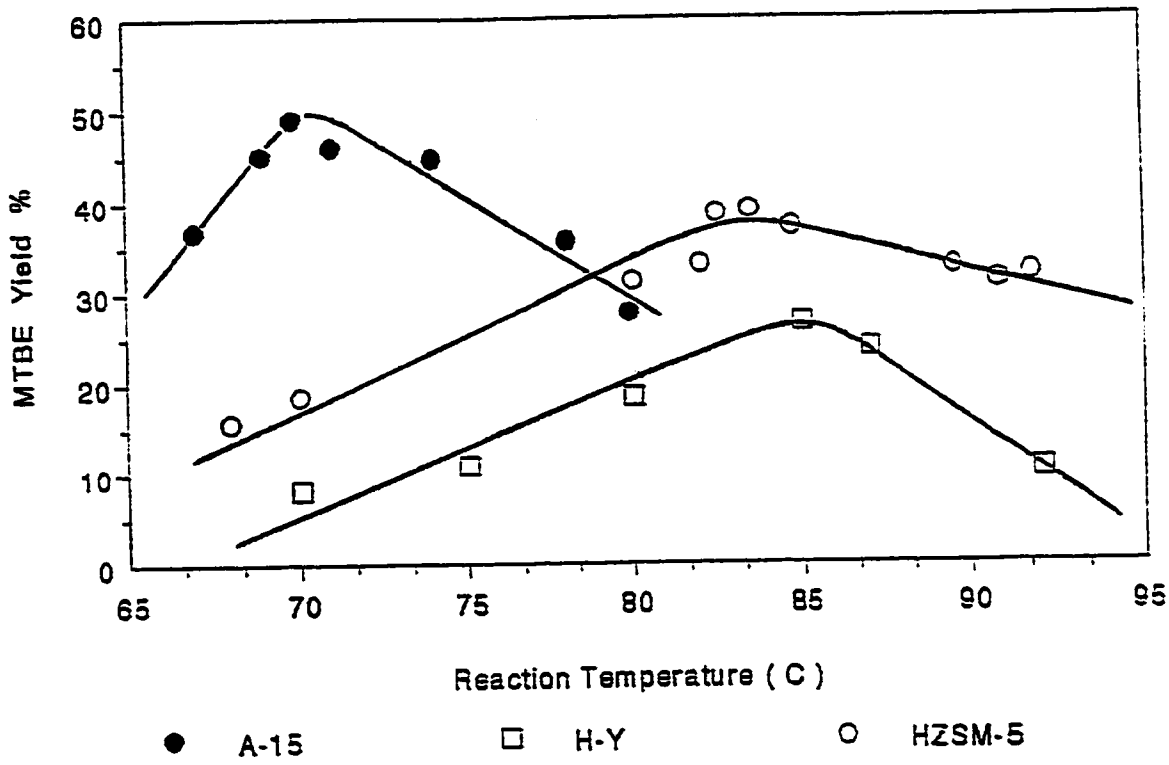

Figure 3.1 : MTBE yield (in % C-atom) versus reaction temperature(°C), obtained with the Amberlyst-15 (●), H-ZSM-5 (○) and H-Y (□) catalysts.

Table 3.3 : Yield of MTBE in % C-atom as a function of reaction temperature obtained with the commercial Amberlyst-15.

Reaction temperature (°C)	MTBE Yield (% C-atom)	C-8 Yield (% C-atom)	Selectivity to MTBE (%)
67	36.8	1.95	95.0
69	45.1	4.42	91.1
70	48.5	5.80	89.3
71	46.0	6.05	88.4
74	44.8	7.42	85.8
78	35.7	10.21	77.8
80	29.9	13.84	68.4

g) was much less active than the ZSM-5 zeolite due to its lower acid strength. The ZSM-5 zeolite, although having a high acid strength, only showed a moderate catalytic activity among the three catalysts because of its lower acid density. As for the A-15 resin, the very high catalytic activity was due to both a high acid density (4.81 meq H^+ / g, see Table 3.0) and a high acid strength.

The important amount of C-8 by-products obtained with the commercial A-15 resin is mainly favored by its large pore structure within the mesopore range 25 – 35 nm. Zeolite catalysts produced no C-8 by-products in the case of HZSM-5 zeolite or very low amount of C-8 by-products in the case of HY zeolite when compared to the A-15 resin, owing to their narrow micropore structure, i.e. 5.4 × 5.6 Å and 5.1 × 5.5 Å for the ZSM-5 zeolite (Figure 3.2) and 7.4 Å for the HY zeolite (Figure 3.3). Within zeolite pore and channel network, only suitable sized molecules such as MTBE or ETBE are selectively formed. The ZSM-5 pore diameter was too small to allow the formation of bulky diisobutene by-products (transition state selectivity) within its channel network, whereas the slightly larger pore size HY zeolite with its supercage system (1.2 nm) appeared more favorable for their formation. As a result, HZSM-5 zeolite showed a higher product selectivity to MTBE than HY zeolite (see Tables 3.1 and 3.2). The small amount of by-products observed with HY zeolite could be formed only within its small portion of mesopores. As for the A-15 resin, the lower selectivity to MTBE was ascribed to the important amount of by-products formed within its large mesopore

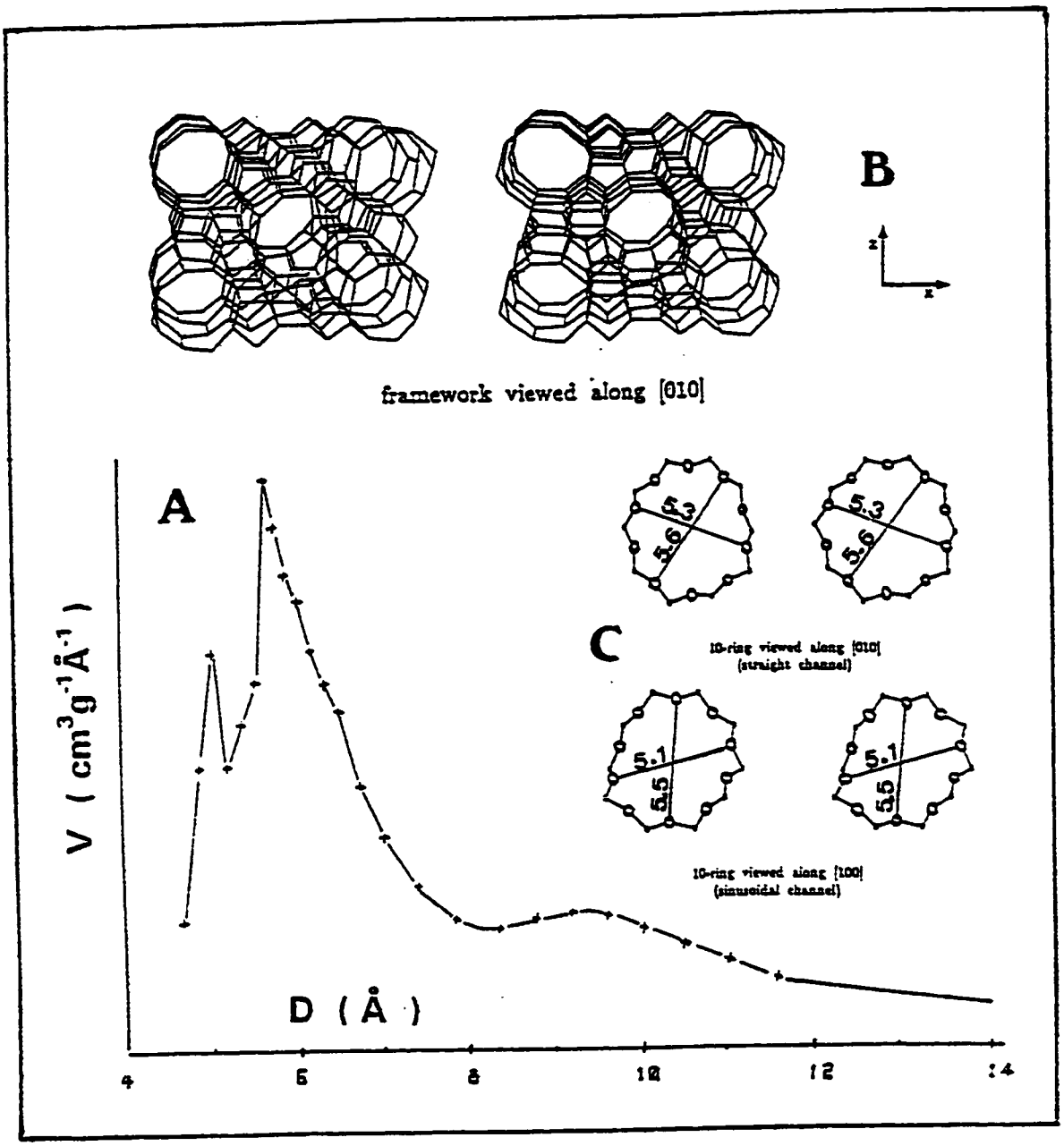

Figure 3.2 : Micropore size distribution (A) of ZSM-5 zeolite and its theoretical structure (B) and pore system (C).
V : volume of N_2 adsorbate physisorbed, D : pore diameter

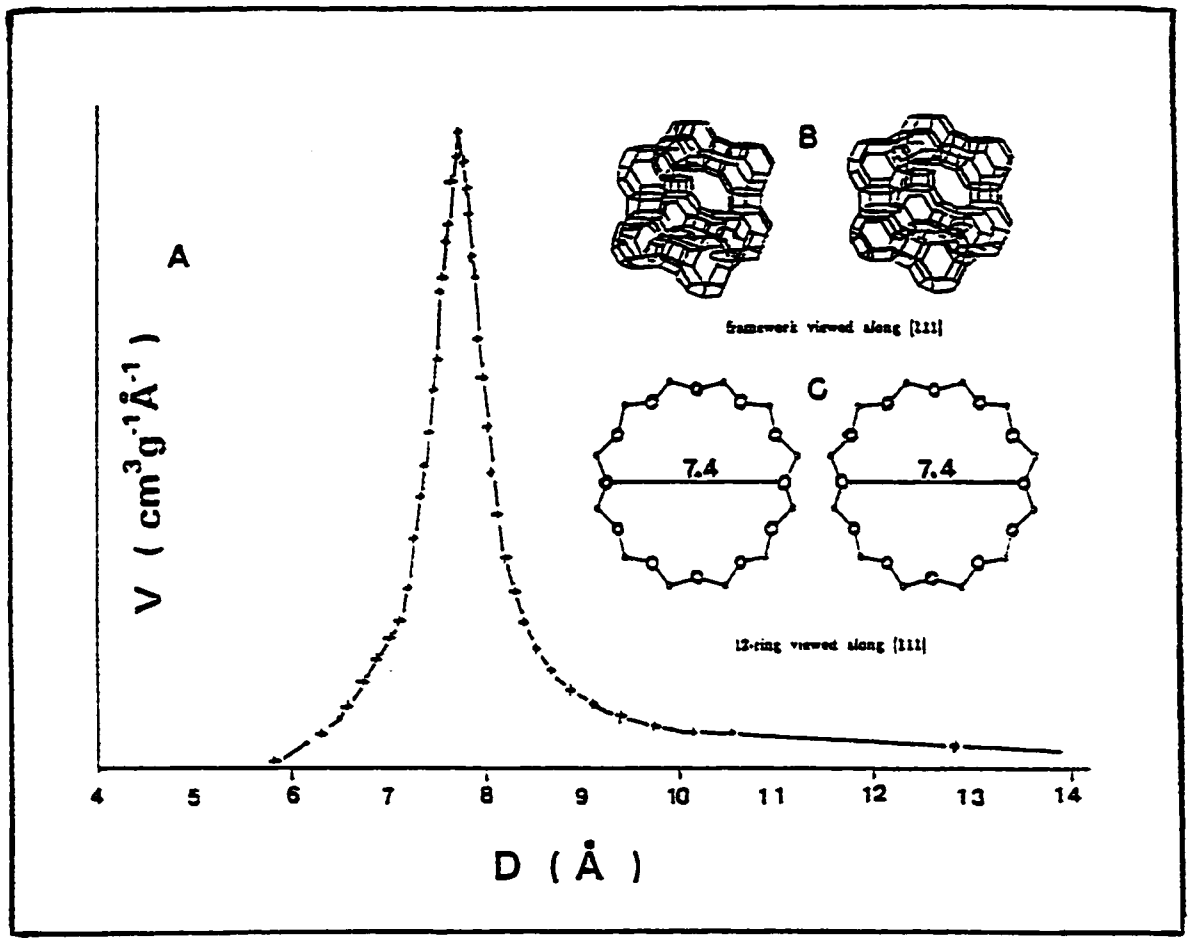

Figure 3.3 : Micropore size distribution (A) of Y zeolite and its theoretical structure (B) and pore system (C).
V : volume of N_2 adsorbate physisorbed, D : pore diameter

structure. In addition, with A-15 resin and HY zeolite, there was also a linear increase in the formation C-8 by-products versus reaction temperature which was due to a higher amount of isobutene available resulting from the reverse reaction of MTBE decomposition occurring especially at reaction temperatures higher than those corresponding to the maxima of MTBE conversion (11).

Although exhibiting a lower catalytic activity in terms of MTBE yield, zeolites materials offered a superior advantage over the commercial A-15 resin which is the shape selectivity of their pore and channel structure : no C-8 by-products were produced with ZSM-5 zeolite, and only small amounts were observed with HY zeolite. In industry, where huge amounts of isobutene reactants are involved in the MTBE production, this advantage represents a remarkable and promising economic asset for the process, by preventing the loss of a large amount of isobutene through the formation of undesirable by-products. Moreover, owing to this interesting shape selectivity to MTBE, zeolites only required a low methanol to isobutene feed ratio of 1:1 instead of the higher feed ratio of 1.24:1 presently used in industry for the A-15 resin. This aspect represents a substantial economic interest with respect to the commercial resin catalyst for which high production costs are involved in the separation and recycling of methanol excess used to reduce the formation of isobutene oligomers. The simple increase of the reaction temperature could not enhance the MTBE yield because of the severe

thermodynamic equilibrium limitations which intervene at high temperatures, as illustrated by the bell curve of MTBE conversion versus reaction temperature.

Besides numerous structural advantages that zeolite materials possess, the only remaining limitation factor regarding the industrial application of zeolites in MTBE synthesis resides on their lower catalytic activity with respect to the commercial A-15 resin. In the next sections, we will investigate and propose different chemical treatment methods in order to increase further their original acid density and strength.

3.2 Trifluoromethane sulfonic acid modified ZSM-5 and Y zeolites

As a remedy to the low catalytic activity of zeolite materials in the MTBE synthesis, the incorporation within zeolite structures of an organic Brønsted superacid, the trifluoromethane sulfonic acid commonly called «triflic acid (TFA) », was thus proposed (85). Triflic acid has often been acclaimed as the strongest of all known monoprotic organic acids with its acidity value of – 14.1 on the Hammett acidity scale (91, 92). Previous work done on the dehydration of ethanol (89) using porous materials coated with such a superacid has shown an increase in catalytic activity with a significant reduction of the reaction temperature. In this work, different amounts of TFA were coated onto the HZSM-5 and HY zeolites surface with the aim to enhance their original surface acidity.

3.2.1 HZSM-5 / TFA catalyst

Triflic acid were incorporated onto the H-ZSM5 catalyst at different concentrations in order to determine the optimal level, according to the procedure described in section 2.1.3. The catalytic activity testings were done according to the experimental conditions mentioned in section 2.3.2.

Catalytic results obtained from the TFA coated ZSM-5 zeolites have shown an increased conversion to MTBE with a triflic acid loading of 3 wt % as illustrated in Figure 3.4 and reported in Table 3.4. The maximum conversion to MTBE observed for the 3% TFA loading was 40.2 % at 84 °C. It was only

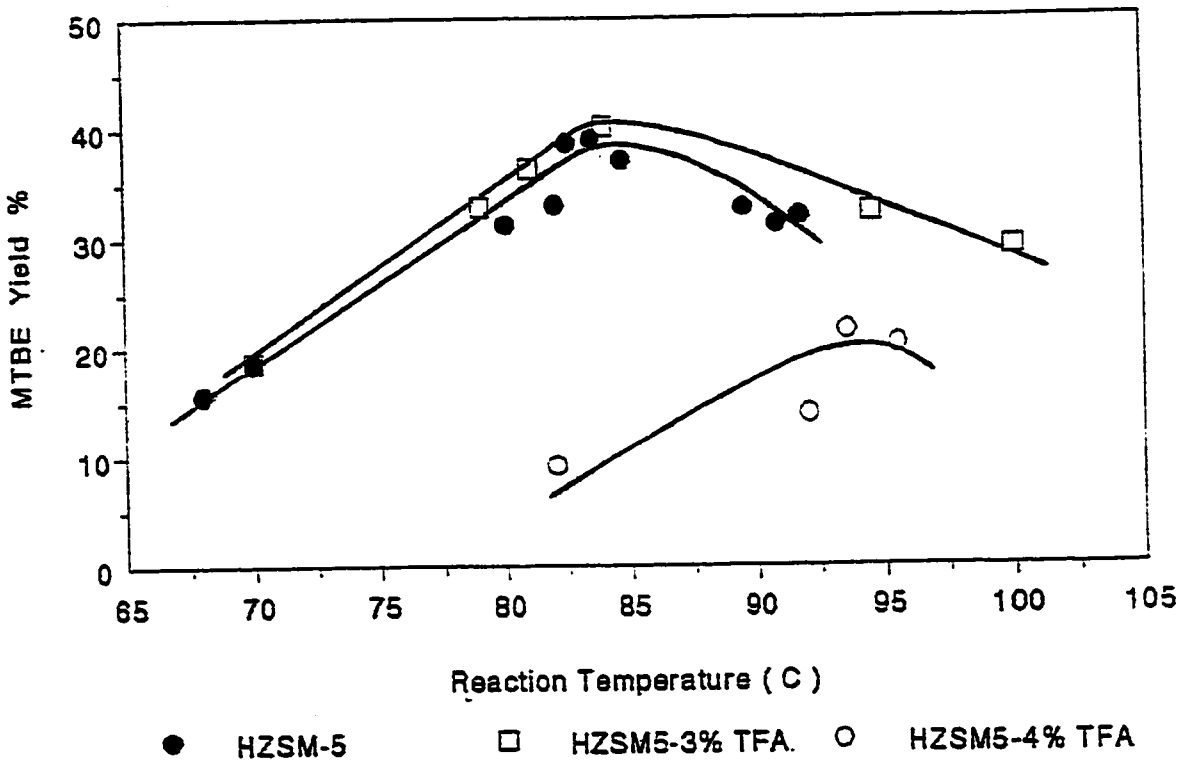

Figure 3.4 : MTBE yield in % C-atom versus reaction temperature (°C), obtained with the H-ZSM-5 (●), H-ZSM5/ 3% TFA (□) and H-ZSM5 / 4 % TFA (○) catalysts.

Table 3.4 : Yield of MTBE in % C-atom as a function of reaction temperature obtained with the HZSM-5 zeolite loaded with triflic acid (TFA)

Catalyst	Reaction temperature (°C)	MTBE Yield (% C-atom)	C-8 Yield (% C-atom)
HZSM-5 - 3 % wt TFA	70	18.7	0.35
	79	32.9	0.48
	81	36.4	0.16
	84	40.2	0.41
	95	32.4	0.23
	100	29.2	0.17
HZSM-5 - 4 % wt TFA	82	9.2	0.05
	92	13.9	0.09
	94	21.6	0.21
	96	20.3	0.10

slightly higher than that of the parent HZSM-5 zeolite, i.e. 39.1 %. Conversely, a higher amount of 4 % triflic acid incorporated which normally increased the total surface acid sites of the catalyst, resulted in a dramatically lower yield of MTBE, i.e. 21.6 %. Thus the small increase in MTBE yield upon loading of 3 % TFA into the H-ZSM5 zeolite was not significant and was indicative of a restriction to the diffusion of isobutene reactants to the acid sites and to the counterdiffusion of MTBE products within the pore and channel network in the presence of bulky triflic acid molecules incorporated onto the zeolite surface. Surface characterization studies by the nitrogen adsorption and desorption technique also supported this observation as shown in Table 3.5 where there was an important decrease by 40 % of the B.E.T. surface area of the HZSM-5 / 3% TFA catalyst with respect to the parent zeolite. This surface area decrease tends to confirm the phenomenon of pore narrowing or pore blockage upon incorporation of triflic acid into the zeolite matrix that limited the access of nitrogen molecules to the pore and channel system during the B.E.T. N_2 adsorption analysis. ZSM-5 belongs to the category of small pore diameter zeolite having an average pore opening of 5.5 Å and therefore is quite sensitive to the incorporation of bulky guest molecules such as triflic acid CF_3SO_3H.

However at the optimal level of 3 % TFA loading, the overall structure of the ZSM-5 zeolite remained preserved as revealed by the very high degree of crystallinity and the unchanged Si / Al ratio of the HZSM-5 / 3 % TFA catalyst.

Table 3.5 : Physico-chemical properties of the H-ZSM-5 and H-ZSM-5 /3 % TFA catalysts.

Samples	Si / Al	TFA loading (wt %)	Degree of Crystallinity (%)	B.E.T. Surface Area (m^2 / g)
H-ZSM-5	18	0	100	360
H-ZSM-5 / 3 % TFA	18	3	99	209

Thus there was no significant dislodgment of the framework Al atoms upon reaction of the triflic acid with the zeolite surface as it was usually observed for other acid treatments of zeolite materials (34).

The small but finite amount of C-8 by-products collected in this series of triflic acid loading HZSM-5 may come from the minute portion of mesopore generated within the zeolite structure under the corrosive action of the organic superacid. However, the latter effect did not provoke any serious damage to the whole micropore structure owing to the low concentration of triflic acid loaded.

Previous works (89,90a) done on the thermal analyses of triflic acid loaded ZSM-5 zeolites have shown that TFA although having a boiling point of 161°C at atmospheric pressure, was quantitatively removed only at temperatures above 240°C once incorporated into the ZSM-5 matrix. This indicated that triflic acid molecules were not simply adsorbed on the zeolite surface but firmly anchored to it by chemisorption.

Doping HZSM-5 zeolite with an organic superacid did not represent an ideal solution to increase the total surface acidity due to the pore narrowing effect exerted by the TFA guest molecules. Nevertheless, the inherent shape selectivity of ZSM-5 structure, its high acidity strength as well as its high thermal and chemical stability still make this zeolite the matrix of choice for further improvements in terms of acidic properties provided that : (i) the size of the incorporated molecules does not affect seriously the diffusion of reactants, their

access to the surface active sites as well as the counter-diffusion of MTBE products, and (ii) the chemical nature of the incorporated molecules and the subsequent treatment of the doped zeolite materials does not damage the crystallinity of the ZSM-5 structure.

3.2.2 HY / TFA catalyst

As in the previous case of HZSM-5 zeolite, a preliminary series of catalytic testings were performed with different triflic acid loadings for HY zeolite and at different reaction temperatures. The results showed a similar amount of 3 % TFA loading as the best superacid concentration incorporated in terms of both textural properties and catalytic activity. Table 3.6 and Figure 3.5 report the percent conversion of isobutene to MTBE versus reaction temperature for the parent HY zeolite and two TFA loaded HY catalysts. At 3 % TFA loading, there was a sharp increase in the catalytic activity of the doped HY zeolite up to 45.8 % with respect to that of the parent zeolite of 26.7 % (see Table 3.2). This conversion level, comparable to that of the commercial A-15 resin of 47.5 % (see Figure 3.1), was accompanied by a much lower rate of C-8 by-products formed, i.e. below 1 % as compared to about 5 % (see Table 3.3 and Figure 3.10) produced with the commercial A-15 resin. This consequent decrease was likely due to the narrowing of the Y zeolite pore system by the adsorbed TFA species which hindered the formation of bulky isobutene dimers. At higher TFA loading of 4 % there was a

Table 3.6 : Yield of MTBE in % C-atom as a function of reaction temperature obtained with the HY zeolite loaded with triflic acid (TFA).

Catalyst	Temperature (°C)	MTBE Yield (% C-atom)	C-8 Yield (% C-atom)
HY - 3 % wt TFA	71	18.6	0.53
	78	32.9	0.48
	80	42.5	0.16
	82	42.1	0.41
	84	45.8	0.23
	87	40.2	0.17
	88	45.3	0.90
	92	26.6	1.06
	97	8.6	0.47
	98	12.2	0.50
HY - 4 % wt TFA	71	17.1	0.42
	80	23.1	0.51
	85	30.2	0.54
	90	32.4	0.83
	94	25.9	0.78

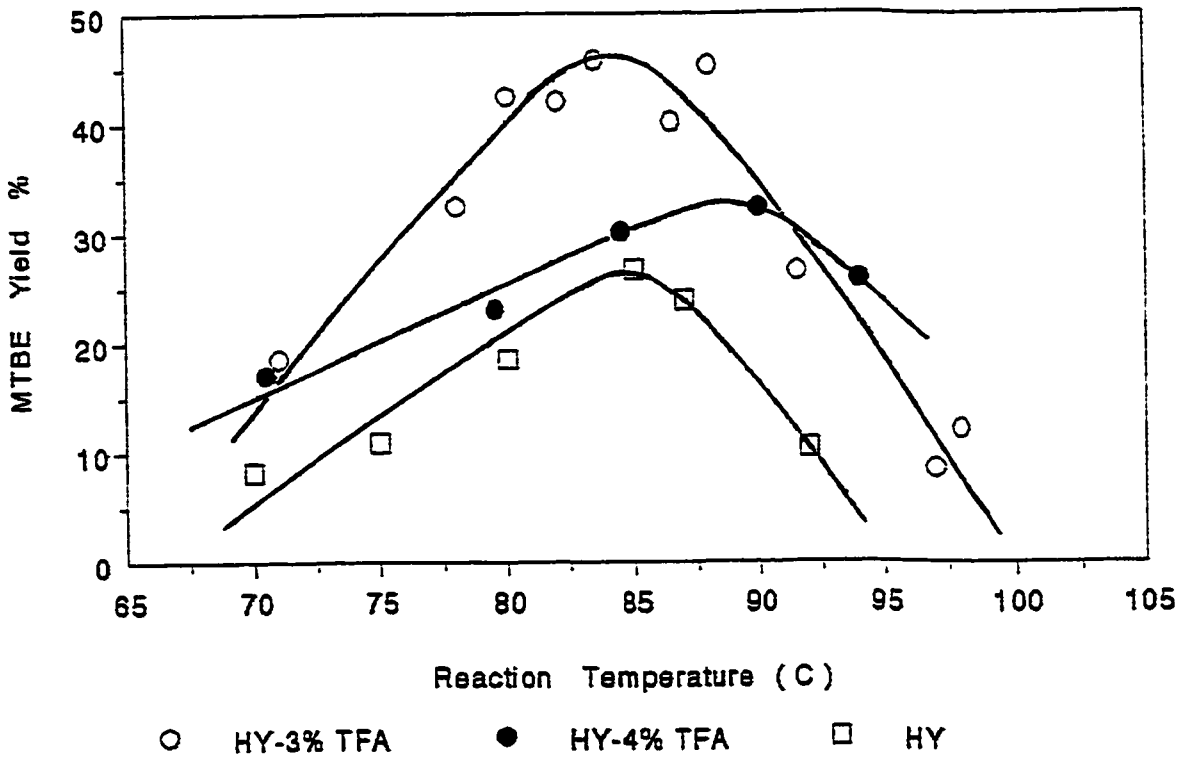

Figure 3.5 : MTBE yield in % C-atom versus reaction temperature (°C), obtained with the H-Y (□), H-Y / 3 % TFA (○) and H-Y / 4 % TFA (●) catalysts.

significantly lower conversion to MTBE : this was the expected consequence of the pore narrowing effect upon TFA coating which either restricted the access of isobutene molecules to the active sites or limited the diffusion of MTBE products. The maximum of MTBE conversion for both the HY parent and the HY / 3 %TFA were located at about 85°C, whereas for the HY / 4 %TFA, this maximum conversion was shifted to 90°C.

3.2.2.1 Characterization studies

The results of characterization studies of HY and HY/ 3 %TFA are reported in Table 3.7. Upon coating with 3 % TFA, the Si / Al ratio of the resulting catalyst was unchanged and the decrease in the degree of crystallinity was not significant. This indicates that at 3 % TFA coating, the Y-type zeolite structure remained almost intact owing to a moderate amount of superacid incorporated.

Two sets of values of the surface area determined according to the BJH method (90b) and the volume of nitrogen adsorbed are reported in Table 3.8 for the parent HY zeolite and the 3 % TFA loaded HY zeolite. The first corresponded to the zeolite type micropores and the second to the combined mesopores and macropores. There was an important decrease by about 50 % of the B.E.T. surface area and of the volume of nitrogen adsorbed for the TFA coated HY zeolite. These decreases were mainly related to the micropore region of the zeolite where occurred the pore narrowing or pore blockage phenomenon exerted by the

Table 3.7 : Textural properties of the H-Y and H-Y / 3 % TFA catalysts.

Sample	Si / Al	Degree of Crystallinity (%)	B.E.T. Surface Area (m^2 / g)
H-Y	2.5	100	428
H-Y / 3% TFA	2.5	99	222

Table 3.8 : Sorptive properties of the H-Y and H-Y / 3 % TFA catalysts.

Sample (Si / Al)	Degree of Crystallinity (%)	B.E.T. Surface Area (m^2 / g)	B.J.H. [75] cumulative desorption method Surface Area (m^2 / g) micro[1]	meso + macro[2]	Volume of N_2 adsorbed (cc / g) micro	meso + macro
H-Y (2.5)	100	428	348 (79 %)	92 (21%)	0.165 (52%)	0.150 (48%)
H-Y / 3% TFA (2.5)	99	222	154 (67%)	75 (33%)	0.073 (35%)	0.136 (65%)

1 : micropores having diameter less than 2 nm
2 : mesopores and macropores having diameters in the range of 2 – 300 nm

incorporated triflic acid molecules firmly anchored inside the pore and channel network. These adsorbed species created a steric hindrance to the nitrogen probe molecules during B.E.T. adsorption analysis and the result was a lower accessible surface area and a lower volume of nitrogen adsorbed.

The mesopore network of the HY / 3 % TFA is represented in Figure 3.6 by a sharp peak at 4 nm that also remained unaltered upon TFA loading. It was very likely that only the mesopores and a portion of the micropore system of the HY / 3 % TFA catalyst were involved in the catalytic reaction. Thus, the important increase in MTBE conversion, which was twice as high as that of the parent zeolite (see Table 3.2 and Table 3.6), was ascribed not only to the increase of surface acidity upon TFA incorporation but also to the larger micropore size of the Y-type zeolite (7.4 Å as compared to 5.5 Å in ZSM-5) and to the existence of these relatively narrow mesopores which contributed to the counterdiffusion of MTBE products. However this bimodal pore system did not affect the shape selectivity of the TFA treated HY catalyst as illustrated in Figure 3.10 by the lower amount of C8 by-products obtained (below 1 %) with respect to that of the parent HY zeolite (up to 4.6 %).

Thermal analysis of the parent HY and the TFA treated HY zeolites including DTA and TGA analyses were illustrated in Figures 3.7 and 3.8. The TGA plot of HY / 3 % TFA showed a quantitative removal of the incorporated TFA species at high temperatures starting from 280 °C up to about 330 °C. On

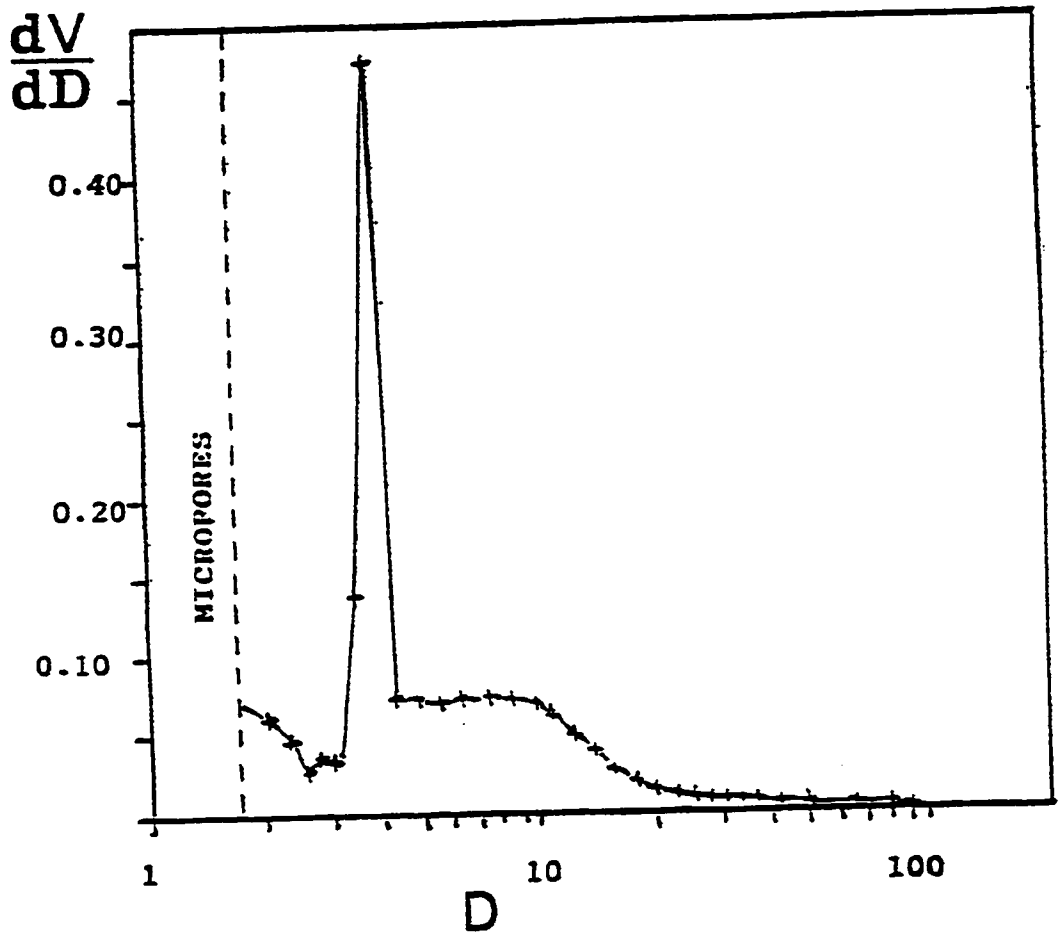

Figure 3.6 : Pore size distribution (mesopore region) of the H-Y/TFA catalyst. V (Volume of nitrogen adsorbed) and D (pore diameter) are expressed in cc/g and nm (10^{-9} m) respectively.

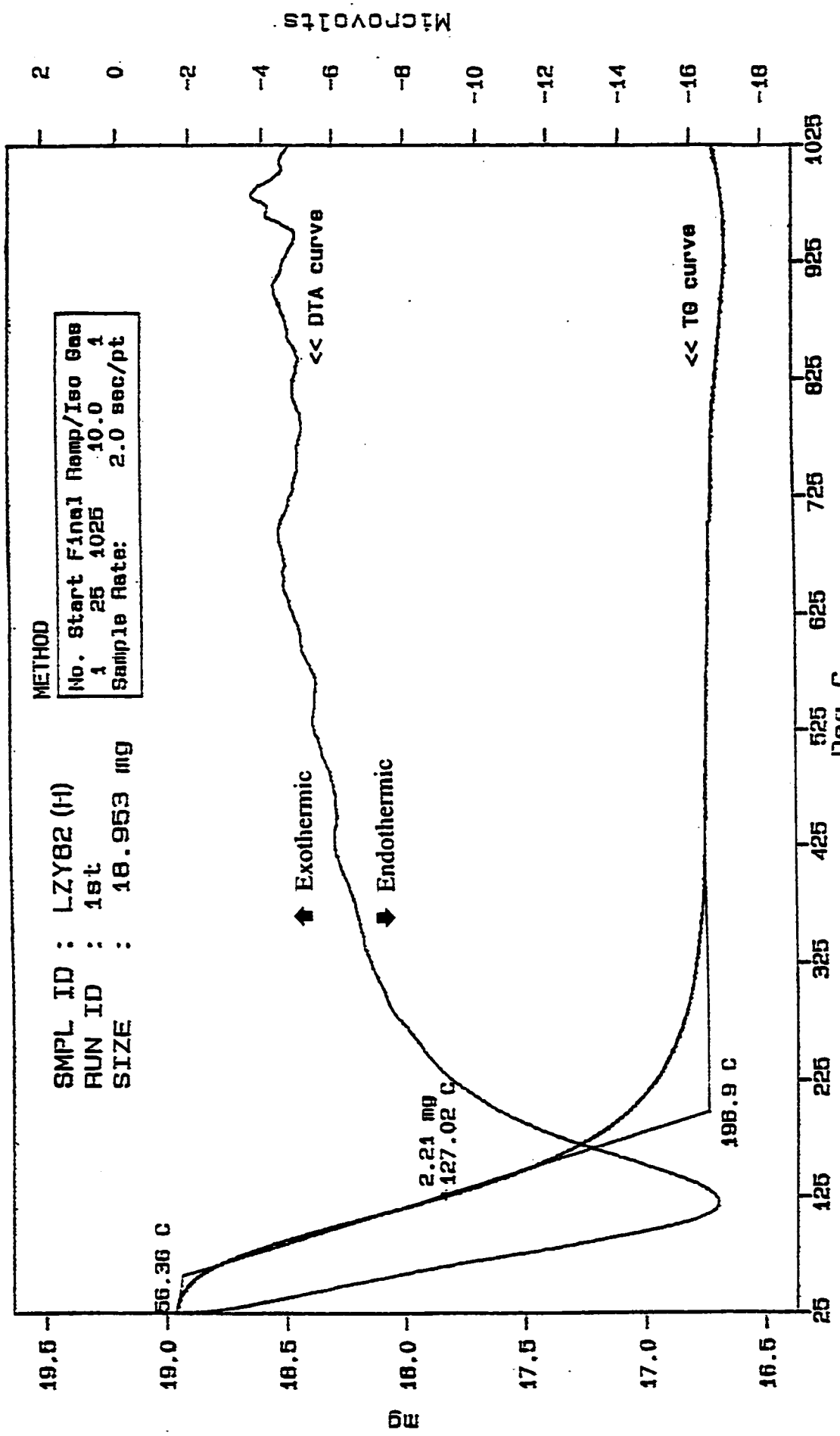

Figure 3.7 : TGA and DTA thermogram of the parent H-Y catalyst.

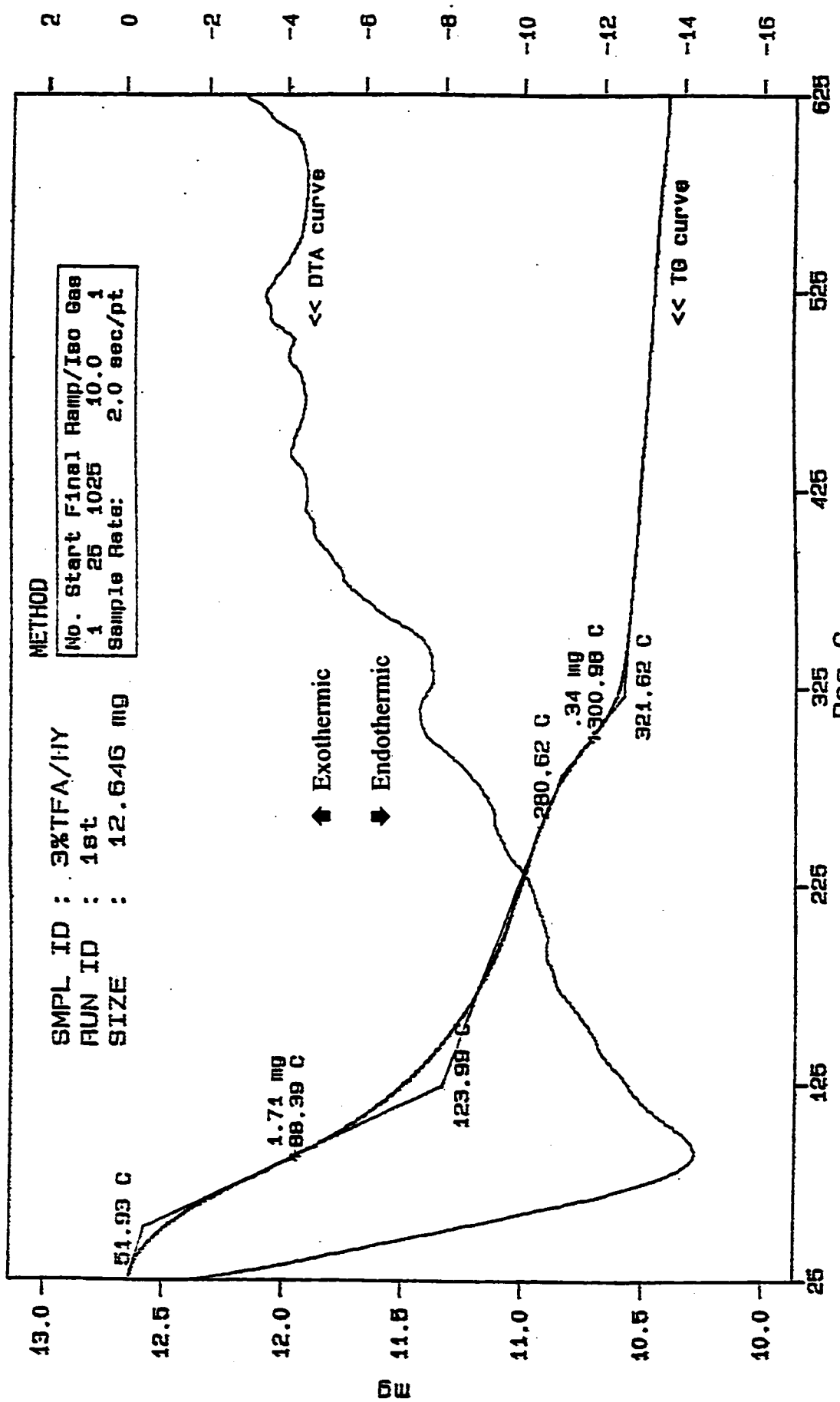

Figure 3.8 : TGA and DTA thermogram of the H-Y / 3 % TFA catalyst.

both TGA plots, the first weight loss occuring in the temperature range 50 °C to 125 °C corresponds to the removal of adsorbed moisture from the Y zeolite structure. Since the normal boiling point of triflic acid is 161°C, its very high temperature of desorption from the HY zeolite matrix shows that TFA species are not simply adsorbed onto the zeolite structure, but they are strongly attached to the zeolite surface by chemisorption bonding. The DTA curve obtained with HY / 3 % TFA upon heating in the presence of air is very complex (see Figure 3.8). When compared to the same curve for HY parent zeolite (0 % TFA) (see Figure 3.7), it can be seen that, after the initial dehydration peak, when TFA is present, the baseline recovery is very much wiggly, making it very difficult to interpolate the baseline and identify the numerous peaks. The most likely interpretation results in the following characteristics :

- an endothermic peak in the temperature range 190 – 275°C (see Figure 3.8), that could be ascribed to the breakage of the bonding of chemisorbed TFA species,
- an exothermic peak in the range 275 – 325°C, which most likely, represents the reaction of the desorbed TFA species with the zeolite surface,
- an endothermic peak in the range 325 – 360°C that could result from the structural rearrangement of the zeolite surface following the reaction with desorbed TFA species,
- and, an exothermic peak in the range 360 – 480°C which results from the stabilization of the ZSM-5 structure upon heating at higher temperatures.

Following our work on the TFA incorporation onto HY zeolite, Nikolopoulos et al. (100) hypothesized that the increase in catalytic activity upon TFA loading could be ascribed to the presence of some extra framework Al species detected by ^{27}Al MAS-NMR, the latter species being extracted from the HY zeolite matrix by the corrosive action of strong superacid. However, at the present stage of research there is actually no experimental evidence supporting their hypothesis for the following reasons : (i) the optimal concentration of TFA incorporated of 3 % represented a relatively small amount used and the activation temperature applied in the following step was quite limited, i.e. 120°C, with respect to the thermal stability of HY zeolite, (ii) at the level of 3% TFA loading, the resulting catalyst did not undergo any significant structural collapse as evidenced by its almost unchanged degree of crystallinity, i.e. 99 % (see Table 3.7) and (iii) in case some framework Al atoms have been extracted from the zeolite matrix, a lower catalytic activity should be observed instead, because this amount of extra-framework Al atoms represented an equivalent loss in terms of Brønsted acid sites from the resulting catalyst. However, in their hypothesis, no qualitative evaluation of these extra-framework Al species has been given and the maximum yield of MTBE obtained by the authors corresponded to a 2 % TFA loading as compared to 3 % in our case.

3.2.2.2 Catalytic activity

For the HY / 3 % TFA catalyst which represents the best catalyst in terms of textural properties and catalytic activity, a series of experiments were carried out in order to determine the effects of contact time and reaction temperature on the MTBE and on the ETBE conversions. The catalytic results of MTBE synthesis are reported in Tables 3.9 and 3.10, and on Figure 3.9 and those of ETBE synthesis in Tables 3.11 and 3.12, and on Figure 3.10.

Figure 3.9 shows the yield of MTBE plotted versus contact time observed at 72 °C, 87 °C and 98 °C respectively. The best temperature for the MTBE production was 87 °C, with maximum yield in MTBE obtained at contact time 2.8 hr. At higher reaction temperatures, there was likely a competition between the formation and the decomposition of MTBE which significantly reduced the final yield of MTBE (88). The yield of C-8 by-products collected at 87 °C, which is also reported on figure 3.9, did not exceed 1.5 % C-atom at highest contact times. Oligomers of isobutene higher than C-8 (actually C-12) were observed and detected by GC-MSD only at reaction temperatures higher than 90°C. At the optimal reaction temperature of 87 °C, the production of dimethyl ether (DME) and other hydrocarbons was practically negligible (less than 1 % C-atom). Lower production of DME was also observed by Chang et al (93).

Figure 3.11 illustrates the formation of C-8 by-products as a function of reaction temperature for the H-ZSM5/ 3%TFA, H-Y and H-Y/ 3%TFA catalysts in

Table 3.9 : Yield of MTBE in % C-atom as a function of Contact Time obtained with HY - 3% TFA catalyst at 87 °C.

Reaction temperature (°C)	W.H.S.V. ($hour^{-1}$)	Contact Time (hour)	MTBE Yield (% C-atom)	C-8 Yield (% C-atom)
87	5.88	0.17	1.1	0.0
	3.85	0.26	1.4	0.0
	2.94	0.34	1.4	0.0
	2.63	0.38	1.9	0.0
	1.30	0.77	3.2	0.07
	0.62	1.62	6.7	0.1
	0.60	1.65	8.1	0.4
	0.47	2.15	22.1	0.5
	0.44	2.29	38.9	0.7
	0.40	2.51	40.6	1.5
	0.39	2.52	45.1	1.2
	0.38	2.64	44.3	1.3
	0.37	2.72	42.9	1.1
	0.36	2.81	47.8	1.39
	0.34	2.93	45.8	1.45
	0.33	3.05	45.0	1.3
	0.32	3.10	39.8	0.9

Table 3.10 : Yield of MTBE in % C-atom as a function of Contact Time obtained with HY - 3% TFA catalyst at 72 °C and 98 °C.

Reaction temperature (°C)	W.H.S.V. ($hour^{-1}$)	Contact Time (hour)	MTBE Yield (% C-atom)	C-8 Yield (% C-atom)
72	2.78	0.36	0.7	0.0
	1.30	0.77	1.1	0.0
	0.60	1.66	1.9	0.0
	0.40	2.48	18.5	0.42
	0.34	2.93	30.9	0.68
98	3.13	0.32	1.6	0.0
	2.13	0.47	2.4	0.0
	1.67	0.60	2.9	0.02
	1.28	0.78	3.9	0.04
	0.39	2.59	15.8	0.18
	0.36	2.78	35.6	0.34
	0.35	2.84	27.2	0.22

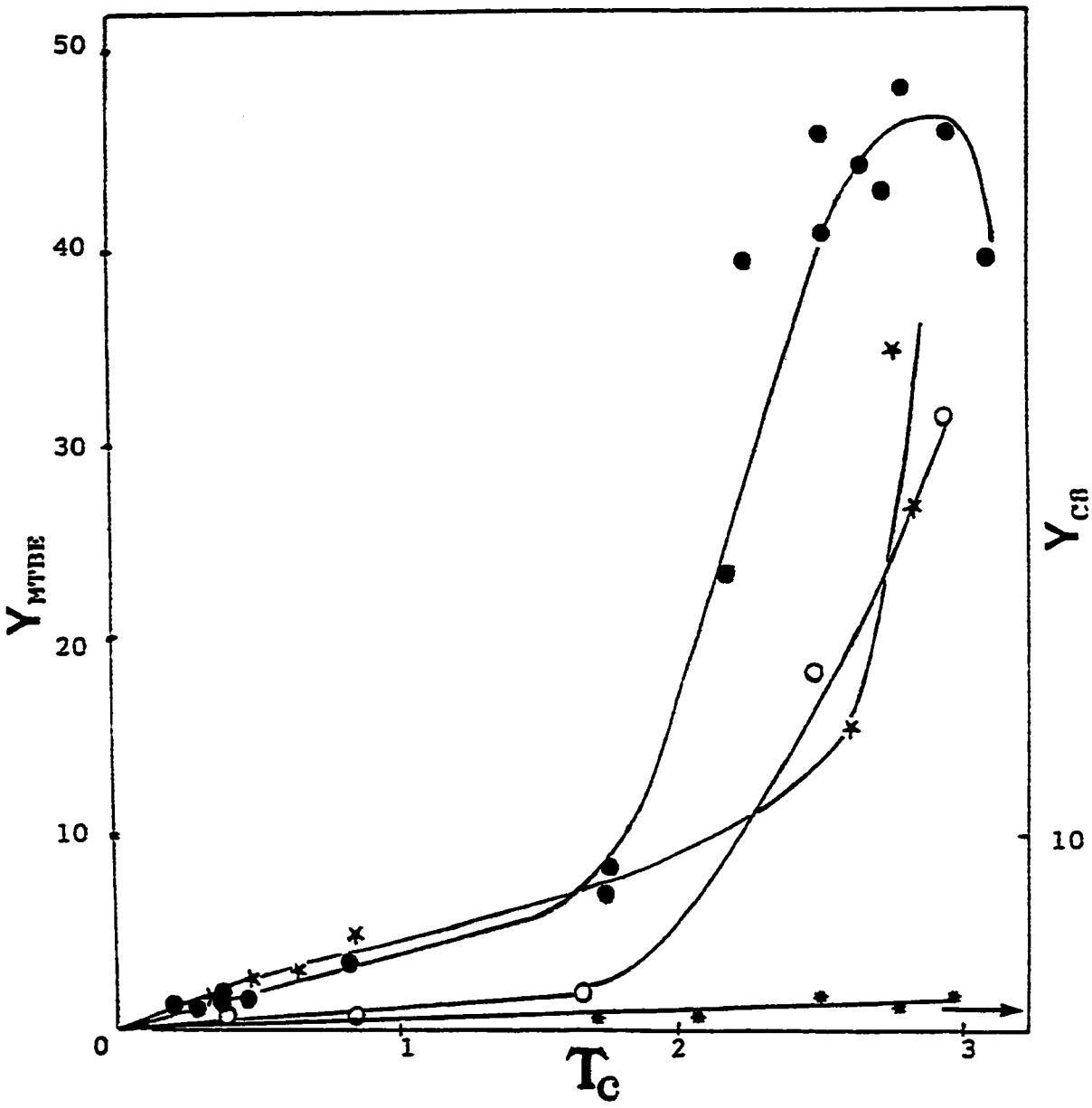

Figure 3.9 : Yield of MTBE in % C-atom versus contact time T_c in hour at (○) = 72°C, (●) = 87°C and (★) = 98°C obtained with HY/ 3% TFA catalyst. (*) = Yield of C8 by-products at 87°C

Table 3.11 : Yield of ETBE in % C-atom as a function of Contact Time obtained with HY - 3% TFA catalyst at 90 °C.

Reaction temperature (°C)	W.H.S.V. ($hour^{-1}$)	Contact Time (hour)	ETBE Yield (% C-atom)	C-8 Yield (% C-atom)
90	2.33	0.43	1.5	0.0
	1.52	0.66	8.7	0.04
	1.27	0.79	13.2	0.15
	1.11	0.90	13.0	0.0
	1.09	0.92	13.6	0.0
	1.05	0.95	12.3	0.0
	1.02	0.98	11.5	0.0
	0.79	1.26	16.0	0.15
	0.65	1.53	18.7	0.26
	0.63	1.59	18.5	0.5
	0.47	2.13	25.3	0.17
	0.44	2.25	21.3	0.02
	0.41	2.43	33.6	1.1
	0.39	2.55	25.7	0.3
	0.38	2.64	22.4	0.5
	0.36	2.75	22.8	1.2
	0.35	2.79	21.5	0.4
	0.34	2.86	21.3	0.6
	0.33	3.02	20.4	1.5
	0.32	3.11	22.6	0.9

Table 3.12 : Yield of ETBE in % C-atom as a function of Contact Time obtained with HY - 3% TFA catalyst at 82 °C and 105 °C.

Reaction temperature (°C)	W.H.S.V. ($hour^{-1}$)	Contact Time (hour)	ETBE Yield (% C-atom)	C-8 Yield (% C-atom)
82	1.79	0.56	1.1	0.03
	1.28	0.78	1.4	0.01
	0.37	2.73	6.7	0.15
	0.33	3.03	13.9	0.24
	0.18	5.58	15.3	0.51
105	5.00	0.20	1.1	0.0
	2.17	0.46	2.3	0.0
	1.47	0.68	2.5	0.01
	1.14	0.88	7.0	0.0
	0.57	1.74	19.4	0.42
	0.45	2.21	20.4	0.76
	0.43	2.30	15.1	0.52
	0.42	2.38	12.6	0.18

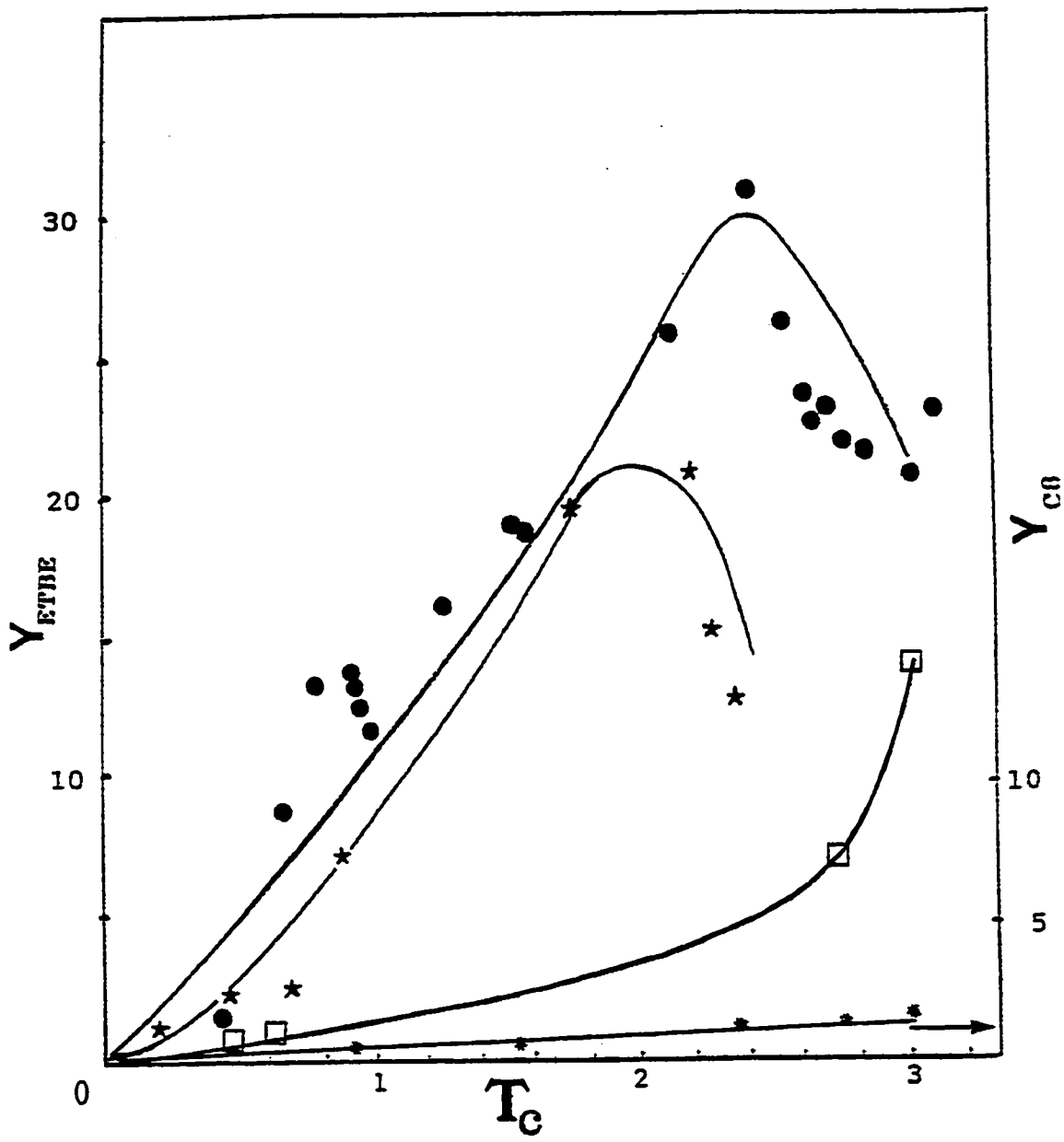

Figure 3.10 : Yield of ETBE in % C-atom versus contact time T_c in hour at (□) = 82°C, (●) = 90°C and (★) = 105°C obtained with HY/ 3% TFA catalyst. (*) = Yield of C8 by-products at 90°C

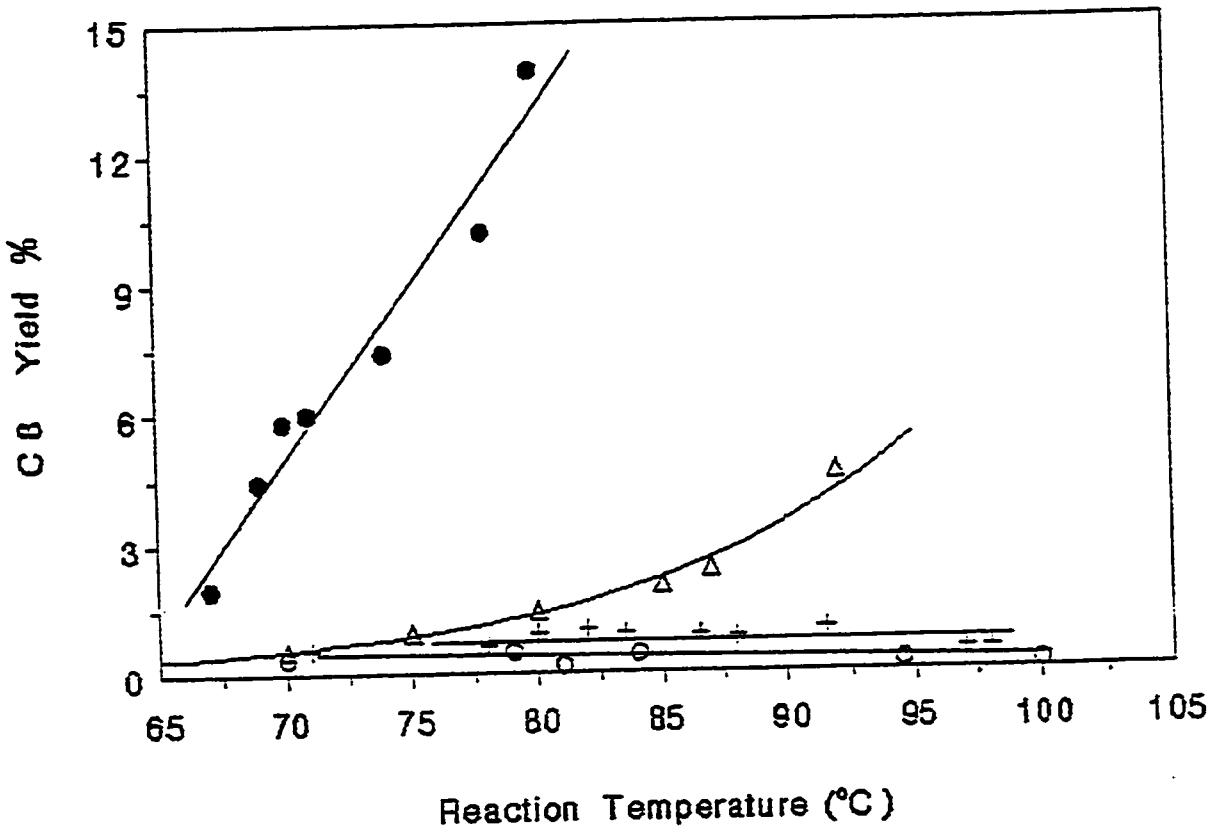

Figure 3.11 : C-8 by-products yield in % C-atom versus reaction temperature (°C), obtained with the Amberlyst-15 (•), the H-Y / 3 % TFA (+), the H-Y (Δ), and the H-ZSM-5/3 % TFA (O) catalysts in the MTBE synthesis.

comparison with the commercial A-15 resin. For the catalysts not containing TFA, a general trend of gradual increase in the formation of C-8 by-products with reaction temperature is observed. This can be attributed to a higher amount of isobutene available resulting from the reverse reaction of MTBE decomposition at high temperatures. However this gradual increase was more important with the A-15 resin due to its large mesopore structure (25-35 nm) but was much less pronounced for the zeolite based catalysts because of their smaller micropore system of which pore diameter ranges from 5.2 to 7.4 Å. As expected, the lowest production of C-8 by-products is obtained with TFA loaded H-Y and H-ZSM5, as compared to the parent H-Y zeolite, and this can be attributed to the pore narrowing effect by the TFA molecules which imposed a space constraint on the formation of such bulky C-8 dimers.

In terms of catalyst stability, runs totaling more than 50 hours carried out at 87 °C with contact time 2.6 hr and a methanol / isobutene feed ratio of 1.2 showed no significant loss (less than 5 %) of catalytic activity.

Since the HY / 3% TFA catalyst showed an important enhancement of catalytic activity for the MTBE synthesis, with no significant production of C-8 by-products, it was decided to perform a series of catalytic testings for the ETBE synthesis using this successful catalyst. ETBE is a related compound of MTBE with very similar antiknock properties. Although not widely produced at the present time (6b) for economic reasons, ETBE will undoubtedly gain in

importance in the near future, owing to recent advances in ethanol production from biomass, that will lower markedly the price of ethanol (98).

The same trends (maximum activity with respect to reaction temperature and contact time) were observed for the ETBE synthesis. The maximum ETBE yield observed at 90 °C for a contact time of 2.4 hr is reported in Figure 3.10. However, the maximum yield of ETBE obtained (33.6 %) is much lower than that of MTBE (47.8 %) because of the parallel and competitive reaction with ETBE formation, namely the dehydration of ethanol to diethyl ether. The expected consequence of this side reaction is a significant decrease in the amount of adsorbed ethanol, normally available for the synthesis of ETBE, which underwent dehydration to form diethyl ether (DEE). The important yield of DEE produced from ethanol dehydration compared to the negligible amount of dimethyl ether derived from methanol condensation in MTBE synthesis could be ascribed to its low activation energy (85), i.e. 56 kJ /mol. Another reason for the significantly high yield of DEE observed could be the steric factor of these relatively large ethanol molecules (with respect to methanol) which tends to hinder the diffusion of bulky isobutene molecules within the zeolite channel system, once preferentially adsorbed onto the inner zeolite pore wall by their polar character (with respect to isobutene molecules). This unbalanced population of reactants on the zeolite surface increased the likelihood of the ethanol molecules residing together, making them more prone to react with each other through the

dehydration pathway and thereby affecting the etherification reaction. The same phenomenon was much less likely to occur in the case of MTBE synthesis where smaller methanol molecules can diffuse away from one another, resulting in a negligible amount of dimethyl ether being detected.

In ETBE synthesis, at reaction temperatures higher than 80 °C, some hydrocarbons (HC*) from C-1 to C-11 other than C-8 and higher oligomers of isobutene were produced (see Table 3.13), mainly at high contact times as shown in Figure 3.12. As illustrated in this figure, the opposite trends of formation of diethyl ether and of hydrocarbons (HC*) versus contact time, observed for two different reaction temperatures, suggests that these hydrocarbons (HC*) are derived from diethyl ether. These data is in good agreement with earlier results obtained by R. Le Van Mao et al. in a study of the dehydration of ethanol (86). It is also worth noting that in both the MTBE and ETBE synthesis, the yields of C-8 hydrocarbons resulting from the acid-catalyzed dimerization of isobutene were, as expected, practically similar.

To remedy to the undesired effects of these side reactions, the dilution of the ethanol feed with different concentrations of water was studied. The results reported in Table 3.14 showed that for the feed concentration of ethanol / water of 1:9, there was a drastic reduction of the formation of diethyl ether and hydrocarbons (HC*), and to a lesser extent the production of C-8 dimers of isobutene. However, at this dilution there was also a decrease, although more

Table 3.13 : Yield of Diethyl Ether (DEE) and Hydrocarbons other than oligomers of isobutene (HC*) in % C-atom as a function of Contact Time obtained with HY - 3% TFA catalyst at 90 °C and 105 °C in the synthesis of ETBE.

Reaction temperature (°C)	W.H.S.V. ($hour^{-1}$)	Contact Time (hour)	DEE Yield (% C-atom)	HC* Yield (% C-atom)
90	4.76	0.21	16.8	0.3
	3.03	0.33	20.8	0.4
	1.75	0.57	25.2	0.4
	1.04	0.96	19.8	4.4
	0.82	1.22	15.2	6.3
	0.59	1.69	5.6	8.8
	0.50	2.00	2.8	10.8
	0.38	2.61	2.2	11.2
105	2.44	0.41	4.36	3.4
	1.61	0.62	6.30	5.2
	1.06	0.94	4.48	6.8
	0.66	1.51	1.08	10.3
	0.42	2.39	0.50	13.6

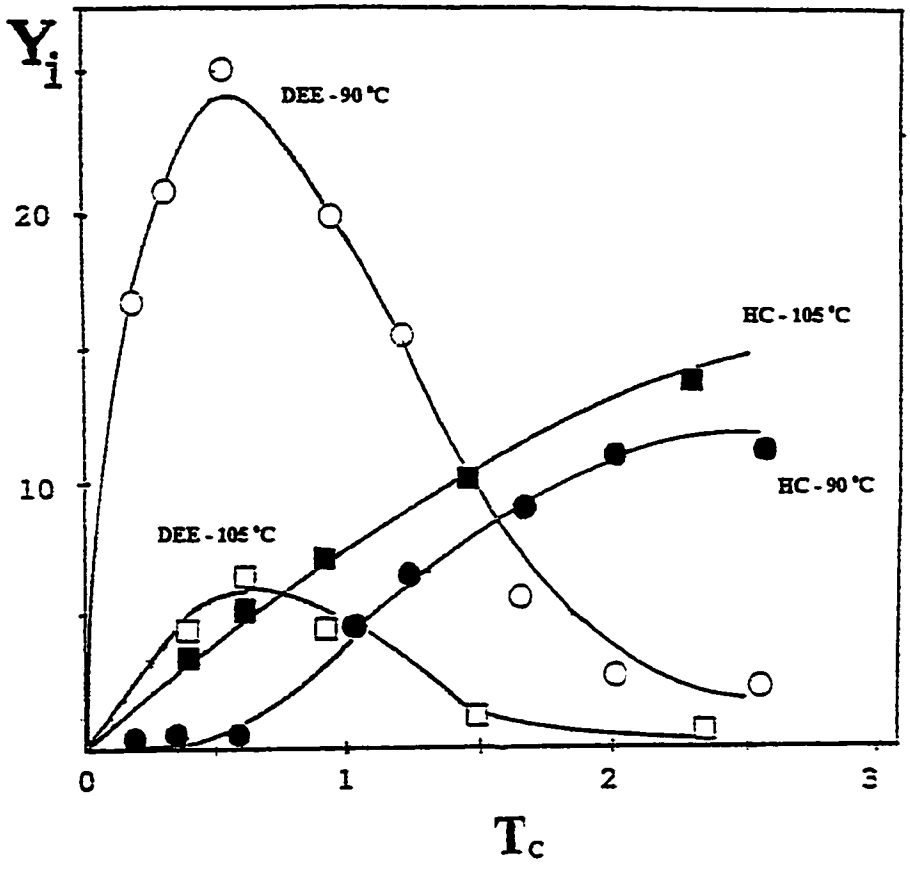

Figure 3.12 : Yield of Diethyl Ether and Hydrocarbons (other than oligomers of isobutene) in % C-atom versus contact time T_C (in hour) obtained at different reaction temperatures with the HY/3% TFA catalyst in the ETBE synthesis.

For i = DEE : ○ = 90 °C and □ = 105 °C

For i = HC : ● = 90 °C and ■ = 105 °C

Table 3.14 : Effect of the dilution of feed ethanol with water in the synthesis of ETBE on the HY / 3% TFA catalyst.

Reaction conditions :

- Temperature : 90 °C
- Contact time : 1.5 hour
- Ethanol / Isobutene ratio : 1.2

Feed	Y_{ETBE}	Y_{DEE}	Y_{C8}	Y_{HC*}
100 % Ethanol	20	11	0.6	10
50 vol % Ethanol / 50 vol % water	22	8	0.5	8 **
10 vol % Ethanol / 90 vol % water	16	1	0.2	0.5 **

Y_i : Yield of product i in % C-atom

Y_{HC*} : Yield in $C_1 - C_{11}$ Hydrocarbons excluding the isobutene oligomers.

** : mostly ethylene.

moderate, (by only 20 %) of the yield of ETBE, which is due to a strong competition between water and ethanol molecules for adsorption on the zeolite surface acidic sites.

3.2.2.3 Kinetic studies

A kinetic study was carried out on the successful HY / 3% TFA catalyst for which high catalytic activities for the synthesis of MTBE and ETBE were observed.

According to Hill (94), for any heterogeneous catalytic reaction, several physical and chemical steps take place in an orderly sequence as follows :

- mass transfer of the reactants from the main body of the fluid to the exterior surface of the catalyst particles,
- molecular diffusion of the reactants from the exterior surface of the catalyst particle into the interior pore structure,
- chemisorption of the reactants on the catalyst surface,
- reaction on the catalyst surface involving several steps,
- desorption of chemically adsorbed species from the surface of the catalyst,
- transfer of the products from the interior of the catalyst pores to the external surface of the catalyst particles by molecular diffusion,
- mass transfer of the products from the exterior surface of the particles into the bulk of the fluid.

In order to evaluate the apparent activation energy, some assumptions were made (94a). First, the mass transfer of reactant species between the catalyst particles and the bulk of fluid was not a limiting step in the process and therefore could be neglected. Detailed kinetic studies on different types of acid-catalyzed reactions carried out in our laboratory on several zeolite catalysts by R. Le Van Mao et al (94b) have confirmed that the influence of the above mentioned mass transfer of reactants has practically no effect on the catalytic activity. Second, the molecular diffusion of reactants and products, the energy of which was considered to be small under the present operating conditions regarding the flow rate and reaction temperature, was assumed to be negligible and thus was not taken into account. Hence, the whole catalytic process depended essentially on the adsorption, the reaction itself and the desorption step. The etherification reaction (of both MTBE and ETBE) as well as the adsorption step are exothermic while desorption is endothermic. The apparent activation energy can be expressed as follows :

$$E_{app} = E_{ads} + E_{rxn} - E_{des}$$

In general, the activation energy of a reaction can be determined according to the Arrhenius equation, if the reaction rate at various temperatures are known :

$$k = A \exp (- E_a / RT) \qquad (3.1)$$

where k is the rate constant,

A the pre-exponential factor,

R the universal gas constant, and

T the reaction absolute temperature (in K).

In the gas phase synthesis of MTBE, the reaction rate could be expressed as follows :

$$r = k\,[Iso]^n\,[MeOH]^m \qquad (3.2)$$

where [Iso] and [MeOH] represent the molar concentrations of isobutene and methanol respectively. Assuming that gaseous reactants behave like ideal gases :

$$P_i\,V = n_i\,R\,T$$

the concentration of each gaseous reactant i will be :

$$[\,i\,] = n_i\,/\,V = P_i\,/\,R\,T$$

Then, equation (3.2) can be rearranged as follows :

$$r = k\,(P_{Iso})^n\,(P_{Me})^m\,/\,(RT)^{n+m} \qquad (3.3)$$

where r is the reaction rate,

k the rate constant,

P_{Iso} the partial pressure of isobutene,

P_{Me} the partial pressure of methanol, and

n, m are the orders of reaction of isobutene and methanol respectively.

In the present case, for bimolecular reactions where two reactants (isobutene and methanol) are involved, the reaction rate could be expressed by the consumption rate of either reactants :

$$r = -\,d\,[Iso]\,/\,dt = -\,d\,[MeOH]\,/\,dt$$

In kinetic investigations for a static system, t usually represents the reaction time over which the variation of reactant concentrations is followed. However, in a catalytic reaction where a plug flow system is involved, t represents the contact time for the reaction which is the average time that a reactant molecule takes to pass through the catalyst bed.

In this work, since the conversion to MTBE product was determined from the initial concentration of isobutene converted, the reaction rate is the normal rate of consumption of isobutene, and it could also be expressed as follows as a function of contact time (t) :

$$r = -d[Iso]/dt = -1/RT \times d P_{Iso}/dt \qquad (3.4)$$

where [Iso] is the concentration of isobutene,

and P_{Iso} the partial pressure of isobutene.

P_{Iso} may also be expressed as a function of C_t , the isobutene C-atom percent conversion to MTBE, as follows :

$$P_{Iso} = (100 - C_t)\, P^{o}_{Iso}$$

where P^{o}_{Iso} is the initial partial pressure of isobutene.

Thus, $d P_{Iso}/dt = - P^{o}_{Iso}\, dC_t/dt \qquad (3.5)$

From (3.5), the general form of reaction rate (3.1) becomes :

$$r = P^{o}_{Iso}/RT \times dC_t/dt$$

$$r = K_1 (dC_t/dt)$$

where the constant $K_1 = P^{o}_{Iso}/RT$

Therefore, the initial reaction rate r_o, defined at contact time t = 0, is given by

$$r_o = r_{t=0} = K_1 \, (dC_t / dt)_{t=0} \qquad (3.6)$$

However, according to (3.3) the initial rate r_o could be expressed as :

$$r_o = k \, (P^o_{Iso})^n \, (P^o_{Me})^m \, / (RT)^{n+m}$$

where P^o_{Me} is the initial partial pressure of methanol.

By substituting the expression of rate constant k from the Arrhenius equation in (3.1), the initial rate becomes :

$$r_o = (P^o_{Iso})^n \, (P^o_{Me})^m \, / (RT)^{n+m} \times A \, \exp(-E_a / RT)$$

$$r_o = K_2 \, A \, \exp(-E_a / RT) \qquad (3.7)$$

with constant $K_2 = (P^o_{Iso})^n \, (P^o_{Me})^m \, / (RT)^{n+m}$

A series of catalytic MTBE and ETBE reactions were carried out at different temperatures and at various contact times approaching the time $t_o = 0$, for which initial conversion rates of isobutene to the corresponding ether were taken into account for the determination of the apparent activation energy. The results of MTBE and ETBE conversions versus contact time at different reaction temperatures are reported in Tables 3.15, 3.16 and plotted on Figures 3.13 and 3.1.4. For each set of etherification reactions performed at a given temperature, the experimental results expressed in terms of isobutene C-atom percent conversion (C_t) were fitted to a function f(t) of contact time t, using a non-linear regression algorithm from the software "Slidewrite Plus" (95). The fitting function f(t)

Table 3.15 : Yield of MTBE at various contact times and reaction temperatures on the HY- 3% TFA catalyst.

Reaction temperature (°K)	Contact time T_c (hour)	MTBE Yield (% C-atom)	Initial rate* r_o (% C-atom $hr^{-1}.g^{-1}$)
343	0	0	1.13
	0.36	0.7	
	0.77	1.1	
	1.06	1.1	
	1.53	1.9	
360	0	0	4.54
	0.26	1.1	
	0.34	1.4	
	0.38	1.9	
	0.77	3.2	
	1.62	6.7	
	1.65	8.1	
369	0	0	4.96
	0.32	1.6	
	0.47	2.4	
	0.60	2.9	
	0.78	3.9	

(*) : r_o obtained by extrapolation of $T_c \rightarrow 0$.

Table 3.16 : Yield of ETBE at various contact times and reaction temperatures on the HY-3% TFA catalyst.

Reaction temperature (°K)	Contact time T_c (hour)	MTBE Yield (% C-atom)	Initial rate* r_o (% C-atom $hr^{-1}.g^{-1}$)
338	0	0	0.32
	0.74	0.2	
	1.06	0.3	
	1.52	0.5	
355	0	0	2.51
	0.56	1.1	
	0.78	1.4	
	2.73	6.7	
364	0	0	11.13
	0.60	1.4	
	0.79	7.7	
	0.90	12.9	
	1.12	12.9	
	1.89	19.3	

(*) : r_o obtained by extrapolation of $T_c \rightarrow 0$.

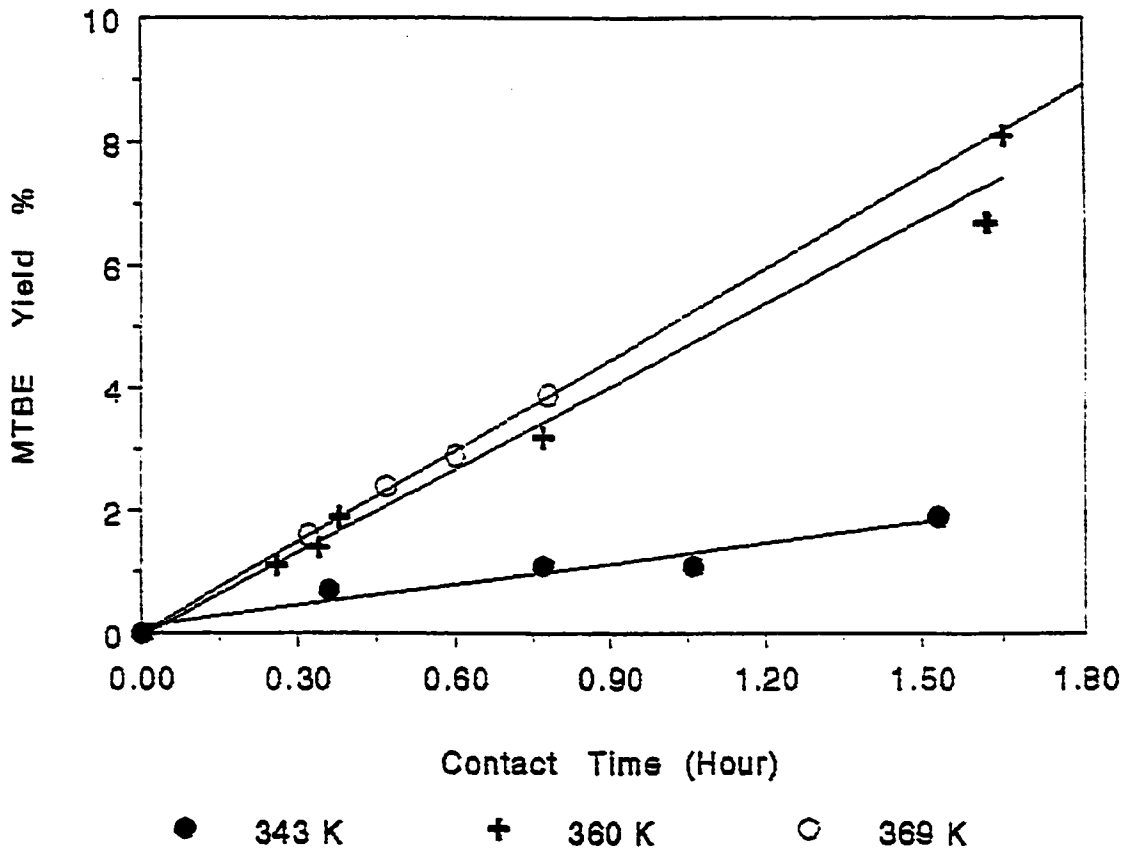

Figure 3.13 : MTBE Yield (in % C-atom) as a function of contact time T_c in hours at different reaction temperatures (K).

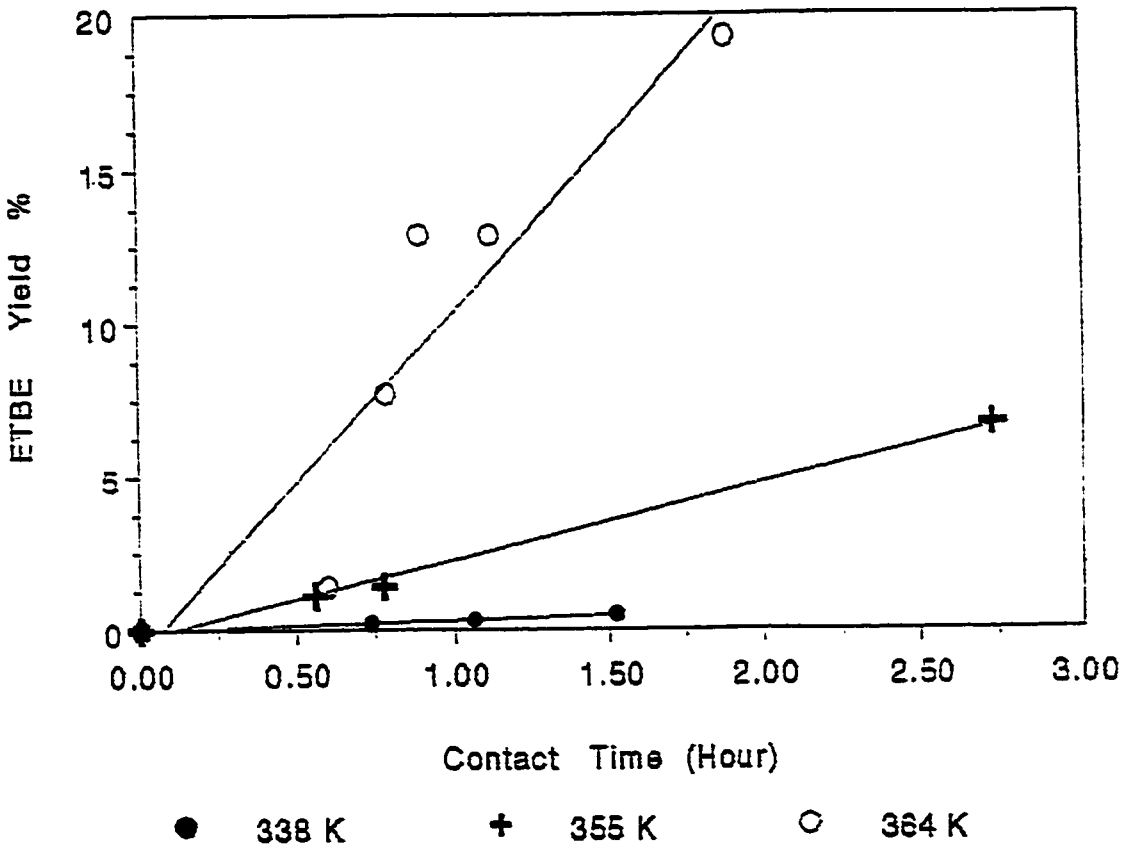

Figure 3.14 : ETBE Yield (in % C-atom) as a function of contact time T_c in hours at different reaction temperatures (K).

providing the best correlation factor was a third-order polynomial function in the form :

$$C_t = a + b\,t + c\,t^2 + d\,t^3$$

where a, b, c, d are constants with constant a being equal to zero, since no conversion was possible ($C_t = 0$) at zero contact time ($t = 0$) when the reactants were not in contact yet with the catalyst.

Then the initial reaction rate was determined by taking the derivative of the fitting function f(t) and extrapolating the conversion C_t to zero contact time,

$$r_o = \lim_{t \to 0} \frac{d[C_t]}{dt} = \lim_{t \to 0} \frac{d[f(t)]}{dt}$$

which then gave a constant value b, owing to the linearity of experimental C_t versus contact time t :

$$r_o = b \qquad (3.8)$$

The initial reaction rate of MTBE synthesis at each temperature is reported in Table 3.1.5 and that of ETBE in Table 3.16.

From equations (3.7) and (3.8),

$$r_o = b = K_2\, A\, \exp(-E_a / RT)$$

$$r_o = A'\, \exp(-E_a / RT)$$

where the constant $A' = K_2\, A$

Finally,

$$\ln r_o = \ln A' - E_a / RT$$

The value of the apparent activation energy E_{app} was evaluated from the plot of $\ln r_o$ versus $10^3/T$, which gave a straight line having a slope $-E_a/10^3$ R. As illustrated in Figure 3.15 for both ethers, satisfactory correlation factors of 0.97 and 0.995 were found for MTBE and ETBE plots respectively.

The estimated apparent activation energy for MTBE was 64.3 ± 6 kJ/mol, a value comparable to those found in the literature for the A-15 resin, ranging from 71 kJ / mol (12) to 82 kJ/mol (88). For an acid in solution, methyl sulfuric acid and paratoluene sulfonic acid, a higher value 91 kJ/mol has been reported. As pointed out by Gicquel and Torck (88), lower values of apparent activation energy were partly due to diffusion limitations of reactants within the pore and channel network. Another possible cause for this lowering of E_{app} stems from the saturation of the active sites on zeolite surface by methanol molecules (88) with respect to isobutene because of their smaller size and their higher polarity (when compared to both isobutene and ethanol molecules). The resulting unbalance in the population of the species of the two reactants at the vicinity of the active sites resulted in a lower MTBE conversion at small contact time, hence the expected lowering of the estimated value of E_{app}. This phenomenon which was normally less pronounced in the case of ETBE for the aforementioned reasons was exemplified partly by its higher value of E_{app} .

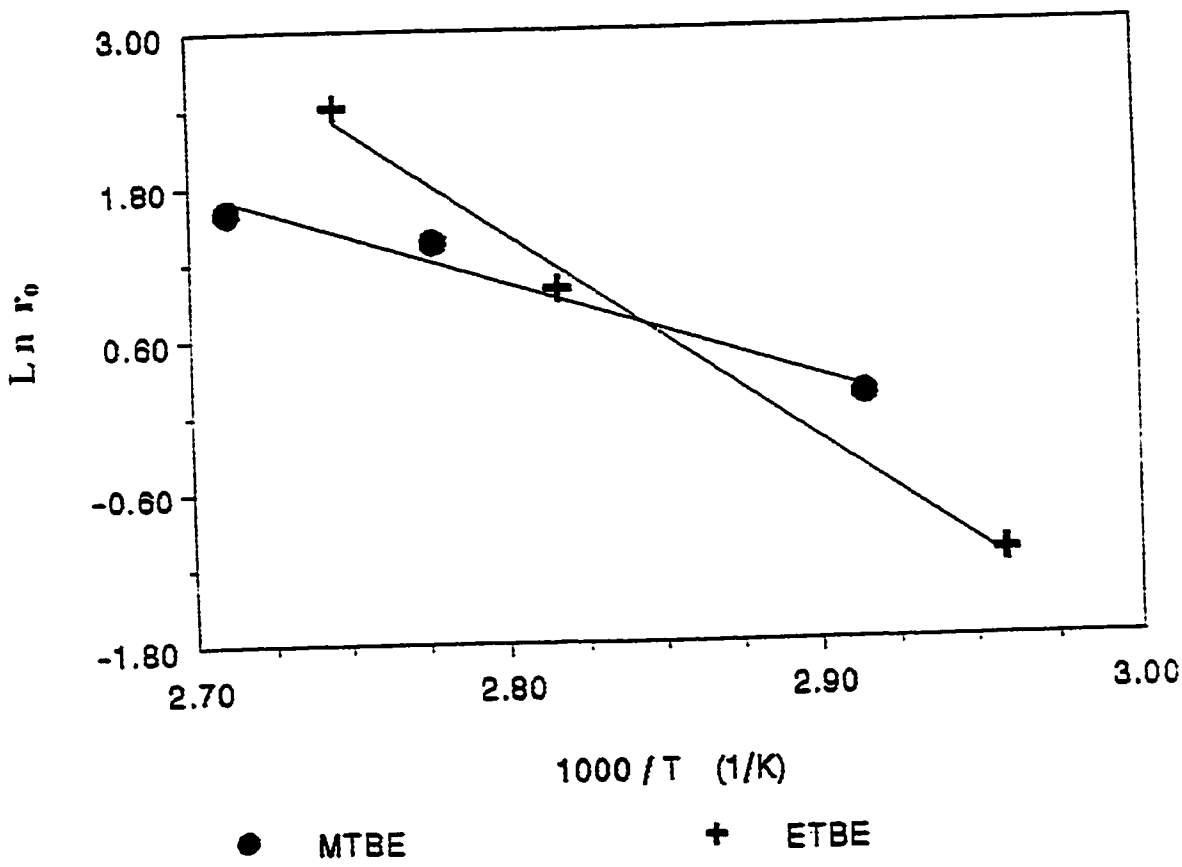

Figure 3.15 : Arrhenius plot of the initial rates (in % C-atom hr^{-1} g^{-1}) of MTBE (●) and ETBE (✚) obtained with the H-Y / 3% TFA catalyst.

For ETBE, the value obtained for the apparent activation energy of 133.4 ± 15 kJ/mol was relatively high because of the presence of competitive reactions such as the dehydration of ethanol to diethyl ether (already significant at 90 °C) and probably the ETBE decomposition at high temperatures. The resulting lower concentration of ethanol available for the ETBE synthesis was likely the direct cause of such a high apparent activation energy (88). In the literature a lower apparent activation energy (82 kJ/mol) was reported for ETBE synthesis (96) performed on a smaller pore sized H-Mordenite (0.67 × 0.70 nm). This moderate E_{app} value contributed to confirm the general trend mentioned above in the case of MTBE by Gicquel and Torck (88), and also to validate the relatively high E_{app} found in this work for a larger pore diameter (0.74 nm for the micropore system in addition to the 4 nm mesopore system) Y-type zeolite.

The comparable range of E_{app} estimated in this work with respect to those found in the literature, the relatively low range of temperatures used for the acquisition of kinetic data as well as the very straight line obtained for the Arrhenius plot constituted a good indication of the quasi absence of mass transport limitations within the TFA doped HY catalyst.

3.2.3 Conclusion

The incorporation of an organic superacid (TFA) in moderate concentration (3 % wt.) into the large pore Y-type zeolite represents a successful method of

increasing the total acidity of zeolite catalysts. It results in a remarkable enhancement of the catalytic activity in MTBE gas phase synthesis to the level similar to that of the commercial A-15 resin with a negligible production of undesirable by-products (see Table 3.17). The best temperature corresponding to the maximum yield of MTBE was found to be 87 °C at contact times varying from 2.5 to 2.8 hours. The synthesis of ETBE, a close cousin and a potential rival to MTBE, carried out on the same catalyst and at similar reaction conditions did not yield the same performance as that observed for MTBE synthesis because of the parallel and competitive reaction of ethanol dehydration and the important production of hydrocarbons other than oligomers of isobutene occurring at high reaction temperatures.

However the incorporation of such an organic superacid (TFA) onto the medium pore sized ZSM-5 zeolite did not produce a significant catalytic activity increase as that observed with the Y-type zeolite. The reason is the pore narrowing effect resulting from the loading of bulky TFA species within the small pore and channel network of ZSM-5 which hindered the diffusion of reactants and products. The temperature required for the maximum MTBE yield was about the same as with the Y-type zeolite.

Nevertheless ZSM-5 still represents an attractive zeolite matrix for its high chemical and thermal stability and mainly for its interesting shape selectivity

Table 3.17 : Maximum yield of MTBE obtained with the TFA loaded zeolites.

Catalyst	Amberlyst-15	HZSM-5 / 3 % TFA	H-Y / 3 % TFA
Reaction Temperature (°C)	70	85	87
MTBE Yield (% C-atom)	47.5	40.8	46.1
C-8 Yield (% C-atom)	4.4	0.2	0.4
Selectivity to MTBE (%)	91.5	99.5	99.1

(99.5 %, see Table 3.2.4) in the gas phase synthesis of MTBE even at a low methanol / isobutene feed ratio (99a).

In the next sections, we will focus our efforts either on improving the acid strength of ZSM-5 zeolite by incorporation into its structure suitable sized guest molecules having strong acidic properties or on increasing its acid density by the controlled modification of the framework Si content.

3.3 Fluorinated ZSM-5 zeolite

The incorporation of fluorine based organic superacid i.e. triflic acid has shown an important increase in catalytic activity mainly with large pore Y-type zeolite with no significant production of isobutene dimers and oligomers. However the incorporation of such a superacid did not produce any significant activity enhancement for the medium pore sized ZSM-5 zeolite which is characterized by an excellent shape selectivity in the gas phase synthesis of MTBE (99a). According to recent investigation studies from A. Kogelbauer et al., the dealumination of zeolites that resulted from the triflic acid loading on HY zeolite appeared to be the main cause of such a catalytic activity enhancement (99b).

In this section, are described investigations of the incorporation of fluoride species as electron withdrawing compounds onto the ZSM-5 matrix for its superior characteristics mentioned earlier and especially for the promising prospect of this method in increasing the surface acidity of zeolite catalysts (101a). Previous work done by A. Kogelbauer et al. using this method with HY zeolite have shown that "fluoride modification did not result in an MTBE synthesis activity enhancement unless it was coupled with a high temperature activation process" (101). However in their catalyst preparation procedure, only a unique activation temperature i.e. 400°C was applied to the whole series of fluoride incorporated catalysts and the result was simply "a monotonous increase in catalytic activity with increasing fluoride ions concentration " (100).

In addition, unlike the bulky triflic acid molecules which created steric constraints within the medium pore system of ZSM-5 zeolite, the ammonium fluoride precursors used in this method were much smaller and thus were not subjected to any steric hindrance in the diffusion through ZSM-5 structure. Owing to their smaller size, NH_4F precursors can be distributed more homogeneously within the whole ZSM-5 pore and channel structure.

In this study the emphasis was placed on the effect of the amounts of NH_4F precursors incorporated and particularly on the influence of the final activation temperatures used, which constitutes the key factor of the new catalytic behavior observed with fluoride modified ZSM-5 catalysts. A mechanism of the zeolite surface modification as a function of the final activation temperature is proposed based on the coherent set of data collected from different characterization techniques. The proposed mechanism serves as basis for rationalizing the observed catalytic activity in correlation with the temperature modified surface acidity.

3.3.1 Characterization studies

3.3.1.1 Physico-chemical properties of the untreated parent zeolites

The results of characterization studies of the untreated zeolites (parent sodium form and acid form) are compiled in Tables 3.18 and 3.19. Chemical analysis results reported in Table 3.18 showed no significant change in the Si/Al molar ratio after the ion-exchange of the as purchased Na-ZSM5 to generate the

Table 3.18 : Chemical composition of the untreated zeolites (powder form, activated at 450 °C overnight) in wt % on the dry oxide basis.

Sample	SiO_2 (wt %)	Al_2O_3 (wt%)	Na_2O (wt%)	Si/Al
Na-ZSM5	93.6	3.9	2.49	20.5
H-ZSM5	96.0	3.9	0.18	21.0

Table 3.19 : Physico-chemical properties of the untreated zeolites (powder form, activated at 450 °C overnight)

Sample	Si/Al	Degree of crystalinity (%)	BET surface area (m^2/g)	
			Total	Micropores
Na-ZSM5	20.5	100	332	254
H-ZSM5	21.0	93	364	267

parent acid form H-ZSM5 zeolite. The latter constituted the starting material for fluoride incorporation studies in this work. The crystallinity of the as purchased Na-ZSM5 zeolite is taken arbitrarily as being equal to 100 %. A minor decrease (7 %) of the degree of crystallinity was observed upon conversion to H-ZSM5 (see Table 3.19). The slight increase of the BET total surface area of the H-ZSM5 with respect to the Na-ZSM5 zeolite was probably due to the leaching of intraporous amorphous materials remaining from the zeolite synthesis which occurred within the Na-ZSM5 (101b). The micropore surface area of the obtained acid form H-ZSM5 zeolite were quite comparable with that of the parent sodium form Na-ZSM5.

3.3.1.2 Physico-chemical properties of the fluoride modified zeolites

The characterization results of fluoride incorporated H-ZSM5 are reported in Table 3.20. It can be seen that for concentrations of ammonium fluoride loading up to 2.60×10^{-3} mol / g zeolite, there was little loss of crystallinity and of the BET surface area, for both the total surface area and the micropore surface area as compared to the parent H-ZSM5 zeolite. This indicated that, within the chosen NH_4F concentration range, and at the final activation temperature of 450°C, the structure of the ZSM5 zeolites remained preserved. At the NH_4F concentration of 2.60×10^{-3} mol / g zeolite a slightly larger decrease in micropore surface area and crystallinity degree were observed. However, at higher NH_4F concentrations,

Table 3.20 : Physico-chemical properties of the fluorinated ZSM-5 zeolites (extrudates with 10 wt % of bentonite), all activated at T_f = 450 °C.

Sample	Initial NH_4F loading (10^{-3} mol.g^{-1})	Degree of crystalinity (%)	BET surface area (m^2/g)	
			Total	Micropores
HZSM-5	0	100	328	238
H-ZSM5/F7	0.05	100	336	266
H-ZSM5/F4	1.00	100	336	248
H-ZSM5/F3	1.87	100	333	241
H-ZSM5/F5	2.60	99	313	224
H-ZSM5/F6	3.10	88	314	207
H-ZSM5/F6*	3.10	87	313	196

(*) activated at 500 °C overnight

regardless of whether the fluorinated catalyst was activated at 450°C or 500°C, there was a serious loss in the degree of crystallinity and a significant decrease in the micropore surface area, which are indicative of the partial structural collapse of the resulting zeolite material. The latter effect was the expected consequence of a combined action of a high NH_4F loading and a relatively high thermal activation.

Table 3.21 reports the concentration of the actual fluoride ions incorporated into the zeolite catalyst, determined by use of a fluoride-ion selective electrode technique, as a function of the activation temperature for two NH_4F concentrations F3 and F6. These results showed maximum amounts of fluoride ions incorporated in the activation temperature range 400°C to 450°C for F3 and 450 °C for F6. This indicates that the insertion of an optimal amount of fluoride ions into the ZSM-5 structure according to our fluorination procedure was satisfactorily achieved at 400 - 450°C. The lower F^- content obtained at 500°C was ascribed to the partial removal of the inserted fluoride ions to form fluoro-complexes of Si and Al (109) when the catalyst was submitted to high activation temperature.

The lowest F^- content recorded at 325°C does not really reflect the actual F^- ions inserted into the zeolite structure. In fact when the F3 / 325°C catalyst sample was submitted to F^- ions analysis it was first calcined at 750°C before the acid treatment. Thus, part of the HF chemisorbed at 325°C was accidentally inserted onto the zeolite structure in very short period of time under the sufficiently high activation temperature of the calcination step and then part of these recently

Table 3.21 : Variation of Fluoride content with the initial ammonium fluoride loading and the final activation temperature.

Catalyst	Initial NH_4F loading (10^{-3} mol.g^{-1})	Final activation temperature (°C)	F^- content * (wt.%)
H-ZSM5	0	450	0
H-ZSM5/F3	1.87	325	2.4
H-ZSM5/F3	1.87	400	2.8
H-ZSM5/F3	1.87	450	2.7
H-ZSM5/F3	1.87	500	2.2
H-ZSM5/F6	3.10	450	4.3

(*) : as determined by fluoride selective electrode analysis.

inserted F^- ions were rapidly extracted from zeolite debris. The result was a low amount of F^- ions measured. As a matter of fact, it was shown by R.B. Borade et al. that the effective incorporation of F^- ions into β-zeolite actually starts at ca. 450°C (109).

The highest amount of incorporated fluoride ions was found for the highest (F6) concentration. At the activation temperature of 450°C, there were practically equal fractions of fluoride ions actually inserted (ca. 76 % and 73 %) onto the zeolite structure as reported for both of the two NH_4F concentrations F3 and F6, which indicated that our procedure of ammonium fluoride incorporation and thermal activation as well as the fluoride ions analysis were reliable and reproducible.

3.3.1.3 FT-IR studies

In the following section, only the frequency shifts and absorbance maxima of FT-IR bands are reported. The corresponding FT-IR spectra are shown in appendix A-2. Table 3.22 reports the frequencies of the framework region for the F3 and F6 fluoride incorporated ZSM5 zeolites activated at different temperatures. These results show that for F3 concentration there is practically no change in the framework region frequencies when activated at 325°C, but at 450°C and 500°C there are slight shifts in frequencies towards higher values with respect to the parent zeolite. These frequency shifts are greater (+4 to +8 cm^{-1}) with the highest

Table 3.22 : FT-IR band position in the framework region. (resolution = 1 cm^{-1}).

Sample	Activation temperature (°C)	Wavenumber (cm^{-1})				
H-ZSM5	450	549	622	799	1103	1225
H-ZSM5/F3	325	550	624	799	1104	1227
H-ZSM5/F3	450	551	625	801	1104	1227
H-ZSM5/F3	500	551	625	801	1104	1228
H-ZSM5/F6	450	553	627	803	1105	1231
H-ZSM5/F6	500	553	627	803	1106	1232

Initial ammonium fluoride loading (in 10^{-3} mol / g zeolite) :

F3 = 1.87 ; F6 = 3.10

NH_4F concentration F6 activated at 400°C and 500°C and indicated that some significant structural changes occurred within the resulting zeolite framework. These frequency shifts of the structural bands towards higher values are characteristic of the dealumination of zeolite (118). These structural changes taking place within F6 catalysts were better illustrated by the dramatic lowering of the absorbance values of three characteristic bands shown in Table 3.23. The 1104 cm^{-1} band corresponds to the asymmetric stretching of framework Si-O-Si or Si-O-Al bonds, whereas the 800 – 870 cm^{-1} and 1625 cm^{-1} bands corresponding to the in-plane bending of the Si-OH groups and the bending of $O\text{-}H_{water}$ adsorbed on the Si-OH respectively. These IR spectra constitutes an indirect probe of the acid site density. The decrease of absorbance of these bands is much smaller for the F3 catalysts activated at 450°C and 500°C than for the F6 catalysts, and is indicative of only minor surface changes or structural modifications. As for the F3 / 325°C catalyst, the similarity of the absorbance values of these characteristic bands with those of the parent zeolite revealed that the framework structure of the resulting material remained practically unchanged when activated at 325°C. The large decrease of absorbance observed for the H-ZSM5 / F6 catalysts activated at 450°C and 500°C was attributed to an intense corrosive action of a high fluoride content on the zeolite framework which lead to a serious loss of tetrahedral Al atoms and silanol groups, especially at 500°C where dehydroxylation and replacement of –OH groups by the inserted fluoride ions occurred.

Table 3.23 : Absorbances of FT-IR bands in the low frequency region. The absorbances are expressed in arbitrary units (A.I. = area of peak / weight of the wafer in g, with concentration of zeolite equal to 2.5 wt %)

Sample	Activation temperature (°C)	1104 cm^{-1} (10^2 A.I.)	800-870 cm^{-1} (A.I.)	1625 cm^{-1} (A.I.)
H-ZSM5	450	1.98	4.6	9.6
H-ZSM5/F3	325	1.97	4.5	10.2
H-ZSM5/F3	450	1.60	3.7	6.7
H-ZSM5/F3	500	1.60	3.6	6.4
H-ZSM5/F6	450	0.82	2.9	2.2
H-ZSM5/F6	500	0.42	1.2	0.8

Initial ammonium fluoride loading (in 10^{-3} mol / g zeolite) :

F3 = 1.87 ; F6 = 3.10

1104 cm^{-1} : asymmetric stretching of Si–O–Si and Si–O–Al

800 - 870 cm^{-1} : in plane bending of Si–OH and HO–Si–OH

1625 cm^{-1} : bending of OH_{water} adsorbed on SiOH

Given the best catalytic activity and textural properties of the H-ZSM5 / F3 catalyst, FT-IR of adsorbed pyridine were achieved for this catalyst in order to determine the relative contribution of Brønsted and Lewis acid sites as well as the influence of dehydroxylation (starting to occur from 450°C) on the total surface acidity. The relative contribution of Brønsted and Lewis acid sites to the total surface acidity is represented by the B / L and the B / (L,B) ratios. The results reported in Table 3.24 clearly show two main points : (i) there is a general decrease of these ratios observed for both the F3 loaded H-ZSM5 and the parent zeolite due to the dehydroxylation effect on activation at 500°C ; (ii) the higher B / L ratio of the H-ZSM5/F3/450°C catalyst and the larger decrease of both of its B/L and B/(L,B) ratios upon dehydroxylation with respect to the parent zeolite indicates that additional Brønsted acid sites have been created upon fluorination of H-ZSM5 zeolite at the F3 concentration followed by thermal activation at 450°C.

3.3.1.4 Methanol chemisorption tests

In order to understand better the high catalytic activity and selectivity of H-ZSM5 / F3 catalysts in MTBE synthesis, it was decided to study their adsorption behaviors at 80°C with respect to methanol and the impact on the diffusion of reactants and products through the ZSM-5 pore and channel network. Methanol chemisorption data are reported in Table 3.25 for the F3 loaded H-ZSM5 catalysts activated at different temperatures. The F6 loaded H-ZSM5 and the parent zeolite

Table 3.24 : FT-IR study of the adsorbed pyridine (ratios of band areas).

Sample	Activation temperature (°C)	$B^{(1)} / L^{(2)}$	$B^{(1)} / (L,B)^{(3)}$
H-ZSM5	450	2.2	0.8
H-ZSM5	500	1.9	0.7
H-ZSM5/F3	450	2.4	1.0
H-ZSM5/F3	500	1.2	0.7

(1) 1547 cm^{-1} band assigned to (pyridine adsorbed on) Bronsted acid sites

(2) 1446 cm^{-1} band assigned to Lewis acid sites

(3) 1491 cm^{-1} band assigned to both acid sites.

Table 3.25 : Methanol chemisorption at equilibrium on fluorinated H-ZSM5 zeolites.

Catalyst	Initial NH_4F loading (10^{-3} mol.g^{-1})	Activation temperature (°C)	Methanol chemisorption (10^{-3} mol/g zeolite)	$R_{Me/Al}$*
H-ZSM5	0	450	2.6	3.3
H-ZSM5/F3	1.87	325	1.9	2.4
H-ZSM5/F3	1.87	400	2.2	2.9
H-ZSM5/F3	1.87	450	2.2	2.8
H-ZSM5/F3	1.87	500	2.3	3.0
H-ZSM5/F6	3.10	500	1.5	1.9

(*) : $R_{Me/Al}$ = Molar ratio of MeOH / Al

Operating conditions : 80 °C under a vacuum of 10^{-2} Torr.

were used as references. It is known that polar methanol adsorbates preferentially on the Brønsted acid sites located close to the framework Al atoms (108); each framework tetrahedral Al atom corresponds to a Brønsted acid site. The ratio $R_{Me/Al}$ represented the number of methanol molecules adsorbed on each Brønsted acid site. The low amount of MeOH chemisorbed recorded for F3 / 325°C was mainly due to the pore blockage or pore narrowing effect caused by the HF species which were chemisorbed onto the zeolite pore walls. Another reason for this could be the repulsive effect exerted by the fluoride species towards methanol adsorbate molecules. When the catalysts were activated at 400°C and 450°C, the chemisorbed HF molecules were either desorbed and evacuated from the zeolite pore system or firmly inserted onto the zeolite surface, thereby leaving more intracrystalline space available for a significantly higher amount of MeOH to chemisorb on the zeolite surface (see Table 3.25). This phenomenon was more marked at a higher activation temperature 500°C allowing a slightly higher amount of MeOH to chemisorb. As for the H-ZSM5 / F6 catalyst activated at 500°C, the lowest amount of MeOH chemisorbed was recorded and could be ascribed to the lower number of framework Al (or Brønsted acid) sites resulting from the serious structural collapse (see Table 3.20) and to the intense repulsive effect which the fluoride ions, inserted in high concentration, exerted towards methanol adsorbates (see Table 3.25).

All the catalytic tests were performed with a methanol pre-admission period of 15 min in order to ensure the production of a maximum MTBE yield. Previous works done on the preliminary catalytic tests with simultaneous admission of methanol and isobutene showed a dramatically low yield of MTBE, (ca. 7–8 %) with respect to that obtained with the standard testing procedure requiring MeOH pre-admission. Beside the lower yield of MTBE collected, there was a gradual change in the appearance of the catalyst from the normal white to a yellow brown color. This was due to the bulky isobutene dimers that were formed and trapped within ZSM-5 channel intersections, because of their large size and thus hindered the diffusion of reactant molecules within the pore and channel network. This fact demonstrated the important role of pre-admitted methanol in the protection of Brønsted acid sites against the access of isobutene molecules and in the prevention of the undesired isobutene dimerization.

3.3.1.5 ^{27}Al MAS – NMR studies

Figures 3.16 to 3.21 show the ^{27}Al MAS-NMR spectrum of the parent H-ZSM5 zeolite (taken as the reference spectrum), and that of the fluoride incorporated H-ZSM5/F3 catalysts activated at four different temperatures (325°C, 400°C, 450°C and 500°C) and of the H-ZSM5/F6 activated at 450°C. Only the latter catalyst was significantly different from the H-ZSM5 reference, and showed an intense side band at ca. 0 ppm chemical shift, which is characteristic of extra-

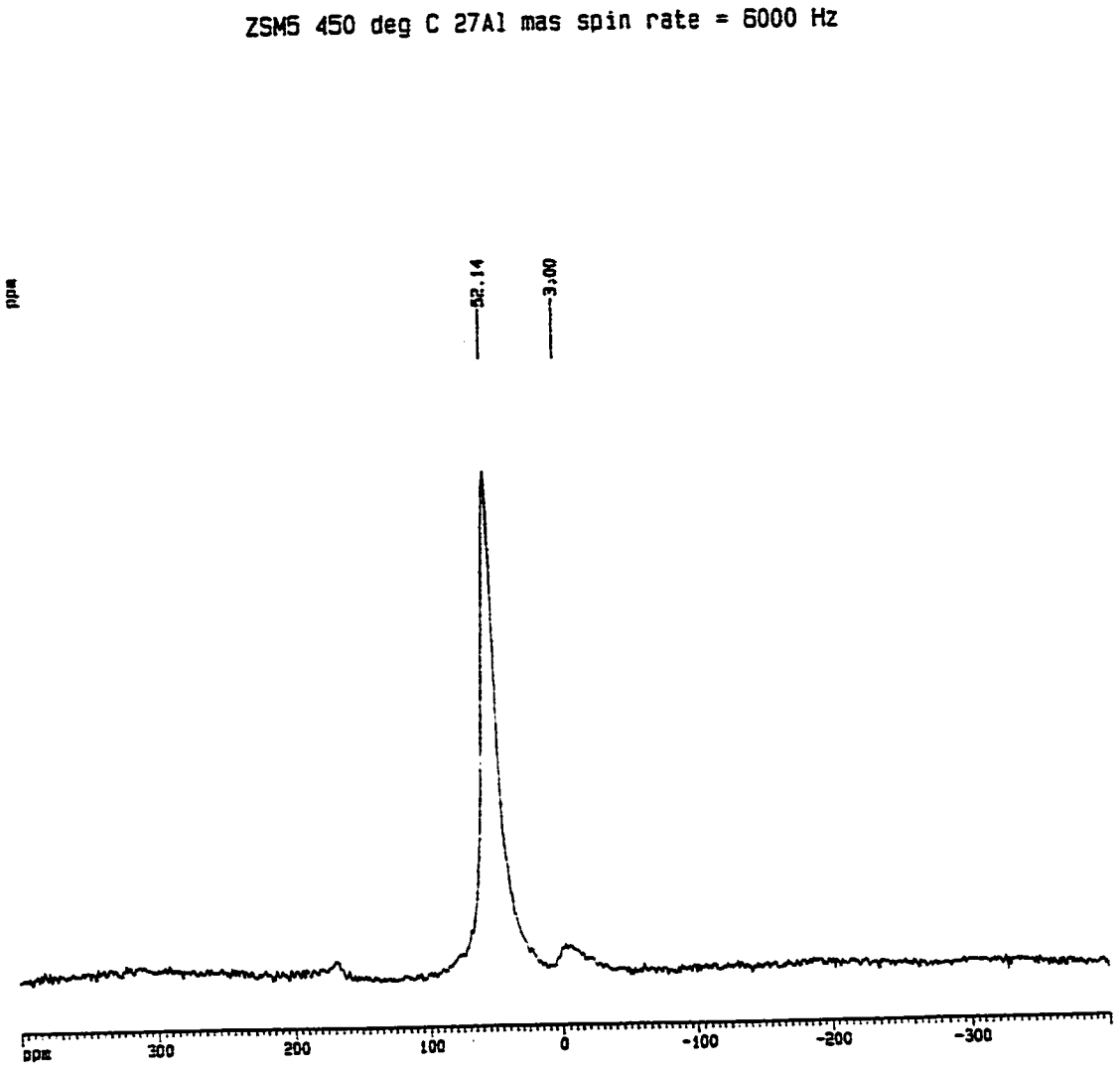

Figure 3.16 : ^{27}Al MAS-NMR spectrum of the parent H-ZSM5 / 450°C sample. In abscisa : chemical shift expressed in ppm with respect to reference octahedral $Al[(OH_2)_6]^{3+}$ at the origin.

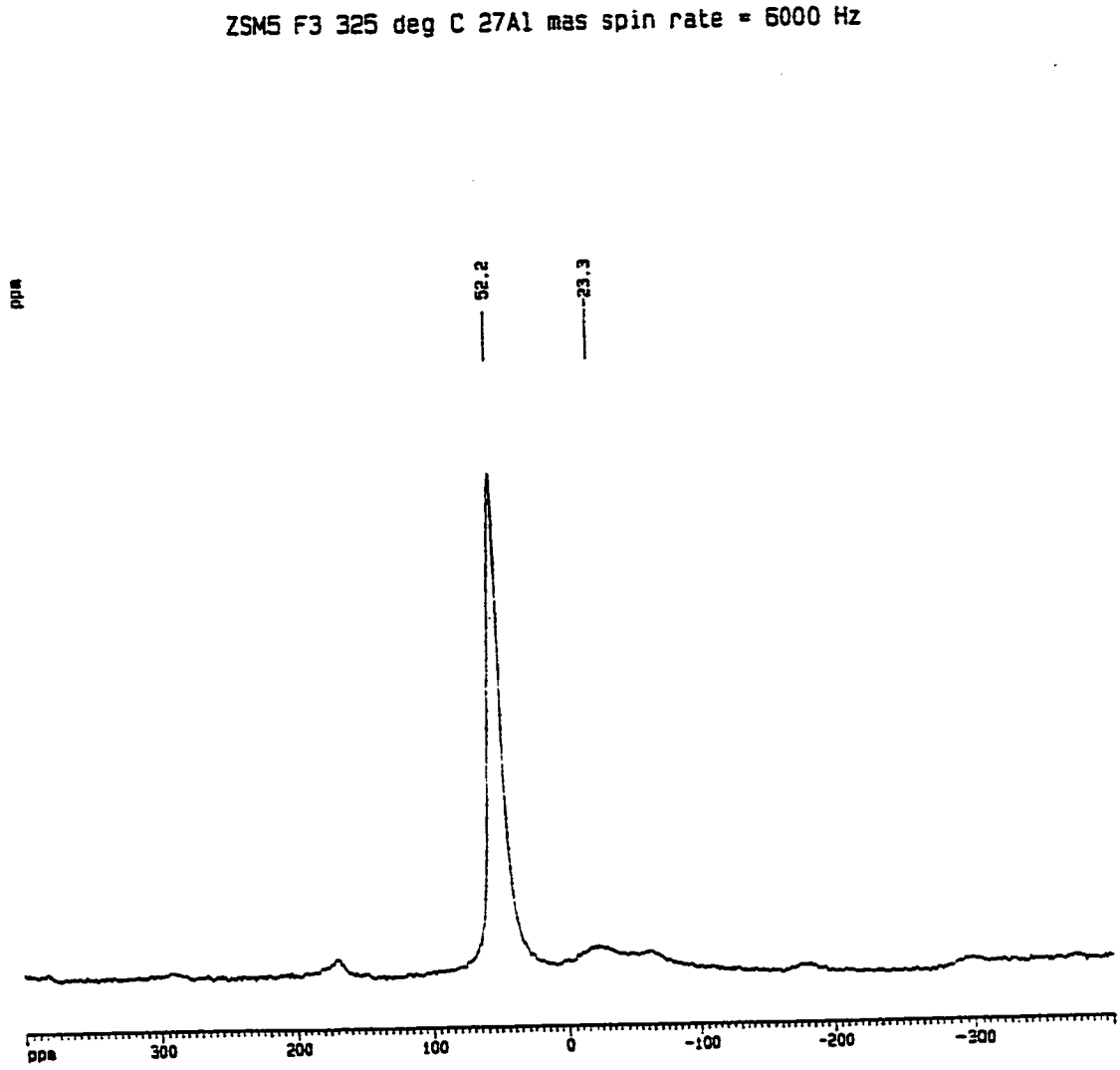

Figure 3.17 : ^{27}Al MAS-NMR spectrum of H-ZSM-5 / F3 / 325°C sample. In abscisa : chemical shift expressed in ppm with respect to reference octahedral $Al[(OH_2)_6]^{3+}$ at the origin.

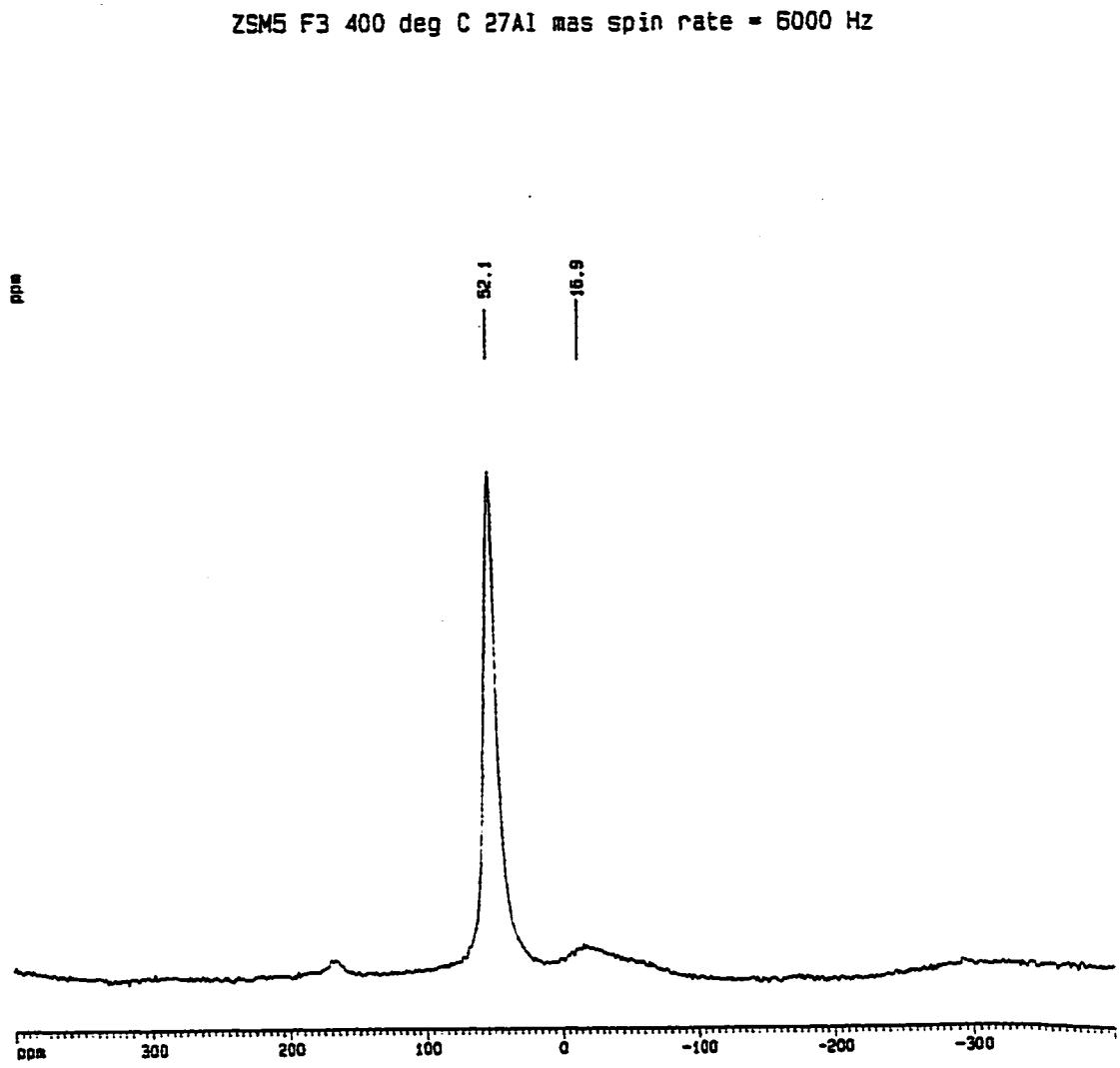

Figure 3.18 : ^{27}Al MAS-NMR spectrum of H-ZSM-5 / F3 / 400°C sample. In abscisa : chemical shift expressed in ppm with respect to reference octahedral $Al[(OH_2)_6]^{3+}$ at the origin.

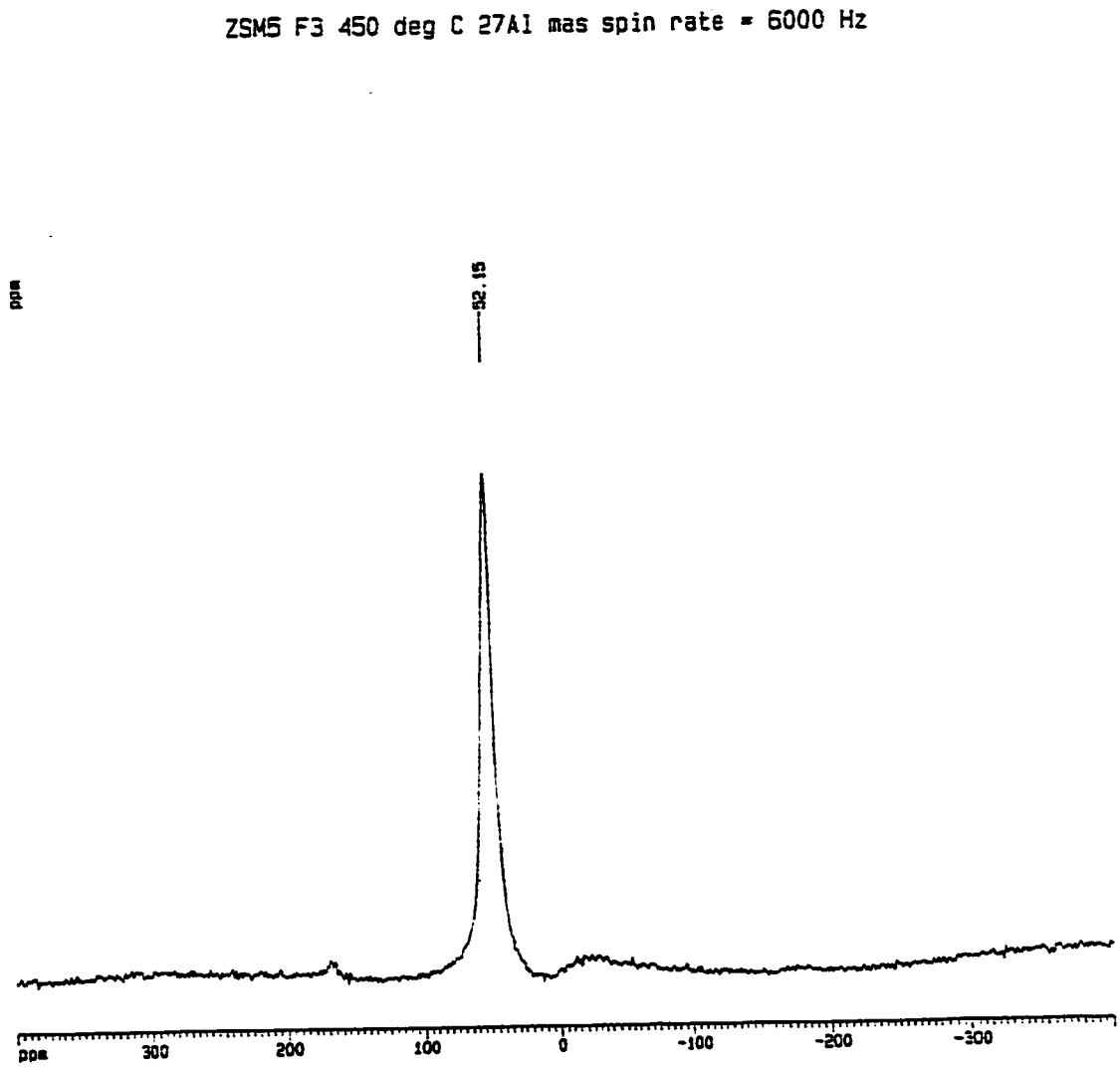

Figure 3.19 : ^{27}Al MAS-NMR spectrum of H-ZSM-5 / F3 / 450°C sample. In abscisa : chemical shift expressed in ppm with respect to reference octahedral $Al[(OH_2)_6]^{3+}$ at the origin.

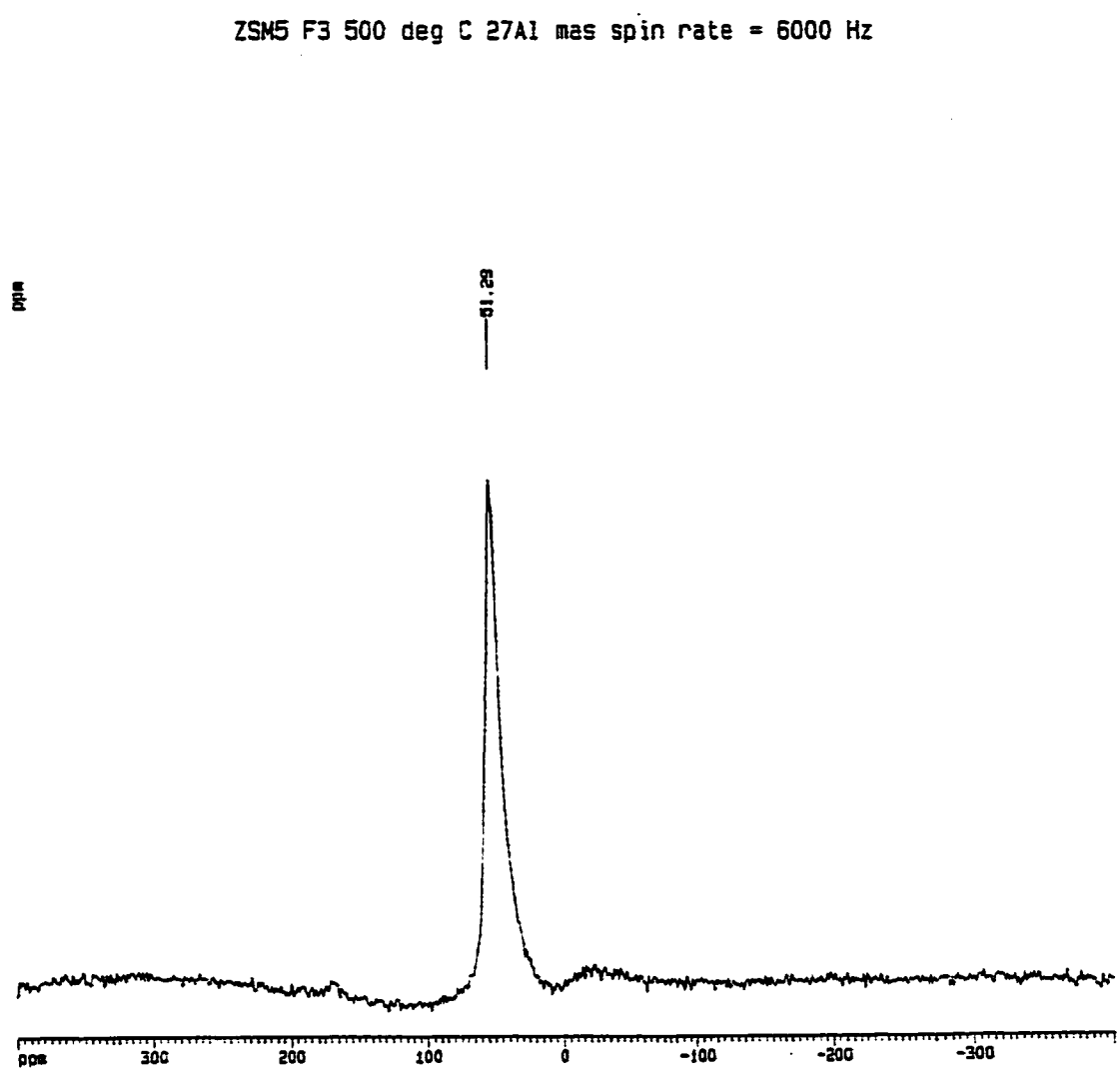

Figure 3.20 : ^{27}Al MAS-NMR spectrum of H-ZSM-5 / F3 / 500°C sample. In abscisa : chemical shift expressed in ppm with respect to reference octahedral $Al[(OH_2)_6]^{3+}$ at the origin.

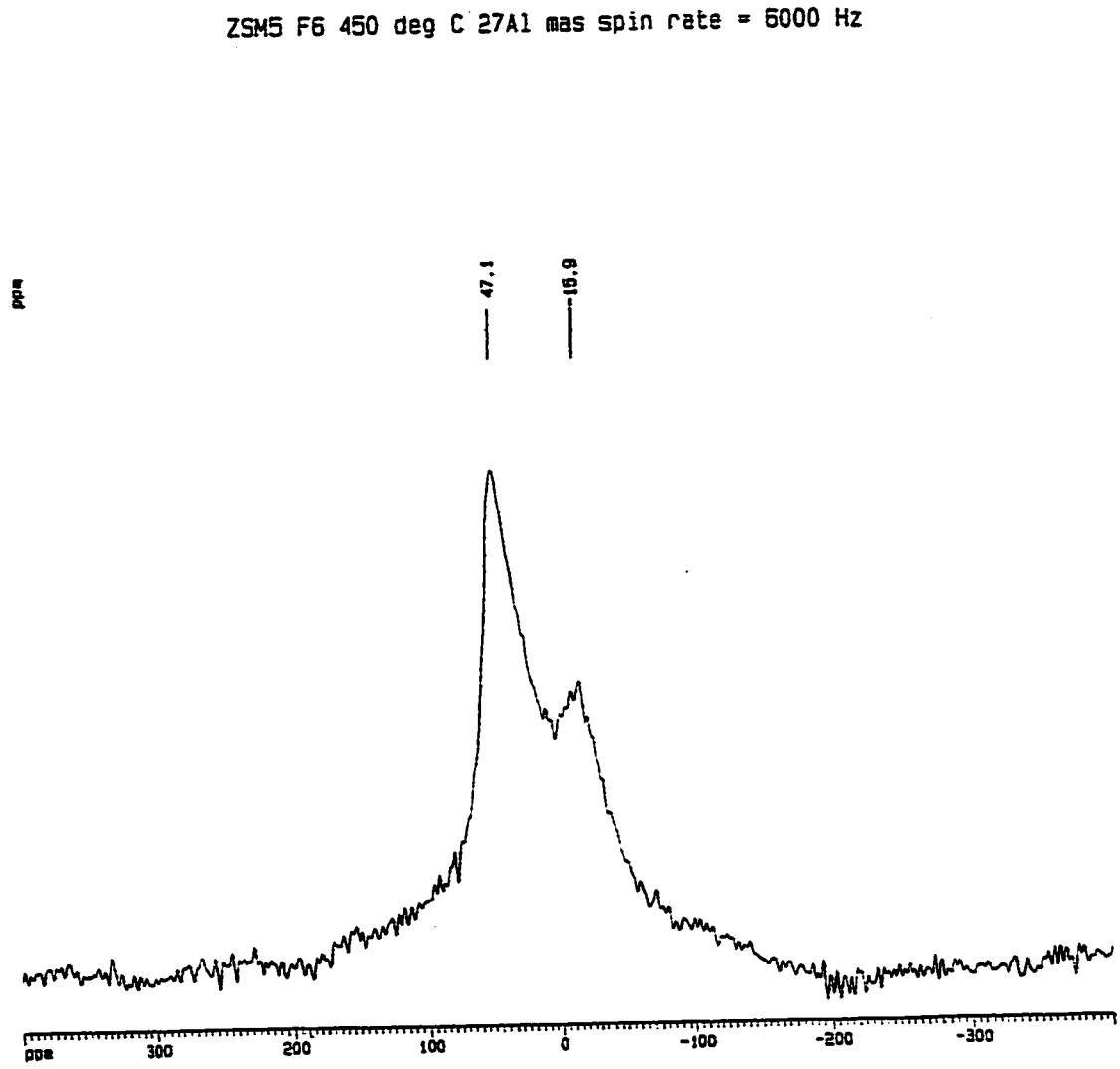

Figure 3.21 : ^{27}Al MAS-NMR spectrum of H-ZSM-5 / F6 / 450°C sample. In abscisa : chemical shift expressed in ppm with respect to reference octahedral $Al[(OH_2)_6]^{3-}$ at the origin.

framework Al atoms that were extracted from the zeolite structure under the corrosive action of the HF released when a high concentration of NH_4F was used (F6 = 3.10×10^{-3} mol / g zeolite). For the parent H-ZSM5 zeolite and for all the H-ZSM5 / F3 catalysts activated at temperatures up to 500°C : (i) the ^{27}Al MAS–NMR spectra exhibited a sharp band at ca. 52 ppm characteristic of the framework tetrahedral Al atoms ; (ii) there was no noticeable amount of extra-framework Al atoms as illustrated by the insignificant side band at ca. 0 ppm which was quite similar to that observed for the parent zeolite, indicating the absence of any structural modification. This means that with the low NH_4F concentration F3 (of 1.87×10^{-3} mol / g zeolite) and for activation temperatures as high as 500°C, the ZSM5 zeolite framework was not damaged by the corrosive action of released HF species. Our X-Ray diffraction studies and BET surface measurements (see Table 3.20) also confirmed this observation with the unchanged degree of crystallinity and micropore surface area for F3 catalysts activated at temperatures up to 500°C.

3.3.1.6 Determination of the acid site density and strength

The acid sites density of F3 loaded H-ZSM5 catalysts determined by ammonia-TPD technique are reported in Table 3.26 and the profiles of acid strength (of the best catalysts) provided by the same technique are plotted in Figure 3.22. The acid density of the H-ZSM5 parent zeolite was taken as the reference. The symbol $R_{H+/Al}$ is defined as the ratio of the number of measured

Table 3.26 : Determination of the acid sites density by the ammonia temperature programmed desorption method (back-titration).

Catalyst	Initial NH_4F loading (10^{-3} mol.g^{-1})	Final activation temperature (°C)	Density of acid sites (10^{-3} mol.g^{-1})	$R_{H+/Al}$ *
H-ZSM5	0	450	0.78	1.0
H-ZSM5/F3	1.87	325	0.70 **	0.9
H-ZSM5/F3	1.87	400	1.05	1.3
H-ZSM5/F3	1.87	450	1.04	1.3
H-ZSM5/F3	1.87	500	0.62	0.8
H-ZSM5/F6	3.10	450	0.63	0.8

* : $R_{H+/Al}$ = atomic ratio of acid sites / tetrahedral Al atoms

** : no accurate measurement possible (see text).

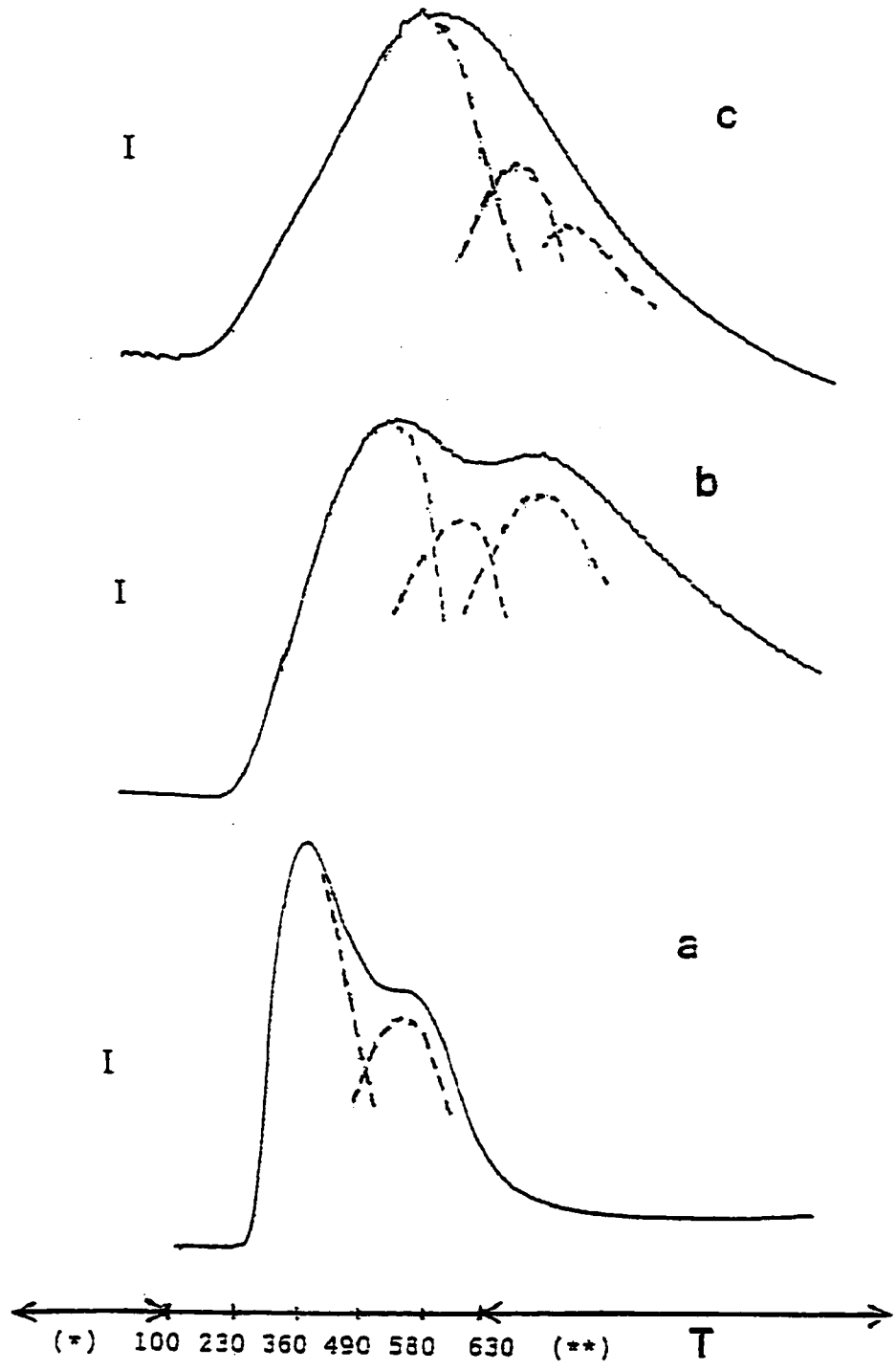

Figure 3.22 : Ammonia temperature programmed desorption profile of : a) H-ZSM5 ; b) H-ZSM5 / F3 (450 °C) and c) H-ZSM5 / F3 (500 °C). T = ammonia desorption temperature in °C ;
In Y axis : I = response of the TCD detector, in arbitrary units.
(*) and (**) = constant temperatures, 100 °C and 630 °C, respectively.

Brønsted acid sites over the number of framework tetrahedral Al sites and represents the relative acid sites density of each catalyst with respect to the parent zeolite.

For the H-ZSM5 / F3 catalyst activated at 325°C, it was not possible to assess accurately the acid site density due to the presence of chemisorbed HF species on the zeolite surface, which recombined with the ammonia probe molecules during the adsorption phase of ammonia to form ammonium fluoride within the zeolite channel network. These recombined ammonium fluoride species block the zeolite pore system, and thus, restrict the access of other ammonia probe molecules to some acid sites deeply located inside the zeolite pore and channel network. The result was a lower acid density measured (with respect to parent zeolite) which did not reflect the total acid sites density of the catalyst, since the latter would normally include both the original parent H-ZSM5 acid sites and the additional HF chemisorbed acid sites newly created. Moreover, during the temperature programmed desorption phase of ammonia, these ammonium fluoride species were also desorbed from the zeolite surface and they actually formed a very thin powder layer deposited on the glass wall of the outlet tube of the reactor. They are actually representative of the extra acid sites created by the HF species chemisorbed on the zeolite surface. For this reason, the ammonia TPD profile of the H-ZSM5/F3/ 325°C catalyst could not be measured satisfactorily for the study of its acid strength.

The highest acid site density was found for the F3 catalysts activated at 400°C and 450°C and correspond to an increase of 30 % with respect to the parent zeolite acid density. These values, which are considered to be optimal, suggest that extra Brønsted acid sites have been created for the F3 fluoride loaded H-ZSM5 catalysts when they were activated at 400°C and 450°C. However catalytic results showed a highest maximum MTBE yield (44.9 %) with the final activation temperature 450°C, whereas a lowest MTBE yield (37.5 %) was reported for the final activation temperature 400°C.

At the activation temperature of 500°C, the substantially lower acid site density was ascribed to the dehydroxylation effect which reduced significantly the Brønsted acid sites by 20 % with respect to the parent zeolite. Simililarly, the low acid site density measured for the H-ZSM5 / F6 catalyst activated at 450°C stemmed from a partial structural collapse which resulted from a higher amount of ammonium fluoride incorporated, followed by an activation temperature of 450°C. This partial structural collapse was also evidenced by the XRD and BET characterization techniques (see Table 3.20).

The ammonia TPD profiles of the parent H-ZSM5 zeolite and of the H-ZSM5 / F3 catalysts activated at 450°C and 500°C are plotted on Figure 3.22. They show a semi-quantitative distribution of acid strengths for each catalyst with respect to the parent zeolite.

In comparison to the parent zeolite, the F3 loaded H-ZSM5 catalysts exhibit : (i) an increase in strength for the population of weak and medium acid sites as revealed by the shift of the corresponding first and second peaks to higher desorption temperatures, (ii) a substantial increase in the population of the strongest acid sites, which was almost insignificant within the parent zeolite as shown by the important shoulder at highest desorption temperatures for the 450°C activated catalyst and a moderate tail at the same desorption temperatures region for the 500°C activated catalyst. This indicates that upon incorporation of highly electronegative fluorine into the ZSM5 structure, there is a general increase in the strength of all the acid sites already present in the parent H-ZSM5 zeolite resulting from the inductive effect of inserted fluoride ions which polarize the neighboring O–H bonds and render the H atoms more labile and thus more acidic.

At the highest desorption temperature, i.e. at 630°C, the important shoulder observed in profile (b) with respect to the moderate tail in profile (c) indicates that there is a significantly higher concentration of the strongest acid sites when the F3 loaded catalyst is activated at 450°C than when activation is carried out at higher temperatures. The serious decrease of the strong acid sites concentration at 500°C is due to the well known dehydroxylation phenomenon which starts to occur above 450°C. The population of the weak and of the medium acid sites are roughly comparable for both final activation temperatures, 450°C and 500°C.

3.3.2 Catalytic activity

The results of MTBE yield versus activation temperature obtained with the H-ZSM5 / F3 catalyst (concentration F3 of NH_4F loading : 1.87×10^{-3} mol / g zeolite) are reported in Table 3.27 and plotted in Figure 3.23. They show a strong dependence of the catalytic activity on the final activation temperature of the catalyst. Surprisingly, the MTBE yield showed two maxima (42.9 % and 44.9 %) at two different final activation temperatures (T_f), 325°C and 450°C, respectively, and one minimum at 400°C. The maximum (II) observed at T_f = 450°C was clearly higher than that reported as maximum (I) at T_f = 325°C. Both maximum MTBE yields are significantly higher than that of the parent H-ZSM5 zeolite (i.e. 34.2 %), with the maximum (II) being close to that of the commercial A-15 resin (47.5 %).

Moreover, for activation temperatures lower than 300°C, there was no significant activity enhancement, indicating that (102) :

(i) the decomposition of the ammonium fluoride incorporated into the zeolite starts at 10 to 20°C higher than the decomposition temperature of crystalline ammonium fluoride i.e. 240°C as measured by thermogravimetric and differential thermal analysis (see Figure 3.24), and

(ii) within the temperature range from 250°C to 300°C, gaseous ammonia released by the ammonium fluoride decomposition was not completely evacuated from the zeolite pore and channel system and thereby greatly affected the diffusion of

Table 3.27 : Variation of MTBE yield with the final activation temperature for the ZSM-5 / F3 catalyst.

Catalyst	Initial NH_4F loading (10^{-3} mol.g^{-1})	Final activation temperature (°C)	MTBE yield (C-atom %)	Total oligomers of C_{4-} (C-atom %)
H-ZSM5	0	450	34.2	0.0
H-ZSM5/F3	1.87	250	21.3	0.0
		300	35.6	0.0
		325	42.9	0.0
		340	41.1	0.0
		350	39.3	0.0
		375	37.7	0.0
		400	37.5	0.0
		425	41.4	0.0
		450	44.9	0.0
		475	40.5	0.0
		500	41.2	0.0

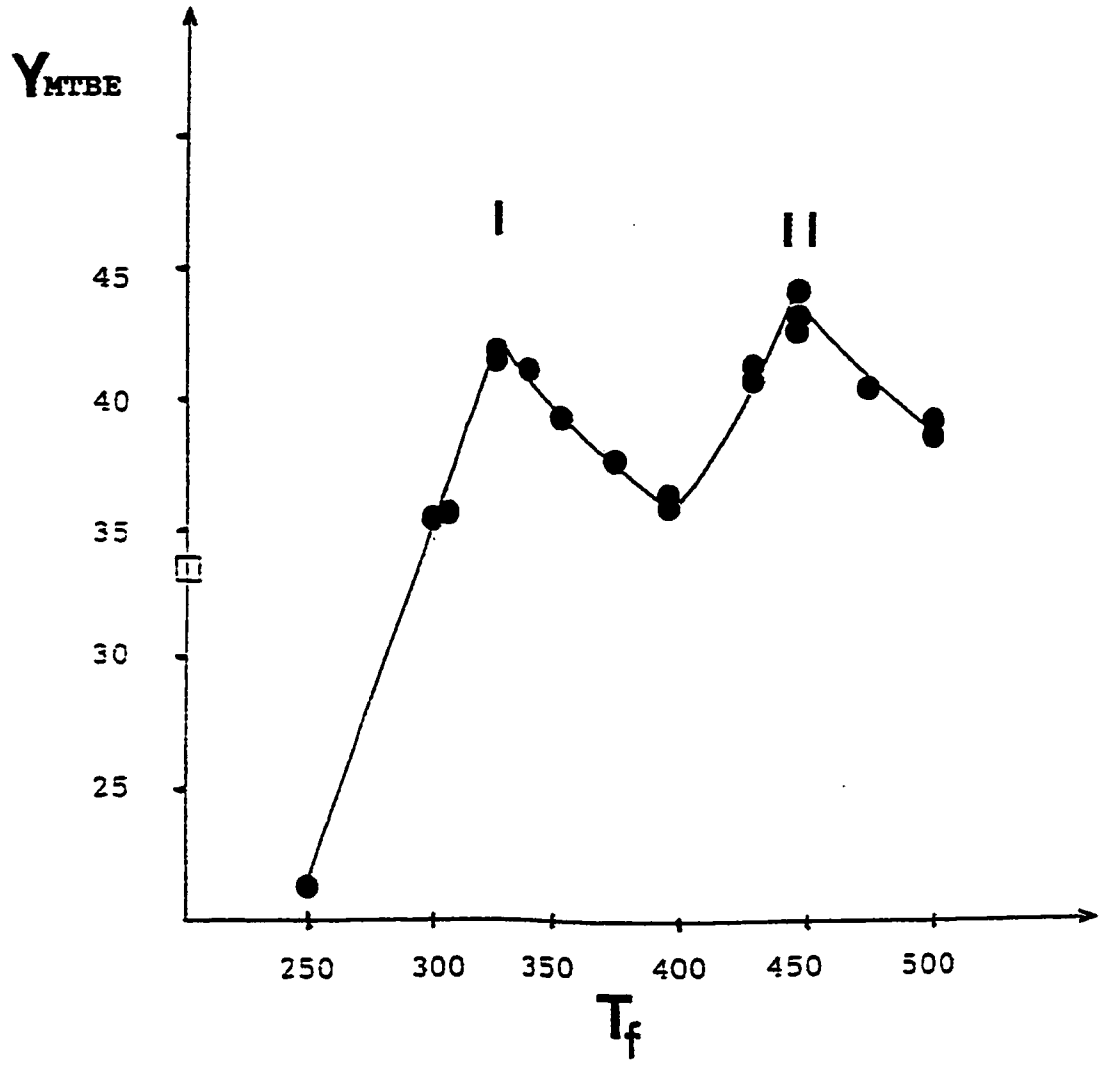

Figure 3.23 : MTBE yield (in C-atom %) versus final activation temperature T_f (T_f in °C) with the H-ZSM5 / F3* catalyst (●)
(□) : MTBE yield of the parent zeolite.
* concentration F3 = 1.87×10^{-3} mol NH_4F / g zeolite

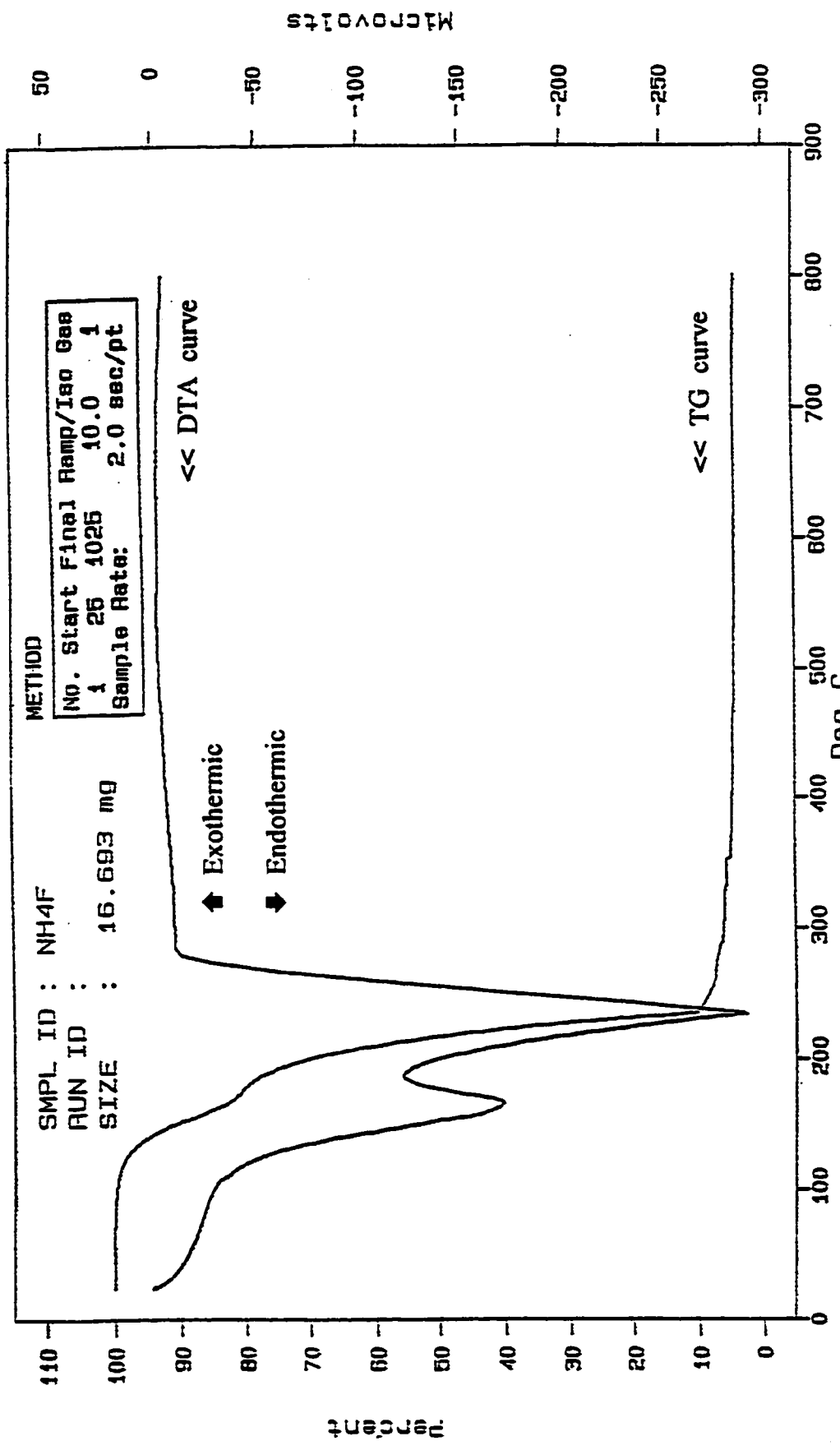

Figure 3.24 : TGA and DTA thermogram of ammonium fluoride.

reactants (and products as well) and their access to the surface acid sites. For this reason, the catalytic activity (21.3 %) was much lower than that of the parent zeolite (34.2 %).

The above trends of catalytic activity were also observed for another series of fluoride incorporated H-ZSM5 catalysts having variable ammonium fluoride loadings in the range 0.05×10^{-3} to 2.60×10^{-3} mol / g zeolite and activated at four different temperatures (see Table 3.28) :

- a) For catalysts having medium ammonium fluoride loading between 1.00×10^{-3} and 2.60×10^{-3} mol / g zeolite, there were two maximum yields of MTBE at 325°C and 450°C respectively, with the maximum recorded at 450°C being the highest as previously mentioned. With such values of fluoride loadings and activation temperatures, there was no significant modification of the textural properties of the F^- modified catalysts in terms of degree of crystallinity, BET total surface area and micropore surface area (see Table 3.20). Thus, in this range of NH_4F concentration and activation temperature, the zeolite framework was not damaged, and little dealumination effect caused by HF species occured.

- b) The optimal fluoride ion concentration required to obtain the maximum MTBE yield was found to be F3 : 1.87×10^{-3} mol / g zeolite, while a fluorination level beyond 2.60×10^{-3} mol / g zeolite had adverse effects on the catalytic activity i.e. the decrease in MTBE yield and the loss of the two maxima characteristic (see Table 3.1.8). In addition, there was no noticeable amount of

extra-framework Al atoms formed for the H-ZSM5 / F3 catalysts as revealed by the ^{27}Al MAS-NMR spectra in Figures 3.17 to 3.20. Practically all the Al atoms present in these catalyst samples remained tetrahedral, i.e. within the zeolite framework as demonstrated by the presence of a unique band at ca. 52 ppm.

- c) For the lowest ammonium fluoride loading (F7), the two maximum MTBE yields were shifted to 400°C and 500°C respectively with lower MTBE yields as expected when compared to those corresponding to the medium range of NH_4F concentrations. The second maximum recorded at 500°C, an activation temperature at which lower MTBE yields were obtained for all the other NH_4F concentrations in this series, could be attributed to the very low amount of fluoride ions incorporated with a corrosive action not intense enough to damage the zeolite structure. Hence, all the active acid sites were still intact and the result was the highest MTBE yield recorded at that temperature. As a matter of fact, it is known that the parent H-ZSM5 zeolite can withstand activation temperatures as high as 550°C during 14 hours without undergoing any detectable partial structural collapse.

- d) For the highest ammonium fluoride loading F6 catalyst, lower MTBE yields were reported with only one maximum at 450°C. The reason for this global decrease of catalytic activity was ascribed to the partial structural collapse of the zeolite framework, which results from an intense corrosive action of a high amount of HF species (released from the decomposition of NH_4F incorporated in

high concentration) under high activation temperatures. This partial structural collapse is illustrated in Table 3.20 by the decreased value of degree of crystallinity recorded and the decreased micropore surface area and in Figure 3.21 by the appearance of an extra-framework Al side band at nearly 0 ppm on the ^{27}Al MAS-NMR spectrum.

The value of the MTBE yield collected at 325°C for the F6 concentration was significantly lower than those obtained for other NH_4F concentrations at the same temperature and it was even lower than that of the parent zeolite (see Table 3.28). This difference could be explained by the pore blockage or pore narrowing effect exerted by the very high amount of HF species chemisorbed on the zeolite surface which restricted the diffusion of reactants and products within the zeolite pore system. As a matter of fact, at the next higher activation temperature, i.e. 400°C, where part of the HF chemisorbed was desorbed and evacuated from the pore and channel system thereby allowing a better diffusion for reactants and products, there was a sharp increase of the MTBE yield from 33.3 % to 39.8 %. Thus the concentration F6 represented the limit above which beneficial effect due to the increase in surface acid density is cancelled out by pore blockage sructural damage, and therefore no improvement of activity takes place. The two lowest values of MTBE yields in this series obtained at 500°C for the two highest NH_4F loading F5 and F6 were quite similar : 31.1 % and 31.2 %. They both reflected a

Table 3.28 : Variation of the MTBE yield with the ammonium fluoride loading and the final activation temperature of H-ZSM5 catalysts

Catalyst	Initial NH_4F loading (10^{-3} mol.g^{-1})	Final temperature of activation (°C)	MTBE yield (C-atom %)
H-ZSM5	0	450	34.2
H-ZSM5/F7	0.05	325	37.6
		400	40.2
		450	38.9
		500	41.4
H-ZSM5/F4	1.00	325	42.8
		400	38.8
		450	43.0
		500	39.7
H-ZSM5/F3	1.87	325	42.9
		400	37.5
		450	44.9
		500	41.2
H-ZSM5/F5	2.60	325	42.5
		400	37.4
		450	44.5
		500	31.2
H-ZSM5/F6	3.10	325	33.3
		400	39.8
		450	40.8
		500	31.1

partial structural collapse which resulted from the combined effect of a high fluoride loading and a high activation temperature.

It is worth mentioning that the activation temperature of 400°C that was normally used by A. Kogelbauer et al. (100) only corresponded to a minimum yield (37.5 %) of MTBE reported in this work (see Figure 3.23), a minimum which still remains significantly higher than that of the parent zeolite (34.2 %). As expected, practically no C-8 by-products were detected for both of these two series of catalytic testings, suggesting that the concentration range of fluoride ions incorporated and the various activation temperatures used in this work did not significantly affect the shape selectivity of the fluoride modified H-ZSM5 catalysts.

3.3.3 A proposed mechanism for surface modification by fluoride ions.

In order to explain better the catalytic behavior of the fluoride modified H-ZSM5 / F3 catalyst regarding the surprising presence of two maximum yields of MTBE, a mechanism of the zeolite surface transformation as a function of the final activation temperature is proposed here and described on Figure 3.25. It takes into account the results of both catalytic activity and characterization studies collected from various analytical techniques such as the FTIR (of pyridine adsorbed H-ZSM5/F3), the methanol adsorption test, and the ammonia temperature programmed desorption (TPD) analysis.

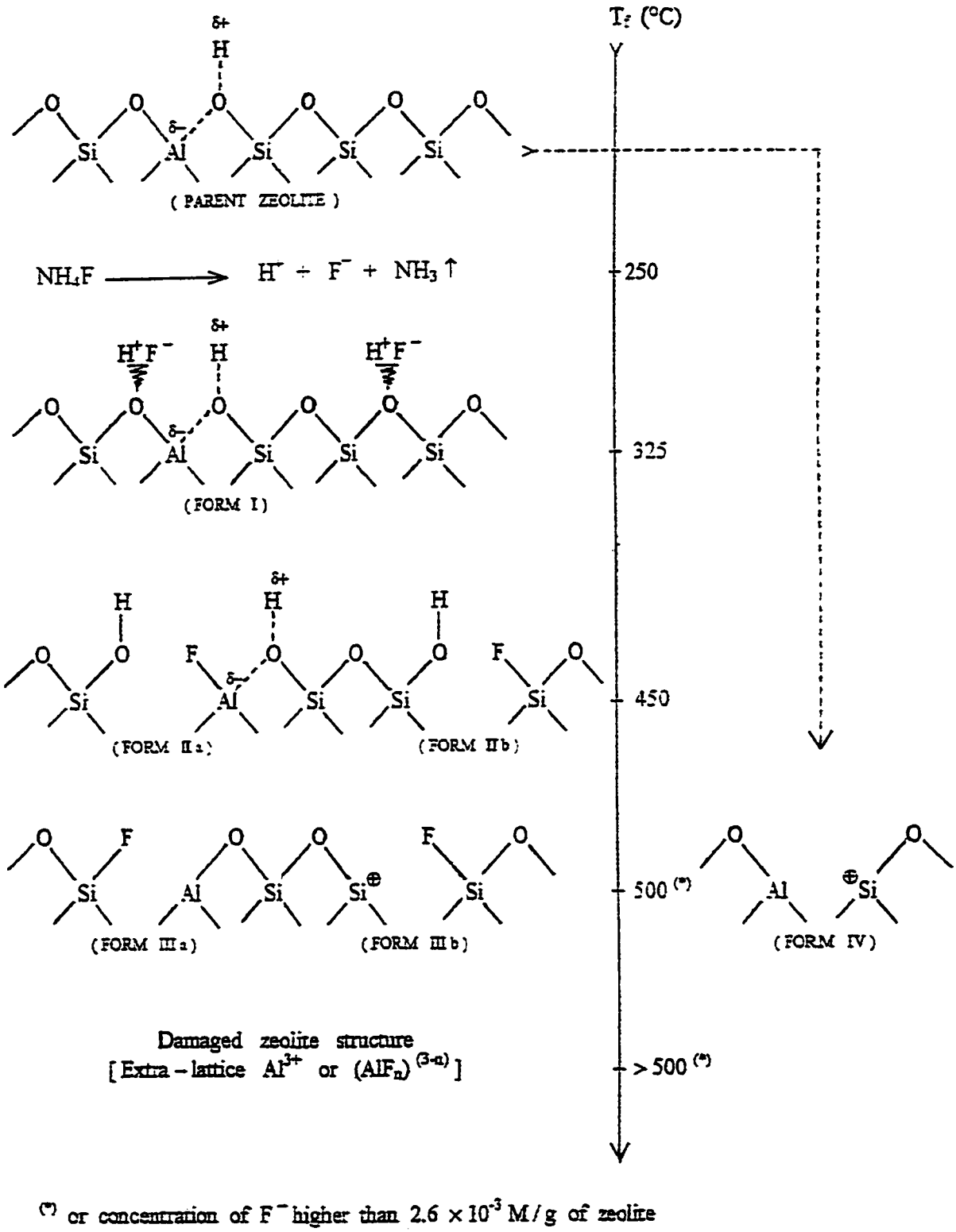

(*) or concentration of F^- higher than 2.6×10^{-3} M/g of zeolite

Figure 3.25 : Mechanism of the formation of active sites as a function of final activation temperature (T_f in °C).

On Figure 3.25, the structure on the top represents the untreated parent zeolite acidic form and the corresponding dehydroxylated form (form IV) when activated at 500°C (103). In this thermal transformation of the parent zeolite structure, two Brønsted acid sites are destroyed to generate two Lewis acid sites consisting of tri-coordinated atoms of Al and Si as shown in the form IV (see Figure 1.8 and ref. 104).

The proposed mechanism of the zeolite surface modification by ammonium fluoride could be explained as follows versus the increasing final activation temperatures :

- a) At activation temperatures below 325°C, the zeolite surface does not undergo any detectable modification and is quite similar to that of the parent zeolite (Figure 3.25), but with the following differences in correlation with the catalytic activity (see Table 3.27) : (i) At 250°C, when the incorporated ammonium fluoride just starts to decompose, the pore and channel network of ZSM5 zeolite are still crowded with gaseous NH_3 and HF species released from the NH_4F decomposition. Their presence seriously affects the diffusion of reactants (and products) within the zeolite channels and their access to the surface active sites. The result is a poor catalytic activity (21.3 %), which was much lower than that of the parent zeolite (34.2 %, see Table 3.27); (ii) at 300°C almost all of the gaseous ammonia has been evacuated from the zeolite pore and channel network and the

catalyst exhibits a catalytic activity (35.6 %) at a level which is comparable with that of the parent zeolite (34.2 %, see Table 3.27).

- b) At the activation temperature of 325°C, some HF species which were generated from the decomposition of NH_4F, are chemisorbed on the zeolite surface as described by form (I) on Figure 3.25. The surface acidity associated with these HF chemisorbed species contributes to the increase in the acid site density of H-ZSM5 / F3 catalyst with respect to the parent zeolite. This increase in surface acidity results in a significant enhancement of the catalytic activity, resulting in the first maximum MTBE yield observed for the medium range of F^- loadings. However the determination of the total acid site density by ammonia TPD technique gives a lower value than that expected (see Table 3.26). The reason for this discrepancy was the presence of the HF species (in the form of H_3O^+... F^- ion pairs or simply H^+... F^-) chemisorbed onto the zeolite pore walls which recombined with ammonia adsorbate molecules during the adsorption phase of NH_3-TPD analysis to form ammonium fluoride. The presence of the latter species within the pore and channel system creates a steric hindrance to the diffusion of other ammonia molecules and restricts their access to active sites located deeply inside the zeolite micropore network. As a matter of fact, during the temperature programmed desorption phase of chemisorbed ammonia, a thin layer of ammonium fluoride species was formed on the glass wall of the outlet tube of the reactor as revealed by a qualitative analysis. Because of this difficulty, the

ammonia TPD profile of acid strength could not be achieved satisfactorily for a better understanding of the resulting high catalytic activity (42.9 %) in terms of percent C-atom IB converted to MTBE. This hindrance effect was also observed with the methanol adsorption test achieved at equilibrium (see Table 3.25). There is a remarkable consistency in the way the amounts of chemisorbed methanol and ammonia are affected by such a partial pore blocking effect or probably by the repulsive action from the F^- anions, as evidenced by the simultaneous decrease of the two molar ratios $R_{H+/Al}$ (Table 3.26) and $R_{Me/Al}$ (Table 3.25). These ratios are indicative of the degree of coverage of the original zeolite acid sites (corresponding to the framework Al tetrahedral sites) by the chemisorbed ammonia and methanol molecules, respectively. On the other hand, FT-IR frequency and absorbance measurements in the low-frequency and in the framework region of the H-ZSM5/F3 samples show that the 1104 cm^{-1} band, assigned to the asymmetric stretching of framework Si-O-Si or Si-O-Al bonds (105,106), did not experience any significant frequency shift (see Table 3.22) or decrease in intensity (see Table 3.23) with respect to the parent zeolite. This indicates that there is no significant change in the number of these framework T-O-T bonds upon activating at 325°C (T representing framework tetrahedral Al or Si atoms). The acid sites density as well as the ratio $R_{Me/Al}$ determined by the back titration of ammonia TPD method showed a substantial increase of almost 35 % with respect to the parent zeolite as reported in Table 3.26. Similarly, the unique

and sharp band at ca. 52 ppm on Figure 3.1.7 also confirms the tetrahedral configuration of all the remaining Al atoms present in the catalyst sample. Moreover, the X-ray diffraction shows no change in the zeolite structure (see Appendix) and in the degree of crystallinity with respect to the parent zeolite (Table 3.20). Nevertheless, these adsorbed (H^+... F^-) ion pairs contributes to an increase of the MTBE yield when compared to the activity level of the parent zeolite (Fig. 3.23 and Table 3.28).

- c) With increasing activation temperature (T_f > 325 °C), some chemisorbed (H^+ F^-) species are slowly desorbed from the zeolite surface, thus decreasing the surface acidity and the result was a gradual decrease of the MTBE yield (Fig. 3.23). At this stage, the zeolite surface is quite similar to the structural form (I) described for the activation temperature 325°C with however a lower number of H^+F^- species chemisorbed on the surface.

- d) At the activation temperature of 400°C, the reaction of the zeolite surface with the protons of the remaining (H^+... F^-) ion pairs resulted in the formation of new hydroxyl groups (Figure 3.25). At that stage, the zeolite surface is most likely similar to the structural representation form at 450°C based on the similar characterization results, including (i) the fluoride ions content, (ii) the amount of methanol chemisorbed, (iii) the acid sites density and (iv) the ^{27}Al MAS-NMR which shows that ZSM-5 structure is preserved with a high Brønsted acid density, excluding the HF chemisorbed species. The associated catalytic activity, although

remaining higher than that of the parent zeolite, was still lower than the maximum yield (II) observed at 450°C, and this is most likely due to diffusion limitations. The impact of the latter effect is gradually reduced as the activation temperature is increased beyond 400°C, and it results in an increase of catalytic activity up to the maximum yield (II) observed at 450°C (see Figure 3.23).

- e) At 450°C, the incorporation of these HF species into the zeolite framework results in optimal " acidity – diffusion " conditions on the zeolite surface with : (i) more readily available diffusion pathways for the reactants in the zeolite micropores resulting mainly from an optimal activation temperature which conferred appropriate local rearrangement of the pore system of the zeolite crystal lattice. This is demonstrated by a higher amount of methanol chemisorbed on the zeolite surface as compared to the parent zeolite (see Table 3.25) ; and (ii) a higher density of acid sites, corresponding to an increase of 35 % with respect to the parent zeolite, which results from the contribution of these newly formed acidic hydroxyl groups (see Table 3.26) as well as the highest catalytic activity recorded at the maximum (II) of MTBE yield. These newly formed acidic hydroxyl groups result from the reaction of the zeolite surface with the H^+F^- ion pairs (proton attack) under the action of a relatively high thermal activation. Their formation also favors the simultaneous insertion of fluoride ions onto the zeolite surface as exemplified by forms IIa and IIb in Figure 3.25. The decrease in absorbance of the (1103 - 1106 cm^{-1}) band characteristic of the T-O-T bond

reveals the breakage of some of the surface Si-O-Si or Si-O-Al bonds (see Table 3.23) of the zeolite primary units. The breakage of these surface T-O-T bonds, being considered as local events under the combined effects of the acidic proton (from H^+ F^-) and a relatively high activation temperature, could not be compensated by any global readjustment as in the case of a normal "proton attack" (107). In our case, the loss of some bonds of the zeolite primary units is evident because of a decrease in the values of the absorbance at the FT-IR wavenumber of 1104 cm^{-1} (from 325°C to 450°C, see Table 3.23). In addition, the presence of F–Al bonds adjacent to some bridged hydroxyl groups (form IIa of Fig. 3.25), similar to one of the acid site forms observed by Becker and Kowalak (110), increases the strength of the latter acidic groups through the strong electron-withdrawing effect induced by fluorine. This is in agreement with the fact that fluorine is the strongest electronegative element of the periodic table and is characterized by an electronegativity value of 4.0 according to Pauling's scale of electronegativity (127). This increase in acid strength is illustrated in Figure 3.22 by the ammonia TPD profile of the H-ZSM5/F3 catalyst (activated at 450°C) showing an important shoulder peak at high temperatures when compared to the parent zeolite profile which corresponds to the strong acid sites. In fact, while the parent zeolite exhibits two ammonia desorption peaks at ca. 360°C and 550°C (Fig. 3.22.a), the H-ZSM5/F3 catalyst activated at 450 °C shows three desorption peaks at ca. 370°C, 560°C and 630°C (Figure 3.22.b), the last desorption peak

corresponding to the strongest acid sites. The consequent enhancement of catalytic activity arising from the increase in density and strength of the surface acid sites is in agreement with Ancilloti's results on the liquid phase reaction, according to which the MTBE synthesis requires a high density of medium – strong acid sites, i.e. from 1 to 5 milliequivalents of H^+ per gram of dry resin catalyst (12). It should be remembered that, with the H-ZSM5 / F3 catalyst activated at 450°C, there is : i) no significant change in the degree of crystallinity and in both total and micropore BET surface areas (Table 3.20) ; and ii) no significant formation of octahedral Al^{3+} species as shown by the corresponding ^{27}Al MAS-NMR spectrum (Fig. 3.19). This means that there is no significant dealumination, the Al atoms under consideration being still in the tetrahedral (or distorted tetrahedral) configuration. Thus, the zeolite surface reached the most favorable "reagent diffusion / acidity" situation at 450°C, resulting in the highest catalytic activity in MTBE synthesis as illustrated by the maximum (II) in Figure 3.23.

- f) At an activation temperature higher than 450 °C, the dehydroxylation of the zeolite surface, i.e. the loss of hydroxyl groups at high temperatures occurs (111,112). This phenomenon is known to produce Lewis acid sites in the zeolite structure which consists of tri-coordinated Al and Si atoms (Form IV of Fig. 3.25) at the expense of the Brønsted acid sites (113). In fact, when the parent zeolite was heated from 450°C to 500°C only, a limited decrease in the values of the B/L and B/(B,L) ratios determined by means of the FT-IR bands of adsorbed pyridine, was

observed (see Table 3.24). The loss of these hydroxyl groups creates more adsorption sites available, whereby a slightly higher amount of methanol chemisorbed as demonstrated in Table 3.25. At 500°C, the extent of breakage of the zeolite surface Si-O-Si and Si-O-Al bonds was the same as that observed at 450°C, as revealed by the similar decrease in absorbance of the 1104 cm^{-1} band which corresponds to the loss of some bonds of the zeolite primary units (Table 3.23).

With the H-ZSM5/F3 catalyst activated in the same way, the following surface rearrangement took place :

- transfer of the F^- ions from the F–Al bond of form IIa to the adjacent Si atom to give a more stable conformational form IIIa described in Fig. 3.25. This fluoride ion transfer which results in a more stable Si–F bond (114, 115), is favored by (i) the higher electronegativity of Si atoms with respect to Al, (ii) a higher activation temperature used in this transfer, i.e. 500°C, (iii) the quite comparable bond energies of Si–F and Al–F, i.e. 565 and 583 kJ/mol respectively (126), and (iv) the close proximity of the Si and Al atoms. This fluoride transfer helps prevent the problem of charge constraint on the zeolite surface which arose from the dehydroxylation process in which Si and Al atoms would bear positive and negative formal charges respectively if the fluoride ion remained bonded to the framework Al atoms.

- formation of an electron deficient Si site referred to as form IIIb which derived from the form IIb . The form IIIa has a configuration similar to the Lewis acid site reported by R.B. Borade et al. (109,116). Our hypothesis on the formation of Lewis acid sites IIIa and IIIb upon dehydroxylation at 500 °C is supported by the following experimental results:

(i) With respect to the H-ZSM5/F3 (450°C), the H-ZSM5 / F3 (500°C) catalyst shows a much lower acid sites density (see Table 3.26), which is in good agreement with the significant loss of Brønsted acid sites resulting from the dehydroxylation process, as represented in Fig. 3.25. In addition, there is a significant loss of the F–Al...OH strong acid sites, as illustrated in the ammonia TPD profile (Fig. 3.22-c) by the decrease of the peak at the highest activation temperature (only a shoulder for the catalyst activated at 500 °C), which is due to the Lewis acid site represented by form IIIa. The positively charged tri-coordinated Si atoms represented by form IIIb, resulting from the dehydroxylation process occurring at 500°C, is quite similar to that of the parent zeolite form IV activated at the same temperature. Its charge is balanced by the neighboring negatively charged Al atoms in the bridged form as pictured in Figure 1.8 in chapter I.

(ii) Similarly, the low-coordinate Si site of form IIIb originates from the condensation of the acidic hydroxyl group IIb with a neighboring proton (Fig. 3.25). Form IIIb, which is equivalent to form IV found in the dehydroxylated

parent H-ZSM5 zeolite, has thus some Lewis acid character. The experimental evidence for the formation of this second Lewis acid form in addition to the form IIIa, was obtained by the FT-IR study of pyridine adsorbed on the H-ZSM5 / F3 catalyst. In fact, when this sample was heated from 450°C to 500°C, the B/L and B/(B,L) ratios decreased in a more pronounced way than with the parent H-ZSM5 (Table 3.24). It was obvious that the large variations of these two ratios were induced by a more important decrease in the number of the Brønsted acid sites and, as a consequence, by a more significant increase in the number of the Lewis acid sites.

(iii) However, these Lewis acid sites are not as abundant and as strong as the Brønsted acid sites (form IIa, F–Al...OH configuration of Fig. 3.25), as demonstrated by the ammonia TPD profile of the H-ZSM5/F3/500°C catalyst with the decrease of the shoulder peak (Fig. 3.22.c) when compared to the profile of the H-ZSM5/F3/450°C catalyst in Fig. 3.22.b. Consequently, the lower surface acidity of the H-ZSM5/F3 (500 °C) in terms of both acid density and strength resulted in a lower MTBE yield (Fig. 3.23).

- g) The F^- concentration of the H-ZSM5 / F3 catalyst is quite low in terms of weight percent of F^- incorporated i.e. 3.5 % weight and thus does not cause any serious structural damage in the range of high activation temperatures up to 500°C as evidenced by ^{27}Al MAS-NMR, FT-IR data. The fact that there were no octahedral Al species detected in this fluorinated zeolite when activated at 500°C

(Fig. 3.20), indicates that the actual Lewis acid sites represented by the configurational forms IIIa and IIIb do not correspond to extra-lattice Al species. However, when the fluoride loading is higher than 2.6 x 10^{-3} mol.g^{-1} and the activation temperature is at least 450 °C, there is removal of some Al atoms by the F species, out of the zeolite lattice, probably by formation of fluoroaluminate complexes, $AlF_n^{(3-n)+}$, in agreement with Sur and Bryant (117). The formation of these extra-lattice Al species within the H-ZSM5/F6 catalyst (with a much higher F^- content than the H-ZSM5/F3, see Table 3.21) was clearly evident from : (i) the ^{27}Al MAS-NMR measurements (Fig. 3.21) with the appearance of an important side band at the origin of the spectrum which corresponded to the presence of octahedral Al atoms ; (ii) the X-ray diffraction work (see Table 3.20) which shows a significant decrease in the degree of crystallinity, since the Al that leaves the crystalline zeolite networks form amorphous materials, (iii) the BET surface area measurements (see Table 3.20) which revealed a noticeable decrease of both total and micropore surface areas; and (iv) the FT-IR spectra (Table 3.23) showing a dramatic decrease of the absorbance of the 1104 cm^{-1} band, and significant frequency shifts towards higher values of the FT-IR bands in the framework region.

These observations indicated that some serious dealumination process similar to that reported elsewhere (118, 119) occurred only for the H-ZSM5 / F6 catalyst, but not for the H-ZSM5 / F3 catalyst activated at the same activation

temperatures. It results from this structure degradation a significant decrease of MTBE yield for the F6 catalyst (Table 3.28). Nevertheless, when the formation of these extra-lattice Al species is quite limited in number, as in our fluorinated catalysts, the yield of MTBE remains much higher than that of the parent zeolite.

In the literature, the extra-lattice Al species have often been associated with enhanced MTBE yield (99b,18) or with enhanced activity in other catalytic reactions (116,120,121) where dealuminated zeolites were used as catalysts. Our results raise the following question : "Are the extra-lattice Al species which are produced in dealuminated zeolites, the direct or indirect cause of the enhancement of the MTBE yield, or of activity increase in other reactions, or are they the visible end-products of some Al species not completely dislodged from the zeolite lattice, which actually intervene in the reaction kinetics? ". Our results suggest that the most efficient acid sites for the MTBE synthesis are in the form IIa (Fig. 3.25) which can be easily converted to the more « visible » extra-lattice Al species.

3.3.4 Robustness of the fluorinated zeolite catalyst

In order to assess the robustness of the HZSM5 / F3 catalyst, catalytic testing was performed for a duration of 40 hours and using the same standard experimental conditions as those specified in section 2.3.2. The results show an almost unchanged catalytic activity and product selectivity when compared to those of the HZSM5 / F3 catalyst obtained from standard reaction conditions, i.e.

for a duration of 5 hours (see Table 3.29). Characterization studies, carried out on the long run used catalyst, after it was reactivated in air at 400°C for 4 hours, reveal no change in the catalyst texture in terms of both surface area and relative crystallinity (see Table 3.30). The stability of the textural properties and catalytic activity, after a prolonged catalytic testing, demonstrated that the fluorinated HZSM5 / F3 catalyst developed in this work, exhibits a strong and resistant texture under the specified thermal activation and reaction conditions of MTBE synthesis.

3.3.5 Conclusion

The incorporation of ammonium fluoride in relatively low concentration, followed by stepwise activation at high temperatures, results in a significant enhancement of the surface acidity of the medium pore sized ZSM5 zeolite. The consequent increase in catalytic activity exhibited two maximum yields of MTBE at two different final activation temperatures, 325°C and 450°C. The first one is due to the contribution of HF species chemisorbed on the zeolite surface, whereas the second maximum occurs at a significantly higher temperature, results from the proton attack of the zeolite surface by the chemisorbed H^+F^- ion pairs. In the latter case, there is formation of new Brønsted acid sites and strengthening of some of the acid sites of the parent zeolite by the strong electron withdrawing effect of the inserted fluoride ions. In both cases, the original ZSM-5 zeolite structure remains preserved owing to the quite limited amount of fluoride species incorporated and a

Table 3.29 : Comparative catalytic activity of the used H-ZSM5/F3/40 catalyst

Catalyst	Conversion (% C-atom)	Selectivity to MTBE (%)	Selectivity to C-8 (%)
H-ZSM5 (5 hour - run)	34.2	100	0
H-ZSM5/F3 (5 hour - run)	44.9	100	0
H-ZSM5/F3/40 (40 hour - run)	44.8	100	0

Table 3.30 : Comparative textural properties of the used H-ZSM5/F3/40 catalyst

Catalyst	Relative Crystallinity (%)	BET Surface Area (m^2/g)	
		Total	Micropores
H-ZSM5 (5 hour - run)	100	328	238
H-ZSM5/F3 (5 hour - run)	100	333	241
H-ZSM5/F3/40 (40 hour - run)	100	325	236

moderately high activation temperature. However, since there is some risk of the chemisorbed HF species to be washed out from the zeolite matrix by a prolonged catalyst usage and because of the moderate reaction temperature range below 325°C, fluorine insertion, obtained by activating the fluorinated catalyst at 450°C, is preferred owing to its superior textural advantages. As a matter of fact, once the fluoride ions are firmly inserted onto the zeolite framework at 450°C, the risk of their removal is actually very low or almost insignificant as long as the temperature used for reaction or deactivation remained at 450°C or below. As previously demonstrated, there is some noticeable removal of fluorine species (see Table 3.21), only at substantially higher activation temperatures, i.e. above 500°C, occurring simultaneously with a non negligible collapse of the zeolite structure. The second noteworthy advantage lies on the wider temperature range of application, up to 450°C, available for a great deal of acid catalyzed reactions requiring a higher selectivity and reaction temperatures. In addition, this procedure of fluorination followed by subsequent thermal activation at 450°C could be applied to other types of zeolite materials having different shape selectivities and structural compositions.

3.4 Fluorinated desilicated ZSM-5 zeolite

A method of controlled desilication using aqueous sodium carbonate solution as desilicating agent, developed in our laboratory by Dr. R. Le Van Mao et al. (69), has shown a selective removal of some framework Si atoms from the zeolite structure. The resulting desilicated material, although exhibiting a significant decrease of the Si/Al atomic ratio, does not present any structural change or dislodgment of framework Al atoms from their tetrahedral sites (69), as revealed by ^{27}Al and ^{29}Si MAS-NMR (see Figure 3.26). The resulting increase in the framework Al density results in a significant increase of the cation exchange capacity per unit weight (122) and of the Brønsted acid site density (123). The latter being particularly interesting in acid catalysis will be explored in this section. The smaller micropores created by this method can be modified by activation at high temperatures or by steam treatment in order to generate a single-sized and slightly larger micropore system with respect to the parent zeolite (124). A mechanism for the controlled desilication was proposed by R. Le Van Mao (68), based on the nature of the silicate debris removed, which consists exclusively of sodium orthosilicate Na_4SiO_4, and its dimer, sodium pyrosilicate $Na_6Si_2O_7$ (see Figure 3.27).

In addition, the treatment of H-ZSM5 zeolite with ammonium fluoride and subsequent activation of the resulting material at 450°C provided zeolite catalysts

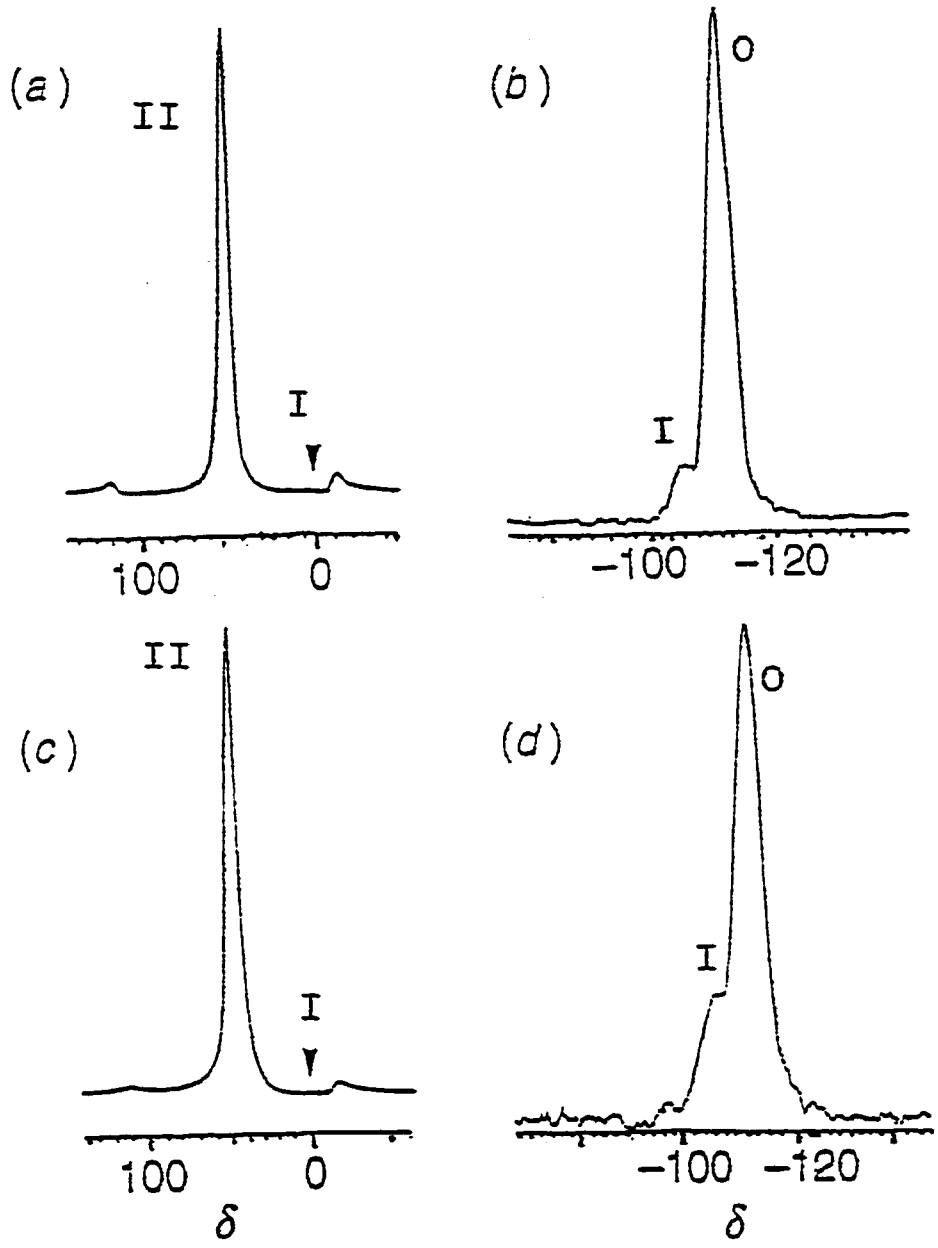

Figure 3.26 : ^{27}Al MAS-NMR spectra [chemical shift with respect to $Al[(OH_2)_6]^{3+}$] of : (a) parent ZSM-5 and (c) desilicated ZSM-5 ; and ^{29}Si MAS NMR spectra [chemical shift with respect to TMS] of : (b) parent ZSM-5 and (d) desilicated ZSM-5. (ref. 69)

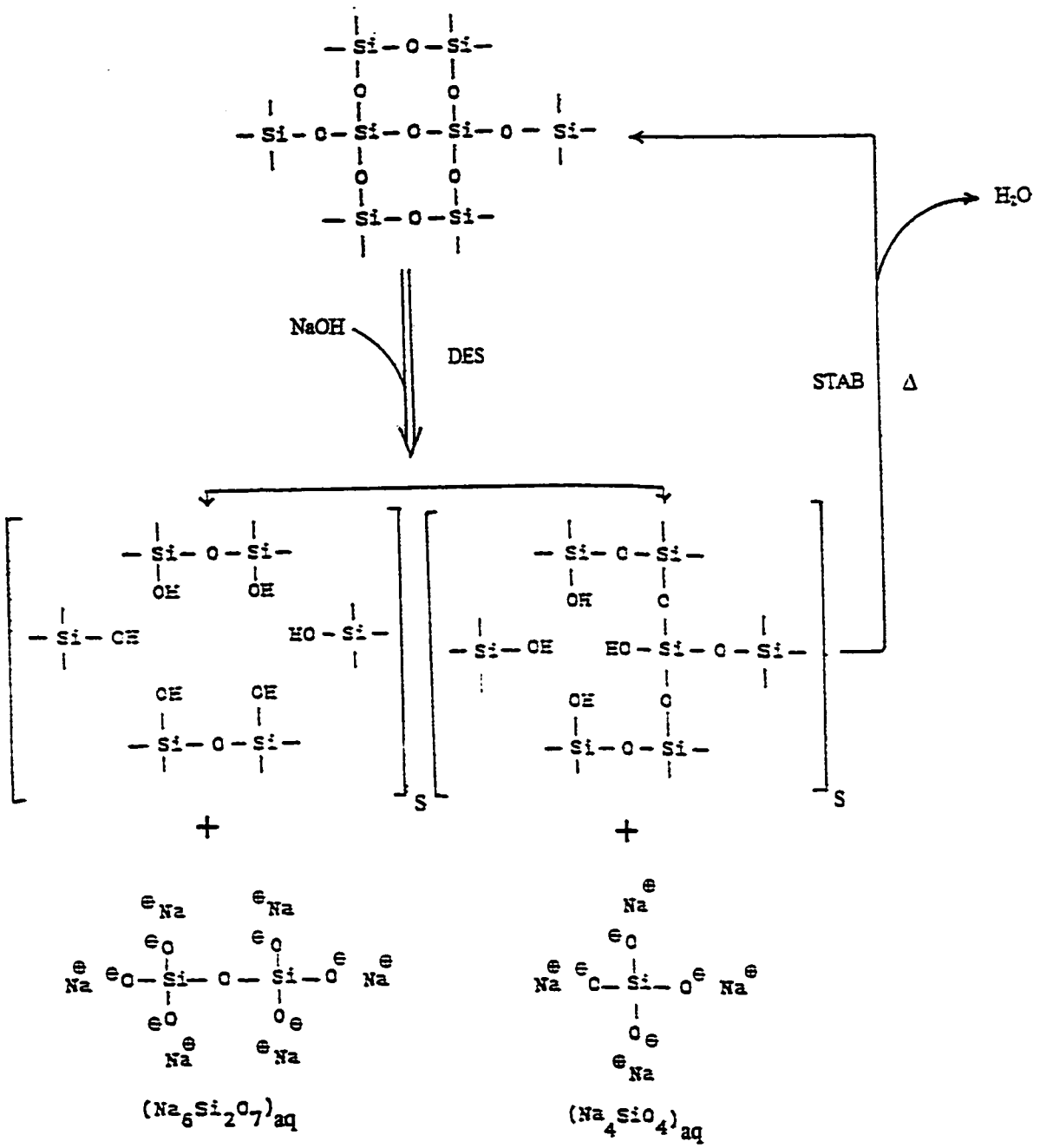

Figure 3.27 : Proposed mechanism for the desilication of ZSM-5 zeolite and the "healing" of the zeolite structure upon thermal activation (ref. 68). (DES = desilication; STAB = stabilization or framework healing)

with a substantial increase in acidic properties in terms of both acid sites density and strength (102).

It results that the objective of this work was to combine sequentially these two modification techniques developed for the ZSM-5 zeolite, i.e. first the controlled desilication, and second, the fluorination / thermal activation treatment in order to prepare a stronger acidic catalyst for the MTBE synthesis.

3.4.1 Characterization studies

3.4.1.1 Physico-chemical properties

Tables 3.31 and 3.32 report the chemical composition and physico-chemical properties of the treated and untreated zeolite materials. It shows clearly an important decrease of the Si / Al atomic ratio by 27 % upon desilication with respect to the parent zeolite, and it results a decrease in the degree of crystallinity (see Table 3.32). However such an important removal of framework Si atoms did not alter the original ZSM5 structure as illustrated by X-Ray diffraction (see Figure 3.28), BET surface area measurement and ^{27}Al and ^{29}Si MAS-NMR (69). The resulting higher Al content which shows an increase of 35 % relative to the parent zeolite, is responsible for the significant increase of cation exchange capacity and acid catalytic properties of the desilicated materials. The Si / Al ratio of the desilicated H-DZSM5 zeolite does not change upon subsequent fluorination and thermal activation (H-DZSM5/F3), therefore, these treatments do not affect

Table 3.31 : Chemical composition of the treated and untreated zeolite catalysts (powder form, activated at 450 °C overnight) in weight % on the dry oxide basis.

Sample	SiO_2 (wt %)	Al_2O_3 (wt%)	Na_2O (wt%)	Si/Al	Na/Al
H-ZSM5	95.9	3.99	0.11	20.4	0.03
H-DZSM5	94.5	5.38	0.12	14.9	0.03
H-ZSM5 / F3	96.0	3.97	0.03	20.5	0.01
H-DZSM5 / F3	94.6	5.34	0.06	15.0	0.02

Table 3.32 : Physico-chemical properties of the treated and untreated zeolite catalysts (powder form activated at 450 °C overnight).

Sample	[Al] (mM / g)	F^- content* (wt. %)	Degree of crystalinity (%)	BET surface area (m^2/g)
H-ZSM5	0.78	0	100	364
H-DZSM5	1.05	0	86	389
H-ZSM5 / F3	0.78 **	2.7	100	370
H-DZSM5 / F3	1.06 **	3.3	87	391

(*) : as determined by fluoride selective electrode analysis.

(**) : determination based on the chemical composition (atomic absorption) and the absence of the MAS-NMR band of ^{27}Al at zero chemical shift with respect to $Al(OH_2)_6^{3+}$ (octahedral Al).

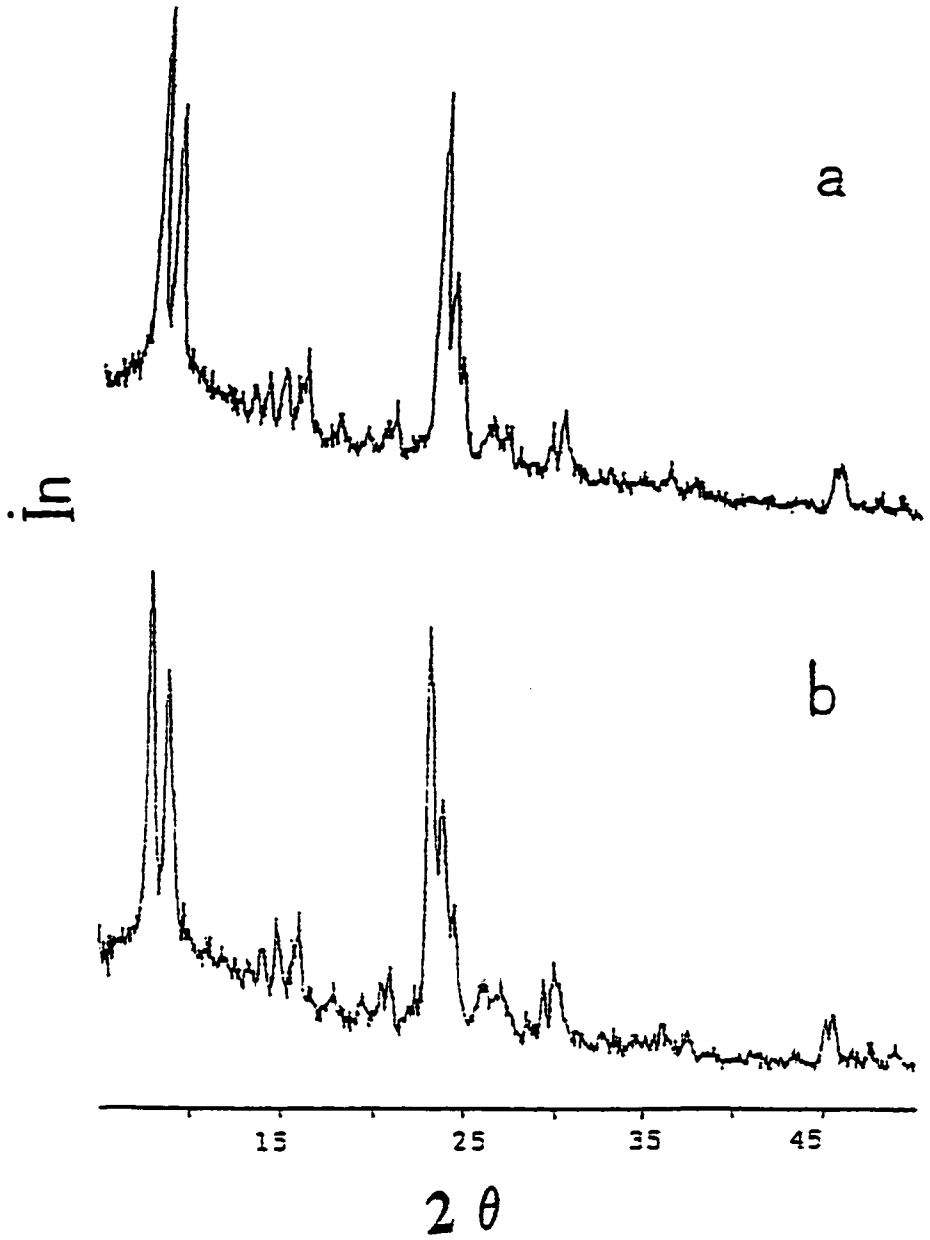

Figure 3.28 : X-ray diffraction patterns of (a) the parent H-ZSM-5 zeolite and (b) the desilicated H-DZSM5 zeolite.
(Intensity In / arbitrary units versus 2θ / degrees)

the Si and Al contents of the framework desilicated zeolite materials. In addition, the higher amount of fluoride ions incorporated, as measured for the H-DZSM5 / F3 catalyst with respect to the H-ZSM5 / F3 (ca. 20 % higher) correlates to the slightly higher BET surface area of desilicated H-DZSM5 /F3 zeolite. This moderate surface area increase (+ 6 %) which was also observed with the H-DZSM5 and H-DZSM5 catalysts (+ 5.4%), results most likely from the corrosive action of basic hydroxide ions on the ZSM-5 zeolite structure (see Table 3.32); a corrosive action not intense enough to provoke a total or partial structural collapse of the zeolite structure but moderately active to slightly enlarge the zeolite surface area through the selective removal of almost 27 % of the framework Si atoms. Subsequent fluorination and thermal activation preserves the extra surface area created by the desilication.

3.4.1.2 Determination of the acid site density and strength

The acid sites density of the desilicated and fluorinated desilicated H-ZSM5 catalysts determined by ammonia-TPD technique are reported in Table 3.33 and the profiles of acid strength provided by the same technique are plotted in Figure 3.29. In order to evaluate quantitatively the distribution of acid strengths in each catalyst, these profiles were deconvoluted according to a previous classification of acid strength performed on the same ZSM-5 zeolite, i.e. weak, medium, strong and very strong (94b). The acid site density of the H-ZSM5 parent zeolite was taken as

Table 3.33 : Determination of the surface acidity by the ammonia - TPD back titration method and the ammonia TPD profile.

Sample	Surface acidity					
	Density(#)	Acid site strength(&)			Δ(*)acidity	$R_{ac/Al}$
	(mM / g)	W + M	S	VS	(%)	
H-ZSM5	0.78	63	21	16	0	1.0
H-DZSM5	1.05	65	23	12	35	1.0
H-ZSM5/F3	1.04	43	27	30	33	1.3
H-DZSM5/F3	1.39	49	29	22	78	1.3

(#) density of the acid sites, expressed in 10^{-3} mol / g of zeolite.

(&) strength of the acid sites (distribution in % obtained by using the deconvolution technique) : Assumptions made in accordance with the desorption temperatures : W = weak ; M= medium ; S = strong and VS = very strong.

(*) % increase in the acid sites density relative to the parent H-ZSM5.

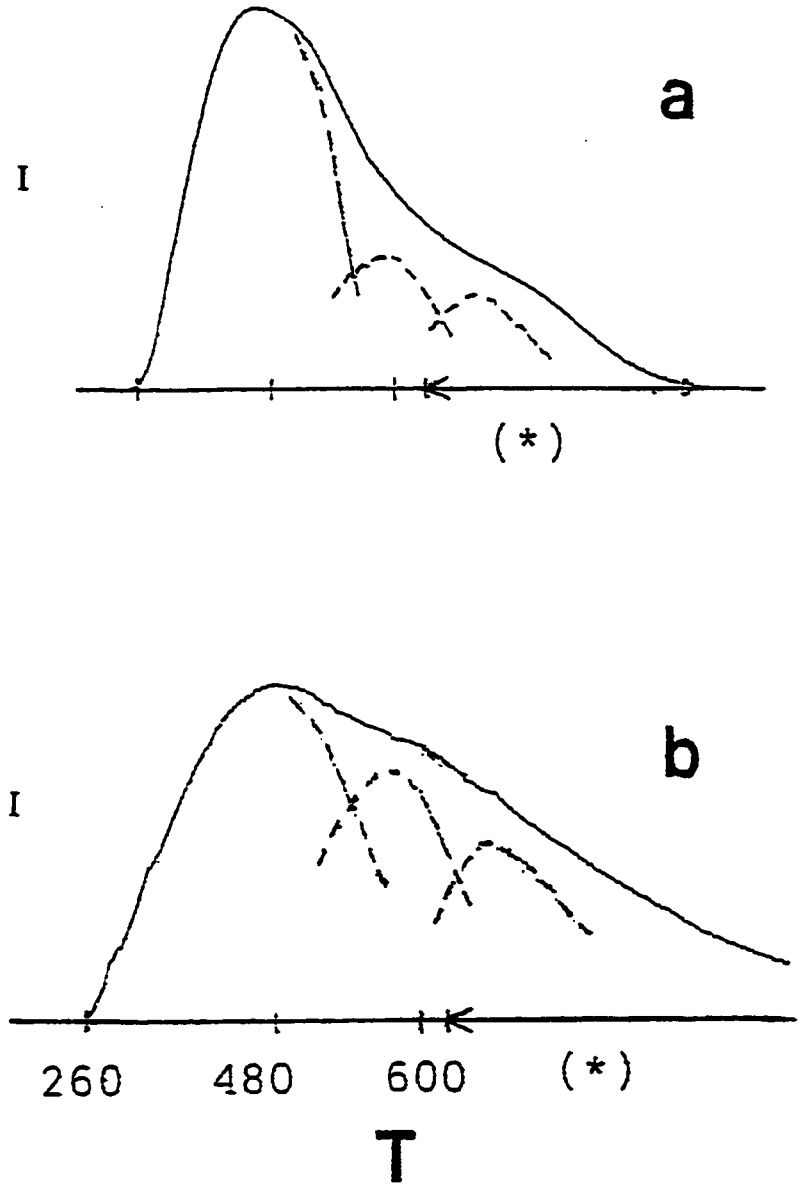

Figure 3.29 : Ammonia - TPD profile of : a) H-DZSM5 and b) H-DZSM5/F3.
T = temperature in °C ; (----) = deconvolution curves ;
(*) = constant temperature (630 °C).
In Y axis : I = response of the TCD detector, in arbitrary units.

the reference. $R_{ac/Al}$ represents the ratio of the measured Brønsted acid sites over the zeolite tetrahedral Al sites.

The titration of the acid sites of H-DZSM5 sample using the ammonia-TPD acid back-titration method gives a density of 1.05×10^{-3} mol / g zeolite (Table 3.33). This is a substantial increase (ca. 35 %) with respect to the parent zeolite and is quasi identical to fluorinated non-desilicated H-ZSM5/F3 zeolite (Table 3.33). Moreover the $R_{ac/Al}$ values which were found to be equal to 1.0 for both the parent H-ZSM5 and the desilicated H-DZSM5, indicates that all the acid sites of the desilicated zeolite were accessible to the ammonia probe molecules. The ammonia TPD profile of the desilicated H-DZSM5, illustrated in Figure 3.29.a, is somewhat similar to that obtained with the parent zeolite (see Figure 3.22.a) and this results in a similar distribution of acid strengths as reported in Table 3.33. Thus, this analogy in acid strength distribution indicates that controlled desilication using sodium carbonate as a desilicating agent does not modify significantly the original acid strength of the parent H-ZSM5 zeolite. It results that the significantly higher MTBE yield with respect to the parent zeolite (see Table 3.34), is a direct consequence of the increased acid site density for the H-DZSM5.

The acid site density found for the fluorinated H-ZSM5 / F3 catalyst, 1.04×10^{-3} mol / g zeolite (Table 3.33) represents an increase of 33 % with respect to the parent H-ZSM5 zeolite. A similar percentage increase is observed for the desilicated H-DZSM5 catalyst upon fluorination : the acid site density of the H-

DZSM5/F3 catalyst was found to be 1.39×10^{-3} mol / g zeolite (see Table 3.33). This represents an increase in acidity of 30 % when compared to the desilicated H-DZSM5. Thus, when compared to the parent H-ZSM5 zeolite, the combination of desilication and fluorination, results in a surprising increase of nearly 80 % of the original acid site density. The ammonia TPD profile of the H-DZSM5 / F3 catalyst reported in Figure 3.29.b illustrates the formation of a higher proportion of strong and very strong acid sites when compared to the H-DZSM5 sample. This shows that the effect of fluorination in non-desilicated and desilicated zeolite is practically similar. These results, together with the fact that there is almost no change of fluoride content of the used catalysts, contributes to confirm the hypothesis of a solid insertion of the fluoride ions onto the zeolite surface, stated in the previous section (Figure 3.25). The appearance of strong acid sites upon fluorination of desilicated H-DZSM5 is due to the strong electron-withdrawing effect of the inserted fluoride ions exerted on the neighboring acidic hydroxyl groups on the zeolite surface. Hence, upon fluorination and subsequent thermal activation of the desilicated H-DZSM5, there is an additional increase in both of the acid site density and strength of the original H-ZSM5 acidity.

For the two fluorinated catalyst samples studied here (H-ZSM5/F3 and H-DZSM5/F3), the same $R_{ac/Al}$ ratio of 1.3 indicates that the fluorination / thermal activation treatment imparted the same effect on the catalyst surface in a quantitative manner. In other words, the extra portion of 30 % of acid site density

in these fluorinated catalysts which are not associated with the tetrahedral Al atoms represents the newly formed acidic hydroxyl groups arising from the reaction of the hydrogen fluoride (H^+F^-)species with the zeolite surface (Figure 3.25). In addition, these fluorinated catalysts (H-ZSM5/F3 and H-DZSM5/F3) also exhibited similar acid strength distributions as reported in Table 3.33 (decrease of the number of weak acid sites and increase of the number of medium and strong acid sites).

Although the desilication or the fluorination of non-desilicated zeolite, applied separately, results in a similar acid site density as shown in Table 3.33 and hence a similar increase in surface acidity with respect to the parent zeolite, their different $R_{ac/Al}$ ratio indicates that the nature of their acid sites is quite different and therefore the numerical similarity is accidental. This is in fact exemplified by the quite different distributions of acid strengths, with that of the desilicated H-DZSM5 being more closely related to that of the parent zeolite. This discrepancy in acid strength distribution is clearly reflected in the different enhancements (2 % and 3 %) of catalytic activity observed for the desilicated H-DZSM5 and the fluorinated H-ZSM5/F3 zeolites (see Table 3.34).

3.4.2 Catalytic activity

The catalytic activity data reported in Table 3.34 are generally in good correlation with the characterization data previously interpreted. The data show

Table 3.34 : MTBE yields obtained at various temperatures (gas phase reaction).

Sample	Reaction temperature (°C)	MTBE yield (C atom %)	Total oligomers of $C_{4=}$ (C atom %)
Amberlyst-15	80	30.0	13.9
	70	47.5	6.3
H-ZSM5	80	34.2	0.0
	70	30.2	0.0
H-DZSM5	80	42.8	0.0
	75	43.7	0.0
	70	36.9	0.0
H-ZSM5/F3	80	44.9	0.0
	70	40.9	0.0
H-DZSM5/F3	80	49.9	0.0
	75	47.7	0.0
	70	46.6	0.0

clearly a two step activity enhancement of the MTBE synthesis upon controlled desilication and subsequent fluorination / thermal treatments.

The controlled desilication treatment, which contributes to increase significantly the H-ZSM5 acid site density, while keeping the acid strength almost unchanged, provides an enhancement of catalytic activity of ca. 25 % with respect to the parent zeolite. In this case the acid strength distribution of the desilicated H-DZSM5 zeolite remains quite similar to that of the parent zeolite, and the same is true for its micropore system (68) since no C-8 dimer by-products were detected after desilication.

As previously shown, fluorination followed by subsequent thermal activation, which increases the acid site density through the reaction of hydrogen fluoride (H^+F^-) species with the zeolite surface, boost the catalytic activity up to 31 % with respect to the parent zeolite. Although the controlled desilication and the fluorination / thermal treatment methods applied separately, generated similar acid sites densities, their resulting acid strengths are not the same and this discrepancy was illustrated by the mild difference in their respective catalytic behaviors (see Table 3.34). Thus, while the higher MTBE yield obtained with the H-ZSM5 / F3 catalyst is ascribed to the electron-withdrawing effect induced by the inserted fluoride ions (see section 3.4.1.2), the enhanced MTBE yield observed with the H-DZSM5 is attributed to a simple increase in the acid site density.

The combination in sequential mode of the desilication and fluorination / thermal activation give a second increase in MTBE yield with respect to the desilicated H-DZSM5 and lead to the surprising overall increase of 46 % of MTBE yield with respect to the parent zeolite, i.e. 49.9 %, a level higher than that observed with the commercial macroporous A-15 resin. The reason for this two step increase can be attributed to the combined effects of several factors : (i) an increase in acid sites density of the original H-ZSM5 zeolite resulting from the selective removal of framework Si atoms, (ii) the formation of new acidic hydroxyl groups resulting from the interaction of hydrogen fluoride (H^+F^-) species with the zeolite surface and (iii) the presence of highly electronegative fluorine, strongly inserted onto the zeolite surface which enhances the strength of the neighboring Brønsted acid sites. In addition, with the fluorinated desilicated H-DZSM5 / F3 there was no noticeable activity decay for a long-lasting run over a period of several days. In the 70 – 80°C temperature range, the successful H-DZSM5 / F3 catalyst behaved even much better than the commercial A-15 resin, not only in terms of MTBE yield, but also because there was no production of oligomers of isobutene as by-products owing to the excellent shape selectivity of ZSM-5 structure (see Table 3.34). These two factors along with the high thermal stability of ZSM-5 zeolite constitute the superior advantages of the fluorinated desilicated H-DZSM5 / F3 catalyst developed in this work over the commercial A-15 resin. On the other hand, in the MTBE synthesis, there is no real advantage

to go over 90°C as an attempt to further increase the MTBE, yield because at higher reaction temperatures, the rate of MTBE formation is seriously limited by the thermodynamic equilibrium factor, with the decomposition of MTBE becoming more and more significant (99a).

3.4.3 Robustness of the fluorinated desilicated zeolite catalyst

In order to evaluate the robustness of the H-DZSM5 / F3 catalyst, catalytic testing was performed for a duration of 40 hours and using the same standard experimental conditions as those specified in section 2.3.2. The results show an almost unchanged catalytic activity and product selectivity when compared to those of the H-DZSM5 / F3 catalyst obtained from standard reaction conditions, i.e. for a duration of 5 hours (see Table 3.35). Characterization studies, carried out on the long run used catalyst, after it was reactivated in air at 400°C for 4 hours, reveal that there was no change in the catalyst texture in terms of both surface area and relative crystallinity (see Table 3.36). The stability of the textural properties and catalytic activity, after a prolonged catalytic testing, demonstrated that the fluorinated desilicated H-DZSM5 / F3 catalyst developed in this work, exhibits a strong and resistant texture under the specified thermal activation and reaction conditions of MTBE synthesis.

Table 3.35 : Comparative catalytic activity of the used H-DZSM5/F3/40 catalyst.

Catalyst	Conversion (% C-atom)	Selectivity to MTBE (%)	Selectivity to C-8 (%)
H-DZSM5 (5 hour - run)	42.8	100	0
H-DZSM5/F3 (5 hour - run)	49.9	100	0
H-DZSM5/F3/40 (40 hour - run)	49.7	100	0

Table 3.36 : Comparative textural properties of the used H-DZSM5/F3/40 catalyst.

Catalyst	Relative crystallinity (%)	BET Surface Area (m^2/g)
H-ZSM5 (5 hour - run)	100	328
H-DZSM5 (5 hour - run)	86	389
H-DZSM5/F3 (5 hour - run)	87	391
H-DZSM5/F3/40 (40 hour - run)	86	387

3.4.4 Conclusion

The combination of the two modification techniques developed in this work for the ZSM-5 zeolite, i.e. desilication and incorporation of fluorine / thermal treatment, has produced a highly efficient catalyst for the MTBE synthesis. Both the density and strength of the acid sites are increased significantly with this sequential preparation procedure. With respect to the parent H-ZSM5 zeolite, the new fluorinated desilicated materials exhibits the following improvements in terms of surface acidity : (i) an increase in acid site density by almost 80 %, and (ii) the formation of significantly stronger acid sites. The fluorinated desilicated catalyst gives a yield of MTBE higher than that of the commercial A-15 resin, with no production of C-8 by-products owing to the shape selective ZSM-5 structure. This preparation procedure can be applied to a wide range of zeolite materials, and the resulting catalyst can be used in several acid catalyzed reactions where a high surface acidity and a specific shape selectivity are required.

CHAPTER IV

CONCLUSION

Presently the industrial production of MTBE is facing an important challenge regarding the choice of an alternative catalyst for the substitution of the commercial Amberlyst-15 resin because of its structural and exploitation related disadvantages. In this perspective, zeolite materials represent the best candidates owing to their superior structural characteristics mainly in the prevention of side reactions. However their lower catalytic activity resulting from a low surface acidity still represents a major drawback for their promising industrial application.

For this purpose, different approaches were attempted in this research work in order to remedy to this problem, and successfully modified zeolite catalysts were obtained.

The method of incorporating an organic superacid (triflic acid) in moderate concentration into the large pore Y-type zeolite produces a highly efficient catalyst showing a remarkable enhancement in catalytic activity with a MTBE conversion similar to that obtained with the commercial A-15 resin and a significantly lower production of isobutene oligomers. However, when applied to the medium pore sized ZSM-5 zeolite, characterized by an excellent shape selectivity in MTBE synthesis, this method did not yield the expected improvements because of a serious pore narrowing effect exerted by the incorporated triflic acid species within ZSM-5 pore and channel network.

Another method of fluoride incorporation onto the ZSM-5 structure using ammonium fluoride as a precursor followed by stepwise thermal activation

produces a substantial increase in zeolite surface acidity in terms of both acid site density and strength. In particular, the catalytic acitvity of the resulting material, which is significantly improved to a level close to that observed with A-15 resin, is characterized by two maxima of MTBE conversion associated to two different activation temperatures, 325°C and 450°C. Based on the satisfactory correlation between characterization data and catalytic results, a mechanism of the zeolite surface modification as a function of final activation temperatures was thus proposed. It takes into account several chemical processes, namely the chemisorption of HF species, the direct insertion of fluoride ions into the zeolite framework as well as the dehydroxylation phenomenon, each of them occurring successively at different activation temperatures, i.e. 325°C, 450°C and 500°C. While the first MTBE maximum yield at 325°C was ascribed to presence of chemisorbed HF species, the second maximum at 450°C slightly higher than the first one, was attributed to the combined action of the newly formed acidic hydroxyl groups and a strong electron withdrawing effect of inserted fluoride ions. According to the proposed mechanism, these newly formed acidic hydroxyl groups which contributes to the increase in acid site density, results from the reaction of the chemisorbed HF species with the zeolite surface accompanied by a simultaneous insertion of fluoride ions onto the zeolite surface. The latter factor in turn enhances the acid strength of the neighboring acidic groups by the strong electron withdrawing effect of fluoride ions. Nevertheless, despite these surface

reactions occurring at relatively high activation temperature, the original ZSM-5 structure and hence its specific shape selectivity remains well preserved, owing to a moderate concentration of ammonium fluoride used and the stepwise method of thermal activation.

A further step of increase in acid sites density was accomplished by the method of controlled desilication which selectively remove framework Si atoms without altering the ZSM-5 zeolite structure. By combining these two modification methods in a sequential mode, i.e. the controlled desilication followed by fluorination / thermal treatment, a stronger acidic catalyst was successfully achieved. Besides a significant enhancement of the zeolite acid strength, this fluorinated desilicated ZSM-5 exhibited an increase in acid sites density by almost 80 % with respect to the original acidity and the resulting catalytic activity in MTBE synthesis was higher than that observed with the commercial A-15 resin with, as an additional advantage, no production of isobutene dimers by-products, contrary to the A-15 resin.

Further work will include the identification of fluoride bonding types involved on the zeolite surface as well as their quantitative estimation by the ^{19}F MAS-NMR technique. It will also be possible to evaluate the relative contribution of Brønsted and Lewis acid sites of the fluorinated desilicated ZSM-5 in the overall catalytic activity by poisoning tests using pyridine and 2,6-dimethylpyridine, since pyridine inhibits both Brønsted and Lewis acid sites

whereas 2,6-dimethylpyridine inhibits selectively BAS due to the steric hindrance constraint. Further tests of catalytic activity in MTBE synthesis with fluorinated desilicated ZSM-5 will also be achieved such as the variation of MTBE yield versus reaction temperature and weight hourly space velocity in order to determine the highest MTBE conversion.

With the remarkable enhancements in both acid site density and strength, and the well preserved structural characteristics of ZSM-5 zeolite, the combined method of controlled desilication and fluorination / stepwise thermal activation at 450°C developed in this work appears promising for the application to a wide range of zeolite materials as well as to many acid catalyzed reactions occurring below 450°C and requiring a high surface acidity and shape selectivity. In addition, since the mechanism of the surface change has been elucidated by different analytical techniques, it is possible to fine tune the surface acidity of zeolite materials by selecting the appropriate activation temperature and / or the concentration of NH_4F incorporated in order to meet the acidity requirements pertaining to each type of acid catalyzed reactions.

CHAPTER V

REFERENCES

REFERENCES

1. D. E. Gushee, *Chemtech, July* 1992, 559
2. M. M. Osman, M. S. Matar and S. Koreih, *Fuel Science and Technology Int'l*, 11(10),1993, 1331
3. W.J. Piel and R.X. Thomas, *Hydrocarbon Processing*, July 1990, 68
4. a. S. J. Ainsworth, *C&EN*, June 10, 1991, 13

   b. G.J. Green and T.Y. Yan, *Ind. Eng. Chem. Res.*, (29), 1990, 1630
5. R. Le Van Mao, R. Carli, H. Ahlafi and V. Ragaini, *Catalysis Letters*, 1990, 321
6. a. J. Tejero, M. Cunill, M. Vila, M. Iborra and J. Tejero, *Ind. Eng. Chem. Res.*, (33), 1994, 2830

   b. D. N. Nakamura, *Hydrocarbon Processing*, January 1995, 15
7. a. R. Trotta and I. Miracca, *Catalysis Today*, (37),1997, 447

   b. V. Fattore, M. Massi Mauri, G. Oriani and G. Paret, *Hydrocarbon Processing*, (60), August 1981, 101

   c. S.A. Nijhuis, F.P.J.M. Kerkhof and A.N.S. Mak, *Ind. Eng. Chem. Res.*, (32), 1993, 2767
8. a. K.P. de Jong, W. Bosch and T.D.B. Morgan, *Stud. Surf. Sci. & Catal.*,(84) 1994, 1175

   b. R.J. Fessenden and J.S. Fessenden, in *Organic Chemistry*, Willard Grant

Press, Boston, Massachusetts, 1979, 280

8. c. S. Romanow-Garcia, *Hydrocarbon Processing*, Jan. 1999, 15

   d. M. Edmond, *National Petroleum News*, 87 (4), 1995, 35

   e. L. Dunn, *Hydrocarbon Processing*, June 1994, 27

   f. S. Romanow-Garcia, *Hydrocarbon Processing*, Nov. 1999, 13

9. A. Chauvel and G. Lefebvre, in *Petrochemical Processes*, Ed. Technip, Paris, 1989, 212

10. N. S. Caetano, J. M. Lourero and A. E. Rodrigues, *Chemical Engineering Science.* (49), 1994, 4589

11. G. Ertl, H. Knozinger and J. Weitkamp in *Handbook of Heterogeneous Catalysis*, Ed. Vch. Wiley, Weinheim, 1997, 1986

12. F. Ancilloti, M. Massi Mauri and E. Pescarollo, *J. Catal.*, (46) 1977, 49

13. a. F. Ancilloti, M. Massi Mauri, E. Pescarollo and L. Romagnoni, *J. Mol. Catal.*, (4) 1978, 37

    b. R.Chavez , R. Olsen and M. Ladisch, *Oil & Gas Journal*, (10), 1994, 66

14. R. Trotta and I. Miracca, in *The catalytic process from laboratory to the industrial plant*, Ed. Italian Chemical Society, Rimini, June 1994

15. a. E.M. Elkanzi, *Chemical Engineering and Processing*, (35), 1996, 131

    b. R. Kunin, E.F. Meitzner, J.A. Oline, S.A. Fisher and N. Frisch, *Ind. & Eng. Chem. Res. & Dev.*, (12), June 1962, 141

16. J.A.Moulin, P.W.N.M. van Leeuwen and R.A.van Santen, *Stud. Surf. Sci. and*

Catal., (79), 1993, 59

17. Ignac J. Jakovac, in *Catalyst Supports and supported Catalysts*, Butterworths Publishers, Stoneham, 1987, 187
18. F. Collignon, M. Mariani, S. Moreno, M. Remy and G. Poncelet, *J. Catal.* (166), 1997, 53
19. P. Chu and G. H. Kuhl, *Ind. Eng. Chem. Res.*, (26), 1987, 366
20. T. Takezono, US. Patent 4,182,913 (1980)
21. F. Lewis and S. Matar, *From Hydrocarbons to Petrochemicals*, Gulf Publishing Co., 1981, 128
22. J. Tejero, M. Cunill and M. Iborra, *J. Mol. Catal.*, (42), 1987, 257
23. H.L. Brockwell, P.R. Sarathy and R. Trotta, *Hydrocarbon Processing*, Sept. 1991, 133
24. K.P. de Jong, W. Bosch and T.D.B. Morgan, *Stud. Surf. Sci. & Catal.*, (96) 1995, 15
25. A. Kogelbauer, J. Reddick and D. Farcasiu, *J. Mol. Catal.*, (103), 1995, 31
26. J. T. Richardson, *Principles of Catalyst Development*, Plenum Press, New York & London, 1989, 77
27. L. Louis Hegedus, Alexis T. Bell, N.Y. Chen and Werner O. Hagg, *Catalysis Design Progress and Perspectives*, Wiley Science Publ., John Wiley & Sons, 1987, 114.
28. M. E. Davis, *Ind. Eng. Chem. Res.*, (30), 1991, 1775

29. D. W. Breck, *Zeolite Molecular Sieves*, John Wiley & Sons Ltd, 1974, 475

30. M. Inomata, M. Yamada, S. Okada, M. Niwa and Y. Murakami, *J. Catal.*, (100), 1986, 264

31. B. C. Gates, in *Catalytic Chemistry*, John Wiley & Sons Inc., 1991, 268

32. D.E.W. Vaughan, *Chemical Engineering Progress*, February 1988, 25

33. G. T. Kerr, *Catal. Rev. Sci. Eng.*, (23), 1981, 281

34. B. C. Gates, in *Catalytic Chemistry*, John Wiley & Sons Inc., 1991, 277

35. I. M. Campbell, in *Catalysis at surfaces*, Chapman & Hall, NY, 1988, 57

36. J.R. Anderson, K. Foger, T. Mole, R.A. Rajadhyaksha and J.V. Sanders *J. Catal.*, (58), 1979, 114

37. R. Szostak, *Molecular Sieves : Principles of synthesis and Identification*, Van Nostrand Reinhold catalysis series, New York, 1989, 31

38. B. C. Gates, *Catalytic Chemistry*, John Wiley & Sons Inc., 1991, 272

39. J. Scherzer, *Octane Enhancing Zeolite FCC Catalysts*, Marcel Dekker, 1990, 44

40. R.M. Dessau, E.W. Valyocsik and M. Goeke, *Zeolites*, (12), 1992, 776

41. F.R. Ribeiro, A.E. Rdrigues, L.D. Rollman and C. Naccache in *Zeolites: Science and Technology*, Martinius Nijhoff ed., The Hague, 1984, 291.

42. N.Y. Topsoe, K. Pedersen and E. G. Derouane, *J. Catal.*, (70), 1981, 41.

43. J.C. Vedrine, A. Auroux, V. Bolis, P. Dejaife, C. Naccache, P.

Wierzchowski, E.G.B. Derouane, J. Nagy, J.P. Gilson, J.H.C. Van Hooff, J.P. Van de Berg and J. Wolthuisen, *J. Catal.*, (59), 1979, 248.

44. H. Auroux, V. Bolis, P. Wierzchowski, P.C. Gravelle and J. C. Vedrine, *J. Chem. Soc. Faraday Trans I*, (75), 1979, 2544.

45. B. C. Gates, *Catalytic Chemistry*, John Wiley & Sons Inc., 1991, 276

46. B. M. Lok, B. K. Marcus and C. L. Augel, *Zeolites*, (6), 1986, 186.

47. J. Cattanach, E. L. Wu and P. B. Venuto, *J. Catal.*, (11), 1968, 342.

48. R. Szostak, *Molecular Sieves : Principles of synthesis and Identification*, Van Nostrand Reinhold catalysis series, New York, 1989, 35.

49. C.T. Chu and C.D. Chang, *J. Phys. Chem.*, (89), 1985, 1569.

50. P. A. Jacobs and R. Von Ballmoos, *J. Phys. Chem.*, (86), 1982, 3050.

51. J. C. Vedrine, in *Guidelines for Mastering the Properties of Molecular Sieves*, Edited by D. Barthomeuf, Plenum Press, New York, 1990, 125

52. W.J. Mortier, in «*Proc. 6th Intern. Zeolite Conf.*», 1984, p. 734

53. J. A. Rabo and G. J. Gajda, in *Guidelines for Mastering the Properties of Molecular Sieves*, Edited by D. Barthomeuf, Plenum Press, New York, 1990, p. 285.

54. M. E. Davis, *Acc. Chem. Res.*, (26), 1993, 111

55. P.B. Weisz and V.J. Frilette, *J. Phys. Chem.*,(64), 1960, 382

56. a. C. Mirodatos and D. Barthomeuf, *J. Catal.*, (93), 1985, 246

b. C. Mirodatos and D. Barthomeuf, *J. Catal.*, (114), 1988, 121

57. D.W. Breck in *Zeolites Molecular Sieves: Structure, Chemistry and Use* Wiley-Interscience Publication, JW & Sons Inc., NY , 1974, Chapter 8

58. A. Dyer in *Intoduction to Zeolite Molecular Sieves*, John Wiley & sons Ltd, 1988, 125

59. S. M. Csicsery, *Zeolites*, Vol 4, July, 1984, 202

60. N.Y. Chen, W.E. Garwood and F.G. Dwyer, in *Shape selective catalysis in Industrial applications*, Marcel Dekker Inc., N.Y., 1989, 17

61. B. C. Gates, *Catalytic Chemistry*, John Wiley & Sons Inc., 1991, 274

62. N.Y. Chen and T.F. Degnan, *Chemical Engineering Progress*, Feb. 1988, p. 32

63. S. Bhatia, in *Zeolite catalysis: Principles and applications*, CRC press Inc., Boca Raton, Florida, 1990, 89

64. J.A. Moulin, P.W.N.M. Van Leeuwen, R.A. van Santen, *Stud. Surf. Sci.& Catal.*, (79), 1993, 262

65. M. E. Davis, *Ind. Eng. Chem. Res.*, (30), 1991, 1677

66. a. J.E. Naber, K.P. de Jong, W.H.J. Stork, H.P.C.E. Kuipers and M.F.M. Post, *Stud. Surf. Sci. Catal.*, vol. 84, 1994, 2198

b. J.S. Magee and G.E. Dolbear, in *Petroleum Catalysis in Nontechnical Language*, Penn Well Publishing Comp., Tulsa OK, 1998,193

67. R. Le Van Mao, A. Ramsaran, S. Xiao, J.H. Yao and V. Semmer, *J. Mater. Chem.*, vol. 3, (5) 1995, 533

68. R. Le Van Mao, S.T. Le, D. Ohayon, F. Caillibot, L. Gelebart and G. Dénès, *Zeolites*, (19), 1997, 270

69. R. Le Van Mao, S. Xiao, A. Ramsaran and J. Yao, *J. Mater. Chem.*, vol. 4, (4) 1994, 605

70. S.B. Kulkarni, V.P. Shiralkar, A.N. Kotasthane, R.B. Borade and P. Ratnasamy, *Zeolites*, (2), 1982, 313

71. S. Brunauer, P.H. Emmett and E. Teller, *J. Am. Chem. Soc.*, (60), 1938, 309

72. M. G. White, *Heterogeneous Catalysis*, Prentice Hall Ed., 1991, 66

73. J. R. Anderson and M. Boudart, *Catalysis Sciences and Technology*, Springer-Verlag, New York, vol.2, 1981, 182

74. I. Langmuir, *J. Am. Chem. Soc.*, (40), 1918, 1361

75. E.P. Barrett, L. G. Joyner and P.R. Halenda, *J. Am. Chem. Soc.*, (73), 1951, 373

76. N.Y. Topsoe, K. Pedersen and Eric G. Derouane, *J. Catal.*, (70), 1981, 41

77. C.V. Hidalgo, H. Itoh, T. Hattori, M. Niwa and Y. Murakami, *J. Catal.*, (85), 1984, 362

78. B.M. Lock, B.K. Marcus and C.L. Angell, *Zeolites*, (6) May, 1986, 185

79. R. Le Van Mao, T. M. Nguyen and J. Yao, *Appl. Catal.*, (61), 1990, 161

80. S. Xiao, R. Le Van Mao and G. Dénès, *J. Mater. Chem.*, 5(8), 1995, 1251

81. N.Y. Topsoe, F. Joensen and E.G. Derouane, *J. Catal.*, (110), 1988, 404

82. R. Le Van Mao, V. Ragaini, G. Leofanti and R. Fois, *J. Catal.*, (81), 1983,

418.

83. G.R. Landolt, *Anal. Chem.*, (43), 1971, 613

84. a. R. Le Van Mao, P. Levesque, G. McLaughlin and L.H. Dao, *Appl. Catal.*, (34), 1987, 163.

b. E. Lundanes and T. Greibrokk, *J. High Resol. Chromato.*,(17), April 1994, 197

c. R. Le Van Mao and L. Dufresne, *Appl. Catal.*, (52), 1989, 1

85. R. Le Van Mao, H. Ahlafi & T.S. Le in : M.E. Davis, S.L. Suib (Eds.), *Selectivity in Catalysis*, ACS Symposium. Series. 517, Washington DC, 1993, p.233

86. T.M. Nguyen and R. Le Van Mao, *Appl. Catal.*, (58), 1990, 119

87. K.J. Chao, T.C. Tasi, M.S. Chen and I.J. Wang, *J. Chem. Soc. Faraday Trans. I*, (77), 1981, 547

88. A. Gicquel and B. Torck, *J. Catal.*, (83), 1983, 9

89. R. Le Van Mao, T. M. Nguyen and G.P. McLaughlin, *Appl. Catl.*, (48), 1989, 267

90. a. R. Le Van Mao and L.Huang, Am. Chem. Soc. National Meeting Boston, U.S.A. (April 22-27, 1990); *Proc. Symp. Novel Methods of Producing Olefins and Aromatics*, April 1990

b. E.P. Barrett, L.G.Joyner and P.P. Halenda, *J. Am. Chem. Soc.*, (73), 1951, 373

91. R.D. Howells and J.D. McCown, *Chem. Rev.* (77), 1977, 69

92. G.A. Olah, G.K.S. Prakash and J. Sommer in *Superacids*, John Wiley & Sons Publishers, 1985, 7

93. K.H. Chang, G.J. Kim and W.S. Ahn, *Ind. Eng. Chem. Res.*, (31), 1992, 125

94. a. C.G. Hill, in *Introduction to Chemical Engineering Kinetics and Reactor Design*, J. Wiley and Sons Ed., 1977, Chap. 6

b. J.H. Yao, Ph. D. Thesis, 1992 and P. Levesque, Ph.D. Thesis, 1987

95. "Slidewrite Plus", Version 4.00, *Advanced Graphics Software Inc.*, CA, USA, 1990

96. G. Larsen, E. Lotero, M. Marquez and H. Silva, *J. Catal.*, (157), 1995, 645

97. J. Xiao and J. Wei, *Chem. Eng. Sci.*, Vol.47, (5), 1992, 1143

98. N. Oktar, G. Dogu, I. Gonderten and T. Dogu, *J. Chem. Tech. & Biotech.*, (74), 1999, 156

99. a. A.A. Nikolopoulos, R. Oukaci, J.G. Goodwin Jr., and G. Marcelin, *Catal. Lett.*, (27), 1994, 149

b. A.A. Nikolopoulos, A. Kogelbauer, J.G. Goodwin Jr., and G. Marcelin, *Appl. Catal. A : Gener.*, (119), 1994, 69

100. A. Kogelbauer, A.A. Nikolopoulos, J.G. Goodwin Jr. and G. Marcelin, in *Zeolites and Related Microporous Materials : State of the Art 1994*, J. Weitkamp, H.G. Karge, H. Pfeifer, W. Holderich (Eds.), Elsevier,

Amsterdam, Vol.84, 1994, 1685

101. a. A.A. Nikolopoulos, A. Kogelbauer, J.G. Goodwin Jr. and G. Marcelin, *Catal. Lett.*, (39), 1996, 173

b. A.K. Ghosh and R.A. Kydd, *Zeolites*, (10), 1990, 766.

102. R. Le Van Mao, T.S. Le, M. Fairbain, A. Muntasar, S. Xiao and G. Dénès *Appl. Catal. A : Gen.*, (185), 1999, 41

103. C. Defosse and P. Canesson, *J. Chem. Soc. Faraday Trans. I*, (11), 1976, 2565

104. R. Borade, A. Sayari, A. Adnot and S. Kaliaguine, *J. Phys. Chem.*, (94), 1990, 5989

105. E.M. Flanigen and H. Khatami, *Adv. Chem. Ser.*, (1), 1971, 201

106. E.F. Vansant, P. Van Der Voort and K.C. Vrancken, *Characterization and Chemical Modification of the Silica Surface, Stud. Surf. Sci. Catal.*, Elsevier, Amsterdam, Vol. 93, 1995, 67

107. J.A. Rabo, G.J. Gajda, in *Guidelines for Mastering the properties of Molecular Sieves*, D. Barthomeuf, E.G. Derouane, W. Holderich Eds. Nato ASI Ser., Plenum Press, New York, Vol. 221, 1990, 273

108. A. Kogelbauer, A.A. Nikolopoulos, J.G. Goodwin Jr. and G. Marcelin, *J. Catal.*, (152), 1995, 122

109. R.B. Borade and A. Clearfield, *J. Chem. Soc. Faraday Trans.*, 3,(91), 1995, 539

110. K.A. Becker and S. Kowalak, *J. Chem. Soc. Faraday Trans. I*, (83), 1987, 535

111. J.C. Vedrine, A. Auroux, V. Boris, P. Dejaivre, C. Naccache, J.B. Nagy, P. Wierzchowski, E.G. Derouane, J.P. Gilson, J.H.C. van Hoof, J.P.van der Berg, and J. Wolthuizen, *J. Catal.*, (59), 1979, 248.

112. E.F Vansant, P, Van Der Voort and K.C. Vranken, in *Characterization and Chemical Modification of the silica surface*, Vol 93, Elsevier Sc., Amsterdam, 1995, p 82 and 104, and references therein.

113. D.W. Breck, in *Zeolite Molecular Sieves*, J. Wiley & Sons, New York (1974), 474.

114. R. K. Marat and A. F. Jansen, *Can. J. Chem.*, (55), 1977, 3845.

115. X. Ou and A.F. Jansen, *Inorg. Chem.*, (36), 1997, 392.

116. A.K. Ghosh and R.A. Kydd, *Zeolites*, (10), 1990, 766.

117. S.K. Sur and R.G. Bryant, *Zeolites*, (16), 1996, 118.

118. B.M. Lok, F.P. Gortsema, C.A. Messina, H. Rastelli and T.P.J. Izod, in *Intrazeolite Chemistry*, Ed. by G.D. Stucky and F.G. Dwyer, ACS Symp. Ser. 218, 1983, 41.

119. C. Coudurier and F. Lefebvre, in *Les Techniques Physiques d'Etude des Catalyseurs*, Edition Technip (Paris), 1988, 53.21.

120. R. von Ballmoos, D.H., Harris and J.S. Magee, in *Handbook of Heterogeneous Catalysis*, Ed. by G. Ertl, H. Knozinger and J. Weitkamp,

VCH Publ., Vol. 4, 1997, p. 1955.

121. M.A. Kuehne, H.H. Kung and J.T. Miller, *J. Catal.*, (171), 1997, 293

122. R. Le Van Mao, N. T. Vu, S. Xiao and A. Ramsaran, *J. Mater. Chem.*, 4, (7), 1994, 1143

123. C. Doremieux-Morin, A. Ramsaran, R. Le Van Mao, P. Batamack, L. Heeribout, V. Semmer, G. Dénès and J. Fraissard, *Catal. Lett.*, (34), 1995, 139

124. R. Le Van Mao, N. Borsuk, D. Ohayon, A. Ramsaran, S.T. Le and G. Dénès *Mat. Res. Soc. Symp. Proc.*, Vol. 454, 1997, p. 73

125. T.S. Le and R. Le Van Mao, *Microp. Mesopor. Mater.*, 34, (1), 2000, 93

126. J.E. Huheey, E.A. Keiter and R.L. Keiter, *Inorganic Chemistry : Principles of Structure and Reactivity*, 4th Ed., Harper Collins : New York, 1993, A-30

127. D. R. Lide, in *CRC Handbook of Chemistry and Physics*, 79th Ed., 1998-1999, 9-74

APPENDICES

APPENDIX 1

X-Ray Diffraction Patterns

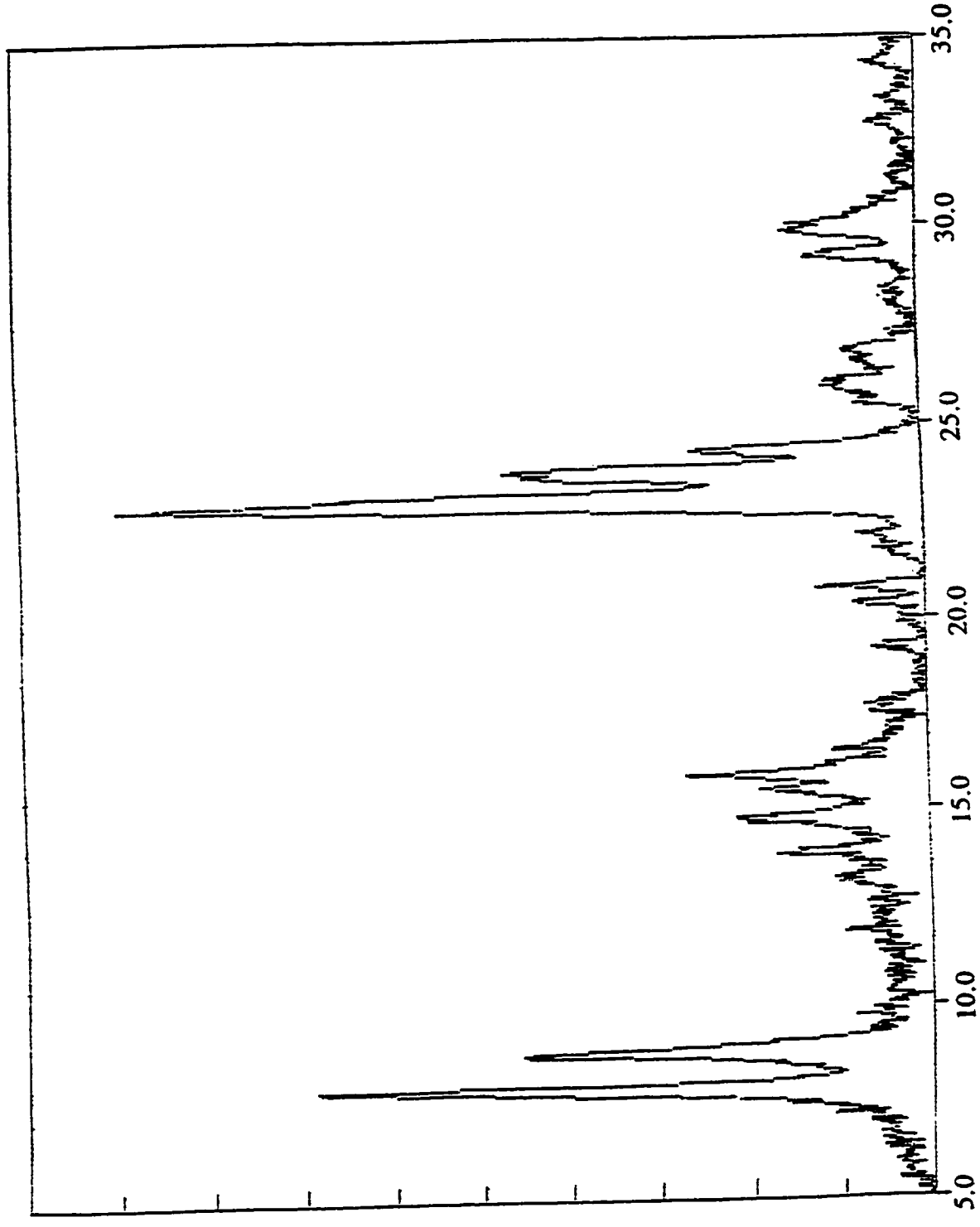

Figure A1.1 : X-Ray diffraction pattern of the parent Na-ZSM-5 zeolite.

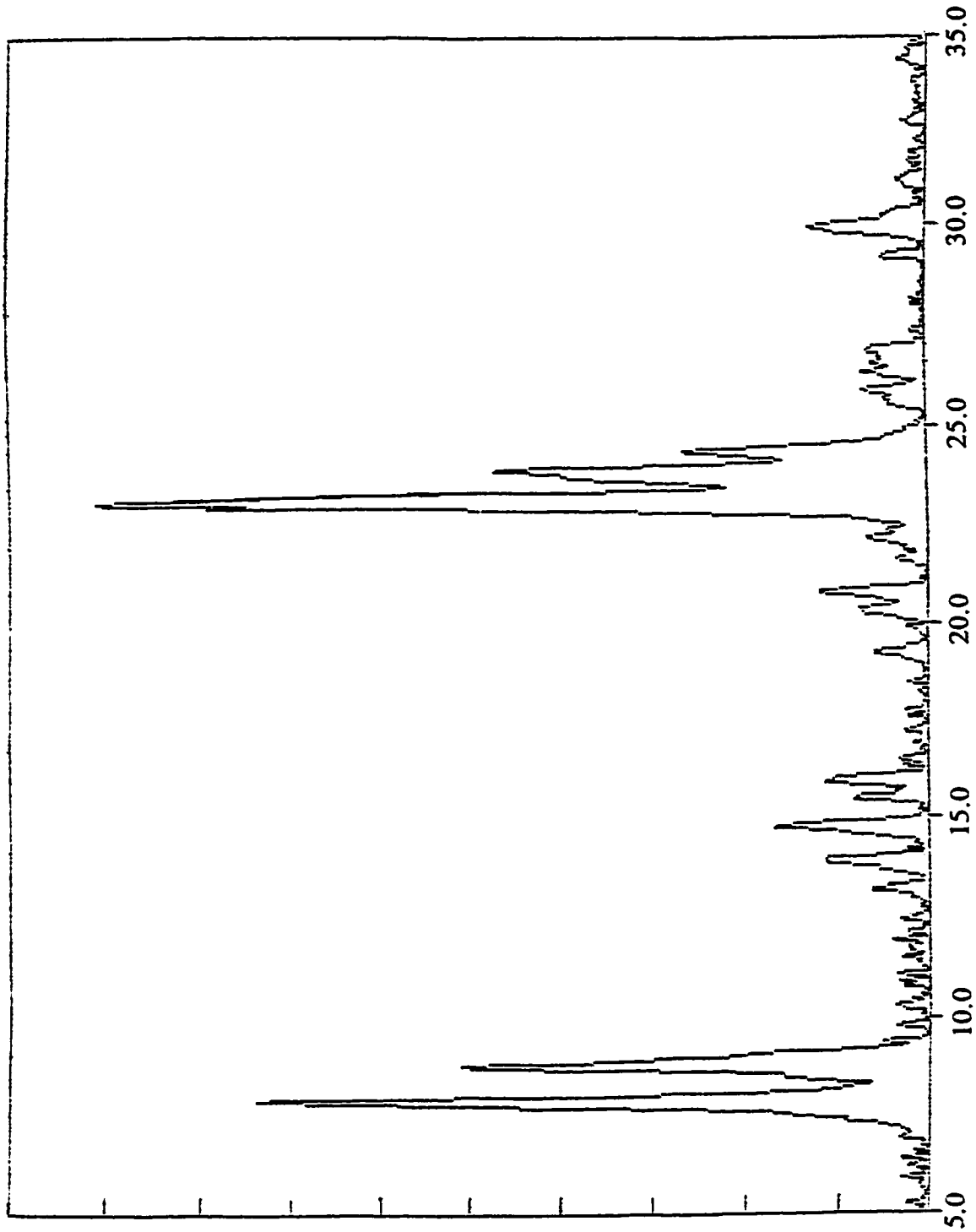

Figure A1.2 : X-Ray diffraction pattern of the parent H-ZSM-5 zeolite.

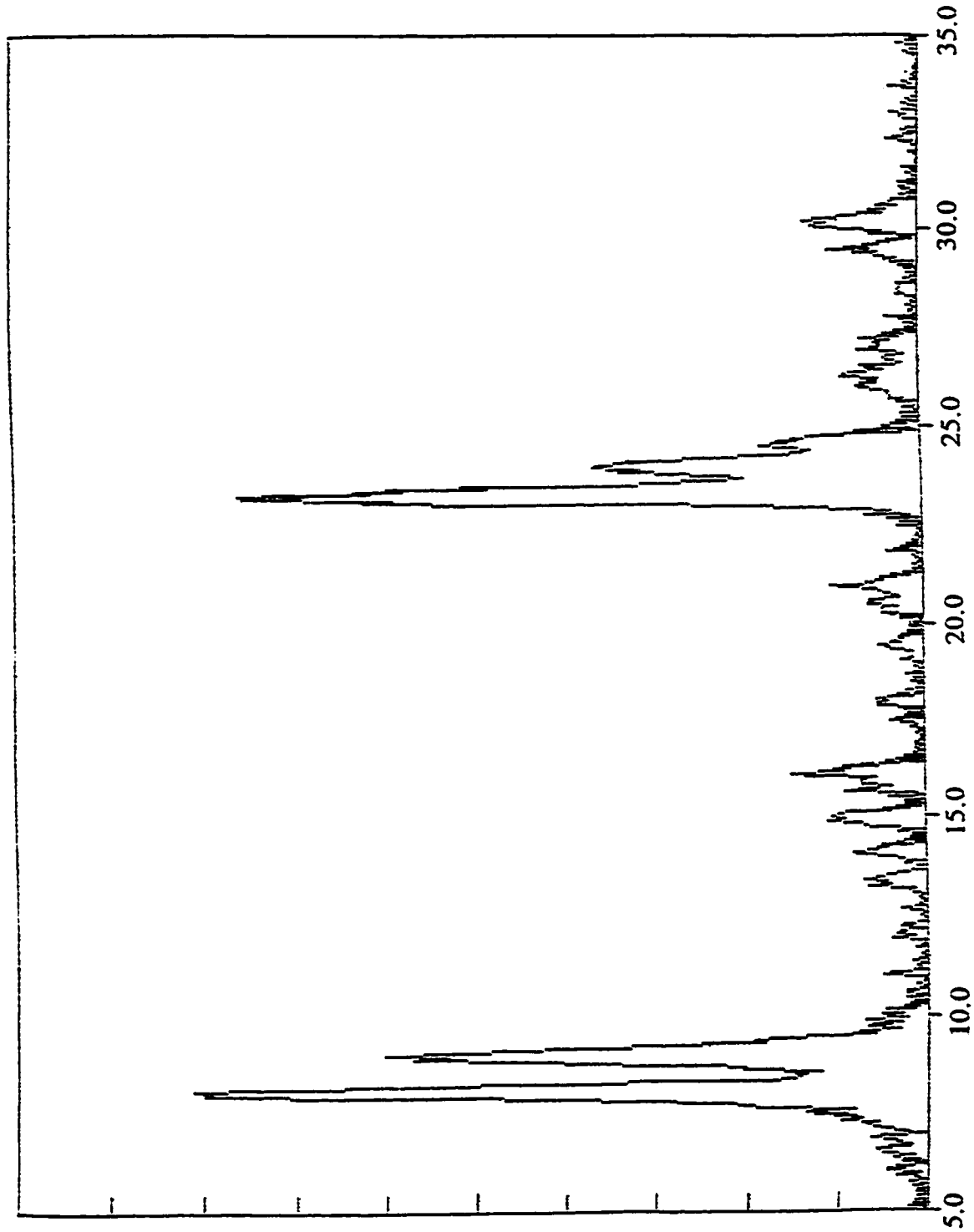

Figure A1.3 : X-Ray diffraction pattern of the desilicated Na-DZSM-5 zeolite.

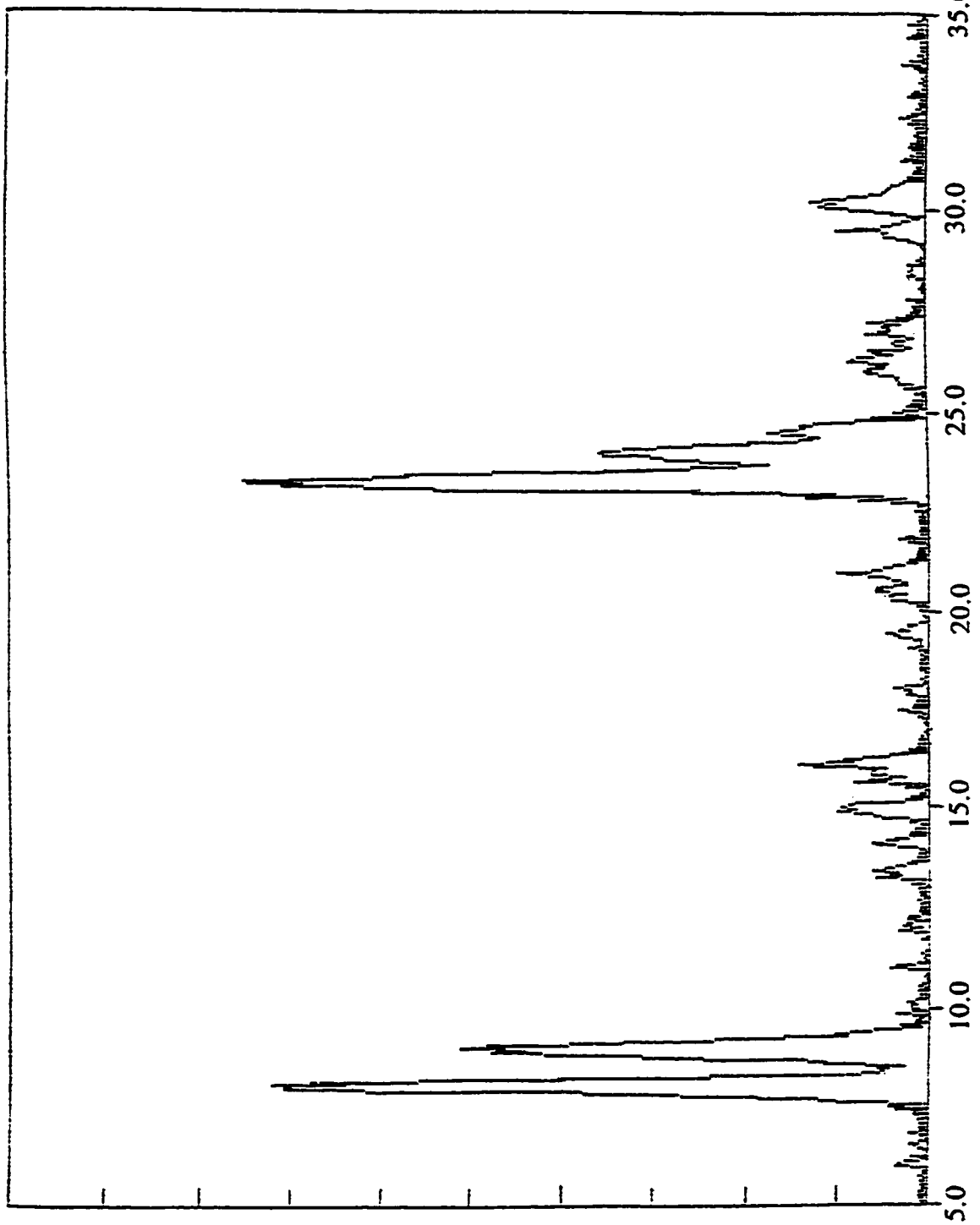

Figure A1.4 : X-Ray diffraction pattern of the desilicated H-DZSM-5 zeolite.

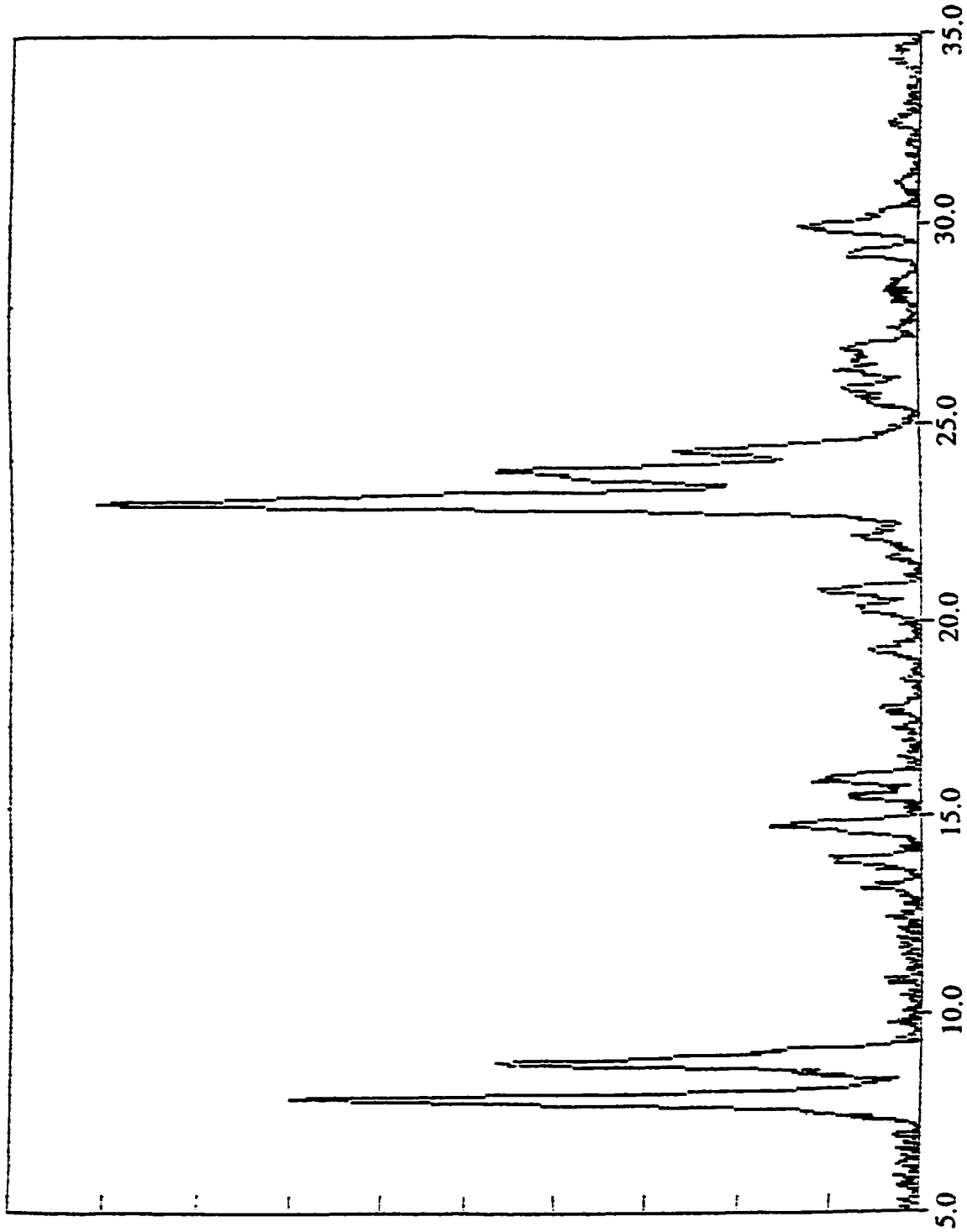

Figure A1.5 : X-Ray diffraction pattern of the H-ZSM-5 / 3 % TFA sample.

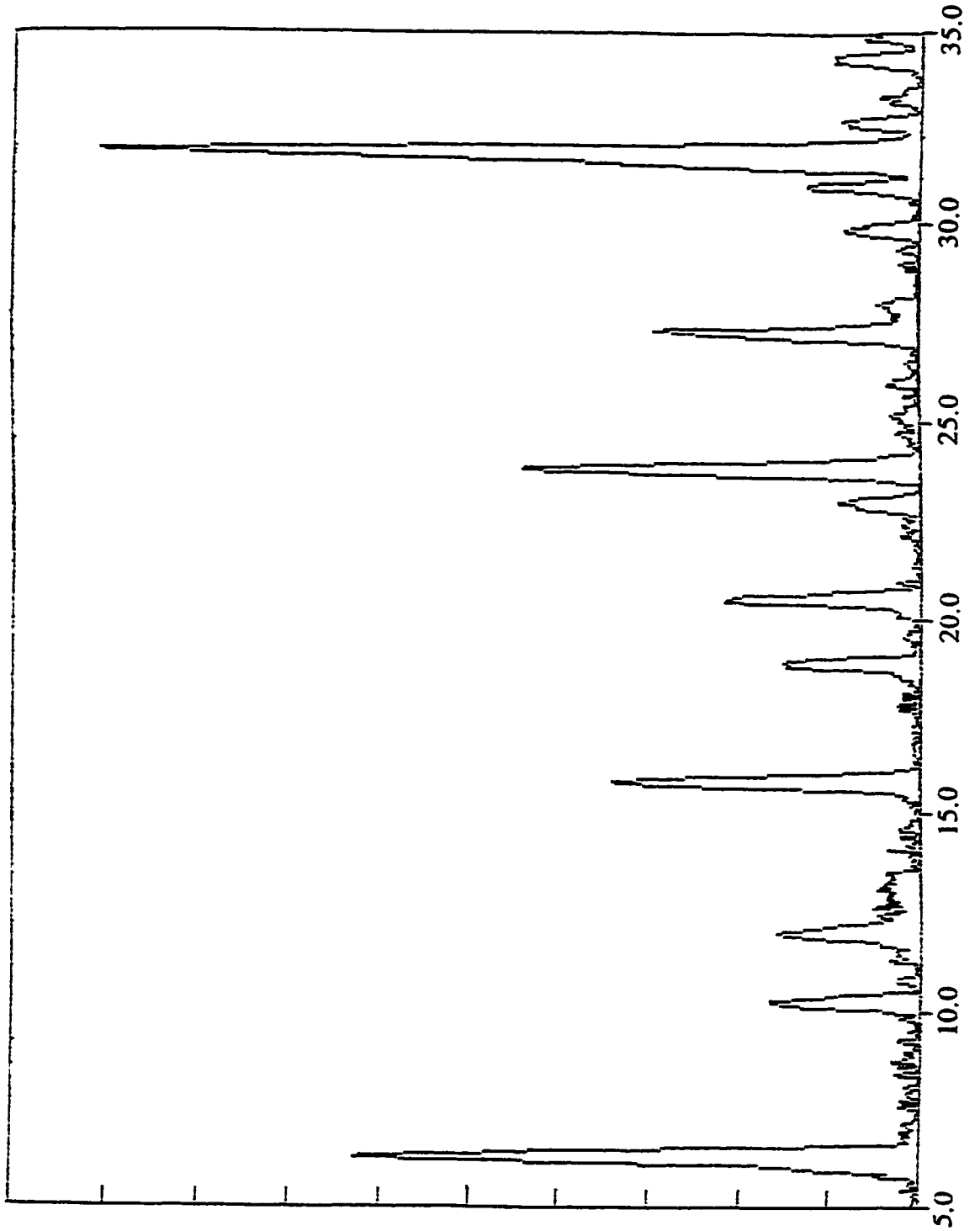

Figure A1.6 : X-Ray diffraction pattern of the parent H-Y zeolite.

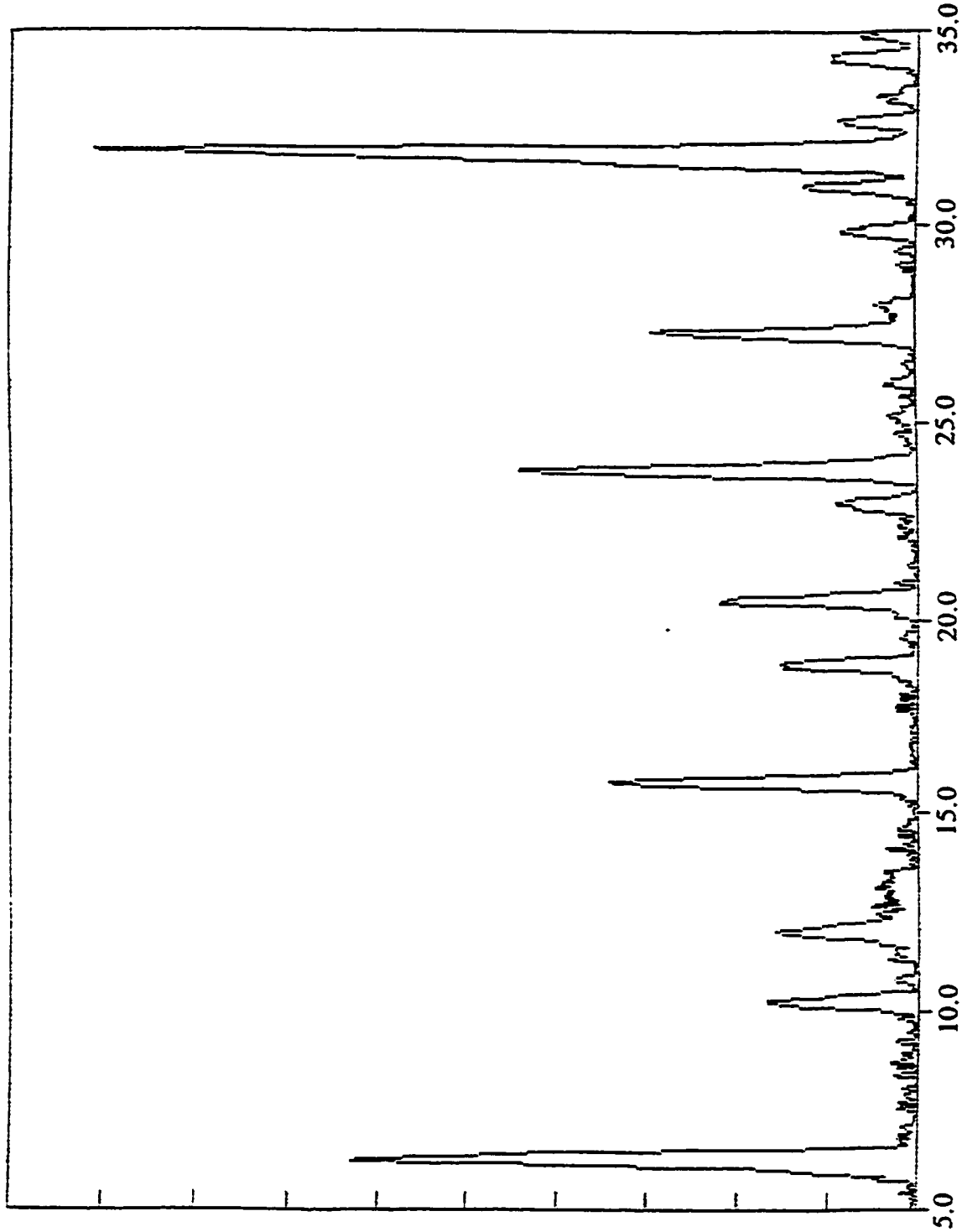

Figure A1.7 : X-Ray diffraction pattern of the H-Y / 3 % TFA sample.

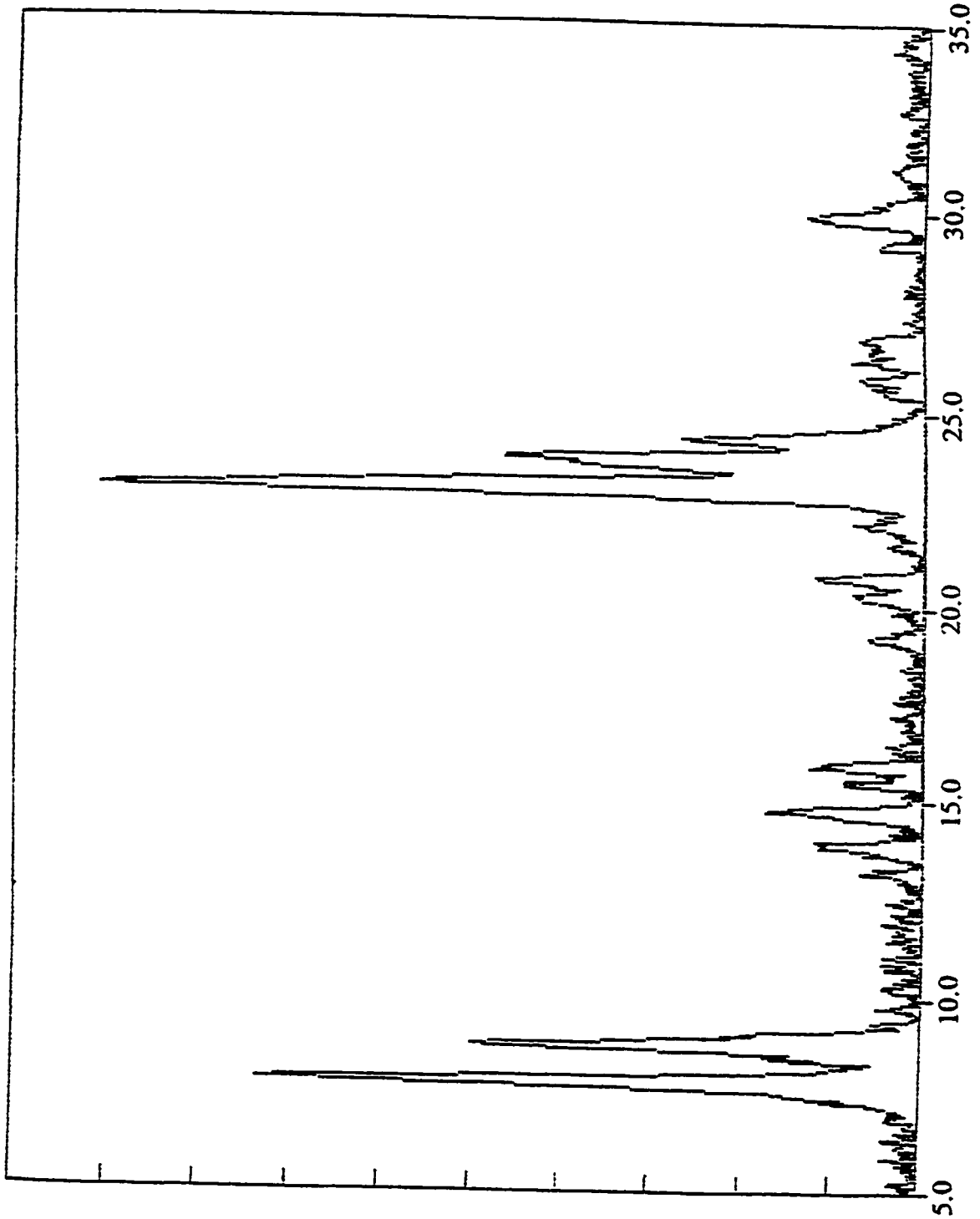

Figure A1.8 : X-Ray diffraction pattern of the fluorinated H-ZSM-5 / F3 / 450°C sample.

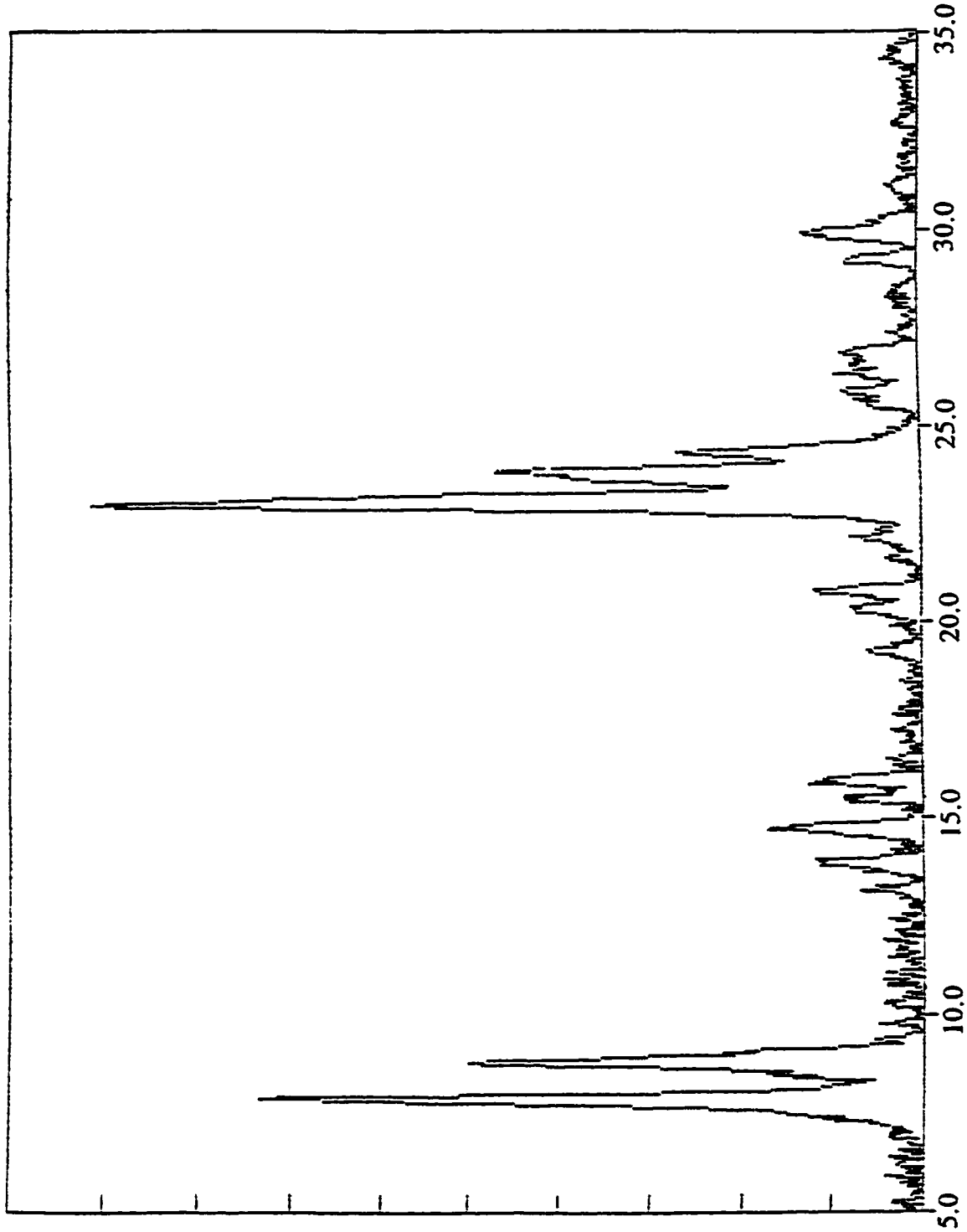

Figure A1.9 : X-Ray diffraction pattern of the fluorinated H-ZSM-5 / F4 / 450°C sample.

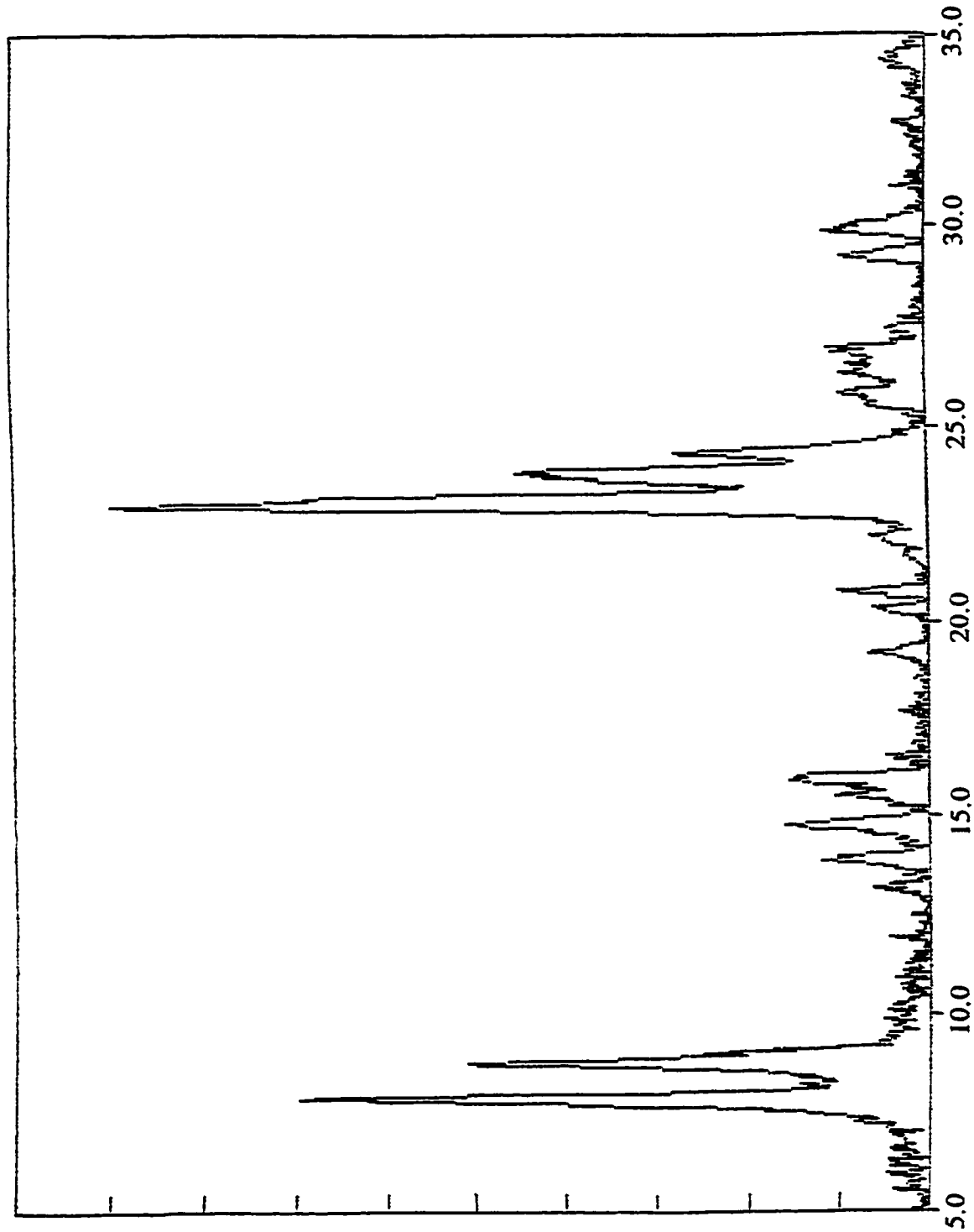

Figure A1.10 : X-Ray diffraction pattern of the fluorinated H-ZSM-5 / F5 / 450°C sample.

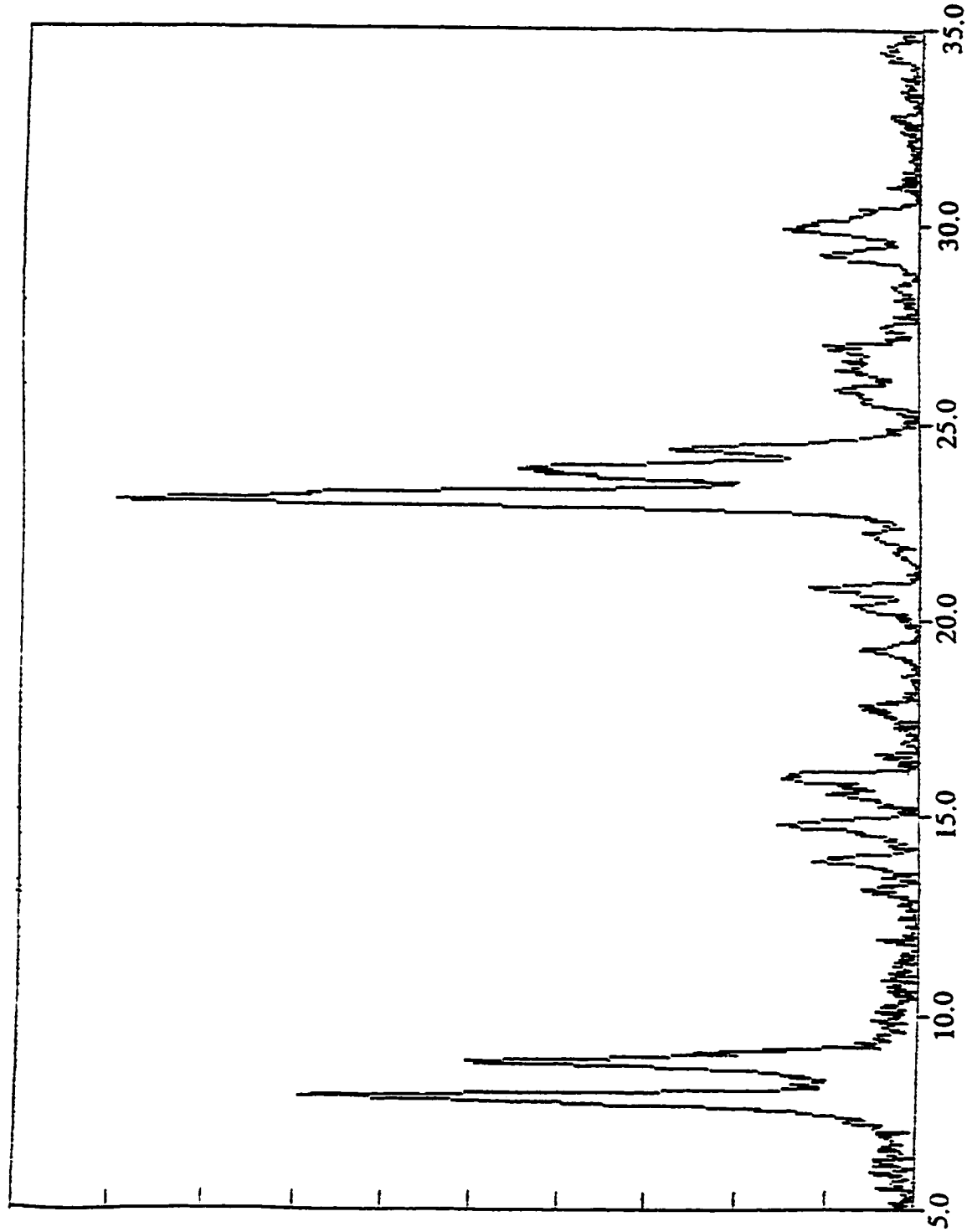

Figure A1.11 : X-Ray diffraction pattern of the fluorinated H-ZSM-5 / F7 / 450°C sample.

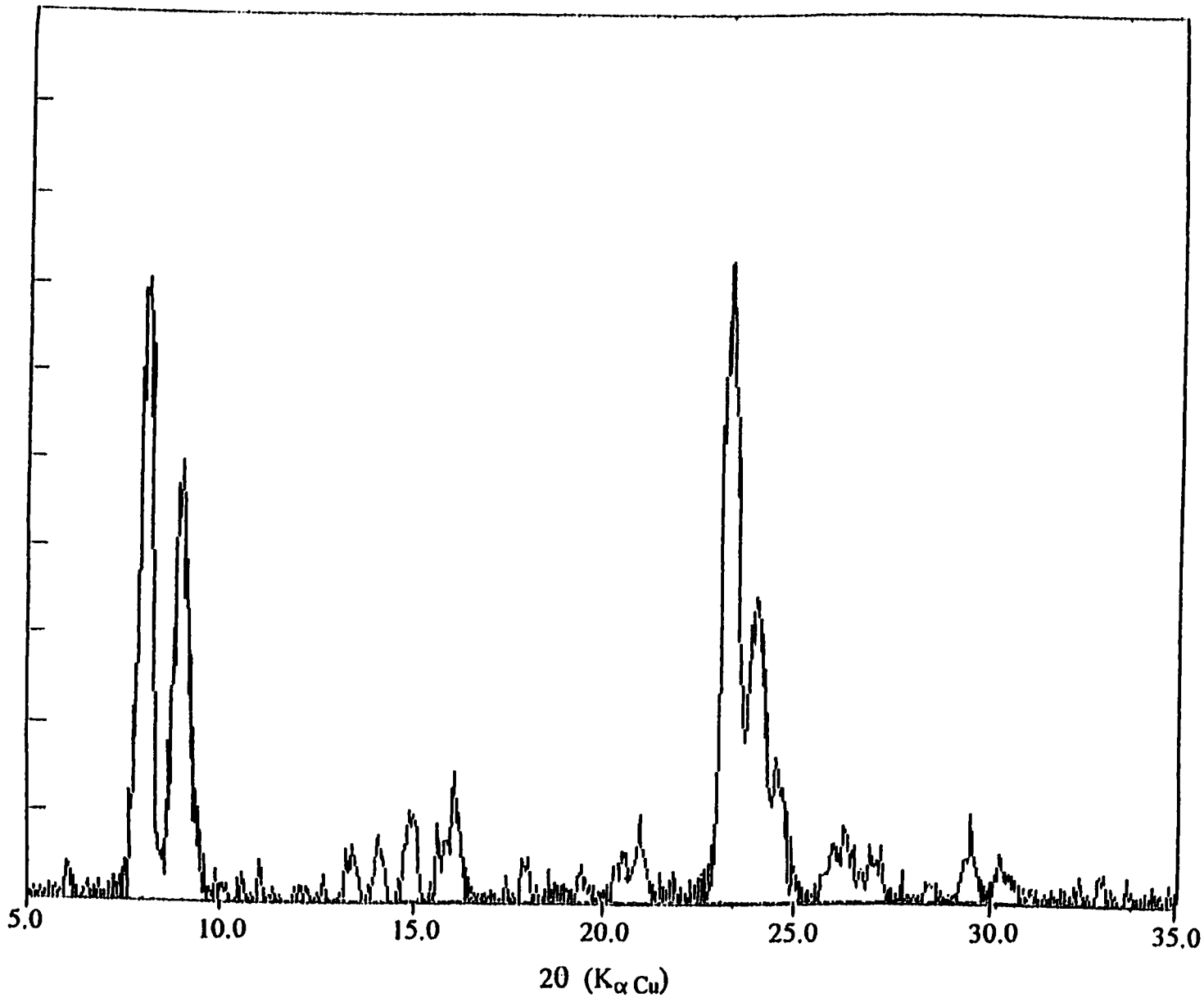

Figure A1.12 : X-Ray diffraction pattern of the fluorinated H-ZSM-5 / F6 / 450°C sample.

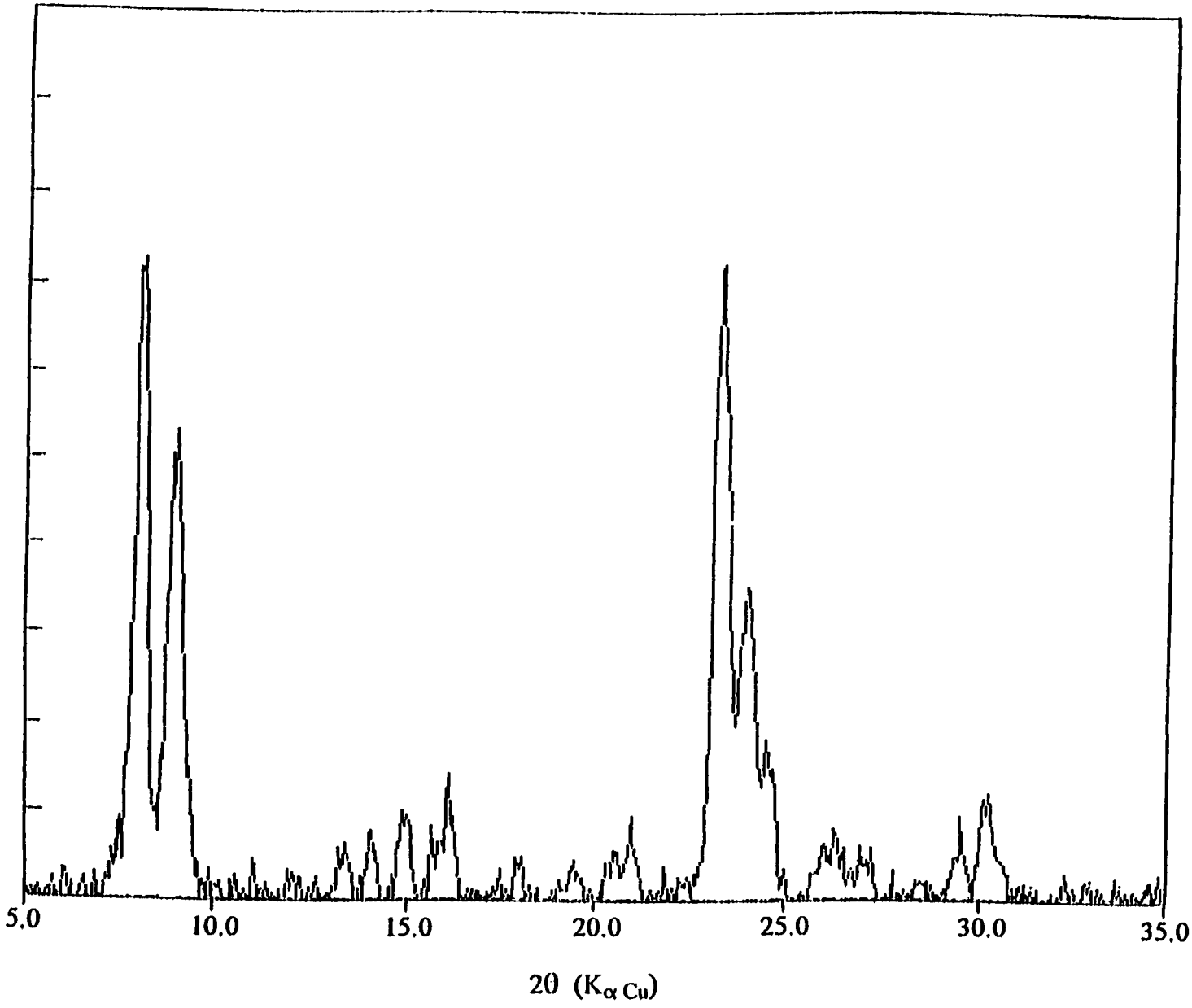

Figure A1.13 : X-Ray diffraction pattern of the fluorinated H-ZSM-5 / F6 / 500°C sample.

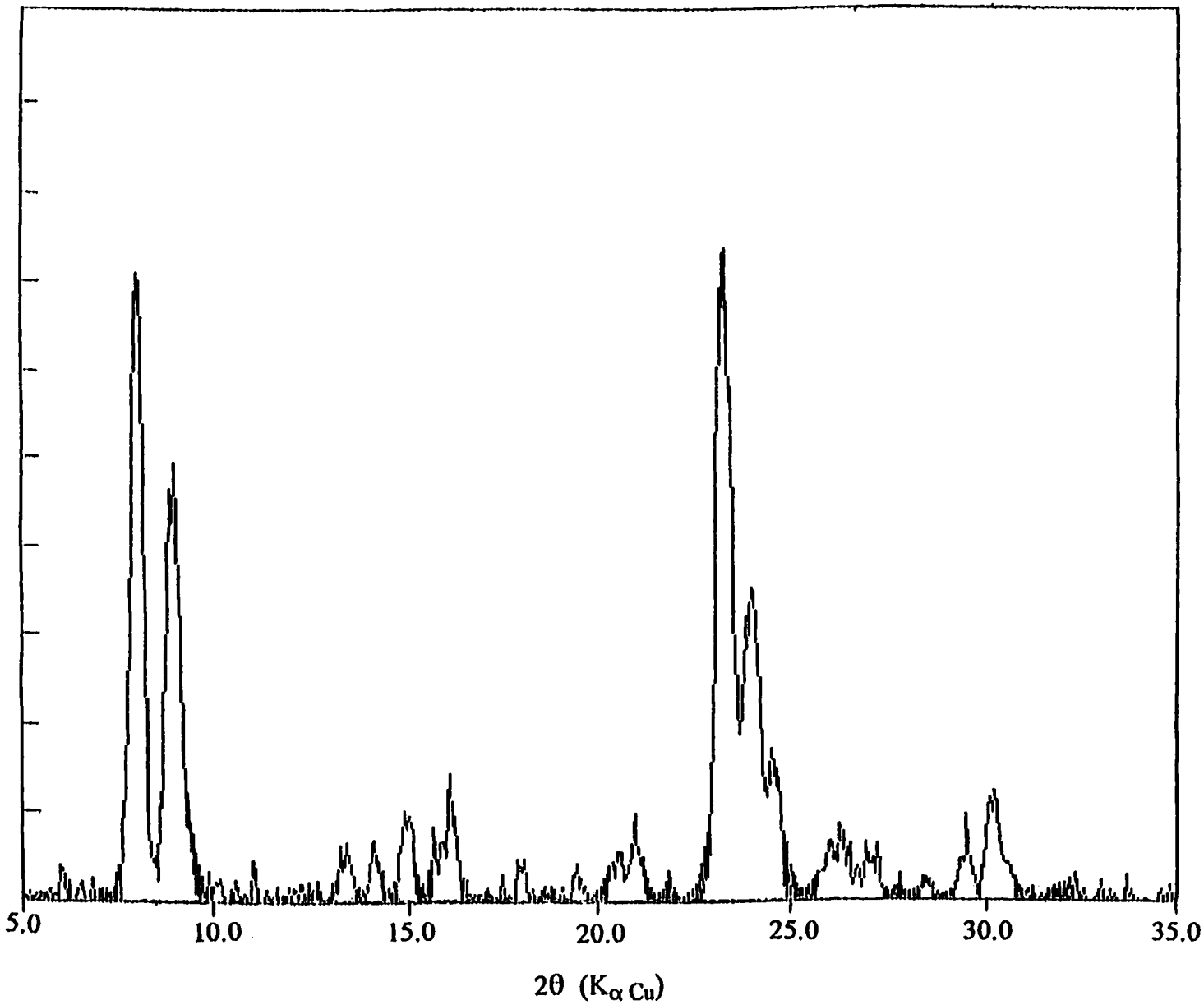

Figure A1.14 : X-Ray diffraction pattern of the fluorinated H-DZSM-5 / F3 / 450°C sample.

APPENDIX 2

FTIR Spectra

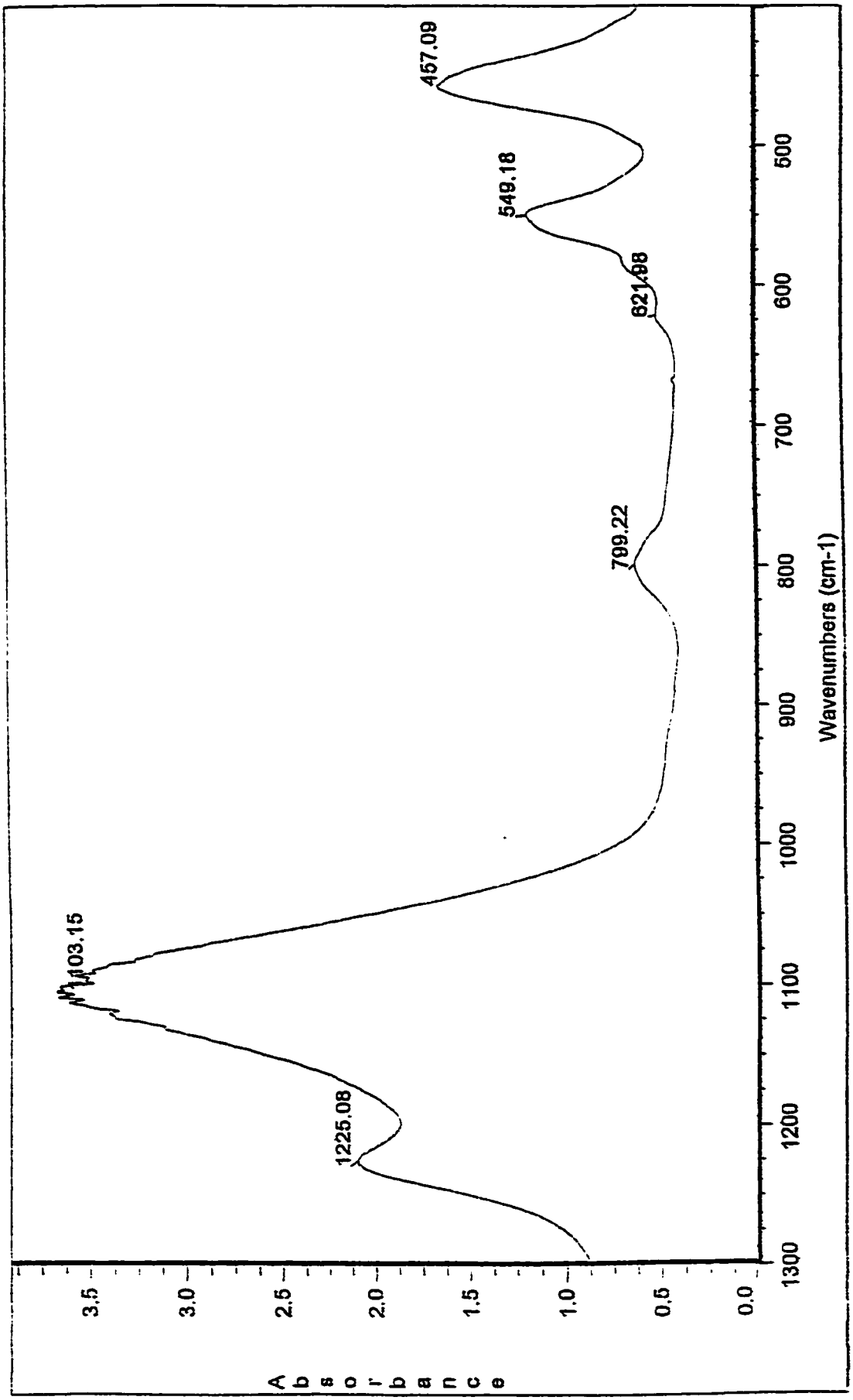

Figure A2.1 : FTIR spectrum of H-ZSM5 sample activated at 450°C in the framework region.

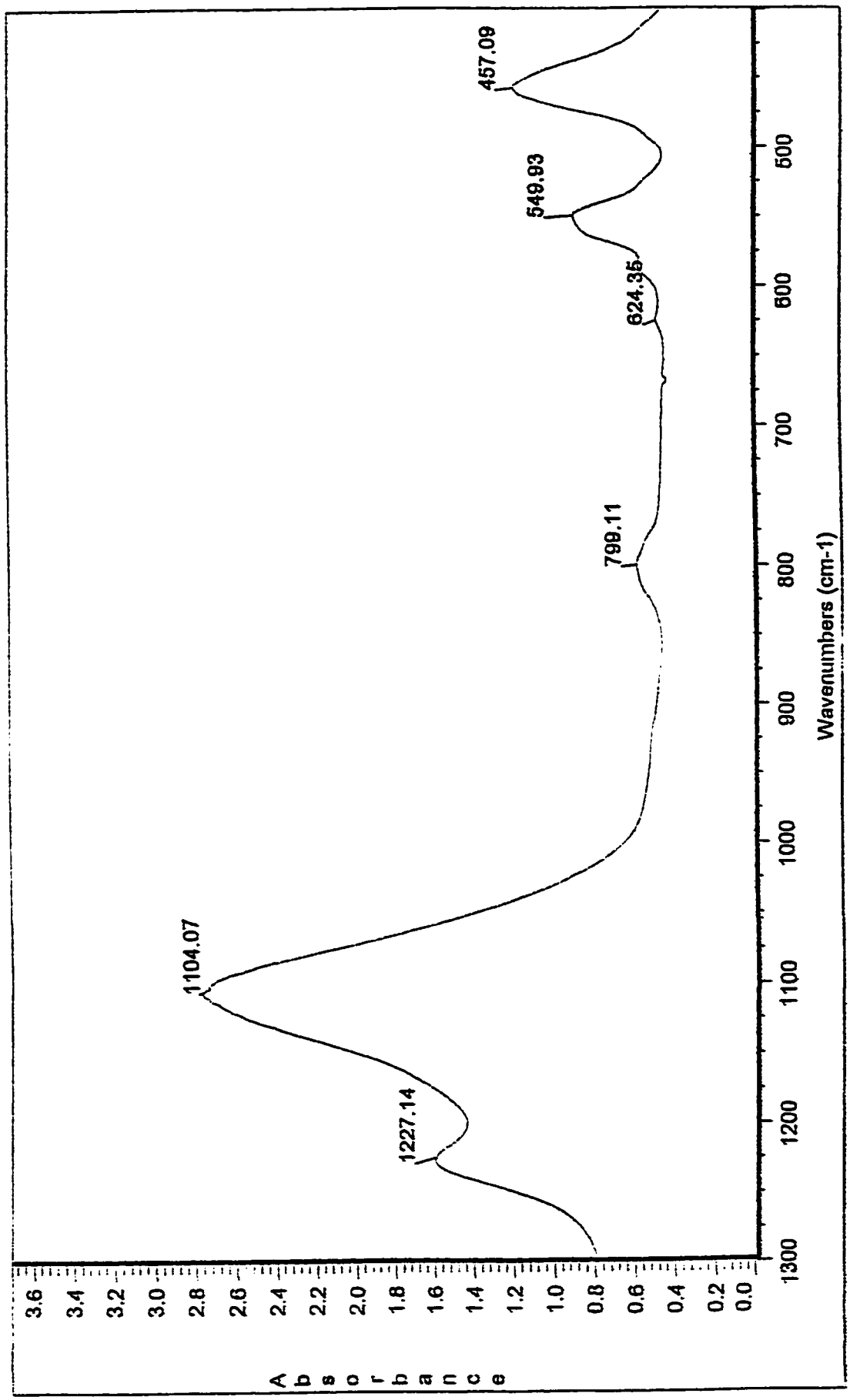

Figure A2.2 : FTIR spectrum of H-ZSM5 / F3 sample activated at 325°C in the framework region.

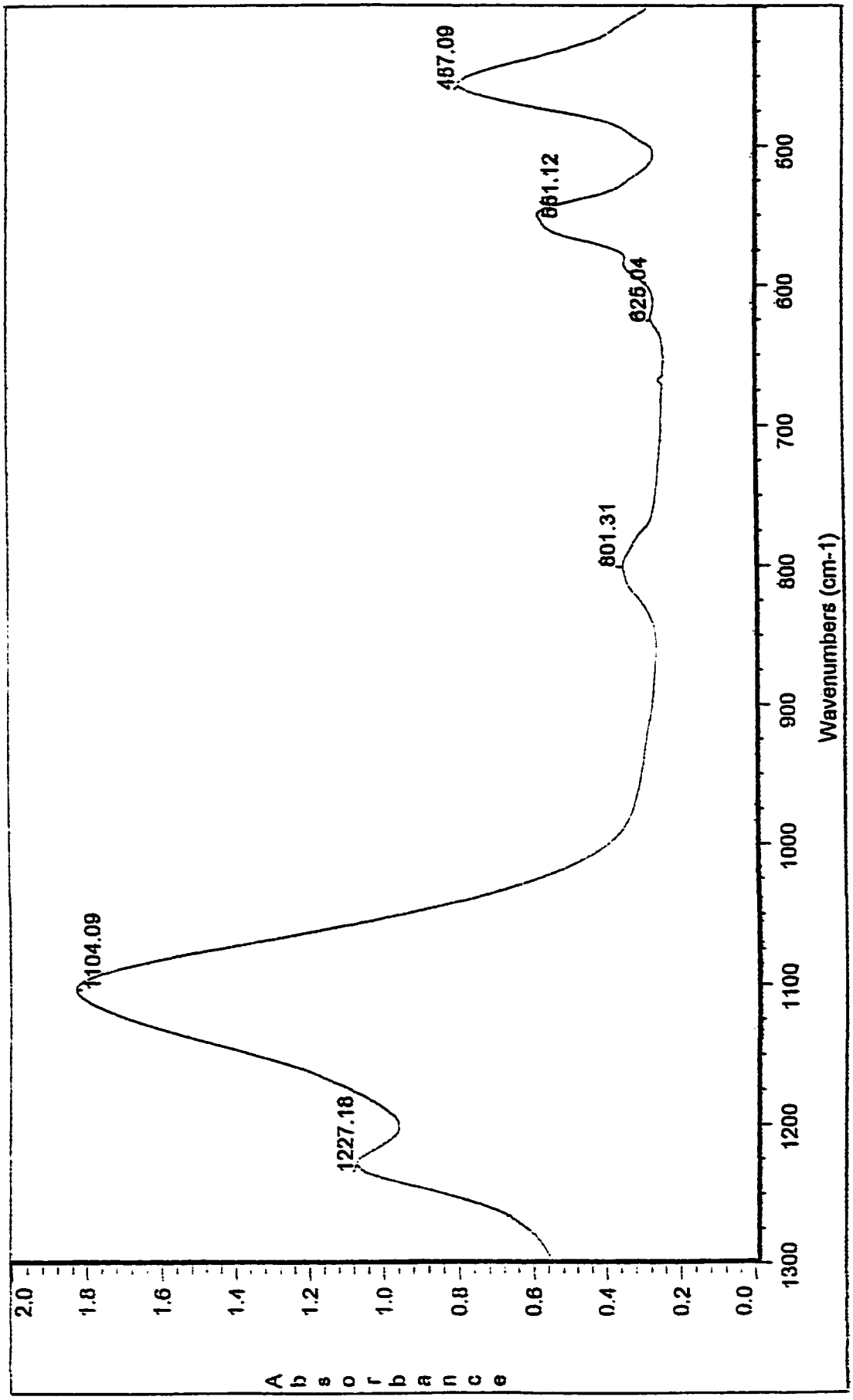

Figure A2.3 : FTIR spectrum of H-ZSM5 / F3 sample activated at 450°C in the framework region.

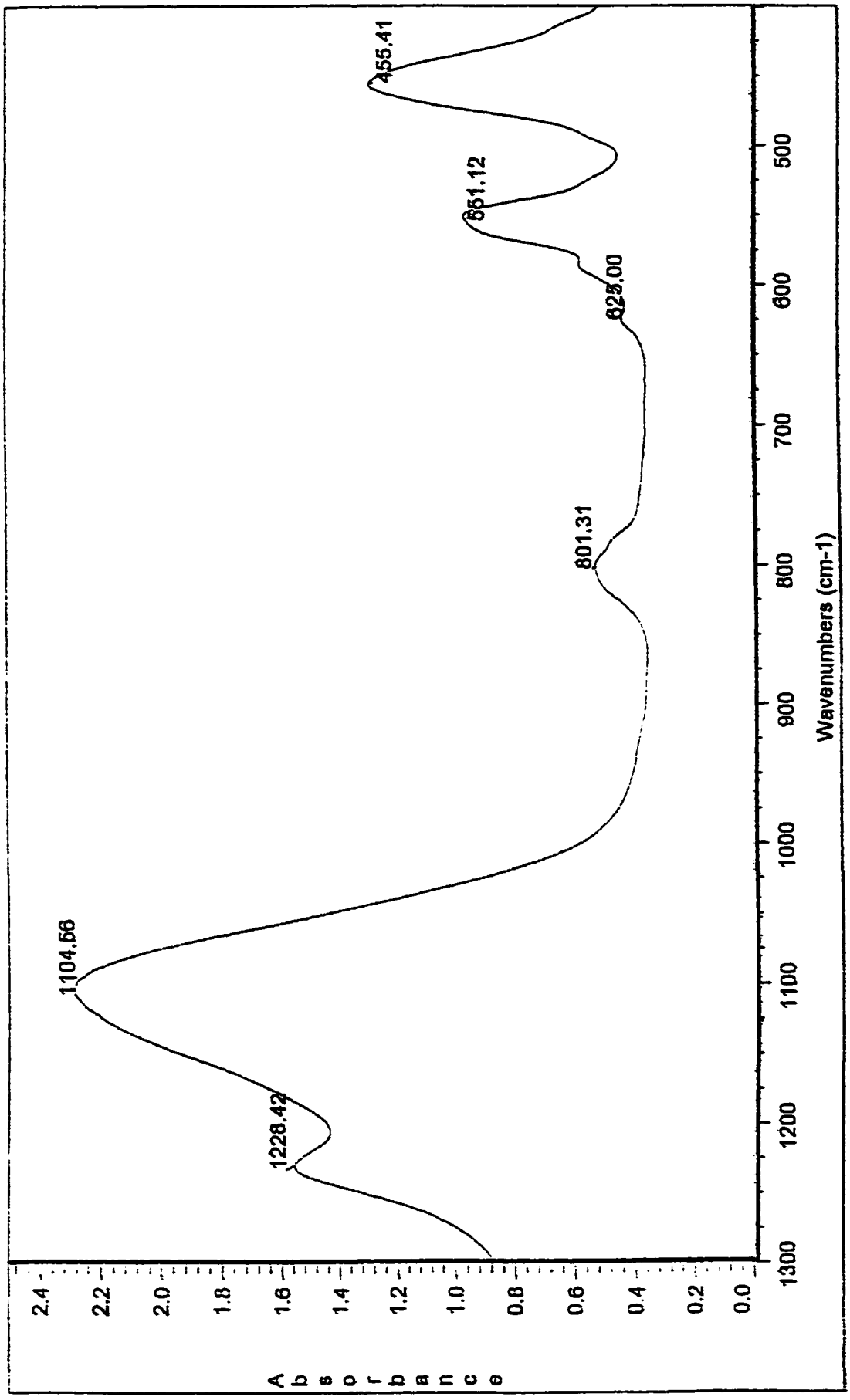

Figure A2.4 : FTIR spectrum of H-ZSM5 / F3 sample activated at 500°C in the framework region.

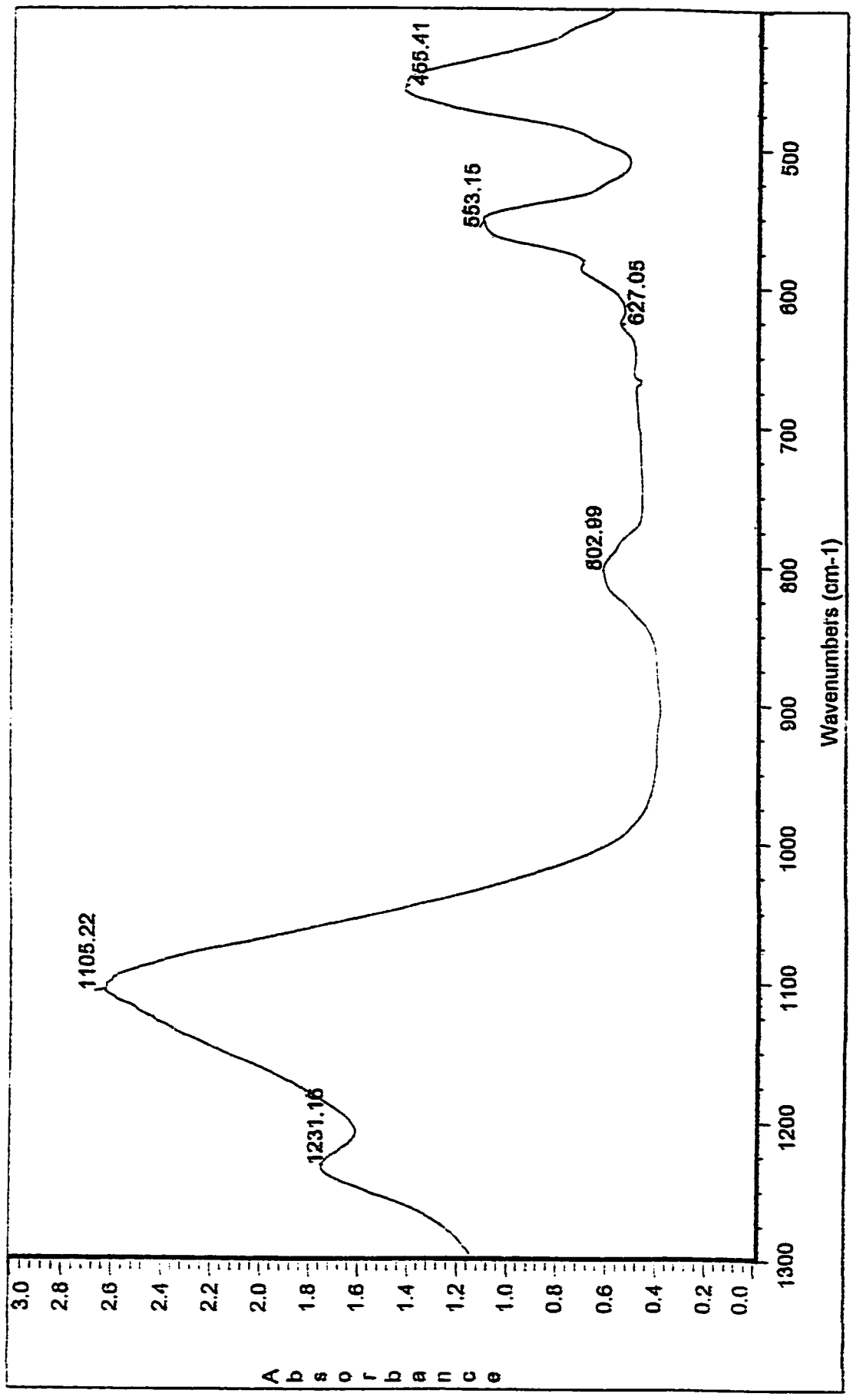

Figure A2.5 : FTIR spectrum of H-ZSM5 / F6 sample activated at 450°C in the framework region.

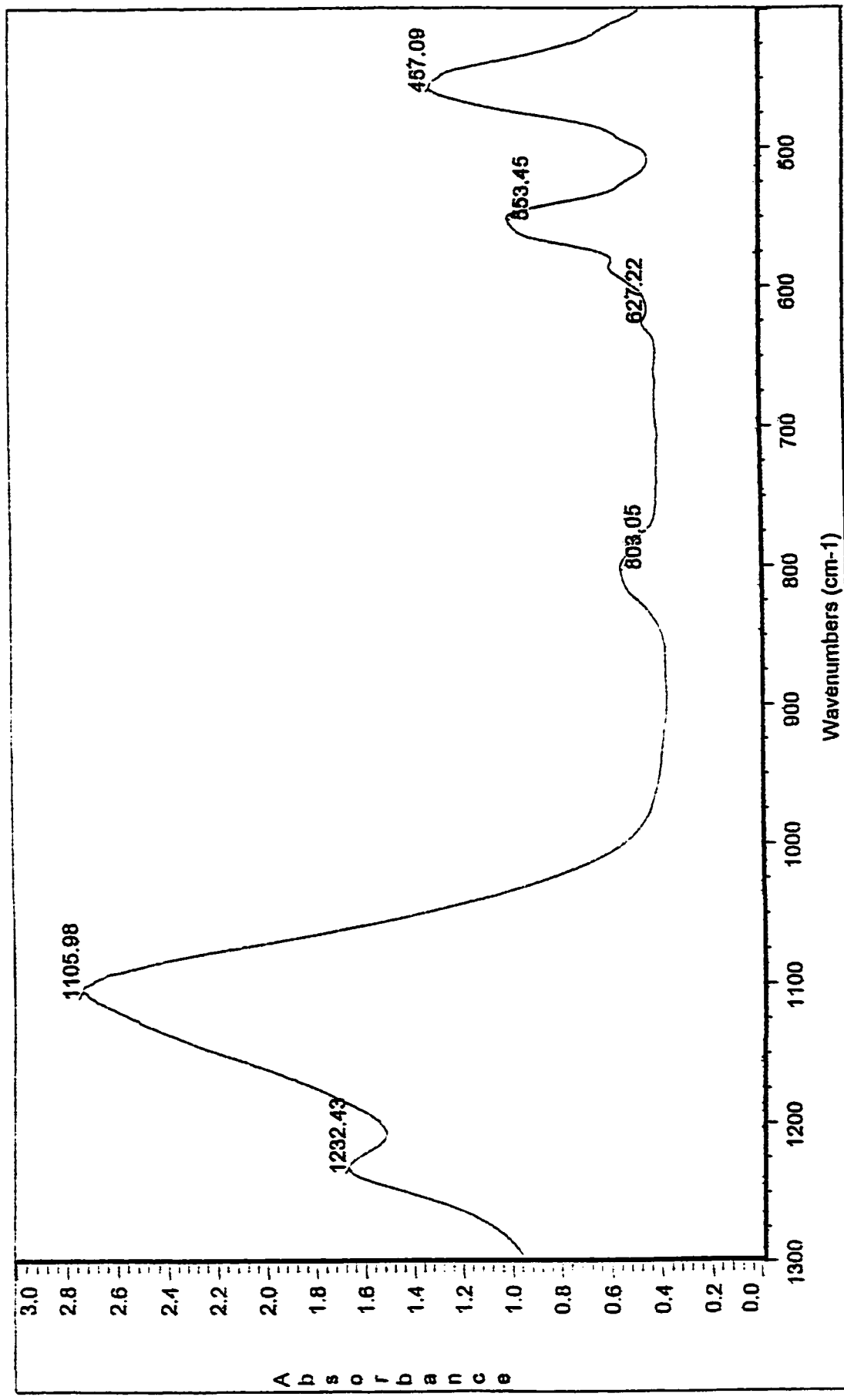

Figure A2.6 : FTIR spectrum of H-ZSM5 / F6 sample activated at 500°C in the framework region.

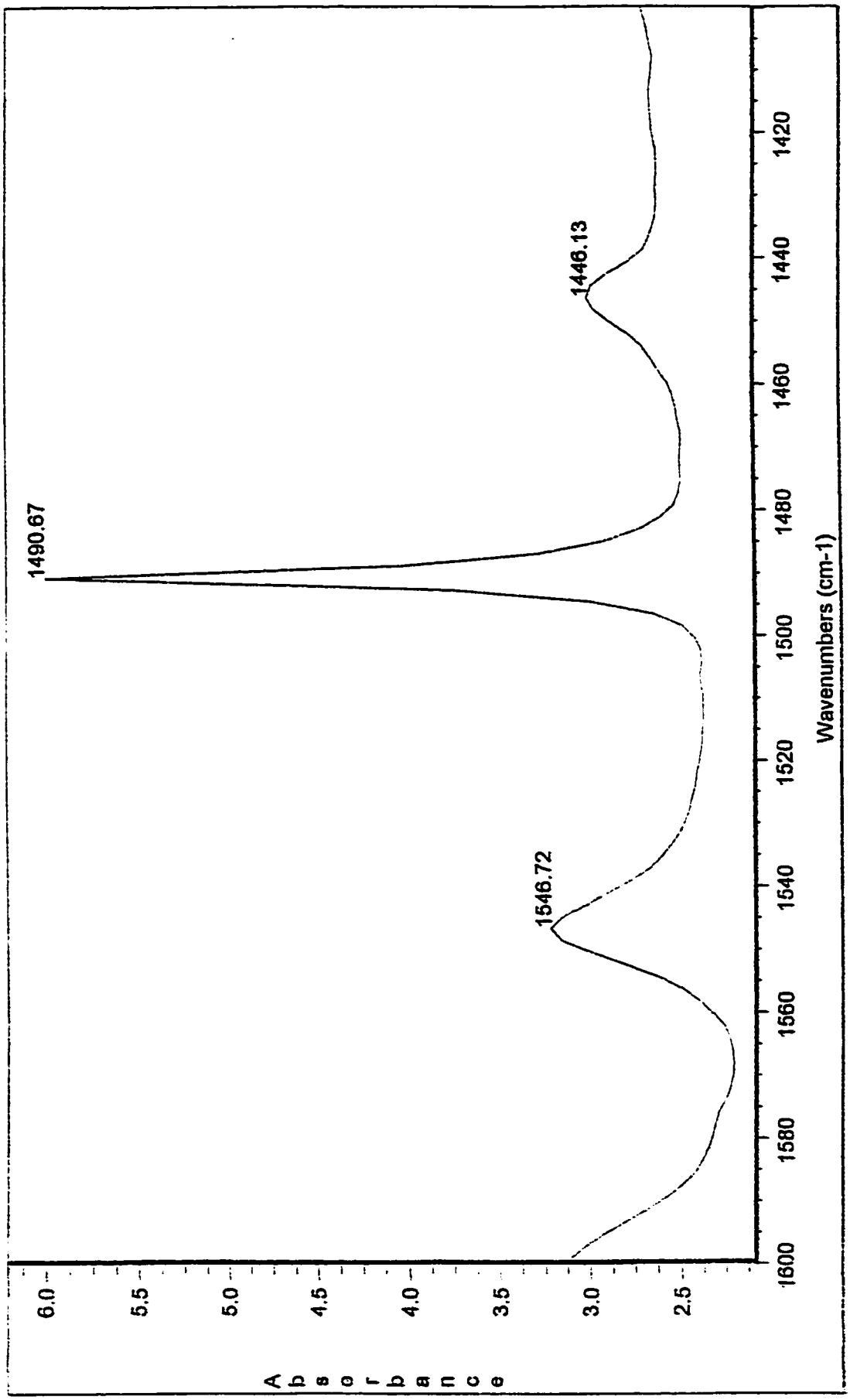

Figure A2.7 : FTIR spectrum of the Pyridine chemisorbed H-ZSM5 sample activated at 450°C.

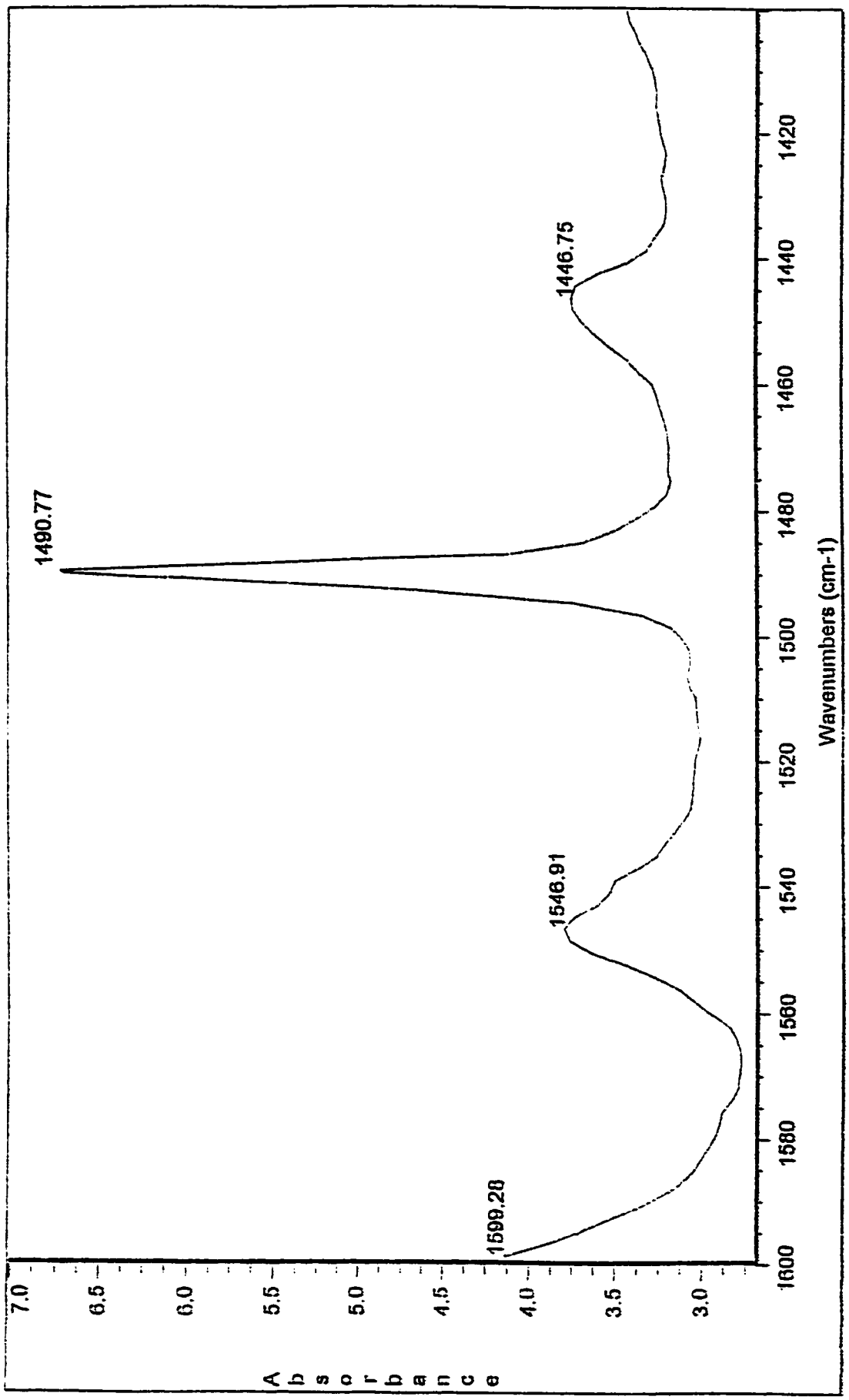

Figure A2.8 : FTIR spectrum of the Pyridine chemisorbed H-ZSM5 sample activated at 500°C.

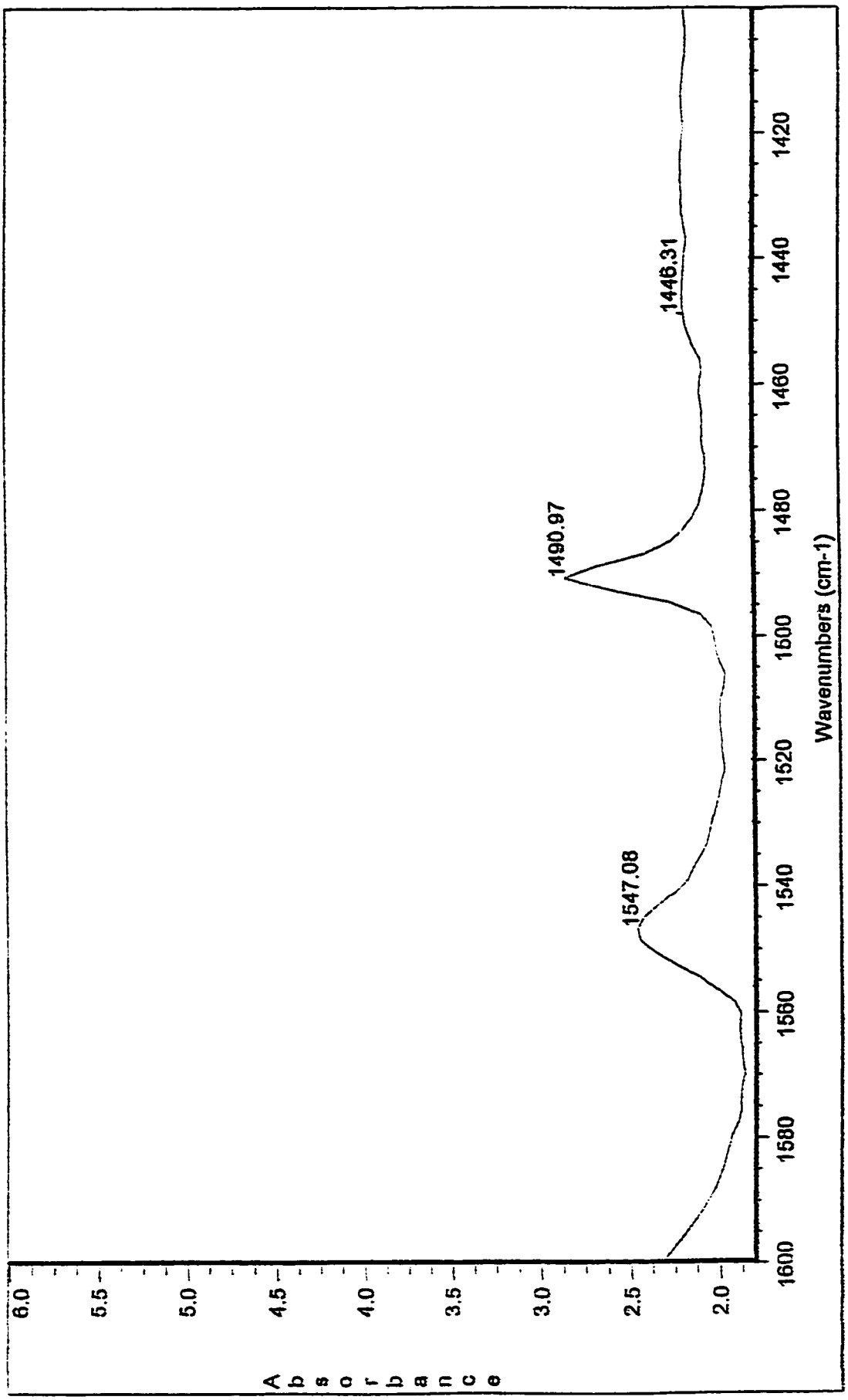

Figure A2.9 : FTIR spectrum of the Pyridine chemisorbed H-ZSM5 / F3 sample activated at 450°C.

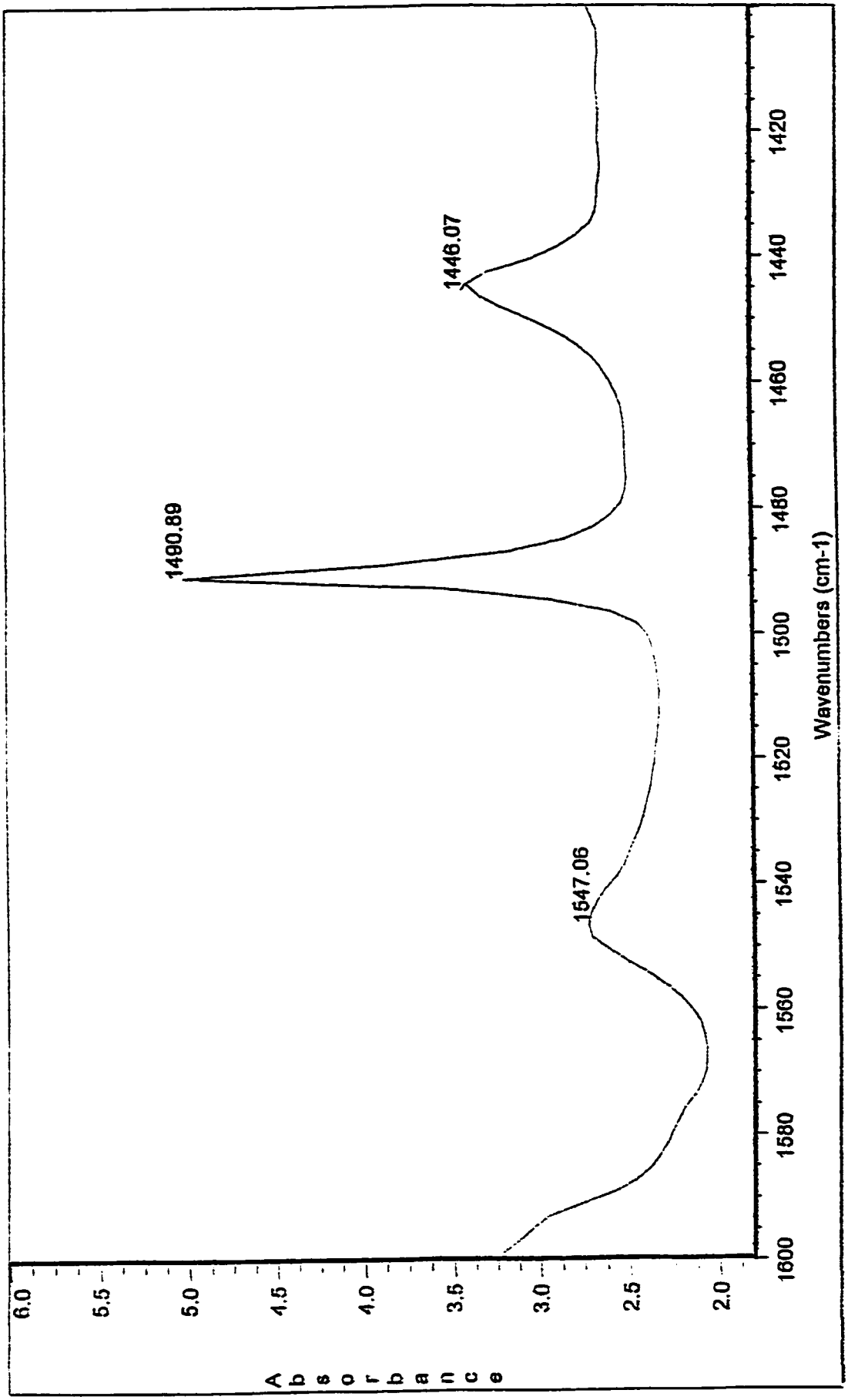

Figure A2.10 : FTIR spectrum of the Pyridine chemisorbed H-ZSM5 / F3 sample activated at 500°C.

APPENDIX 3

Program C++ for the calculation of MTBE conversion

```
// C++ - PROGRAM FOR CALCULATION OF MTBE YIELD
// CONCORDIA UNIVERSITY, CHEMISTRY AND BIOCHEMISTRY DEPARTMENT
#include<stdio.h> // for printf()
#include<conio.h> // for getch()

void main (void)
{
float CONV, PERC81, PERC82, A81, A82, QG, M1, R1, RI, R2, M2, X1, V, T, Qg;
float Y, T3, R3, R4, Z, Mass1, MaoC1, MaoC2, X4, P, X5, WHSV, TK, V6, T6, MC;
float Risob, CC, Rm, PERCL, AL, T9, PERCG, AG, RT;

clrscr();
printf("\n");
printf("\t\tCalculation of the mass of MeOH in the syringe\n");
printf("\n\nEnter the initial mass in g of MeOH in the syringe: ");
scanf("%f",&M1);
printf("\nEnter the mass in g of MeOH in the syringe after the reaction:");
scanf("%f",&M2);
X1=M1-M2; // in  g
printf("\nMass of the MeOH used in the reaction is: %f", X1);
printf("\n**************************************************");

printf("\nConversion of the rate of flow of the exiting gas (Qg), from sec/ml to ml/min.");
printf("\nEnter the volume \"V\" in ml: ");
scanf("%f",&V);
printf("\nEnter the time \"T\" in sec: ");
scanf("%f",&T);
Qg=V/T*60;   // in  ml/min
QG=300/Qg;   // in  sec/5ml
```

```
printf("\nThe flow rate, Qg is: %f sec/5ml", QG);
printf("\nand %f ml/min", Qg);
printf("\n*****************************************************");

printf("\nGive the measured flow rate of isobutene in ml/sec: first enter ml: ");
scanf("%f",&V6);
printf("\nenter sec: ");
scanf("%f",&T6);
printf("\nGive the ambient temperature in K");
scanf("%F",&TK);

R1=T6*5/V6;  // in  sec/5ml
R2=30/R1;  // in  ml/min
//Risob=the flow rate of isobutene in g/hr, for program purpose only
Risob=(2463.366*V6)/(TK*T6); // in g/hr
RI=Risob/56.11 // in  mol/hr

printf("\nThe flow rate of isobutene is %f sec/5ml", R1);
printf("\nor %f ml/min", R2);
printf("\nor %f mol/h", RI);
printf("\n*********************************************************");

printf("\nCalculation of the flow rate of MeOH in g/hr");
printf("\nEnter the total time of the reaction with MeOH in hr");
scanf("%f",&T3);
R3=X1 / T3;        // in  g/hr
printf("\nThe flow rate of MeOH is: %f g/h", R3);
printf("\n*****************************************************");
```

```
R4=R3 / 32.04;  // in  mol/h
printf("\nand %f mol/h", R4);

printf("\nCalculation of the weight of the liquid phase, MTBE in g");
printf("\nEnter the mass of the empty flask in g");
scanf("%f",&MASS1);
printf("\nEnter the mass of the first portion of octanol in g");
scanf("%f",&MAOC1);
printf("\nEnter the mass of the second portion of octanol");
scanf("%f",&MAOC2);
printf("\nEnter the mass of  the empty flask with two portions of octanol and  the
products in g");
scanf("%f",&Y);
X4=MASS1 + MAOC1 + MAOC2;  // in  g
Z=Y-X4;          // in  g
printf("\nThe weight of the liquid phase (MTBE) is:  %fg", Z);
printf("\n**************************************************");

printf("\nCalculation of the mass of standard 2,2DMB added, in g");
printf("\nEnter the mass of the flask and octanol + products and DMB, in g");
scanf("%f",&P);
X5=P-Y;          // in  g
printf("\nThe mass of  2,2DMB is: %f g", X5);
printf("\n**************************************************");

printf("\nCalculation of WHSV, in 1/hr");
printf("\nGive the mass of the catalyst in g used in the reaction");
scanf("%f",&MC);

WHSV=(R3+Risob)/MC;      // in  1/hr
```

```
printf("\nWHSV is: %f 1/h", WHSV);
printf("\n**********************************************************");

printf("\nCalculation of the contact time in hours");
CC=1/WHSV;                    // in  hours
printf("\nThe contact time is: %f  h", CC);
printf("\n**********************************************************");

printf("\nCalculation of the molar ratio of MeOH over isobutene");
Rm=R4/RI;                     // no  units
printf("\nThe Rm= %f', Rm);
printf("\n**********************************************************");

printf("\nCalculation of the percent conversion (CONV) of isobutene to MTBE in the
liquid phase, in percents");
printf("\nGive the average ratio of area percent of MTBE to DMB in the liquid phase");
scanf("%f',&AL);

printf("\nGive the time of the reaction of isobutene in hours");
scanf("%f',&T9);

PERCL=(2.3684*X5*AL*TK)/(R2*T9);       // in  %
printf("\nThe CONV of isobutene to MTBE in the liquid phase is: %f', PERCL,
"percents");
printf("\n**********************************************************************
*****");

printf("\nCalculation of CONV of isobutene to MTBE in the gaseous phase, in
percents");
printf("\nGive the average ratio of area percent of MTBE to DMB in the gaseous phase");
```

```
scanf("%f",&AG);

PERCENTG=(6.758e-3*AG*Qg*TK)/R2;        // in %
printf("\nCONV of isobutene to MTBE in the gaseous phase is: %f", PERCG,
"percents");
printf("\n**********************************************************************
*******");

CONV=PERCG + PERCL;  // in %
printf("\nThe total percent (MTBE) Conv=%f", CONV);
printf("\n*****************************************************");

printf("\nCalculation of CCONV of the byproducts, C8-1, and C8-2");
printf("\nGive the average ratio of area percent of C8-1 and MTBE");
scanf("%f",&A81);
printf("\n Give the average ratio of area percent of C8-2 and MTBE");
scanf("%f",&A82);
PERC81=2.598*X5*TK*A81/(R2*T9);  // in %
PERC82=2.69*X5*TK*A82/(R2*T9);  // in %
printf("\nThe CONV for C8-1 is %f", PERC81);
printf("\n*****************************************************");
printf("\n The CONV for C8-2 is %f", PERC82);
printf("\n*****************************************************");
}
```